MATHEMATICAL MODEL FOR PREDICTING ANISOTROPIC EFFECTS IN PLASTICITY

By

CARL GOTTLIEB LANGNER

A DISSERTATION PRESENTED TO THE GRADUATE COUNCIL OF THE UNIVERSITY OF FLORIDA IN PARTIAL FULFILLMENT OF THE REQUIREMENTS FOR THE DEGREE OF DOCTOR OF PHILOSOPHY

UNIVERSITY OF FLORIDA
1973

DEDICATION

To my wife, Ann, whose constant help and encouragement made this work possible.

ACKNOWLEDGMENTS

The author wishes to thank Professor L. E. Malvern for his help in preparing this dissertation. The author heartily commends Professor Malvern for his courage and faith that enabled him to support and defend his student, the author, even when at times he was not entirely convinced of the worth of his student's unorthodox ideas.

The author acknowledges discussions with the following persons which helped to congeal the basic ideas of the radial element theory: M. A. Eisenberg, I. K. Ebcioglu, E. K. Walsh, R. E. Reed-Hill, P. R. Paslay, N. Cristescu, Ion Suliciu, C. S. Ting, and Richard Johnson. The author received technical help from Guy Demoret, J. D. Macmillan, and Bill Luckhurst. Thanks are also due the National Science Foundation, which helped support the author by Grant No. GK-23452, and to the University of Florida, which provided the majority of computer time used in this study.

TABLE OF CONTENTS

		Page
Acknowledgments		iii
List of Figures		v
Abstract		vii
Chapters		
I	Introduction	1
II	General Concepts of the Radial Element Theory	17
III	A Class of Elemental Stress Vectors for Predicting Elastic Material Behavior	29
IV	A Class of Elemental Stress Vectors for Predicting Elastic-Plastic Material Behavior	41
V	Stress-Strain Behavior for Axial Loading and Reversed Axial Loading	52
VI	Stress-Strain Behavior for the Class of Loadings Involving Fixed Principal Axes	68
VII	Stress-Strain Behavior for Biaxial Loadings and for a General Loading History	91
VIII	Comparisons between the Theory and Experimental Results for Commercially Pure Aluminum	108
IX	Conclusions and Recommendations for Future Work	135
Bibliography		145
Appendices		
A	Computer Programs	152
B	Tabulated Results	162
C	Yield Surfaces in Principal Stress Space	170
D	Yield Surfaces in Principal Strain Space	184
Biographical Sketch		198

LIST OF FIGURES

Figure		Page
1	Basic Concepts of the Theory.	20
2	Spherical Coordinates	34
3	Distribution of Elemental Stress Vectors for Axial Loading from an Initially Isotropic State	54
4	Stress-Strain Behavior for Axial Loading, Small Strain.	57
5	Stress-Strain Behavior for Axial Loading, Large Strain.	58
6	Distribution of Elemental Stress Vectors for Reversed Axial Loading from an Initially Plastic State	61
7	Axial Loading and Reversed Axial Loadings for $\lambda = 0$	65
8	Axial Loading and Reversed Axial Loadings for $\lambda = 1.5$.	66
9	Stress-Strain Behavior for Shear Loadings	74
10	Numerical Errors for Axial Loading; Ordinary Trapezoidal Integration, $\lambda = 0$	76
11	Numerical Errors for Axial Loading; Ordinary Trapezoidal Integration, $\lambda = 1$	77
12	Numerical Errors for Axial Loading; Modified Trapezoidal Integration, $\lambda = 0$	78
13	Numerical Errors for Axial Loading; Modified Trapezoidal Integration, $\lambda = 1$	79
14	Surfaces of Constant Offset Strain for an Initially Isotropic Material.	84
15	Surfaces of Constant Offset Strain after an Axial Loading	85

Figure		Page
16	Surfaces of Constant Offset Strain after a Pure Shear Loading.	86
17	Stress-Strain Curves for Biaxial Strain Loadings	98
18	Stress-Strain Curves for Biaxial Stress Loadings	99
19	Loading Paths for Biaxial Strain with e_{12} Constant	100
20	Loading Paths for Biaxial Strain with e_{11} Constant	101
21	Loading Paths for Biaxial Stress with s_{12} Constant	102
22	Loading Paths for Biaxial Stress with s_{11} Constant	103
23	Apparatus for Tension-Compression Experiments. .	112
24	Specimen for Tension-Compression Experiments . .	113
25	Comparison of Experiment and Theory for Tension-Compression-Tension Tests.	115
26	Comparison of Experiment and Theory for Compression-Tension-Compression Tests.	116
27	Comparison of Experiment and Theory for Axial Loading and Reversed Axial Loading	117
28	Comparison of Experiment and Theory for Axial Loading and Reversed Axial Loading	118
29	Testing Machine for Biaxial Stress Experiments .	121
30	Strainometer and Specimen for Biaxial Stress Experiments.	122
31	Comparison of Experiment and Theory for Biaxial Tests, Axial Stress versus Axial Strain.	127
32	Comparison of Experiment and Theory for Biaxial Tests, Shear Stress versus Axial Stress.	128
33	Comparison of Experiment and Theory for Biaxial Tests, Shear Strain versus Axial Strain.	129
34	Ratio of Stresses Compared with Slope of Strain Path for Large Strains	130

Abstract of Dissertation Presented to the Graduate Council of the University of Florida in Partial Fulfillment of the Requirements for the Degree of Doctor of Philosophy

MATHEMATICAL MODEL FOR PREDICTING ANISOTROPIC EFFECTS IN PLASTICITY

By

Carl Gottlieb Langner

August, 1973

Chairman: Lawrence E. Malvern
Major Department: Engineering Science, Mechanics, and Aerospace Engineering

Existing theories of plasticity do not adequately describe the anisotropic effects of plasticity. Among the effects not easily incorporated into existing theories are the Bauschinger effect and the observed changes in the yield surface during complex loadings. A new theory of plasticity, the radial element theory, is introduced in this dissertation, which predicts stress-strain curves that are similar in shape to the actual stress-strain curves of many metals. The theory predicts a Bauschinger effect of the Masing type that compares closely with experimental data. The theory also agrees fairly well with experimental data for biaxial loadings of the torsion-tension type. In addition, yield surfaces are predicted by

this theory that in some ways are similar to those observed experimentally by others. The most unusual feature of the theory is the occurrence of a nonsymmetric stress tensor for loadings that involve rotations of the principal strain axes relative to the material. The general form of the radial element theory is not restricted to small deformations or to any one type of material behavior. Hence, it may find some use in other fields as well as in plasticity.

CHAPTER I

INTRODUCTION

This work is a contribution to the theory of plasticity, or more specifically, to the theory of isothermal, time-independent, stress-strain relations for polycrystalline metals. A new theory is introduced here for predicting elastic-plastic stress-strain behavior. The new theory is designed primarily to predict the three-dimensional anisotropic effects observed in metals for reversed loadings and for loading histories involving combined stresses. These are precisely the effects that are not predicted very well by existing theories of plasticity.

We begin our discussion of plasticity with some brief definitions of the more frequently used terminology. For detailed discussions of the concepts, terminology, and notations of plasticity theory the reader should consult one or more of the general expositions [1 - 5].[1] Elasticity is the property of a solid material once deformed to return exactly to the shape it had before deformation when all loads

---

[1] Numbers in brackets designate reference articles and books listed in the Bibliography.

are removed. Elasticity implies a one-to-one functional relationship between stress and strain. Plasticity is the property of a material whereby permanent or residual strain develops and is maintained when a certain yield condition is satisfied or exceeded. Yield condition defines the boundary between elasticity and plasticity; it is the set of stress or strain states situated at the outer limits of elastic behavior.

Stress space and strain space are mathematical vector spaces having, respectively, the nine components of the stress or strain tensors as coordinates. In stress or strain space the yield condition forms a hyper-surface called the yield surface. Loading point is the point in both stress and strain space that describes the current state of stress and strain. Residual strain point is a hypothetical loading point, corresponding to an elastic unloading from the current loading point, defined by zero stress. A loading is any motion of the loading point that involves plasticity. Loading path is the locus of the loading point as it moves in both stress and strain space during a loading. Direction of loading is the tangent to the loading path in either stress or strain space. Radial loading is a loading such that the loading path is a straight line passing through the origin in either stress or strain space. Reversed loading is a loading, following after an initial loading, in which the

loading point retraces the original loading path back to and perhaps beyond the origin in either stress or strain space.

Work-hardening is the phenomenon whereby the yield stress increases during any approximately radial loading. More generally, it is the tendency of the yield surface to expand in directions surrounding the direction of loading in stress space. Bauschinger effect is the phenomenon whereby the yield stress, for a hypothetical reversed loading, decreases or follows the loading point during any approximately radial loading. More generally, Bauschinger effect is the tendency of the yield surface to shrink or follow the loading point in directions roughly opposite the loading direction in stress space. The concepts of work-hardening and Bauschinger effect also often include the functional stress-strain relationship that occurs during a radial loading and a reversed radial loading, respectively. Two simple hypotheses regarding work-hardening are isotropic hardening, whereby the yield surface in stress space expands uniformly while maintaining its original shape and position, and kinematic hardening, whereby the yield surface in stress space translates according to a certain rule while maintaining its original shape and size.

In this work, the material under discussion will always possess a domain of elasticity in which the stress-strain relationship is linear and isotropic relative to a current residual strain. The elastic domain always includes the

current loading point but does not necessarily include the current residual strain point. Initially the residual strain is zero and the yield condition is isotropic, so that the stress-strain behavior for a given loading history is independent of the initial direction of loading. Subsequent yield conditions generally are not isotropic, so that loading directions are important in determining the stress-strain relations after initial plastic yielding. In practice, the initial isotropic state of a polycrystalline metal can be restored by annealing or by melting and careful solidification.

Throughout this work we assume that the yield condition is not influenced by mean stress and that the residual or plastic part of the strain occurs at constant volume. The first assumption was confirmed experimentally for several metals by Crossland [6]. From these assumptions it follows that mean stress and mean strain are elastically related. Rate effects (creep and relaxation) are ignored; either the material is inviscid or all loadings occur at the same constant rate. Thermal effects are ignored; either the material is insensitive to temperature changes or deformations occur at the same constant temperature. Since the present subject is stress-strain relations, we can simply disregard the equations of motion and the energy relations of a continuum.

There are two main classes or categories of plasticity theories. The first class we shall call the phenomenological theories, since the basic ideas of this class of theories

are directly concerned with the relationship between stress and strain. The phenomenological theories were developed in a long series of papers [7 - 28] by many authors. Early examples of this class of theories are: (1) the theory of perfect-plasticity which neglects elastic strains, developed by Saint Venant [8], Levy [9], and von Mises [10]; (2) the theory of perfect-plasticity which includes elastic strains, developed by Prandtl [11] and Reuss [15]; and (3) the total deformation theory of Hencky [12]. These early perfect-plasticity theories assumed an isotropic yield surface and no work-hardening, and they required the plastic strain increment to be proportional to the deviator stress. Because they ignored work-hardening, these theories do not represent very accurately the stress-strain behavior of metals. The Hencky theory related stress to the strain rather than to increments of strain and it included work-hardening. This theory has been shown to be unsuitable for describing plastic behavior for any loadings other than radial and near-radial loadings [1]. Because of their simplicity, and in spite of their shortcomings, the above-mentioned theories have been applied extensively to technological problems [1, 2].

The perfect-plasticity theories were generalized by Ros and Eichinger [16], Melan [17], Prager [18], Hill [19], Drucker [20], and others to include work-hardening. The resulting family of theories is known as plastic potential theory, because the plastic strain increment is expressed

as a derivative of a potential function with respect to stress. The simplest and most common form of plastic potential theory combines the ideas of initial elasticity, a smooth initial yield surface (usually the Mises condition), isotropic work-hardening, and a flow rule defined by the requirement that the direction of the plastic strain increment be the same as the normal to the yield surface at the loading point. Further generalizations were made by Koiter [21], Sanders [22], and Hodge [26], who developed the idea that more than one yield surface can be operating simultaneously; this idea permits the formation of corners from an initially smooth yield surface. The concept of kinematic hardening was proposed by Ishlinskii [23] and Prager [24, 25], and a modified form of kinematic hardening was proposed by Ziegler [27]. Mroz [28] proposed a theory which combines the concepts of isotropic hardening, kinematic hardening, multiple yield surfaces, and a field of work-hardening moduli; this theory can be made to predict work-hardening and a piecewise-linear Bauschinger effect.

The phenomenological theories possess two advantages over other plasticity theories. (1) Most of these theories are simple enough to use in the solution of problems involving engineering structures. (2) Numerous experimental studies [29 - 32] have demonstrated the validity of the plastic potential theories for loadings in which the plastic deformation continues without interruption. See Hill [1, pp. 22-32] for

references to early experimental work. These experimental studies generally avoided reversed loadings and unloading followed by reloading in a different direction, situations in which the phenomenological theories do not provide accurate predictions.

There are two principal objections to the phenomenological plasticity theories. (1) The theories lack the unity of a truly predictive theory. By this is meant that as new ideas and new experimental data become available the phenomenological theories must be repeatedly modified and made increasingly complex with new assumptions in order to account for each new phenomenon. A more satisfactory theory would not require this layering of assumption upon assumption, but would predict all essential phenomena with the simplest and most basic form of the theory. (2) There does not appear to be any easy way to include in these theories a realistic Bauschinger effect or any of the related anisotropic changes in the yield surface as a function of the loading history that have been observed experimentally. The first objection is posed here by the author. The second objection, which concerns mainly the continuing lack of an adequate hardening hypothesis, has been stated before in a variety of places; see Zizicas [3(b)], Naghdi [4, p. 144], Green and Naghdi [5, p. 253], Iwan [33, p. 612], and Batdorf and Budiansky [34, p. 323]. The following passage from Iwan [33] is pertinent:

> One such theory, the incremental theory of plasticity, describes the three-dimensional yielding behavior of a material in terms of a yield surface in stress space, along with a flow rule and a work-hardening law. To date, this theory has been applied quite successfully to the rather large class of problems which have to do with the monotonic loading behavior of materials. However, when the theory is extended to the analysis of a cyclic and hysteretic behavior, certain difficulties arise. For the most part, the difficulties result from the requirement that the theory be capable of accounting for a Bauschinger effect. Furthermore, experimental results indicate that this Bauschinger effect should have a specific form; namely, that the stress-strain curves associated with one-dimensional symmetrical closed hysteresis loops should be of the same form as those of stabilized initial loading curve (or cyclic stress-strain curve for cyclic hardening or softening systems) except for an enlargement by a factor of two. The idea that hysteresis loops should have this form was first suggested by G. Masing and is often referred to as Masing's hypothesis. The recent development of the concept of kinematic hardening by Prager has provided a means for introducing a Bauschinger effect into the incremental theory of plasticity but, even with this extension, stress-strain behavior satisfying Masing's hypothesis has only been obtained for the special case of a linear work-hardening law. When the work-hardening is not linear, it would appear that some additional assumptions need to be added to the kinematic hardening hypothesis but as yet these assumptions have not been set forth.

The reader who wishes further information on cyclic loading is referred to two recent papers by Krempl [35] and Feltner and Landgraf [36]. Masing's hypothesis on the form of the stabilized hysteresis curve was originally proposed in the article [37].

Numerous recent papers [32, 38 - 53] have reported experimental investigations of the initial and subsequent yield surfaces in metals. The metals tested included copper, brass, mild steel, and various alloys of aluminum. All papers but one [47] reported biaxial tests performed on tubular specimens. In [38, 40, 50] the tests involved tension and internal pressure, and in [42, 48] the tests involved torsion and internal pressure. The remaining papers reported combined tension and torsion loadings. Most of the papers dealt with the question of whether or not a corner is formed in the yield surface at the loading point. Two methods have been used to study this question. The first method consisted of probing with the loading point in various directions in stress space and thereby detecting a portion of the yield surface according to some given definition of yielding. This was usually done both initially and after a certain pre-strain. The second method consisted of imposing on the material a zigzag loading path in stress space and then measuring and plotting the corresponding plastic strain increments. According to Drucker [20], if the yield surface is smooth then the direction of the plastic strain increment must be normal to the yield surface and independent of the stress increment. If abrupt changes are observed in the direction of the plastic strain vector corresponding to the abrupt changes in the stress vector, then a corner must exist at the loading point.

The following general conclusions can be drawn from the experimental papers [32, 38 - 53]. The initial yield surface is closer to the Mises condition than to the Tresca condition. All subsequent yield surfaces are smooth and convex, and the direction of the plastic strain increment is always very close to the yield surface normal at the loading point. The plastic strain increments appear to depend only very slightly upon abrupt changes in the directions of the stress increments. Subsequent yield surfaces exhibit a region of high curvature surrounding the loading point, but a sharp corner is not formed. A flattened region generally forms on the side of the yield surface opposite the loading point for data plotted in the shear stress-axial stress plane.

The experimentally observed characteristics of the yield surface depend intimately upon which definition of yield is used. A proportional limit definition of yield [32, 40, 41, 52, 53] gives yield surfaces which translate away from the origin in stress space (in the direction of loading) and which drastically change shape while showing little or no cross-effect (lateral expansion or contraction) during a radial loading. A backward-extrapolation definition of yield [42, 48, 49] leads to yield surfaces which expand nearly uniformly while translating very little; here work-hardening and a large cross-effect occur simultaneously. The sensitivity of the yield surface to the yield definition

led one author [47, 50] to report his results as families of curves of constant offset strain; this procedure avoids the subjectivity of the proportional limit definition and the arbitrariness of any other definition.

The second class of plasticity theory may be called the physical theories. Examples of the physical theories are presented in the papers of Batdorf and Budiansky [34], Besseling [54], Hutchinson [55], Lin and Ito [56, 57], and Wells and Paslay [58]. Studies of the micro-structure of metals has led to the following conclusions. (1) Crystallographic slip is the principal process of plastic deformation in face-centered-cubic metals at low and intermediate temperatures [57]. (2) The phenomenon of work-hardening and the Bauschinger effect are due to locked-in stresses produced by large numbers of dislocations that accumulate and become stuck at grain boundaries and around alloying elements in the material [59, Chapter V]. In various ways each of the physical theories has incorporated the ideas of crystalline slip and locked-in stresses. The most notable achievements of the physical theories are prediction of a developing corner in the yield surface at the loading point during plastic deformation [34, 56, 57] and prediction of a Bauschinger effect of the Masing type [54 - 58].

None of the physical theories has been entirely successful. Either the theories are too specialized and complicated to reliably and economically predict stress-strain behavior for

general loading paths [55, 56, 57], or they require specification of special functions such as the initial yield function and the stress-strain function for a monotonic pure tension or pure shear loading [34, 54, 58]. In the latter case the physical theories are conceptually not too much different from the phenomenological theories, most of which also require specification of various functions, presumably to be obtained from empirical data.

The theory of Lin and Ito [56, 57] deserves a special discussion as it is at present the most highly developed of the physical theories. In this theory the material is idealized as a cubical array of sixty-four differently oriented crystals of cubic shape. Each crystal is assumed to have one slip plane with three equally spaced slip directions. Heterogeneous slip and stress fields are calculated from single crystal slip properties subject to conditions of equilibrium and compatibility. The computed initial yield surface of this aggregate is very close to the Tresca condition, whereas the surface in stress space corresponding to a finite offset strain is close to a Mises condition. This observation offers one possible explanation why experimentally observed initial yield surfaces usually appear closer to the Mises than to the Tresca yield condition. The computed yield surface after an initial axial loading is found to have a corner at the loading point, but this corner is "blunt" in the sense that a corresponding surface of constant offset strain has a rounded nose instead of a sharp corner.

The theoretical results presented in this dissertation corroborate the theoretical results of Lin and Ito [56, 57], as discussed above, including prediction of a Bauschinger effect of the Masing type. Coincidentally, both the present theory and the Lin-Ito theory require the specification of four constants, two elasticities and two plasticity constants, in order to be completely determined. However, the basic ideas of the two theories are very different: the Lin-Ito theory is based on the ideas of slip in a three-dimensional crystalline aggregate, whereas the present theory does not make any appeal to the crystalline micro-structure of metals. The present theory has two advantages over the Lin-Ito theory, namely, greater accuracy and greater efficiency. Greater accuracy is achieved since the present theory can be thought of as representing an infinite rather than a finite polycrystalline aggregate. Greater efficiency is achieved since the present theory contains less structural detail, and this allows a greater quantity of results to be computed from a given amount of computer time.

For completeness, we mention three other currently accepted theories of plasticity that do not fit very well into either of the two categories discussed above. The first of these is the continuum theory of dislocations [60, pp. 88-92], which was developed largely by Kröner [61]. This theory is concerned with the exact mathematical description of dislocations in an elastic body, which is

accomplished by replacing the usual Euclidean metric tensor with a Riemannian metric tensor. The second of these theories is the theory of anisotropic fluids proposed and developed by Ericksen [62]; here a fluid is assumed to consist of molecules shaped like dumbbells. This theory has been promoted as a kind of plasticity theory because in the solution for Poiseuille (pipe) flow [62(b)] the material at the center of the flow is found to move as a rigid plug. The third of these theories is the mathematical theory of plasticity introduced by Ilyushin [63]. Functional analysis of the type expounded by Riesz and Nagy [64] is applied to general loading paths in stress and strain space. Relationships are assumed to exist between the curvatures of the loading paths in the two vector spaces. Lensky [65] attempted to connect this theory with experimental data. The author's brief study of these three theories has failed to reveal any concrete predictions of matters vital to plasticity, such as predictions of stress-strain relations and/or changes in the yield surface during plastic deformation.

In this chapter we have briefly outlined most of the existing theories of plasticity, and we have shown that none of these theories is entirely satisfactory for predicting all aspects of experimentally observed stress-strain behavior. This is true even for the restricted situation in which temperature and time effects can be ignored. We conclude that there is still need for further theoretical work in

plasticity. It is in the spirit of Zizicas [3(b), p. 448] that we undertake the development of a new theory.

> Instead of waiting for the physical theories (which take into account the full details of crystallographic structure) to come all the way to meet the mathematical theories, it may prove faster for the mathematical theories to move and meet the physical theories somewhere halfway between the two. One should be prepared to examine, or even replace completely if necessary, the fundamental assumptions of incremental theory. Certainly this theory, in its present form, should not be used as a basis for criticizing or discouraging research work at variance with its predictions. Such a point-of-view may delay important developments. The formulation of a proper set of mathematical stress-strain relations should be guided primarily by the aim of improving as much as possible the description of the physical behavior of materials. If approximations have to be made for mathematical convenience, they can be much better justified after the complications arising from a generally acceptable set of stress-strain relations are clearly demonstrated. A more accurate set always serves as a reference for comparison with approximate relations.

This dissertation introduces a new plasticity theory, hereafter referred to as the radial element theory. This theory is related to the physical theories mentioned above in the sense that special importance is attached to the locked-in stresses. In fact, a new concept is introduced — a set of elemental stress vectors depending on both the direction in space and the loading history at a material point — which exploits the directional aspects of the locked-in stresses in determining the overall stress at a point in a material body. The radial element theory is a purely

mathematical theory; its only connection with empirical data is through specification of four constants: two elasticities (Young's modulus E and Poisson's ratio ν, say), one yield strain ϵ_y, and a work-hardening parameter λ.

Among the successes that have been achieved with the radial element theory are: realistic predictions of work-hardening and a Bauschinger effect of the Masing type (Chapter V); relatively simple calculations to obtain anisotropic yield surfaces for complex loading paths (Chapter VI); a method of calculating stress-strain behavior for any arbitrary loading path (Chapter VII); and good agreement with experimental data on commercially pure aluminum (Chapter VIII). The experimental data are somewhat limited in quantity and accuracy, but they include two different loading situations, cyclic tension-compression loading of a rod and torsion-tension loading applied to a thin-wall tube.

In summary, the most pertinent properties which the radial element theory aims to predict are: (1) isotropic elasticity relative to the current residual strain; (2) isotropic initial yield condition; (3) subsequent yield conditions which are anisotropic, with the anisotropy determined by the history of deformations; (4) inviscid plastic flow, also determined by the deformation history. For tests conducted at a steady loading rate and at constant temperature, these properties describe fairly well the mechanical behavior of most polycrystalline metals.

CHAPTER II

GENERAL CONCEPTS OF THE RADIAL ELEMENT THEORY

In the theory presented here, the yield surfaces, flow rules, and hardening laws are not specified explicitly, as is true of most plasticity theories, but rather they are determined by the theory once a specific definition of an elemental stress vector is adopted. The key to the theory is the relationship that is assumed to exist between the elemental stress vector and the deformation of a radial element, which is the material element that reflects the deformation history in a given direction. Different material stress-strain behavior results if different relationships are assumed between the elemental stress vectors and deformations of the radial elements. Stress is defined in terms of certain integrals of the elemental stress vectors over an infinitesimal ellipsoid.

Suppose we wish to study the stress-strain behavior at a point P in a material body. The mathematical theory for this study can be developed as follows: Consider a spherical surface embedded in the body in its initially undeformed condition and centered at the given point P.

The radius R of the sphere may be finite if the body undergoes only homogeneous deformations. However, if nonhomogeneous deformations are allowed, then the sphere must be considered as infinitesimally small $R \to 0$. Throughout this dissertation we assume the material is a "simple material", that is, one for which the stress tensor at each material point is uniquely determined by the history of the deformation gradient.

During an arbitrary sequence of deformations the sphere will deform continuously into a sequence of ellipsoids of various shapes and orientations. Mathematical description of the undeformed sphere and of any one of the sequence of deformed ellipsoids, relative to a fixed coordinate system, affords the means of defining various finite strain tensors. For any such strain tensor, the principal directions in the deformed configuration must coincide with the principal axes of the ellipsoid, and the principal strain magnitudes must be related by an invertible function to the principal diameters of the ellipsoid. The sequence of strain tensors computed in this manner from a given sequence of deformations comprises the strain history at the given material point P.

For definiteness and because it is useful, we introduce here one example of a finite strain tensor: the logarithmic strain, also sometimes called the natural strain. Let $\underline{n}_\alpha$ ($\alpha = 1,2,3$) be unit vectors directed along the three principal axes of the deformed ellipsoid; let d_α be the corresponding principal diameters; and let "log( )" signify the natural

logarithm function. Then $\lambda_\alpha = d_\alpha/2R$ are the principal stretches and

$$\varepsilon_\alpha = \log(\lambda_\alpha), \quad \alpha = 1,2,3$$
$$\underline{\varepsilon} = \sum_{\alpha=1}^{3} \underline{n}_\alpha \underline{n}_\alpha \log(\lambda_\alpha) \tag{2.1}$$

are the logarithmic principal strains and the logarithmic strain tensor, respectively. The logarithmic strain has the following two advantages over other strain measures for use in connection with the theory of plasticity: (1) mean and deviator components represent exact measures of volume-type and distortion-type deformations, respectively, and (2) experimental results for tension and compression tests give the same stress-strain curve (up to necking or failure) when logarithmic strain is used. The latter fact allows the possibility that an initially isotropic plasticity theory can agree with experimental data. For the many further details concerning finite strain measures the reader is referred to Truesdell and Toupin [66, 241-324] or Malvern [67, pp. 154-182].

The first fundamental concept of the present theory is the radial element. Consider a material element which initially is a differential cone or filament radiating outward from the center P to a point Q on the surface of the undeformed sphere. See Figure 1. This radial element, corresponding to a given fixed direction in the undeformed state, will elongate (or contract) and shear as the sphere deforms into a sequence of ellipsoids during a given deformation history.

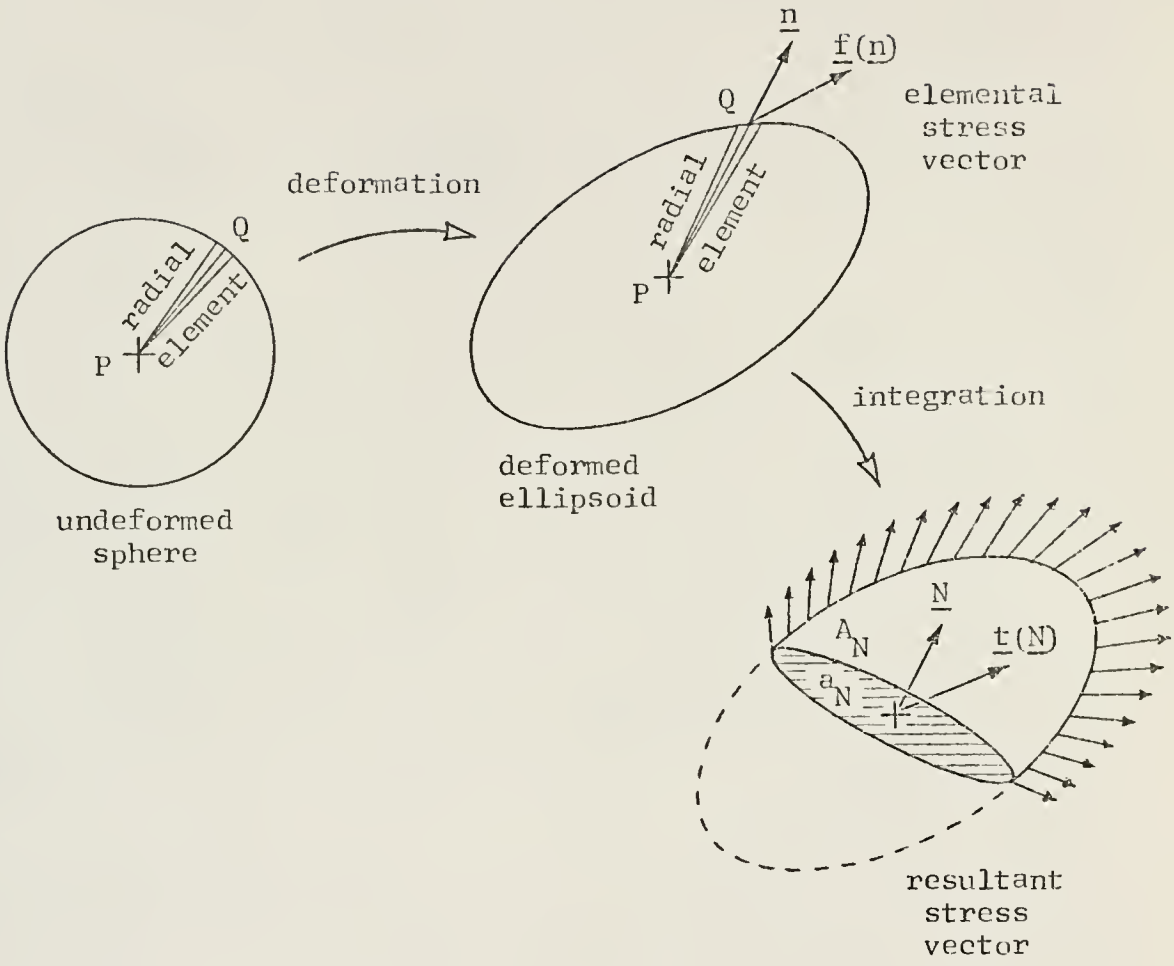

FIGURE 1. BASIC CONCEPTS OF THE THEORY

The second fundamental concept of the theory is the elemental stress vector $\underline{f}$, which we define to act at each point Q on the surface of the deformed ellipsoid. This elemental stress vector is assumed to correspond directly to the radial element along the line PQ. Let $\underline{n}$ be a unit vector in the direction of PQ. Then the set of all elemental stress vectors $\underline{f}(\underline{n})$ corresponding to the set of all radial elements forms a vector field over the ellipsoid. Again refer to Figure 1.

The vector $\underline{f}$ is assumed to depend exclusively on the deformation history of the individual radial element upon which it acts. The overall stress-strain behavior of the material is governed by this relationship which we assume to exist between the elemental stress vector and the deformations of the corresponding radial element. For example, elastic behavior is obtained if this relationship is assumed to be linear and one-to-one, as proved in Chapter III. Elastic-plastic behavior is obtained if the relationship is linear and if the magnitudes of the elemental stress vectors are limited in the manner specified in Chapter IV.

Suppose we are dealing with a material that exhibits elastic-plastic behavior, and suppose that the material has experienced plasticity in certain directions. That is, suppose we computed the elemental stress vectors elastically and we truncated those elemental stress vectors $\underline{f}$ that exceeded a certain yield criterion. Then the plasticity

will be expressed as a reduction of the stress components associated with those directions from the values predicted by elasticity. Anisotropic effects as well as plasticity are introduced into the theory in this manner. These ideas will become clearer to the reader as he progresses through Chapters III and IV.

At this point we must draw a vital distinction between the elemental stress vector used in the radial element theory and the ordinary stress vector introduced by Cauchy [66, p. 537]. Cauchy proved that the stress vector $\underline{t}$ acting on an elemental surface is related to the surface normal unit vector $\underline{n}$ by a homogeneous linear function $\underline{t}(\underline{n}) = \underline{T} \cdot \underline{n}$, where $\underline{T}$ is the stress tensor. This result follows from the principle of linear momentum and is known as the Cauchy stress principle. In the radial element theory $\underline{f}(\underline{n})$ is generalized so that it no longer satisfies the Cauchy stress principle. This generalization of the stress vector is necessary in order to exploit the individual response of material elements oriented in various directions.

If we wish to preserve intact the classical theory of continuum mechanics, it becomes necessary to consider the elemental stress vectors as an entirely separate concept from the Cauchy stress. The elemental stress vectors can be viewed as a structural entity of the material similar to micro-stresses in a dislocation theory or they can be viewed simply as a mathematical device to be used in

generating stress-strain relations. Regardless of how they are viewed we shall continue to develop and use the elemental stress vectors as if they indeed possessed a rigorous mechanical basis.

Ultimately, however, we shall want to use the stress-strain relations generated by the radial element theory in the solution of boundary value problems, such as determination of the bending or twisting of some engineering structure under a set of loads. For this latter purpose we must ignore the details of the radial element theory and accept only the overall stress-strain relations. Finally, we must combine these stress-strain relations with the established principles of continuum mechanics [67, Chapter 5], including the Cauchy stress principle, in order to obtain a meaningful, well-set mechanical problem.

The following equations, which resemble force and moment equilibrium equations, are necessary conditions for the construction of a unique stress tensor.

$$\underline{F} = \int_A \underline{f}\, dA = 0 , \quad \underline{M} = \int_A \underline{r} \times \underline{f}\, dA = 0 \tag{2.2}$$

Here $\underline{r}$ is the radius vector from the center to the ellipsoid surface and A is the total surface area of the deformed ellipsoid. Equations (2.2) represent restrictions on the permissible class of elemental stress vectors; the specific constitutive assumptions for $\underline{f}$ reported in Chapters III and IV do satisfy these restrictions.

The third fundamental concept of the radial element theory comprises the resultant stress vector $\underline{t}$ and the couple stress vector $\underline{c}$, defined as follows:

$$\underline{t}(\underline{N}) = \frac{1}{a_N} \int_{A_N} \underline{f}\, dA\,, \qquad \underline{c}(\underline{N}) = \frac{1}{a_N} \int_{A_N} \underline{r} \times \underline{f}\, dA\,. \tag{2.3}$$

Here $\underline{N}$ is a unit vector normal to the cross-sectional area a_N, and A_N is one-half the surface area of the deformed ellipsoid; both areas a_N and A_N are determined by $\underline{N}$ as shown in Figure 1. Unfortunately, the functions $\underline{t}(\underline{N})$ and $\underline{c}(\underline{N})$ are nonlinear, in general, which eliminates them as direct candidates for the stress tensor and couple stress tensor, respectively.

By comparing equations (2.2) and (2.3), we see that equations (2.2) are equivalent to

$$\underline{t}(\underline{N}) = -\underline{t}(-\underline{N}) \quad \text{and} \quad \underline{c}(\underline{N}) = -\underline{c}(-\underline{N})\,. \tag{2.4}$$

Equations (2.4) state that the resultant stress on one side of a given plane surface is equal and opposite to the resultant stress acting on the other side of the same surface. If these equations were not true then the resultant stress would not be unique, since we would not know which resultant stress vector, i.e., $\underline{t}(\underline{N})$ or $-\underline{t}(-\underline{N})$, to assign to a direction $\underline{N}$.

The following procedure has been tried in conjunction with elastic-plastic behavior for a variety of loadings and seems to yield a unique stress tensor. Suppose we are given a set of elemental stress vectors $\underline{f}(\underline{n})$ distributed over a known deformed ellipsoidal surface. The function $\underline{f}(\underline{n})$ can be quite general, with discontinuities occurring in the

derivatives and in the function itself, provided the vectors are real and provided equations (2.2) or (2.4) are satisfied.[1] Consider any orthogonal triad of unit vectors $\underline{N}_\alpha$ $(\alpha = 1,2,3)$, and compute by means of equation $(2.3)_1$ the three resultant stress vectors $\underline{t}_\alpha = \underline{t}(\underline{N}_\alpha)$ corresponding to these $\underline{N}_\alpha$. In a Cartesian coordinate system with $\underline{N}_\alpha$ as base vectors, the components of $\underline{t}_\alpha$ form a matrix $T = [t_{i\alpha}]$, $(i,\alpha = 1,2,3)$. That is, the components of $\underline{t}_1 = (t_{11}, t_{21}, t_{31})$, $\underline{t}_2 = (t_{12}, t_{22}, t_{32})$, $\underline{t}_3 = (t_{13}, t_{23}, t_{33})$ form the matrix

$$T = \begin{bmatrix} t_{11} & t_{12} & t_{13} \\ t_{21} & t_{22} & t_{23} \\ t_{31} & t_{32} & t_{33} \end{bmatrix} .$$

Note that the second subscript identifies the plane on which the vector acts and the first subscript identifies the component.

Define a positive definite norm in terms of the off-diagonal elements of T by the expression

$$M = (t_{12} + t_{21})^2 + (t_{23} + t_{32})^2 + (t_{31} + t_{13})^2 . \qquad (2.5)$$

We can now search for and obtain an orthogonal triad of unit vectors $\underline{N}'_\alpha$ by the requirement that the norm M be minimum[2] when

---

[1] The maximum generality of the function $\underline{f}(\underline{n})$ that satisfies equations (2.2) and that will permit construction of a stress tensor has not yet been established.

[2] The orthogonal triad of vectors $\underline{N}'_\alpha$ obtained by minimizing the norm M probably is unique for any reasonably well-behaved radial element theory. However, a proof of uniqueness is not available at this time.

the resultant stress vectors $\underline{t}'_\alpha = \underline{t}(\underline{N}'_\alpha)$, or the matrix $T' = T(\underline{N}'_\alpha)$, are computed relative to $\underline{N}'_\alpha$. In fact, for all specific distributions of $\underline{f}(\underline{n})$ considered in this dissertation, the norm M can be made zero by a proper choice of $\underline{N}'_\alpha$. Then T' becomes as diagonal as possible, with $t'_{12} = -t'_{21}$, $t'_{23} = -t'_{32}$, $t'_{31} = -t'_{13}$; and $t'_{11}, t'_{22}, t'_{33}$ are the "principal" resultant stresses.

We now define a resultant stress tensor $\tilde{\underline{T}}$ by the requirement that the components of $\tilde{\underline{T}}$ coincide with the elements of the matrix T' in the special coordinate system with $\underline{N}'_\alpha$ as base vectors. That is, we define $\tilde{t}'_{i\alpha} = t'_{i\alpha}$, where $\tilde{\underline{T}}' = [\tilde{t}'_{i\alpha}]$ is the tensor $\tilde{\underline{T}}$ referred to the coordinate system defined by $\underline{N}'_\alpha$. Relative to any fixed Cartesian coordinate system the components of $\underline{N}'_\alpha$ form a rotation matrix $R = [N'_{i\alpha}]$, and the resultant stress tensor $\tilde{\underline{T}}$ satisfies the transformation equations

$$\tilde{\underline{T}} = R \cdot \tilde{\underline{T}}' \cdot R^T , \quad \tilde{\underline{T}}' = R^T \cdot \tilde{\underline{T}} \cdot R \quad . \tag{2.6}$$

The deviator stress tensor $\underline{S} = [s_{ij}]$ is defined by the equations

$$\underline{S} = \tilde{\underline{T}} + p\,\underline{1} , \quad p = -(t_{11} + t_{22} + t_{33})/3 , \tag{2.7}$$

where $\underline{1} = [\delta_{ij}]$ is the unit tensor and -3p is the trace of the tensor $\tilde{\underline{T}}$ or the matrix T'. The ordinary stress tensor $\underline{\Sigma} = [\sigma_{ij}]$ can be written as

$$\underline{\Sigma} = \underline{S} + \sigma\underline{1} = \tilde{\underline{T}} + (\sigma + p)\,\underline{1} , \tag{2.8}$$

where σ is the mean stress to be determined by a separate relationship between mean stress and mean strain. Equation (2.7) will prove to be most useful in Chapters V, VI, and VII of this dissertation.

The above procedure forms the basis of a general computer program for predicting the stress from a given arbitrary strain history. This computer program is described in Chapter VII and is one of the programs listed in Appendix A. The above procedure is complicated, and it may seem to the reader to be an arbitrary and unnecessarily elaborate exercise of algebraic manipulations. The author has considered this matter in detail and has concluded that the procedure presented is the simplest and most direct method of constructing a stress tensor from a general distribution $\underline{f}(\underline{n})$ of elemental stress vectors.

The most controversial feature of the above procedure is the possibility of predicting a nonsymmetric stress tensor. I could have defined the deviator stress as the symmetric part of the deviator of the tensor $\underline{\underline{T}}$, and this would have given the ordinary symmetric stress tensor. However, my present purpose is to raise the possibility that the stress tensor may actually be nonsymmetric for certain loadings, and so I retain the definitions (2.7) and (2.8). In Chapter VII it is demonstrated that this procedure does predict a nonsymmetric stress for plastic deformations that involve rotations of the principal strain axes.

It may be possible to resolve the couple stress vectors $\underline{c}(\underline{N})$ into a couple stress tensor by a procedure similar to that proposed above for the resultant stresses. However, as our primary interest in this dissertation is with the resultant stresses, hereafter we shall ignore the couple stresses.

Another definition of stress which possibly could be more useful for describing material behavior during a finite strain involves first transferring (via the deformation function) the elemental stress vectors $\underline{f}$ from the deformed ellipsoid to corresponding points on the undeformed sphere. Then the resultant stress vectors $\underline{t}(\underline{N}_\alpha)$ are defined as integrals of the vectors $\underline{f}$ over the hemispheres of radius R that are symmetric about a given set of orthogonal unit vectors $\underline{N}_\alpha$. The stress tensor, in this case analogous to the second Piola-Kirchoff stress tensor, is found from the vectors $\underline{t}(\underline{N}_\alpha)$ as before. The two definitions of resultant stress are not the same, but they can be made equivalent by appropriate choices of the relationship between the elemental stress vectors and the deformations of the radial elements. In the case of stress calculated relative to the undeformed sphere, we must correlate this stress with one of the strain tensors associated with the undeformed state.

CHAPTER III

A CLASS OF ELEMENTAL STRESS VECTORS FOR PREDICTING ELASTIC MATERIAL BEHAVIOR

The general theory presented in Chapter II was valid for finite strains, and in principle it is possible to continue this analysis without invoking small strain approximations. However, by making such approximations the theory is greatly simplified. Questions of which stress and strain measure to use are avoided, and computations of yield surfaces are brought within the scope of a modest computational program. Therefore, in the remainder of this work we shall restrict our attention to the case of infinitesimal strains. For this case, the difference between the deformed ellipsoid and the undeformed sphere is negligible. The elemental vectors $\underline{f}(\underline{n})$ and all integrations to obtain the resultant stresses $\underline{t}(\underline{N})$ may be referred to the surface of the undeformed sphere. For simplicity we shall always consider this sphere to have unit radius $R = 1$.

Let σ_{ij} be the components of stress as defined by equation (2.8) and let ϵ_{ij} be the components of the infinitesimal strain tensor [67, pp. 120-135]. The deviator components s_{ij}, e_{ij} of stress and strain are defined by the following decomposition:

$$s_{ij} = \sigma_{ij} - \sigma\delta_{ij}, \quad e_{ij} = \epsilon_{ij} - \epsilon\delta_{ij} \quad (i,j = 1,2,3)$$

$$\sigma = \frac{1}{3}(\sigma_{11} + \sigma_{22} + \sigma_{33}), \quad \epsilon = \frac{1}{3}(\epsilon_{11} + \epsilon_{22} + \epsilon_{33}) \quad .$$

Here σ, ϵ are the mean stress and mean strain and δ_{ij} is the Kronecker delta. These definitions imply

$$s_{11} + s_{22} + s_{33} = 0, \quad e_{11} + e_{22} + e_{33} = 0 \quad .$$

Throughout the remainder of this work we shall be concerned mainly with relationships involving the deviator components s_{ij} and e_{ij}, instead of the "actual" or "true" stresses and strains, since, as usual, we assume plastic behavior to be confined to these variables. The deviator strain tensor, with components e_{ij}, is real and symmetric by definition, and is assumed known. The deviator stress tensor, with components s_{ij}, is real but not necessarily symmetric, and is the entity that we seek to compute.

We shall have use of the elasticity constants

$$\left.\begin{aligned} &E, \nu \text{ — Young's modulus, Poisson's ratio} \\ &\beta = E/(1 - 2\nu) \quad \text{volume or bulk modulus} \\ &\mu = E/(1 + \nu) \quad \text{shear modulus}^1 \end{aligned}\right\} \quad (3.1)$$

and the following special constants depending on a parameter λ:

$$\varkappa = \mu\left(\frac{4 - 2\lambda}{3 - \lambda}\right), \quad \eta = \mu\left(\frac{4\lambda - 4}{3 - \lambda}\right), \quad \zeta = \varkappa + \eta = \frac{2\mu\lambda}{3 - \lambda} \quad . \qquad (3.2)$$

Our assumption (page 4) that mean stress and mean strain are elastically related can be written simply as $\sigma = \beta\epsilon$.

---

[1] The shear modulus is customarily written as 2μ or $2G$; throughout this dissertation I write it simply as μ to save repeatedly writing the "2."

We require this elastic volume-compressibility relationship to hold at all times.

A specific constitutive assumption for the dependence of the elemental stress vector $\underline{f}$ on the deviator strain tensor $\underline{E}$ is now introduced, which predicts linear elastic behavior when the stress is computed.

$$\underline{f} = \varkappa \underline{E} \cdot \underline{n} + \eta (\underline{n} \cdot \underline{E} \cdot \underline{n}) \underline{n} \tag{3.3}$$

Here $\underline{E} = [e_{ij}]$ is the deviator strain tensor, $\underline{n}$ is a general unit vector, and $\varkappa, \eta$ are the constants defined by equations (3.2). The motivation for considering $\underline{f}$ in this form is that equation (3.3) can be conveniently modified to predict elastic-plastic behavior, which is the main purpose of this dissertation. The modified form of equation (3.3) will be presented in Chapter IV, with further developments presented in Chapters V, VI, VII.

We can prove that $\underline{f}$ in the form of equation (3.3) depends directly on the deformation of a radial element in the direction of $\underline{n}$, which is one of the requirements of the theory expressed in Chapter II. Since $\underline{E}$ is the deviator strain tensor, the inner product $\underline{E} \cdot \underline{n}$ represents the deviator strain vector associated with the unit vector $\underline{n}$. A further contraction of $\underline{E} \cdot \underline{n}$ with $\underline{n}$ gives the magnitude $\underline{n} \cdot \underline{E} \cdot \underline{n}$ of the normal component of the deviator strain vector, and the vector $(\underline{n} \cdot \underline{E} \cdot \underline{n})\underline{n}$ is the normal component. Hence, equation (3.3) defines $\underline{f}$ to be linearly related to the deviator strain vector and the

normal component of the deviator strain vector associated with the radial element in the direction of the unit vector $\underline{n}$.

Further observations can be made by deriving expressions for the normal and tangential (shear) components of $\underline{f}$. The equations

$$\underline{f}_n = (\underline{f}\cdot\underline{n})\underline{n} = \zeta\,\alpha\,\underline{n}$$

$$\underline{f}_t = \underline{f} - \underline{f}_n = \varkappa(\underline{E}\cdot\underline{n} - \alpha\,\underline{n}) \qquad (3.4)$$

where $\alpha = \underline{n}\cdot\underline{E}\cdot\underline{n}$

show that the normal component of $\underline{f}$ is proportional to the normal component of the deviator strain vector in the direction of $\underline{n}$, and that the tangential component of $\underline{f}$ is proportional to the maximum shear component of strain associated with the direction $\underline{n}$. From equations (3.2) and (3.4) it seems reasonable to limit the parameter to the range $0 < \lambda < 2$, since for this range stretch in a given direction is accompanied by a tensile normal component $\underline{f}_n$, and shear in a given pair of directions is accompanied by a tangential component $\underline{f}_t$ corresponding to the same directions, with $\underline{f}_t$ oriented so as to support the shear.

To simplify the calculations we now refer the vectors and tensors to a Cartesian coordinate system that coincides with the principal strain axes. Thus

$$\underline{E} = \begin{bmatrix} e_1 & 0 & 0 \\ 0 & e_2 & 0 \\ 0 & 0 & e_3 \end{bmatrix}, \quad \underline{n} = (\cos\theta_1, \cos\theta_2, \cos\theta_3)$$

where $e_i (i = 1,2,3)$ are the principal deviator strains and $\theta_i (i = 1,2,3)$ are the angles between the vector $\underline{n}$ and the coordinate axes. Substituting these results into equations (3.3) and (3.4) yields

$$\begin{aligned} \underline{f} &= [(\varkappa e_1 + \eta\alpha) n_1,\ (\varkappa e_2 + \eta\alpha) n_2,\ (\varkappa e_3 + \eta\alpha) n_3] \\ \underline{f}_n &= \zeta\alpha\underline{n},\quad \underline{f}_t = \varkappa[(e_1 - \alpha) n_1, (e_2 - \alpha) n_2, (e_3 - \alpha) n_3] \\ \alpha &= \underline{n}\cdot\underline{E}\cdot\underline{n} = e_1 n_1^2 + e_2 n_2^2 + e_3 n_3^2 \end{aligned} \tag{3.5}$$

Additional expressions for $\underline{f}_n$ and $\underline{f}_t$ are given by

$$\left.\begin{aligned} &\underline{f}_n = \frac{\zeta}{2} \sum_{i=1}^{3} \underline{n}\, e_i \cos 2\theta_i,\quad \underline{f}_t = \frac{\varkappa}{2} \sum_{i=1}^{3} \underline{\theta}_i e_i \sin 2\theta_i \\ &\text{where}\quad \underline{\theta}_1 = (\sin\theta_1, -\cot\theta_1 \cos\theta_2, -\cot\theta_1 \cos\theta_3) \\ &\qquad\ \underline{\theta}_2 = (-\cot\theta_2 \cos\theta_1, \sin\theta_2, -\cot\theta_2 \cos\theta_3) \\ &\qquad\ \underline{\theta}_3 = (-\cot\theta_3 \cos\theta_1, -\cot\theta_3 \cos\theta_2, \sin\theta_3)\quad . \end{aligned}\right\} \tag{3.6}$$

The $\underline{\theta}_i$ $(i = 1,2,3)$ are unit vectors tangent to the unit sphere at the point Q determined by the unit vector $\underline{n}$. They each lie in a plane containing one principal strain axis and the vector $\underline{n}$, and they are directed away from the point Q. Equivalence of the two expressions for $\underline{f}_n$ and $\underline{f}_t$ can be shown by substitution.

We now prove that the <u>overall force and torque</u> vanish as required by equations (2.2). Equation $(3.5)_1$ for the elemental stress vectors is used, which is equivalent to equation (3.3) expressed in principal strain coordinates. Introducing spherical coordinates $n_1 = \cos\theta$, $n_2 = \sin\theta\cos\phi$, $n_3 = \sin\theta\sin\phi$, as shown in Figure 2, and imposing the integration limits $0 \le \phi \le 2\pi$, $0 \le \theta \le \pi$, we obtain

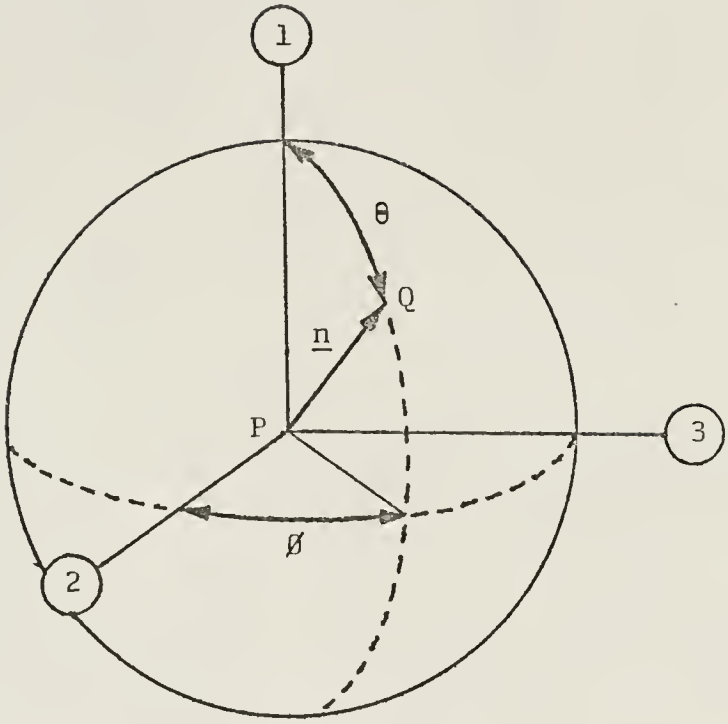

FIGURE 2. SPHERICAL COORDINATES

$$F_1 = \int d\phi \int d\theta \sin\theta\,(f_1)$$

$$= e_1 \int d\phi \int d\theta \sin\theta \cos\theta\,(\kappa + \eta\cos^2\theta)$$

$$+ \eta \int d\phi \int d\theta \sin^3\theta \cos\theta\,(c_2\cos^2\phi + e_3\sin^2\phi)$$

$$= e_1[\phi]_0^{2\pi}\left[\kappa(\tfrac{1}{2}\sin^2\theta) + \eta(-\tfrac{1}{4}\cos^4\theta)\right]_0^{\pi}$$

$$+ \eta[\tfrac{1}{2}(e_2+e_3)\phi + \tfrac{1}{4}(e_2-e_3)\sin 2\phi]_0^{2\pi}\left[\tfrac{1}{4}\sin^4\theta\right]_0^{\pi} = 0$$

$$M_1 = \int d\phi \int d\theta \sin\theta\,(f_3\cos\theta_2 - f_2\cos\theta_3)$$

$$= \kappa(e_3 - e_2)\int d\phi \int d\theta \sin^3\theta \sin\phi\cos\phi$$

$$= \kappa(e_3 - e_2)[\tfrac{1}{2}\sin^2\phi]_0^{2\pi}\left[-\frac{\cos\theta}{3}(2+\sin^2\theta)\right]_0^{\pi} = 0 \quad .$$

Proof that the vector equations (2.2), namely $\underline{F} = \underline{M} = 0$, are valid can be completed by repeating the integrations for the other two axes. A simpler proof is obtained by symmetry, since we can simply permute the indices without affecting the above results.

We now compute the <u>resultant stress vectors</u> with respect to the coordinates along the principal strain axes, using the definition (2.3). We start with the vector $\underline{t}_1 = (t_{11}, t_{21}, t_{31})$ corresponding to the e_1-axis, and again we use the relations $n_1 = \cos\theta$, $n_2 = \sin\theta\cos\phi$, $n_3 = \sin\theta\sin\phi$. This time the integration limits are $0 \le \phi \le 2\pi$, $0 \le \theta \le \pi/2$.

$$t_{11} = \frac{1}{\pi}\int d\phi \int d\theta \sin\theta\,(f_1)$$

$$= \frac{e_1}{\pi}[\phi]_0^{2\pi}\left[\kappa(\tfrac{1}{2}\sin^2\theta) + \eta(-\tfrac{1}{4}\cos^4\theta)\right]_0^{\pi/2}$$

$$+ \frac{\eta}{\pi}[\tfrac{1}{2}(e_2+e_3)\phi + \tfrac{1}{4}(e_2-e_3)\sin 2\phi]_0^{2\pi}\left[\tfrac{1}{4}\sin^4\theta\right]_0^{\pi/2}$$

$$= e_1(\kappa + \tfrac{\eta}{2}) + \tfrac{\eta}{4}(e_2+e_3) = (\kappa + \tfrac{\eta}{4})e_1 = \mu e_1$$

$$t_{21} = \frac{1}{\pi}\int d\phi \int d\theta \sin\theta\,(f_2)$$

$$= \frac{e_2}{\pi}\int d\phi \int d\theta \sin^2\theta\cos\phi\,(\varkappa + \eta\sin^2\theta\cos^2\phi)$$

$$+ \frac{\eta}{\pi}\int d\phi \int d\theta \sin^2\theta\cos\phi\,(e_1\cos^2\theta + e_3\sin^2\theta\sin^2\phi) = 0$$

$$t_{31} = \frac{1}{\pi}\int d\phi \int d\theta \sin\theta\,(f_3)$$

$$= \frac{e_3}{\pi}\int d\phi \int d\theta \sin^2\theta\sin\phi\,(\varkappa + \eta\sin^2\theta\sin^2\phi)$$

$$+ \frac{\eta}{\pi}\int d\phi \int d\theta \sin^2\theta\sin\phi\,(e_1\cos^2\theta + e_2\sin^2\theta\cos^2\phi) = 0$$

The remaining expressions for the resultant stresses can be obtained simply by a permutation of indices.

$$\underline{t}_2 = (t_{12}, t_{22}, t_{32}) = (0, \mu e_2, 0)$$

$$\underline{t}_3 = (t_{13}, t_{23}, t_{33}) = (0, 0, \mu e_3)$$

Following the procedure of Chapter II, we can write the above results in matrix form.

$$T = \begin{bmatrix} t_{11} & t_{12} & t_{13} \\ t_{21} & t_{22} & t_{23} \\ t_{31} & t_{32} & t_{33} \end{bmatrix} = \mu \begin{bmatrix} e_1 & 0 & 0 \\ 0 & e_2 & 0 \\ 0 & 0 & e_3 \end{bmatrix} \tag{3.7}$$

The norm M defined by equation (2.5) vanishes for the matrix T when computed relative to the coordinate system used here. Hence, by definition, the axes of this coordinate system are the principal stress axes and by equation (2.7) the quantities $s_i = t_{ii}$ (no summation) are the principal deviator stresses. These quantities determine a deviator stress tensor $\underline{S} = [s_{ij}]$ which, because of equation (3.7), is related to the deviator strain tensor $\underline{E} = [e_{ij}]$ by the classical elasticity equation

$$\underline{S} = \mu \underline{E} \quad . \tag{3.8}$$

Note that the principal axes of stress and strain coincide, a result that is true in general if and only if the material behavior is isotropic elasticity. Obviously, the definitions $(3.2)_{1,2}$ of the constants $\varkappa, \eta$ were chosen so that the present results, equations (3.7) and (3.8), would emerge.

Equation (3.7) is valid only for resultant stresses computed relative to the principal strain coordinates. It is important in the present theory to know how the resultant stress vectors transform during a change of coordinates. Consider an arbitrary Cartesian coordinate system, related to the principal strain coordinates through an arbitrary orthogonal transformation. Equation (3.3) can be written in component form as

$$\begin{aligned} f_i &= \varkappa \sum_{j=1}^{3} e_{ij} n_j + \eta \alpha n_i, \quad (i = 1,2,3) \\ \alpha &= \sum_{j=1}^{3} \sum_{k=1}^{3} e_{jk} n_j n_k \quad . \end{aligned} \tag{3.9}$$

Introducing spherical coordinates $n_1 = \cos\theta$, $n_2 = \sin\theta\cos\phi$, $n_3 = \sin\theta\sin\phi$, we can rewrite equations (3.9) as

$$\begin{aligned} f_1 &= (\varkappa e_{11} + \eta\alpha)\cos\theta + \varkappa(e_{12}\cos\phi + e_{13}\sin\phi)\sin\theta \\ f_2 &= (\varkappa e_{22} + \eta\alpha)\sin\theta\cos\phi + \varkappa(e_{21}\cos\theta + e_{23}\sin\theta\sin\phi) \\ f_3 &= (\varkappa e_{33} + \eta\alpha)\sin\theta\sin\phi + \varkappa(e_{31}\cos\theta + e_{32}\sin\theta\cos\phi) \\ \alpha &= e_{11}\cos^2\theta + e_{22}\sin^2\theta\cos^2\phi + e_{33}\sin^2\theta\sin^2\phi \\ &\quad + e_{23}\sin^2\theta\sin 2\phi + e_{31}\sin 2\theta\sin\phi + e_{12}\sin 2\theta\cos\phi \quad . \end{aligned} \tag{3.10}$$

After a lengthy evaluation of integrals having the limits $0 \le \phi \le 2\pi$, $0 \le \theta \le \pi/2$, we obtain components of the resultant stress vector $\underline{t}_1 = (t_{11}, t_{21}, t_{31})$ in the new coordinate system as follows:

$$t_{11} = \frac{1}{\pi}\int d\phi \int d\theta \sin\theta\,(f_1) = (\varkappa + \tfrac{1}{4}\eta)e_{11} = \mu e_{11}$$

$$t_{21} = \frac{1}{\pi}\int d\phi \int d\theta \sin\theta\,(f_2) = (\varkappa + \tfrac{1}{2}\eta)e_{21} = \xi e_{21}$$

$$t_{31} = \frac{1}{\pi}\int d\phi \int d\theta \sin\theta\,(f_3) = (\varkappa + \tfrac{1}{2}\eta)e_{31} = \xi e_{31}$$

where $\xi = 2\mu/(3 - \lambda)$. By repeating the integrations with respect to the other two coordinate axes, or simply by permuting the indices, we find

$$\underline{t}_2 = (t_{12}, t_{22}, t_{32}) = (\xi e_{12}, \mu e_{22}, \xi e_{32})$$

$$\underline{t}_3 = (t_{13}, t_{23}, t_{33}) = (\xi e_{13}, \xi e_{23}, \mu e_{33}) \quad .$$

The matrix form

$$T = \begin{bmatrix} t_{11} & t_{12} & t_{13} \\ t_{21} & t_{22} & t_{23} \\ t_{31} & t_{32} & t_{33} \end{bmatrix} = \begin{bmatrix} \mu e_{11} & \xi e_{12} & \xi e_{13} \\ \xi e_{21} & \mu e_{22} & \xi e_{23} \\ \xi e_{31} & \xi e_{32} & \mu e_{33} \end{bmatrix} \tag{3.11}$$

shows that the resultant stress T is linearly related to the strain $\underline{E}$, but that in general the relationship is not tensorial. The exception occurs when $\lambda = 1$, giving simply $T = \mu\underline{E}$. Since strain transforms as a tensor, it follows that in general the resultant stress T does not.

The relationship between the stress and strain tensors and the resultant stress matrix $T = [t_{ij}]$ as computed from equations (2.3) and (3.3) will now be made definite. Let

$\underline{S} = [s_{ij}]$ and $\underline{E} = [e_{ij}]$ be the deviator stress and strain tensors, related here by equation (3.8). If primed and unprimed quantities refer to two different Cartesian coordinate systems, then we have the following transformation equations:

$$e_{ij} = \sum_{k=1}^{3} \sum_{\ell=1}^{3} a_{ik} a_{j\ell} e'_{k\ell} = s_{ij}/\mu = t_{ij}/\gamma_{ij}$$

$$e'_{ij} = \sum_{k=1}^{3} \sum_{\ell=1}^{3} a_{ki} a_{\ell j} e_{k\ell} = s'_{ij}/\mu = t'_{ij}/\gamma_{ij} \qquad (3.12)$$

$$\gamma_{ij} = [\mu \text{ if } i = j \text{ or } \xi = 2\mu/(3 - \lambda) \text{ if } i \neq j] \quad .$$

Here $A = [a_{ij}]$ is an arbitrary rotation matrix, the elements of which obey the orthogonality conditions [67, p. 27].

$$\sum_{k=1}^{3} a_{ik} a_{jk} = \sum_{k=1}^{3} a_{ki} a_{kj} = \delta_{ij} = \begin{cases} 1 \text{ if } i = j \\ 0 \text{ if } i \neq j \end{cases}$$

Although the resultant stress matrix T does not transform as a tensor, we can always construct the deviator stress tensor $\underline{S}$ by first finding the principal axes of T, which are identical to the principal stress axes. Then the elements of $\underline{S}$ can be determined from the elements of T by equation (2.7). The procedure of Chapter II can be rephrased as an eigenvalue problem. Thus, the principal stress axes $\underline{N}_\alpha$ can be found by solving the equation (if a solution exists)

$$\sum_{i=1}^{3} (t_{ij} + t_{ji} - 2\delta_{ij} t_\alpha) N_{i\alpha} = 0, \quad (j, \alpha = 1,2,3) \qquad (3.13)$$

and the eigenvalues t_α are related to the principal deviator stresses s_α by the equations

$$s_\alpha = t_\alpha - (t_1 + t_2 + t_3)/3, \quad (\alpha = 1,2,3) \quad . \qquad (3.14)$$

In solving equation (3.13) it must be recognized that, in general, as for example when plasticity is involved, T is nonsymmetric and $T(\underline{N}_\alpha)$ is a nonlinear function. The fact that $T(\underline{N}_\alpha)$ can be nonlinear requires, in general, an iteration procedure for calculating $\underline{N}_\alpha$, involving solution of a sequence of linear eigenvalue problems of the form (3.13). This topic will be resumed in Chapter VII.

There may exist definitions of the elemental stress vector $\underline{f}$ other than the one proposed by equation (3.3) which would satisfy the equilibrium requirements $\underline{F} = \underline{M} = 0$, and also predict linear elasticity. For example, one could imagine the elemental stress vectors for a cubic lattice, or some other structured lattice, as being zero in all directions except the principal lattice directions. The vectors $\underline{f}$ in these lattice directions, for a given nonzero deformation, would be defined so as to make the resultant stresses finite. Such theories, which may or may not be isotropic, would involve complicated expressions for the elemental vectors and the resultant stresses. In contrast the present theory, based on equation (3.3), involves only simple trigonometric functions. Moreover, studies have shown [60, p. 5] that various microstructural theories of a given class generally lead to the same macroscopic results. Accordingly, the present investigation is restricted to equation (3.3) and to one generalization of equation (3.3) that involves plasticity.

CHAPTER IV

A CLASS OF ELEMENTAL STRESS VECTORS FOR PREDICTING ELASTIC-PLASTIC MATERIAL BEHAVIOR

Plasticity is now introduced into the theory by limiting in a special way the magnitudes of the elemental stress vectors on the unit sphere. Recall the definition of $\underline{f}$ adopted in Chapter III which predicts linear elasticity, namely

$$\underline{f} = \varkappa\, \underline{E}\cdot\underline{n} + \eta(\underline{n}\cdot\underline{E}\cdot\underline{n})\,\underline{n} \qquad (3.3)$$

$$\varkappa = \mu\left(\frac{4-2\lambda}{3-\lambda}\right), \quad \eta = \mu\left(\frac{4\lambda-4}{3-\lambda}\right) \qquad (3.2)_{1,2} \quad .$$

Here $\underline{E}=[e_{ij}]$ is the deviator strain tensor, $\underline{n}$ is a general unit vector, and $\varkappa,\eta$ are elasticity constants.

For plasticity, the elemental stress vectors are not uniquely related to the strain, as in equation (3.3), but are determined by the (time independent) strain history. The deviator strain history $\underline{E}^{(m)}$ at a material point can be defined by a sequence of strain increments $d\underline{E}^{(m)}$; thus

$$\underline{E}^{(0)} = 0, \quad \underline{E}^{(m)} = \underline{E}^{(m-1)} + d\underline{E}^{(m)}, \quad m = 1,2,\ldots,M \quad . \qquad (4.1)$$

This discrete representation of the strain history facilitates computations on a digital computer, as we shall see later. The limit of a continuously varying strain history can be approached by letting each increment $d\underline{E}^{(m)}$ become very

small and at the same time letting the end-point integer M become very large.

The most reasonable assumption regarding plasticity is to limit the magnitude of the tangential (shear) component $\underline{f}_t$ of the elemental stress vector $\underline{f}$. This is in keeping with the physical assumption that plasticity is a phenomenon involving shear stress and unaffected by uniform pressure [68]. Accordingly, equation (3.3) can be generalized to include plasticity as follows:

$$\underline{f}^{(0)} = 0, \quad \underline{f}^{(m)} = \bar{g}\begin{Bmatrix} 1 & \text{if } g_t \le Y \\ Y/g_t & \text{if } g_t > Y \end{Bmatrix}, \quad m = 1,2,3,\ldots$$
$$\bar{g} = \underline{f}^{(m-1)} + \chi\, d\underline{E}^{(m)}\cdot\underline{n} + \eta\, \underline{n}(\underline{n}\cdot d\underline{E}^{(m)}\cdot\underline{n}), \quad g_t = [\bar{g}\cdot\bar{g} - (\bar{g}\cdot\underline{n})^2]^{\frac{1}{2}} \tag{4.2}$$

where Y is a characteristic yield stress. Equations (4.2) represent a procedure of repeatedly calculating a vector $\bar{g}$ and then the magnitude g_t of its tangential component and then the elemental stress vector $\underline{f}^{(m)}$ corresponding to a given deviator strain increment $d\underline{E}^{(m)}$. The initial condition $\underline{f}^{(0)} = 0$ implies that the material initially is in an isotropic annealed condition.

Equations (4.2) yield a solution for $\underline{f}^{(m)}$ in terms of the deviator strain $\underline{E}^{(m)}$ only in the case of a radial loading. Then $d\underline{E}^{(m)}$ and $\underline{E}^{(m)}$ are proportional: $d\underline{E}^{(m)} = c_m d\underline{E}$; $\underline{E}^{(m)} = (c_1 + \ldots + c_m)\, d\underline{E}$. Substituting this result into equations (4.2) we find for radial loading

$$\underline{f}^{(m)} = \bar{g}\begin{Bmatrix} 1 & \text{if } g_t \le Y \\ Y/g_t & \text{if } g_t > Y \end{Bmatrix}$$
$$\bar{g} = \chi\, \underline{E}^{(m)}\cdot\underline{n} + \eta\, \underline{n}(\underline{n}\cdot\underline{E}^{(m)}\cdot\underline{n}), \quad g_t = [\bar{g}\cdot\bar{g} - (\bar{g}\cdot\underline{n})^2]^{\frac{1}{2}} \tag{4.3}$$

Since $\bar{g}$ is computed elastically in terms of the (total) strain $\underline{E}^{(m)}$ and then truncated to yield $\underline{f}^{(m)}$, equations (4.3) represent what is called a total-deformation type theory. Such a theory is valid for radial loadings and approximately valid for near-radial loadings, but it certainly would not predict reasonable results for loading paths that include stress reversals [1, p. 47].

The above definition of $\underline{f}^{(m)}$ could perhaps have been stated with greater mathematical elegance in terms of time derivatives and/or the strain invariants. However, the form presented here is most easily adapted to computer programming. Hence, I have adopted equations (4.2), and in the case of radial loadings equations (4.3), as the basic definitions of $\underline{f}$ to be used throughout the remainder of this work.

Equations (4.2) represent a procedure of computing and then truncating those elemental stress vectors that exceed a certain yield condition. The proposed yield condition tests the magnitude f_t of the tangential component of the elemental stress vector against a characteristic yield stress Y, which is assumed constant for all elemental vectors and all time. The present theory is essentially an incremental-type theory in which each elemental vector obeys the same elastic-perfectly-plastic law. The proposed yield condition predicts an initial yield condition of the Tresca type when expressed in terms of stress or strain, as we shall demonstrate below.

To find the initial yield condition, we assume residual stresses and strains are zero initially, so that the material behaves elastically as discussed in Chapter III. Then we consider those states of stress or strain for which the maximum value of f_t on the unit sphere is equal to Y, the characteristic yield stress. Symbolically

$$\max_{(\text{sphere})} \; [f_t(e^*_{ij})] = Y \tag{4.4}$$

where e^*_{ij} represents a point on the initial yield surface in strain space. In terms of coordinates along the principal strain axes, we can write the tangential component of $\underline{f}$ as

$$\begin{aligned} \underline{f}_t &= \varkappa[(e_1 - \alpha)n_1,\ (e_2 - \alpha)n_2,\ (e_3 - \alpha)n_3] \\ f_t &= (\underline{f}_t \cdot \underline{f}_t)^{\frac{1}{2}} = \varkappa[\sum_{i=1}^{3} e_i^2 n_i^2 - \alpha^2]^{\frac{1}{2}} \\ \alpha &= e_1 n_1^2 + e_2 n_2^2 + e_3 n_3^2 \quad . \end{aligned} \tag{4.5}$$

Let us first investigate the yield condition for the special cases of pure shear and axial strain, whereby $e_2 = -e_1$, $e_3 = 0$, and $e_2 = e_3 = -e_1/2$, respectively. In the case of pure shear

$$\alpha = e_1(n_1^2 - n_2^2), \quad f_t = \varkappa e_1[n_1^2 + n_2^2 - (n_1^2 - n_2^2)^2]^{\frac{1}{2}} \quad .$$

In the case of axial strain

$$\alpha = \tfrac{1}{2} e_1(3n_1^2 - 1), \quad f_t = \tfrac{3}{2}\varkappa e_1 n_1(1 - n_1^2)^{\frac{1}{2}} \quad .$$

For both cases, the maximum value of f_t occurs when $\underline{n} = (\sqrt{\tfrac{1}{2}}, \sqrt{\tfrac{1}{2}}, 0)$, as proved below. Let e_k, e_y denote the deviator yield strains for pure-shear and axial-strain

loadings, respectively, and let $s_k = \mu e_k$, $s_y = \mu e_y$ denote the corresponding deviator yield stresses. That is, at yield $e_k = e_1 = -e_2$, $e_3 = 0$ for a pure-shear loading, and $e_y = e_1 = -2e_2 = -2e_3$ for an axial-strain loading. Invoking equation (4.4) and the above expressions for f_t, we obtain the following equivalence relations among the various measures of yielding:

$$e_k = \frac{3}{4} e_y = \frac{Y}{\varkappa}, \quad s_k = \frac{3}{4} s_y = \frac{\mu Y}{\varkappa} = \left(\frac{3 - \lambda}{2 - \lambda}\right) \frac{Y}{2} \quad . \tag{4.6}$$

We now investigate the yield condition for arbitrary strain conditions. Introducing spherical coordinates $n_1 = \cos\theta$, $n_2 = \sin\theta\cos\phi$, $n_3 = \sin\theta\sin\phi$, we can rewrite equations (4.4) and $(4.5)_2$ as

$$\max_{\theta,\phi} [f_t(\theta, \phi)/\varkappa] = e_k, \text{ where}$$

$$f_t/\varkappa = (e_1^2 \cos^2\theta + e_2^2 \sin^2\theta \cos^2\phi + e_3^2 \sin^2\theta \sin^2\phi - \alpha^2)^{\frac{1}{2}} \tag{4.7}$$

$$= \begin{bmatrix} (e_1 - 2e_2\cos^2\phi - 2e_3\sin^2\phi) e_1 \cos^2\theta - e_2 e_3 \sin^2\theta \sin^2 2\phi \\ + (1 - \sin^2\theta \cos^2\phi) e_2^2 \cos^2\phi + (1 - \sin^2\theta \sin^2\phi) e_3^2 \sin^2\phi \end{bmatrix}^{\frac{1}{2}} \sin\theta \ .$$

Let us now seek the maximum values of the function $f_t(\theta,\phi)$, where the range of variables is $0 \le \theta \le \pi$, $0 \le \phi \le 2\pi$. Note that $f_t = 0$ when $\theta = 0$ and $\theta = \pi$ because of the multiplicand "sin θ." But f_t in general is nonzero. Hence $\max(f_t)$ must occur in the restricted range $0 < \theta < \pi$. Necessary conditions for $\max(f_t)$ to occur at a given point (θ,ϕ) are $\partial f_t/\partial\theta = \partial f_t/\partial\phi = 0$. Thus

$$0 = \frac{\partial}{\partial\theta}(f_t/\kappa)^2 = (A - B\cos^2\phi - C\sin^2\phi)\sin 2\theta$$

$$0 = \frac{\partial}{\partial\phi}(f_t/\kappa)^2 = (B - C)\sin^2\theta \sin 2\phi$$

where $A = (2\alpha - e_1)e_1$, $B = (2\alpha - e_2)e_2$, $C = (2\alpha - e_3)e_3$.

Suppose $0 < \theta < \pi$, so that $\sin\theta \neq 0$. Then

$$(A - B\cos^2\phi - C\sin^2\phi)\cos\theta = 0, \quad (B - C)\sin 2\phi = 0 .$$

The first equation is satisfied if $\theta = \pi/2$, so that $\cos\theta = 0$. In this case, the second equation becomes

$$2(B - C)\sin 2\phi = (e_2 - e_3)^2 \sin 4\phi = 0$$

since $B - C = (2\alpha e_2 - e_2^2) - (2\alpha e_3 - e_3^2) = (e_2 - e_3)^2\cos 2\phi$.

In general, $e_2 \neq e_3$, which implies $\sin 4\phi = 0$. Thus ϕ must have at least one of the values $\phi = n\pi/4$ where $n = 0,1,2,\ldots,8$. Plugging these values into the expression $(4.7)_3$ we find

$$f_t/\kappa = \text{abs}\,(e_2 - e_3)\sin\phi\cos\phi$$

$$= \begin{cases} 0 \text{ if } \phi = 0,\ \pi/2,\ \pi,\ 3\pi/2,\ 2\pi \\ \tfrac{1}{2}\,\text{abs}\,(e_2 - e_3) \text{ if } \phi = \pi/4,\ 3\pi/4,\ 5\pi/4,\ 7\pi/4 \end{cases} .$$

The initial yield condition in this case is

$$e_k = \max_{\theta,\phi}(f_t/\kappa) = \tfrac{1}{2}\,\text{abs}\,(e_2 - e_3)$$

provided the maximum value of f_t occurs at the points $\theta = \pi/2$, $\phi = n\pi/4$ with $n = 1,3,5,7$. Continuing in this manner, or simply permuting indices, we find the following equation which we recognize as the Tresca yield condition.

$$e_k = \tfrac{1}{2}\max(|e_2 - e_3|, |e_3 - e_1|, |e_1 - e_2|) \qquad (4.8)$$

This equation states that yield first occurs when the maximum shear strain (or stress) reaches a critical value.

The directions corresponding to each segment of equation (4.8) can be specified by unit vectors as follows:

$$\begin{aligned} e_k = \tfrac{1}{2}|e_1 - e_2| : \quad & \underline{n} = \sqrt{\tfrac{1}{2}}\ (\pm 1,\ \pm 1,\ 0) \\ e_k = \tfrac{1}{2}|e_2 - e_3| : \quad & \underline{n} = \sqrt{\tfrac{1}{2}}\ (0,\ \pm 1,\ \pm 1) \\ e_k = \tfrac{1}{2}|e_3 - e_1| : \quad & \underline{n} = \sqrt{\tfrac{1}{2}}\ (\pm 1,\ 0,\ \pm 1) \quad . \end{aligned} \tag{4.9}$$

These unit vectors $\underline{n}$ indicate the points on the unit sphere at which yielding first occurs. If the principal strains have distinct values, then only one line of the expressions (4.9) can be valid at any one time. Suppose the first line is valid, which was true for the case of pure shear analyzed previously, and suppose the deformation is continued beyond initial yield. Then there will develop four regions on the unit sphere surrounding the four points $\underline{n} = \sqrt{\tfrac{1}{2}}\ (\pm 1,\ \pm 1,\ 0)$, inside of which the elemental vectors are restricted by the plasticity equation $f_t = Y$. Outside of the four regions $f_t < Y$, and the elasticity equations of Chapter III continue to govern the elemental stress vectors.

In general, the boundary between the elastic and plastic regions on the unit sphere can be very complicated. There is only one situation known to the author in which a closed-form expression for this elastic-plastic boundary exists. If the principal strain axes are fixed in the material and the loading is radial (i.e., the strain magnitudes e_1, e_2, e_3 increase proportionally), then the boundary between the elastic and plastic regions is given by the following equations:

$$e_k^2 = (f_t/\varkappa)^2 = \left(\sum_{i=1}^{3} e_i^2 \cos^2\theta_i\right) - \left(\sum_{i=1}^{3} e_i \cos^2\theta_i\right)^2 \qquad (4.10)$$

or

$$e_k^2 = \left\{\begin{matrix}(e_1 - 2e_2\cos^2\phi - 2e_3\sin^2\phi)\, e_1\cos^2\theta - e_2 e_3 \sin^2\theta \sin^2 2\phi \\ + (1-\sin^2\theta\cos^2\phi)\, e_2^2\cos^2\phi + (1-\sin^2\theta\sin^2\phi)\, e_3^2\sin^2\phi\end{matrix}\right\} \sin^2\theta \ .$$

The complexity of the foregoing equations for the elastic-plastic boundary on the unit sphere — even for the restrictive situation of fixed strain axes and radial loading — obviously limits the number and type of closed-form solutions that may exist for the stresses when plasticity is involved. Two closed-form solutions, obtained for pure axial loading and reversed axial loading, form the subject matter of Chapter V. Other solutions, which do not necessarily involve fixed axes or radial loadings, were obtained numerically via the digital computer and are presented in Chapters VI and VII.

We now prove that if the principal strain axes are forever <u>fixed</u> in the material, then the principal stress axes are also fixed and the two sets of axes coincide. The proof follows from the symmetry of the function $\underline{f}(\underline{n})$ relative to the principal strain axes. Equations (4.3), which are valid for radial loadings, can be expressed in principal strain coordinates as follows:

$$\underline{f} = \bar{g}\, F(g_t/Y), \quad g_t = \varkappa(e_1^2 n_1^2 + e_2^2 n_2^2 + e_3^2 n_3^2 - \alpha^2)^{\frac{1}{2}}$$

$$\bar{g} = \varkappa(e_1 n_1, e_2 n_2, e_3 n_3) + \eta\alpha\underline{n}, \quad \alpha = e_1 n_1^2 + e_2 n_2^2 + e_3 n_3^2 \qquad (4.11)$$

where $F(x) = [1 \text{ if } x \le 1;\ 1/x \text{ if } x > 1]$.

Let us calculate the elemental stress vectors corresponding to the four unit vectors $\underline{n} = (a, \pm b, \pm c)$, where a, b, c are positive constants subject to the restrictions $a^2 + b^2 + c^2 = 1$. Thus

$$\begin{aligned}
\underline{n}_{(1)} &= (a, b, c) : \underline{f}_{(1)} = [\varkappa(e_1 a, e_2 b, e_3 c) + \eta\alpha(a, b, c)] F(g_t/Y) \\
\underline{n}_{(2)} &= (a, -b, c) : \underline{f}_{(2)} = [\varkappa(e_1 a, -e_2 b, e_3 c) + \eta\alpha(a, -b, c)] F(g_t/Y) \\
\underline{n}_{(3)} &= (a, b, -c) : \underline{f}_{(3)} = [\varkappa(e_1 a, e_2 b, -e_3 c) + \eta\alpha(a, b, -c)] F(g_t/Y) \\
\underline{n}_{(4)} &= (a, -b, -c) : \underline{f}_{(4)} = [\varkappa(e_1 a, -e_2 b, -e_3 c) + \eta\alpha(a, -b, -c)] F(g_t/Y)
\end{aligned} \tag{4.12}$$

where $g_t/Y = (e_1^2 a^2 + e_2^2 b^2 + e_3^2 c^2 - \alpha^2)^{\frac{1}{2}}/e_k$.

Consider now the sum of these four elemental vectors

$$\sum_{i=1}^{4} \underline{f}_{(i)} = 4a\,(\varkappa e_1 + \eta\alpha)\, F(g_t/Y)\,(1,0,0) \quad . \tag{4.13}$$

This sum has a nonzero component in the e_1-direction only.

From equation (2.3) we see that the resultant stress vector $\underline{t}_1$ is computed by integrating the differential vector $d\underline{t}_1 = \underline{f}\, dA/\pi$ over the hemisphere defined by $n_1 \geq 0$, where $\underline{n} = (n_1, n_2, n_3)$ is an otherwise arbitrary unit vector. An equivalent vector $\underline{t}_1$ is obtained by integrating the differential vector

$$d\underline{t}_1 = (\underline{f}_{(1)} + \underline{f}_{(2)} + \underline{f}_{(3)} + \underline{f}_{(4)})\, dA/\pi \tag{4.14}$$

where $\underline{f}_{(i)}$ are defined above; here each component $\underline{f}_{(i)}\, dA/\pi$ is integrated over one quadrant of the given hemisphere. By comparing equations (4.13) and (4.14) we conclude that $\underline{t}_1$ has a nonzero component in the e_1-direction only. Similarly, we find that $\underline{t}_2$ points in the e_2-direction and $\underline{t}_3$ points in the e_3-direction. We conclude that for a radial loading

the resultant stress matrix $T = [t_{i\alpha}]$ is diagonal ($t_{i\alpha} = 0$ if $i \neq \alpha$) when computed relative to fixed principal strain axes. Recall that the principal stress axes are identical to the principal axes of the matrix T.

The same conclusion can be reached similarly for the case of fixed principal strain axes and arbitrarily varying strain increments de_1, de_2, de_3. Although I omit details in order to save space, I offer the following outline of this proof: First assume a given distribution $\underline{f}^{(0)}(\underline{n})$ of elemental stress vectors which is symmetric in the sense of equations (4.12). Then introduce an arbitrary strain increment and compute the new elemental stress vectors $\underline{f}^{(1)}(\underline{n})$. Proof follows by observing that the distribution $f^{(1)}(\underline{n})$ is also symmetric in the sense of equations (4.12). The general case in which the principal strain axes rotate relative to the material is too complicated to allow such simple conclusions to be derived.

The following is a discussion of the essential features of the radial element theory as regards computing elastic-plastic stress-strain behavior from equation (4.2). This discussion should help the reader to understand the developments of the theory presented in the next three chapters. Consider a loading and unloading of an initially isotropic material that involves plasticity. Before loading the elemental stress vectors $\underline{f}(\underline{n})$ associated with a given material particle are all zero; here $\underline{n}$ represents the set of unit

vectors pointing in all possible directions. During loading the vectors $\underline{f}(\underline{n})$ vary with the strain according to equations (4.2), and the stress is computed in terms of these $\underline{f}(\underline{n})$ by the procedure of Chapter II. When unloading occurs the stress drops to zero; however, the strain and the set of elemental stress vectors $\underline{f}_0(\underline{n})$ after unloading generally are not zero. This situation is analogous to a beam which, after plastic bending, has a residual curvature and locked-in stresses even when the bending moment is zero. (This beam analogy applies to many parts of the present theory.)

The importance of the residual stress vectors $\underline{f}_0(\underline{n})$ is that, for any fixed material particle and any moment of time, this set of vectors contains all the information about past deformation history sufficient to predict the future mechanical behavior. Suppose we are given a finite increment of strain $\Delta \underline{E}$ along a known strain path. Then knowledge of $\underline{f}_0(\underline{n})$ and $\Delta \underline{E}$ enables us to compute the elemental stress vectors $\underline{f}(\underline{n})$, and hence the stress, corresponding to this new increment of strain. Furthermore, from the set of vectors $\underline{f}_0(\underline{n})$, we are able to compute the entire yield surface at each step of a strain history, as will be demonstrated in Chapter VI.

CHAPTER V

STRESS-STRAIN BEHAVIOR FOR AXIAL LOADING AND REVERSED AXIAL LOADING

Consider a monotonic loading with fixed principal strain axes in which the principal deviator strains are maintained in the constant ratio $e_2 = e_3 = -e_1/2$. This case is called axial strain or axial loading, and includes the common tension and compression tests of a cylindrical specimen. Referring the deviator strain tensor to the principal strain axes, we can define axial loading by the following expressions:

$$\underline{E} = \begin{bmatrix} e & 0 & 0 \\ 0 & -e/2 & 0 \\ 0 & 0 & -e/2 \end{bmatrix}, \qquad \begin{array}{l} e(0) = 0 \text{ and } e(t) \geq 0 \\ \text{or } e(t) \leq 0 \text{ for } t > 0 \end{array} . \tag{5.1}$$

For this case we can use equations (4.3) to compute the elemental stress vectors $\underline{f}$. We begin by computing $\bar{g} = (g_1, g_2, g_3)$.

$$\begin{aligned} \alpha &= \underline{n}\cdot\underline{E}\cdot\underline{n} = e(n_1^2 - n_2^2/2 - n_3^2/2) = \tfrac{1}{2} e(3n_1^2 - 1) \\ g_1 &= (\eta\alpha + \varkappa e)n_1 = \tfrac{1}{2} e\, n_1(3\eta n_1^2 + a) \\ g_2 &= (\eta\alpha - \varkappa e/2)n_2 = \tfrac{1}{2} e\, n_2(3\eta n_1^2 - \zeta) \\ g_3 &= (\eta\alpha - \varkappa e/2)n_3 = \tfrac{1}{2} e\, n_3(3\eta n_1^2 - \zeta) \end{aligned} \tag{5.2}$$

Here $a = 2\varkappa - \eta$ and $\zeta = \varkappa + \eta$. Normal and tangential components of $\bar{g}$ are given by

$$\begin{aligned} \bar{g}_n &= \zeta\, \alpha\, \underline{n} = \tfrac{1}{2}\zeta\, e(3n_1^2 - 1)(n_1, n_2, n_3) \\ \bar{g}_t &= \varkappa(\underline{E}\cdot\underline{n} - \alpha\,\underline{n}) = \tfrac{3}{2}\varkappa\, e[(1 - n_1^2)n_1, -n_1^2 n_2, -n_1^2 n_3] \\ g_t &= (\bar{g}_t \cdot \bar{g}_t)^{\frac{1}{2}} = \tfrac{3}{2}\varkappa\, e\, n_1 (1 - n_1^2)^{\frac{1}{2}} \quad . \end{aligned} \tag{5.3}$$

With these results the expression for $\underline{f}$ becomes

$$\underline{f} = \bar{g}\begin{cases} 1 & \text{if } g_t/Y \le 1 \\ Y/g_t & \text{if } g_t/Y > 1 \end{cases}, \quad \frac{g_t}{Y} = \frac{e}{e_y}\sin 2\theta \tag{5.4}$$

where θ is the spherical coordinate defined by $n_1 = \cos\theta$. We recall from equation (4.6) that $e_y = 4Y/3\varkappa$ is the yield strain for axial loading. For convenience we define three new variables ξ_1, ξ_2, ψ, as follows:

$$\xi_1 = \frac{\pi}{4} - \frac{\psi}{2}, \quad \xi_2 = \frac{\pi}{4} + \frac{\psi}{2}, \quad \cos\psi = \frac{e_y}{e} \quad . \tag{5.5}$$

Then $\underline{f} = \bar{g}\begin{cases} 1 \text{ for } 0 \le \theta \le \xi_1 \text{ or } \xi_2 \le \theta \le \pi - \xi_2 \text{ or } \pi - \xi_1 \le \theta \le \pi \\ \cos\psi/\sin 2\theta \quad \text{for } \xi_1 \le \theta \le \xi_2 \text{ or } \pi - \xi_2 \le \theta \le \pi - \xi_1 \end{cases}$. (5.6)

This situation is illustrated in Figure 3. We see that plasticity develops in two expanding parallel bands on the unit sphere, centered on the circles $\theta = \pi/4$ and $\theta = 3\pi/4$, for the case of axial loading. Resultant stresses are computed as follows:

$$\begin{aligned} t_{11} &= \frac{1}{\pi}\int_0^{2\pi} d\phi \int_0^{\pi/2} d\theta \sin\theta (f_1) \\ &= 2\int_{S_1} d\theta \sin\theta (g_1) + \cos\psi \int_{S_2} d\theta \sec\theta (g_1) \\ &= e\left[3\eta\left(-\frac{\cos^4\theta}{4}\right) + a\left(\frac{\sin^2\theta}{2}\right)\right]_{S_1} + \frac{e_y}{2}\left[3\eta\left(\frac{2\theta - \sin 2\theta}{4}\right) + a\theta\right]_{S_2} \\ &= \mu(e + e_y\psi - e\sin\psi) = s_y(\psi - \tan\psi + \sec\psi) \end{aligned} \tag{5.7}$$

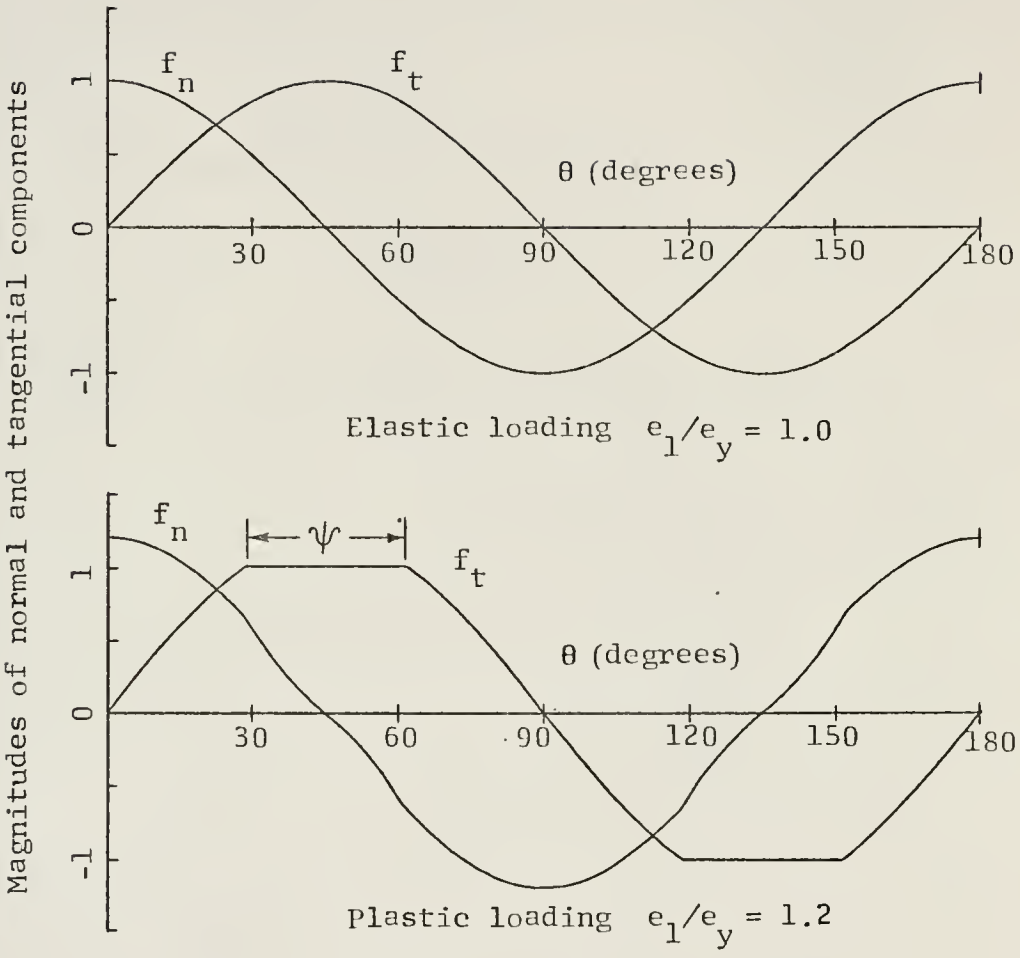

FIGURE 3. DISTRIBUTION OF ELEMENTAL STRESS VECTORS FOR AXIAL LOADING FROM AN INITIALLY ISOTROPIC STATE

$$t_{22} = \frac{1}{\pi}\int_{-\pi/2}^{\pi/2} d\phi \int_{o}^{\pi} d\theta \sin\theta (f_2)$$

$$= \frac{2}{\pi}\int_{S_o} d\phi \int_{S_1} d\theta \sin\theta (g_2) + \frac{\cos\psi}{\pi}\int_{S_o} d\phi \int_{S_2} d\theta \sec\theta (g_2) \qquad (5.8)$$

$$= \frac{2e}{\pi}\left[3\eta\left(\frac{4\theta - \sin 4\theta}{32}\right) - \zeta\left(\frac{2\theta - \sin 2\theta}{4}\right)\right]_{S_1} + \frac{e_y}{\pi}\left[3\eta\left(\frac{\sin^2\theta}{2}\right) + \zeta \log(\cos\theta)\right]_{S_2}$$

$$= -\frac{s_y}{\pi}\left[\left(\frac{\pi}{2} - \psi\right)\sec\psi + \left(\frac{3-3\lambda}{3-\lambda}\right)\sin\psi + \left(\frac{2\lambda}{3-\lambda}\right)(\log\cos\xi_1 - \log\cos\xi_2)\right] .$$

The integration limits in equations (5.7) and (5.8) are given in set theory notation as

$$S_o = \left(-\frac{\pi}{2}, \frac{\pi}{2}\right), \quad S_1 = \left((0,\theta_1),(\theta_2,\frac{\pi}{2})\right), \quad S_2 = (\theta_1, \theta_2) .$$

Here we have used identities such as

$$\sin^2\xi_1 = \cos^2\xi_2 = \tfrac{1}{2}(1 - \sin\psi), \quad \sin 2\xi_1 = \sin 2\xi_2 = \cos\psi$$
$$\sin^2\xi_2 = \cos^2\xi_1 = \tfrac{1}{2}(1 + \sin\psi), \quad \cos 2\xi_1 = -\cos 2\xi_2 = \sin\psi .$$

By symmetry considerations we find

$$t_{33} = t_{22}, \quad t_{23} = t_{32} = t_{31} = t_{13} = t_{12} = t_{21} = 0 .$$

The principal stress axes coincide with the principal strain axes, and so we can use equation (2.7) or equation (3.14) to solve for the components of the deviator stress tensor. Letting $p = -(t_{11} + t_{22} + t_{33})/3$ and $L = \log\cos\xi_1 - \log\cos\xi_2$, we obtain

$$p = -\frac{s_y}{3}\left[\psi - \tan\psi + \frac{2\psi}{\pi}\sec\psi - \frac{6}{\pi}\left(\frac{1-\lambda}{3-\lambda}\right)\sin\psi - \frac{4L}{\pi}\left(\frac{\lambda}{3-\lambda}\right)\right]$$

$$\left.\begin{aligned} s_1 = -2s_2 = -2s_3 = s_y\Big[&\frac{2}{3}(\psi - \tan\psi) + \left(1 - \frac{2\psi}{3\pi}\right)\sec\psi \\ &+ \frac{2}{\pi}\left(\frac{1-\lambda}{3-\lambda}\right)\sin\psi + \frac{4L}{3\pi}\left(\frac{\lambda}{3-\lambda}\right)\Big] \end{aligned}\right\} \qquad (5.9)$$

where $s_y = \mu e_y = Y(\frac{1-\lambda/3}{1-\lambda/2})$ is the yield stress for axial loading. Equation (5.9) and the following expression for the deviator strains are the desired results for predicting stress-strain behavior in the case of axial loading.

$$e_1 = -2e_2 = -2e_3 = e_y \sec \psi, \quad 0 \leq \psi < \pi/2 \tag{5.10}$$

Figures 4 and 5 show stress-strain curves calculated and plotted for various values of the parameter λ. We see that the slope of the stress-strain curves and the stress relative to yield both increase with increasing values of λ. Hence, we are justified in calling λ a work-hardening parameter. The data of Figure 4 lend support to the suggestion of Chapter III that λ be limited to the range $0 < \lambda < 2$. When $\lambda < 0$ we see that the stress reaches a maximum and then falls with increasing strain. The material is unstable, which is an unrealistic and undesirable material property. Not obvious from Figure 4 but true nonetheless is the fact that the slope ds_1/de_1 is greater than the elastic modulus μ for $\lambda > 2$ and for certain values of the strain. When this occurs, the residual strain becomes negative for a positive loading; here again the material is unstable [69].

The reader is referred to Tables B-1 and B-2 of Appendix B, where stress and strain are tabulated for five values of the work-hardening parameter λ. These tabular values, based on the closed-form solution of equations (5.9) and (5.10), will be compared with the approximate numerical results of Chapter VI, in order to establish the accuracy of the latter. The

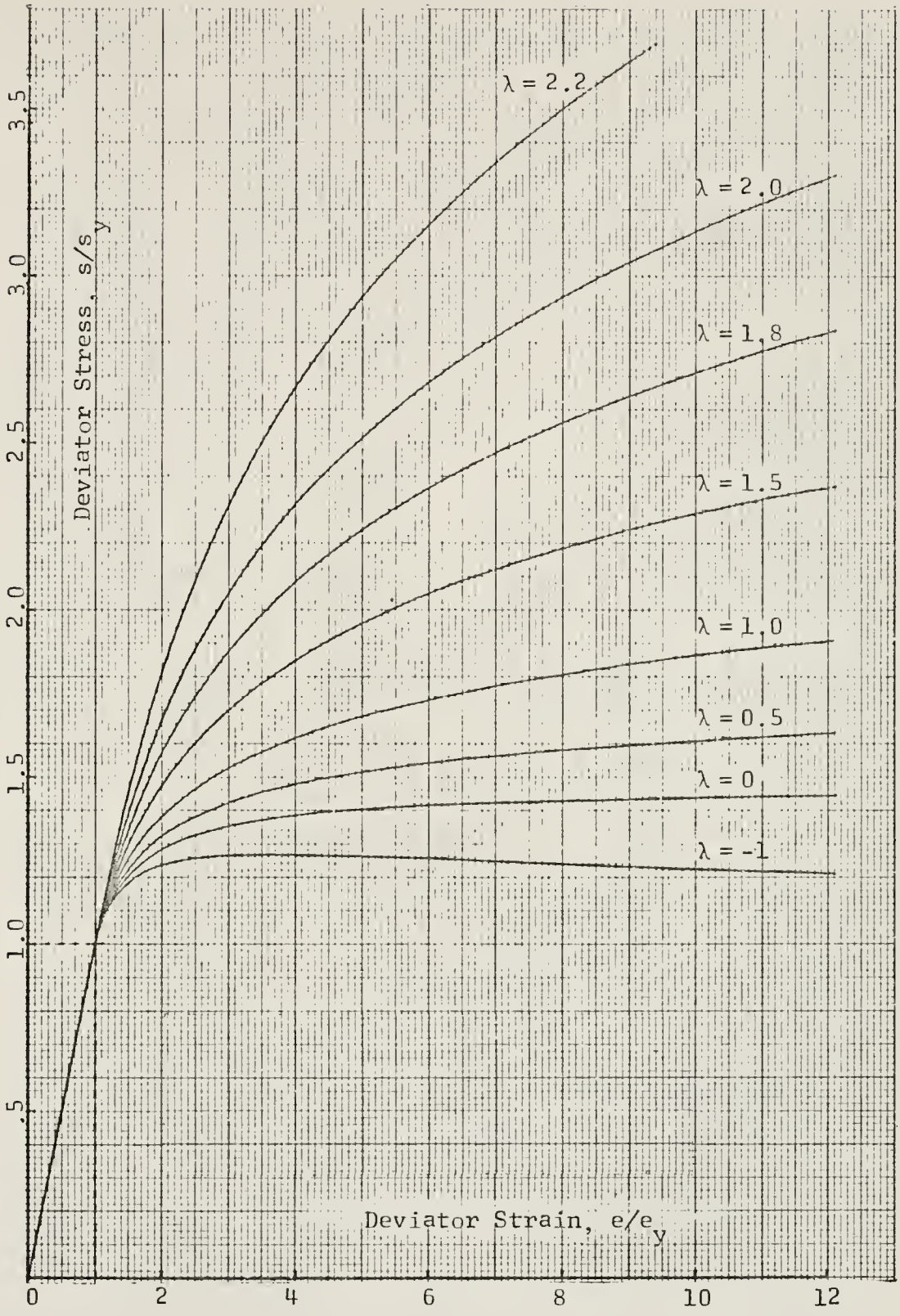

FIGURE 4. STRESS-STRAIN BEHAVIOR FOR AXIAL LOADING, SMALL STRAIN

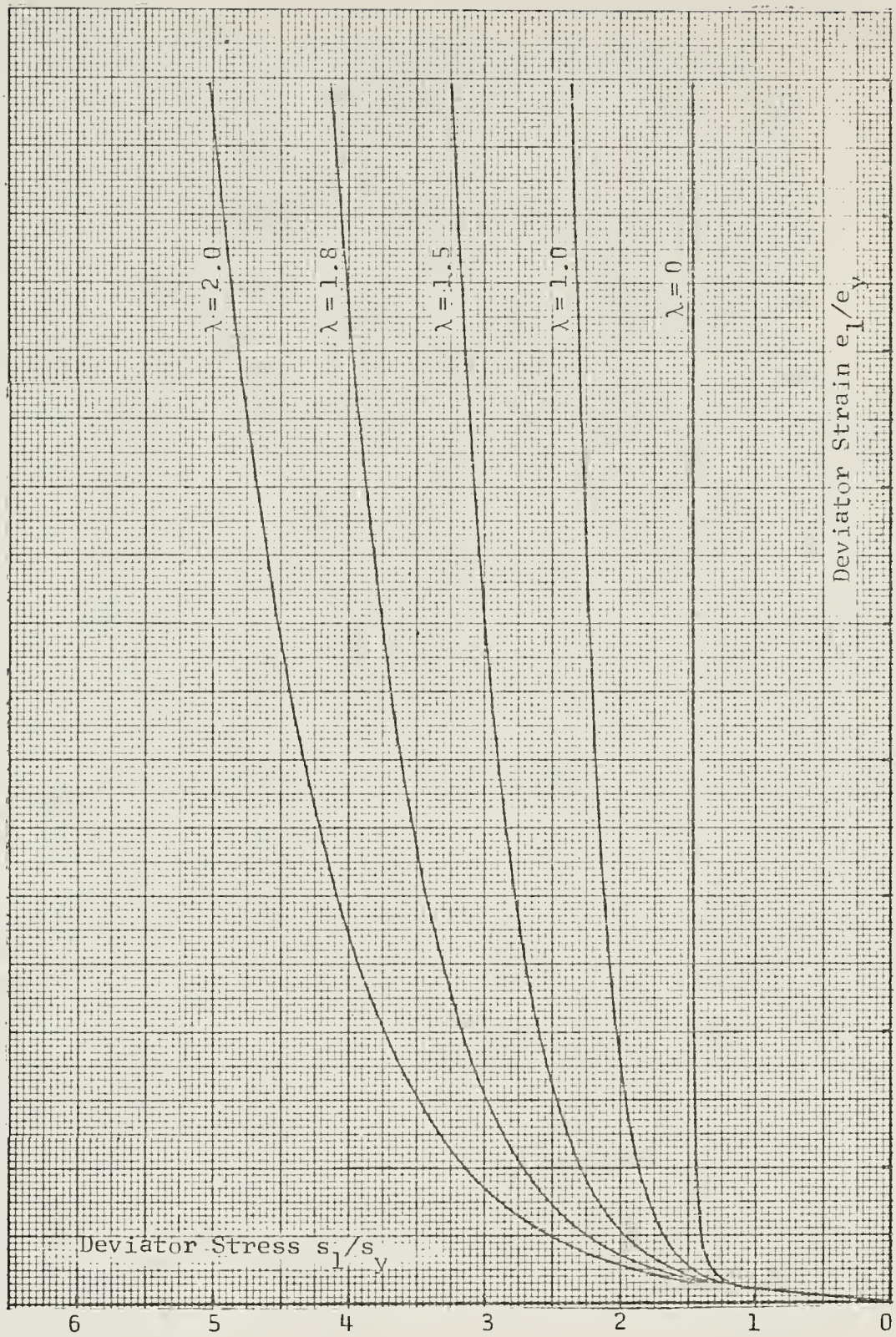

FIGURE 5. STRESS-STRAIN BEHAVIOR FOR AXIAL LOADING. LARGE STRAIN

reader is also referred to Program A-1 of Appendix A, which is the computer program used to generate the data of Figures 4 and 5 and Tables B-1 and B-2. The programming language of Appendix A is BASIC.

The prediction of various stress-strain curves raises the possibility of fitting the present theoretical results with experimental uniaxial test data. Perhaps there are certain metals and certain values of the theoretical parameter λ for which the theory and experiments can be matched reasonably well. The reader is referred to Chapter VIII, where we have attempted to fit the theory with experimental results on commercially pure polycrystalline aluminum. The present theoretical results are expressed in terms of the deviator stresses and strains. In order to make comparisons with experimental data these quantities must be converted to true stresses and strains. The following results, easily obtained and applicable for either uniaxial tension or uniaxial compression, are presented without derivation:

$$\sigma_1 = 3 s_1/2, \quad \sigma_2 = \sigma_3 = 0$$
$$\epsilon_1 = e_1 + s_1/2\beta, \quad \epsilon_2 = \epsilon_3 = -e_1/2 + s_1/2\beta \quad . \tag{5.11}$$

We now investigate the case of <u>reversed axial loading</u>. As before, $\underline{f}(\underline{n})$ has rotational symmetry about the e_1-axis, and so depends only on the spherical coordinate angle θ. Assume a given material body is loaded axially into the plastic range so that the initial stress-strain behavior is

predicted by equations (5.9) and (5.10) derived above. Figure 6a shows the distribution of the elemental stress vectors $\underline{f}$ as a function of the angle θ for one such loading. We observe that plasticity has occurred because the slope of $\underline{f}(\theta)$ is discontinuous. Now superimpose an axial loading of the opposite sense (i.e., with reversed signs) onto the given loading, as shown in Figures 6b through 6d. Figure 6b is approximately the distribution of elementary stress vectors which gives zero resultant stress. Figures 6c and 6d show distributions of the elemental stress vectors after yield has occurred for the reversed loading. Note that Figure 6d is exactly a mirror image of Figure 6a. If the material were loaded cyclically between equal tensile and compressive limits, then the elemental stress vectors would alternate indefinitely between two mirror image distributions.

In view of the behavior of the function $\underline{f}(\theta)$ shown in Figure 6 and described above, only two additional parameters are needed to describe the distributions of $\underline{f}$ during a reversed loading. We denote the two parameters ψ_1 and ψ_2. During the initial loading ψ_1 is variable and equal to ψ used previously, and $\psi_2 = 0$. During the reversed loading ψ_1 is constant and equal to the maximum value of ψ that occurred in the initial loading, and ψ_2 is variable in the range $0 \le \psi_2 \le \psi_1$. Define a vector field $\underline{h} = (h_1, h_2, h_3)$ by

$$\begin{aligned} h_1 &= \tfrac{1}{2}(3\eta \cos^2\theta + a)\, e_y \cos\theta \\ h_2 &= \tfrac{1}{2}(3\eta \cos^2\theta - \zeta)\, e_y \sin\theta \cos\phi \\ h_3 &= \tfrac{1}{2}(3\eta \cos^2\theta - \zeta)\, e_y \sin\theta \sin\phi \end{aligned} \qquad (5.12)$$

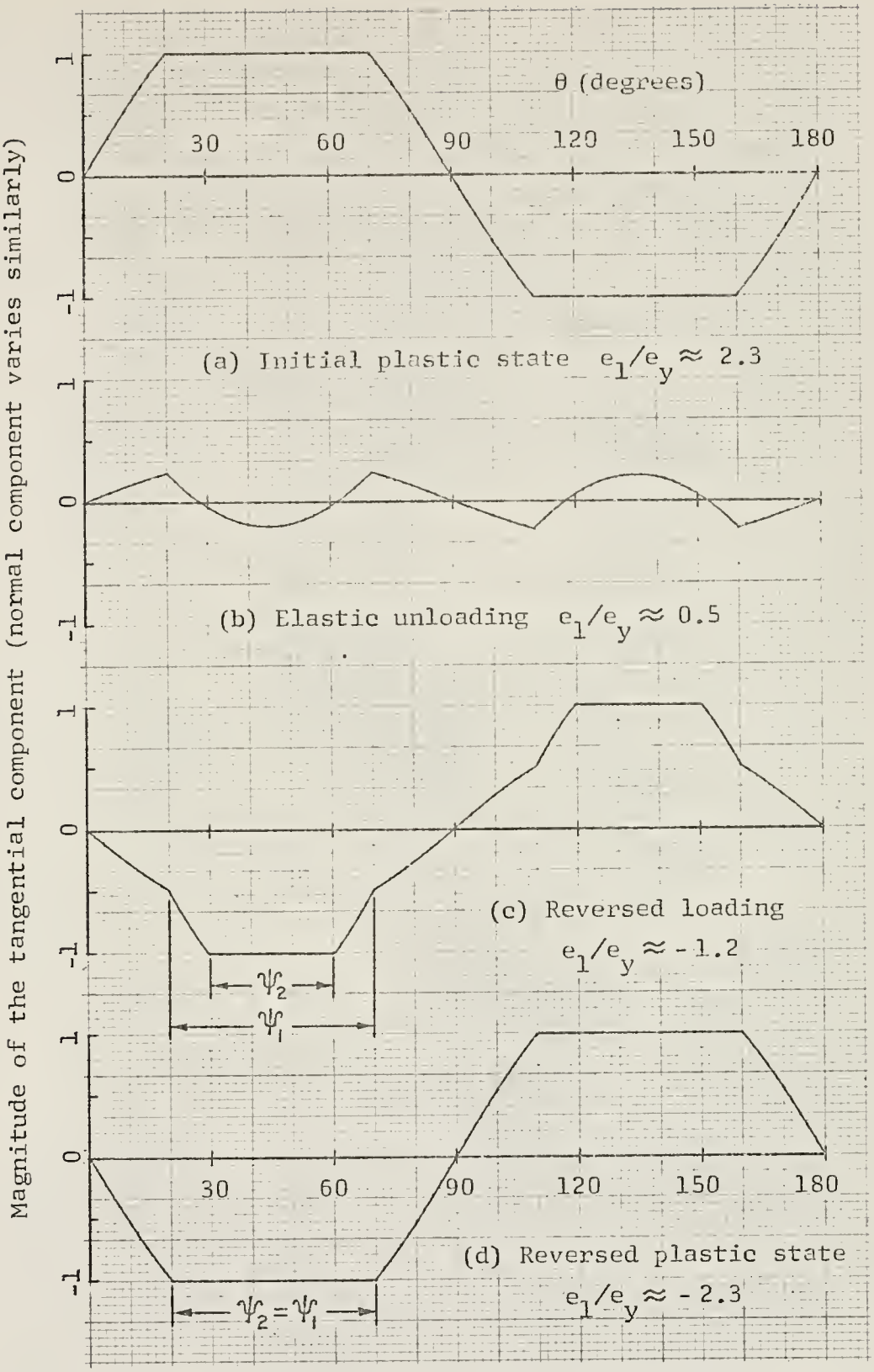

FIGURE 6. DISTRIBUTION OF ELEMENTAL STRESS VECTORS FOR REVERSED AXIAL LOADING FROM AN INITIALLY PLASTIC STATE

where θ, ϕ are the spherical coordinates of Figure 2 and $0 \le \theta \le \pi$, $0 \le \phi \le 2\pi$, unless specified otherwise. As before, $a = 2\kappa - \eta$ and $\zeta = \kappa + \eta$. We can express the elemental stress vector $\underline{f}$ in terms of $\underline{h}$ as follows.

1. Initial elastic loading $\underline{f} = \underline{h} \cos \psi_1$, $-\pi \le \psi_1 \le 0$ (5.13a)

2. Elastic-plastic loading $0 \le \psi_1 \le \pi/2$

$$\underline{f} = \underline{h} \begin{Bmatrix} \sec \psi_1 & \text{for } \theta \in S_1 \\ \csc 2\theta & \text{for } \theta \in S_2 \end{Bmatrix} \tag{5.13b}$$

3. Elastic unloading $-\frac{\pi}{2} \le \psi_2 \le 0 \le \psi_1 < \frac{\pi}{2}$, ψ_1 constant

$$\underline{f} = \underline{h} \begin{Bmatrix} \sec \psi_1 & \text{for } \theta \in S_1 \\ \csc 2\theta & \text{for } \theta \in S_2 \end{Bmatrix} - 2\underline{h} \cos \psi_2 \tag{5.13c}$$

4. Reversed elastic-plastic loading $0 \le \psi_2 \le \psi_1 < \frac{\pi}{2}$, ψ_1 constant

$$\underline{f} = \underline{h} \begin{Bmatrix} \sec \psi_1 & \text{for } \theta \in S_1 \\ \csc 2\theta & \text{for } \theta \in S_2 \end{Bmatrix} - 2h \begin{Bmatrix} \sec \psi_2 & \text{for } \theta \in S_3 \\ \csc 2\theta & \text{for } \theta \in S_4 \end{Bmatrix} \tag{5.13d}$$

5. Reversed elastic-plastic loading $0 \le \psi_1 \le \psi_2 < \frac{\pi}{2}$, ψ_1 constant

$$\underline{f} = -\underline{h} \begin{Bmatrix} \sec \psi_2 & \text{for } \theta \in S_3 \\ \csc 2\theta & \text{for } \theta \in S_4 \end{Bmatrix} \tag{5.13e}$$

Here S_1, S_2, S_3, S_4 are sets of real numbers defined by

$$\xi_1 = \frac{\pi}{4} - \frac{\psi_1}{2}, \quad \xi_2 = \frac{\pi}{4} + \frac{\psi_1}{2}, \quad \zeta_1 = \frac{\pi}{4} - \frac{\psi_2}{2}, \quad \zeta_2 = \frac{\pi}{4} + \frac{\psi_2}{2} \tag{5.14}$$

$$S_1 = ((0,\xi_1),(\xi_2,\pi-\xi_2),(\pi-\xi_1,\pi)), \quad S_2 = ((\xi_1,\xi_2),(\pi-\xi_2,\pi-\xi_1))$$

$$S_3 = ((0,\zeta_1),(\zeta_2,\pi-\zeta_2),(\pi-\zeta_1,\pi)), \quad S_4 = ((\zeta_1,\zeta_2),(\pi-\zeta_2,\pi-\zeta_1)) \ .$$

Resultant stresses are computed from the equations

$$\underline{t}_i = (t_{1i}, t_{2i}, t_{3i}) = \frac{1}{\pi} \int_{A_i} \underline{f} \, dA, \ (i = 1,2,3) \ . \tag{5.15}$$

As before, since the principal strain axes are fixed in the material, we have the relations

$$s_i = t_{ii} - (t_{11} + t_{22} + t_{33})/3, \quad (i = 1,2,3, \text{ no sum}) . \tag{5.16}$$

Plugging appropriate expressions for $\underline{f}$ from equations (5.13) into equations (5.15) and (5.16), and performing the integrations, we find the following closed-form solutions. Here $L_1 = \log\cos\xi_1 - \log\cos\xi_2$ and $L_2 = \log\cos\zeta_1 - \log\cos\zeta_2$. Cases 1 and 2, having to do with initial loadings, were derived previously and are not repeated here.

3. Elastic unloading $-\frac{\pi}{2} \le \psi_2 \le 0 < \psi_1 < \frac{\pi}{2}$, ψ_1 constant

$$e_1 = -2e_2 = -2e_3 = e_y(\sec\psi_1 - 2\cos\psi_2)$$

$$s_1 = -2s_2 = -2s_3 = s_y\left[\frac{2}{3}(\psi_1 - \tan\psi_1) + \left(1 - \frac{2\psi_2}{3\pi}\right)\sec\psi_1 + \frac{2}{\pi}\left(\frac{1-\lambda}{3-\lambda}\right)\sin\psi_1 + \frac{4L_1}{3\pi}\left(\frac{\lambda}{3-\lambda}\right) - 2\cos\psi_2\right] \tag{5.17}$$

4. Reversed elastic-plastic loading $0 \le \psi_2 \le \psi_1 < \frac{\pi}{2}$, ψ_1 constant

$$e_1 = -2e_2 = -2e_3 = e_y(\sec\psi_1 - 2\sec\psi_2)$$

$$s_1 = -2s_2 = -2s_3 = s_y\left[\frac{2}{3}(\psi_1 - \tan\psi_1) - \frac{4}{3}(\psi_2 - \tan\psi_2) + \left(1 - \frac{2\psi_1}{3\pi}\right)\sec\psi_1 - \left(2 - \frac{4\psi_2}{2\pi}\right)\sec\psi_2 + \frac{2}{\pi}\left(\frac{1-\lambda}{3-\lambda}\right)\sin\psi_1 - \frac{4}{\pi}\left(\frac{1-\lambda}{3-\lambda}\right)\sin\psi_2 + \frac{4}{3\pi}\left(\frac{\lambda}{3-\lambda}\right)(L_1 - 2L_2)\right] \tag{5.18}$$

5. Reversed elastic-plastic loading $0 \le \psi_1 \le \psi_2 < \frac{\pi}{2}$, ψ_1 constant

$$e_1 = -2e_2 = -2e_3 = -e_y\sec\psi_2$$

$$s_1 = -2s_2 = -2s_3 = -s_y\left[\frac{2}{3}(\psi_2 - \tan\psi_2) + \left(1 - \frac{2\psi_2}{3\pi}\right)\sec\psi_2 + \frac{2}{\pi}\left(\frac{1-\lambda}{3-\lambda}\right)\sin\psi_2 + \frac{4L_2}{3\pi}\left(\frac{\lambda}{3-\lambda}\right)\right] \tag{5.19}$$

Equations (5.17), (5.18), and (5.19) satisfy "Masing's hypothesis" [37], whereby the stress-strain curve of reversed loading is exactly double in size, although rotated 180-degrees and translated, compared with the stress-strain curve of the initial loading. Symbolically

$$\begin{aligned}
&1,2.\ \text{Initial loading:}\quad s = s(e),\ 0 \le e \le e_m \\
&3,4.\ \text{Reversed loading:}\quad \begin{cases} s' = s_m - 2s(e), & s_m = s(e_m) \\ e' = e_m - 2e, & 0 \le e \le e_m \end{cases} \\
&5.\ \text{Reversed loading:}\quad s' = -s(e),\ e' = -e,\ e \ge e_m
\end{aligned} \tag{5.20}$$

For Case 5, where $\psi_2 \ge \psi_1$, the stress-strain curve of reversed loading is identical in size, but rotated 180-degrees about the origin, compared with the continuation of the initial stress-strain curve. This phenomenon, too, is considered a part of Masing's hypothesis. The present result is to be expected because Masing's hypothesis is a general property of mechanical systems composed of elastic-perfectly-plastic elements [33].

Figures 7 and 8 show computed results of axial and reversed axial loadings for $\lambda = 0$ and $\lambda = 1.5$, respectively. The large effect of the parameter λ on the stress-strain behavior can be seen by comparing these graphs. Two related phenomena appear on both graphs, namely the presence of a Bauschinger effect and constancy of the elastic range. The Masing hypothesis, discussed above and embodied in equations (5.20), is readily discernible from Figure 7 or 8. A special

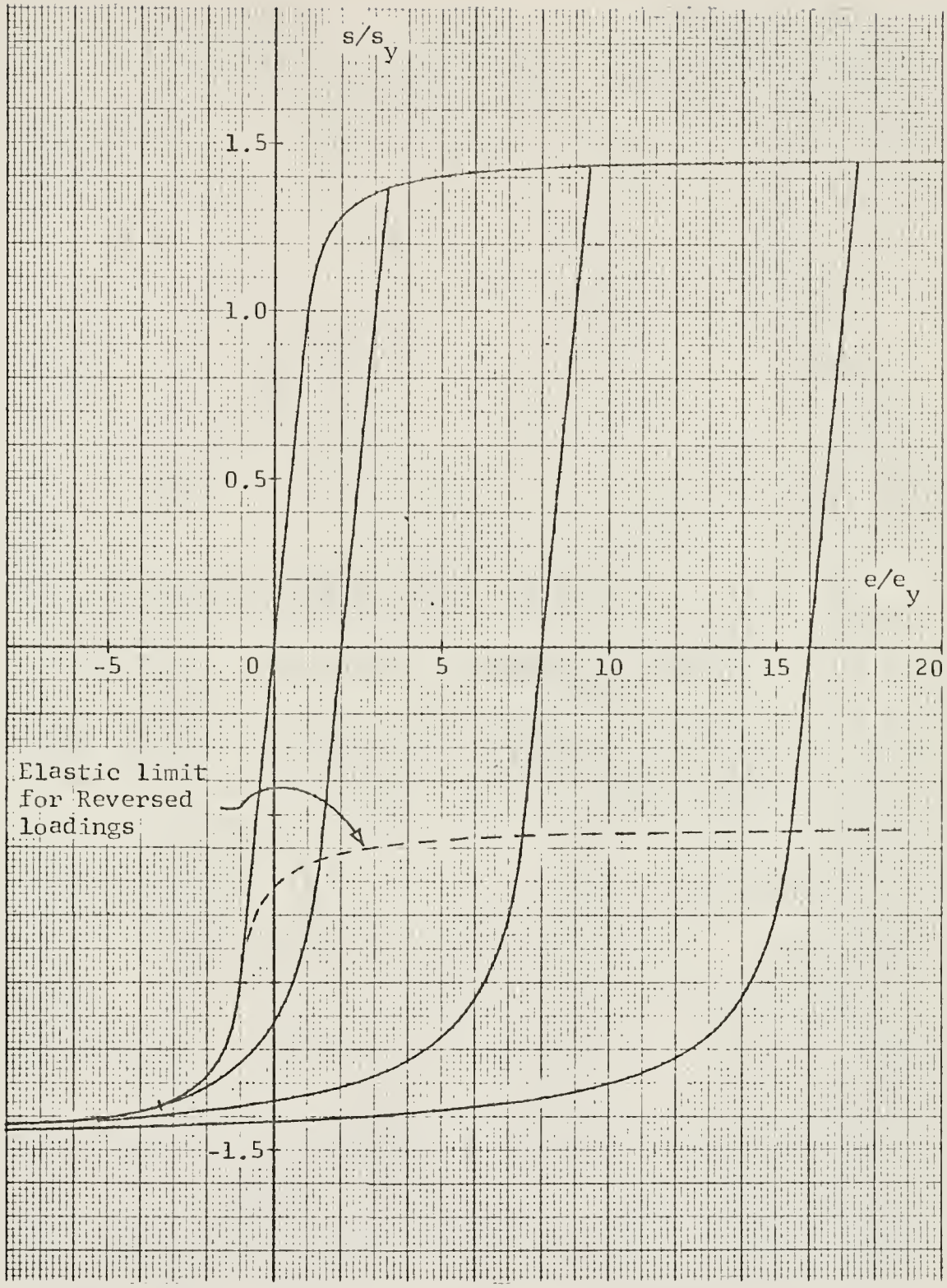

FIGURE 7. AXIAL LOADING AND REVERSED AXIAL LOADINGS FOR $\lambda = 0$

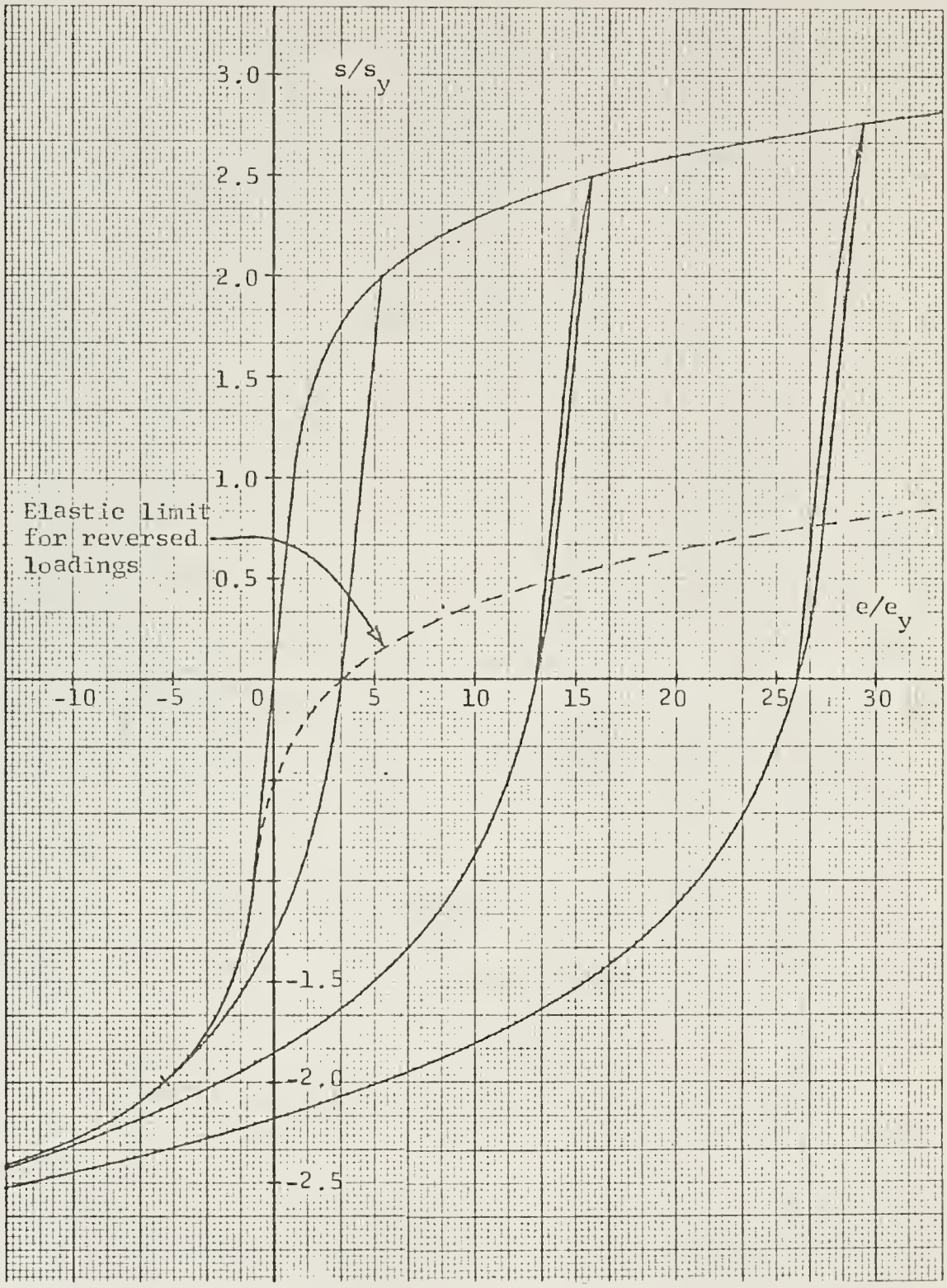

FIGURE 8. AXIAL LOADING AND REVERSED AXIAL LOADINGS FOR $\lambda = 1.5$

phenomenon appears in Figure 8 but not in Figure 7, namely the hysteresis loop of unloading and reloading that involves plasticity. The reloading curves may be obtained either from a straightforward extension of the closed-form results of Chapter V, or by a direct application of the numerical methods of Chapter VI. Note that the hysteresis loops of unloading-reloading are present only for certain values of λ and certain values of strain, as defined by the condition $s/s_y > 2$.

One further result relating to uniaxial stress-strain behavior can be derived from equations (5.9) and (5.10). Introducing identities such as

$$\sin\psi = \cos(2\delta), \quad \sec\psi - \tan\psi = \tan\delta$$

$$\log\cos\xi_2 = \log\sin\delta = \log\delta - \delta^2/6 - \delta^4/180 - \ldots$$

$$\delta\sec\psi = \csc(2\delta) = \tfrac{1}{2} + \delta^2/3 + 7\delta^4/15 + \ldots$$

where $\delta = \xi_1 = \pi/4 - \psi/2$, we can easily show that

$$\lim_{e_1\to\infty} \frac{s_1}{s_y} = \lim_{\delta\to 0} \frac{s_1}{s_y} = \frac{\pi}{3} + \frac{4}{3\pi}\left[\frac{3-2\lambda}{3-\lambda} - \lim_{\delta\to 0}\left(\frac{\lambda\log\delta}{3-\lambda}\right)\right] . \qquad (5.21)$$

We conclude from equation (5.21) that a limiting stress corresponding to large values of strain exists if and only if $\lambda = 0$, in which case

$$\lim_{e_1\to\infty} \frac{s_1}{s_y} = \frac{\pi}{3} + \frac{4}{3\pi} = 1.4716107\ldots.$$

CHAPTER VI

STRESS-STRAIN BEHAVIOR FOR THE CLASS OF LOADINGS INVOLVING FIXED PRINCIPAL AXES

Consider a class of loadings in which the principal strain axes are fixed relative to the material, but where the principal strain magnitudes can vary arbitrarily.

$$\left.\begin{aligned} &\varepsilon_i(0) = 0, \quad \varepsilon_i = \varepsilon_i(t) \text{ for } t > 0 \\ &e_i = \varepsilon_i - (\varepsilon_1 + \varepsilon_2 + \varepsilon_3)/3, \quad (i = 1,2,3) \end{aligned}\right\} \tag{6.1}$$

This class of loadings is more general than the axial loadings studied in Chapter V; axial loadings are included here as a special case. The following equations govern the elemental stress vectors and the resultant stresses:

$$\left.\begin{aligned} &\underline{f}^{(0)}(\underline{n}) = 0, \ \underline{f}^{(m)} = \bar{g}\begin{cases} 1 & \text{if } g_t \le Y \\ Y/g_t & \text{if } g_t > Y \end{cases}, \ m = 1,2,3,\ldots \\ &\bar{g} = \underline{f}^{(m-1)} + \kappa d\underline{E}^{(m)}\cdot\underline{n} + \eta\underline{n}(\underline{n}\cdot d\underline{E}^{(m)}\cdot\underline{n}), \ g_t = [\bar{g}\cdot\bar{g} - (\bar{g}\cdot\underline{n})^2]^{\frac{1}{2}} \end{aligned}\right\} \tag{6.2}$$

$$\left.\begin{aligned} &\underline{t}_1 = \frac{1}{\pi}\int_0^{2\pi} d\phi \int_0^{\pi/2} d\theta \, \underline{f} \sin\theta, \quad \underline{t}_2 = \frac{1}{\pi}\int_{-\pi/2}^{\pi/2} d\phi \int_0^{\pi} d\theta \, \underline{f} \sin\theta \\ &\underline{t}_3 = \frac{1}{\pi}\int_0^{\pi} d\phi \int_0^{\pi} d\theta \, \underline{f} \sin\theta \quad . \end{aligned}\right\} \tag{6.3}$$

Here $\underline{f}^{(m-1)}$ and $\underline{f}^{(m)}$ are the elemental stress vectors before and after application of a given strain increment $d\underline{E}^{(m)}$. Again we refer vectors and tensors to the principal strain coordinates, and we use spherical coordinates θ,ϕ where convenient.

In Chapter IV we proved that if the principal strain axes are fixed in the material throughout a deformation, then the principal stress axes are fixed and coincident with the strain axes. Since these conditions apply in the present case, we can compute the principal deviator stresses s_i from the equations

$$\begin{aligned} s_i &= t_{ii} - (t_{11}+t_{22}+t_{33})/3, \quad (i=1,2,3, \text{ no sum}) \\ \underline{t}_i &= (t_{1i},t_{2i},t_{3i}) = \frac{4}{\pi}\int_0^{\pi/2} d\phi \int_0^{\pi/2} d\theta\, \underline{f} \sin\theta \quad . \end{aligned} \tag{6.4}$$

Equation $(6.4)_2$ follows from equations (6.3) by symmetry considerations similar to equations (4.12). As noted in Chapter IV, the boundary between elastic and plastic regions on the unit sphere can be very complicated for a general loading. In fact, due to the complicated nature of this elastic-plastic boundary, there probably does not exist a closed-form solution for the class of problems discussed here. Therefore, we shall be forced to derive a numerical procedure, or <u>algorithm</u>, to be used in conjunction with a digital computer, for solving equations (6.1) through (6.4).

Consider a finite grid of points covering one octant of a unit sphere and based on the spherical coordinates θ,ϕ. Thus

$$\theta_i = iP, \quad \phi_j = jP, \quad (i,j=0,1,\ldots,N) \tag{6.5}$$

where N is a grid-spacing integer and $P=\pi/2N$. The integral of a function $f(\theta,\phi)$ over a spherical octant can be approximated by the <u>trapezoidal rule formula</u> as follows:

$$\int_0^{\pi/2} d\phi \int_0^{\pi/2} d\theta\, f \sin\theta = \sum_{i=0}^{N} \alpha_i \left[\frac{f_{i0} + f_{iN}}{2} + \sum_{j=1}^{N-1} f_{ij} \right] + \varepsilon$$

where $f_{ij} = f(\theta_i, \phi_j)$, $\alpha_i = (P/2)(\cos\theta_{i-1} - \cos\theta_{i+1})$ (6.6)

$$\alpha_o = (P/2)(1 - \cos\theta_1), \quad \alpha_N = (P/2)\cos\theta_{N-1} \quad .$$

If the function $f(\theta,\phi)$ is continuous and possesses continuous first and second derivatives, then the truncation error ε for the trapezoidal integration formula is bounded.

$$\text{abs } \varepsilon < \max_{\theta,\phi} \frac{(\pi/2)^4}{12N^2} (f_{\theta\theta} + f_{\phi\phi} \sin^2\theta) \sin^2\theta \qquad (6.7)$$

Here $f_{\theta\theta}$ and $f_{\phi\phi}$ are partial derivatives and $0 \le \theta, \phi \le \pi/2$. Equations (6.6) can be derived by summing the product of the area and the average functional value for each patch of the finite grid. The inequality (6.7) is derived by expanding the function $f(\theta,\phi)$ in a two-dimensional Taylor's series [70, p. 187] and substituting the result into equation (6.6).

As an alternative integration formula consider the following modified trapezoidal rule:

$$\int_0^{\pi/2} d\phi \int_0^{\pi/2} d\theta\, f \sin\theta = \sum_{i=0}^{N} \alpha_i \left[\frac{f'_{i0} + f'_{iN}}{2} + \sum_{j=1}^{N-1} f'_{ij} \right] + \varepsilon'$$

where $f'_{ij} = f(\theta'_i, \phi'_j)$, $\theta'_i = \phi'_i = iP$ for $i = 1,2,\ldots,N-1$ (6.8)

$$\theta'_o = \phi'_o = P/6, \quad \theta'_N = \phi'_N = \pi/2 - P/6 \quad .$$

Here $\alpha_i (i = 0,\ldots,N)$ are defined in equations (6.6). It can be shown that the truncation error ε' for equation (6.8) is of order N^{-3}, instead of N^{-2} as in the case of equation (6.6). That is, the integration formula (6.8) converges

faster than (6.6) as the finite grid is refined. Proof that ϵ' is order N^{-3} follows by combining Taylor's series and the Euler-MacLaurin summation formula [70, p. 154], both suitably generalized to two dimensions.

Now consider numerical integration of the elemental stress vectors $\underline{f}$ over a spherical octant, as required by equations (6.4). In particular, let us apply equations (6.6) to the three components $f_k (k = 1,2,3)$ of $\underline{f}$ relative to the principal strain coordinates. Initially during a loading, the material is elastic and the functions $f_k(\theta,\phi)$ possess continuous derivatives of all orders. Here the inequality (6.7) provides a bound on the truncation error. After plasticity occurs the functions $f_k(\theta,\phi)$ still are continuous, but the derivatives $\partial\theta^m \partial\phi^n f_k$ of all orders are discontinuous along the boundary between elastic and plastic regions on the unit sphere. Hence, in general, the inequality (6.7) does not hold true after plasticity has occurred.

Equations (6.6) and (6.8) are the basic numerical integration formulae to be used in the remainder of this work, even though the functions to be integrated generally will have discontinuous derivatives. When plasticity occurs we simply are forced to establish the numerical accuracy by comparisons with the exact solutions of Chapter V, instead of by inequalities such as (6.7). As we shall see, the numerical error can be made arbitrarily small by using a sufficiently large grid-spacing integer N.

Let us comment briefly on the choice of integration formula. I could have chosen a more complicated, higher-order polynomial formula — of the Gauss type, say — instead of the trapezoidal rule. The discontinuous derivatives of $\underline{f}(\theta,\emptyset)$ again would have rendered invalid the usual error estimates. Experience with equations (6.6) and (6.8) has shown that, except for integrations in the elastic range, there is very little to be gained by using an equation with truncation error of order N^{-3} instead of N^{-2}. Therefore, I doubt whether any significant improvement of accuracy can be achieved from any higher-order integration formula when the first derivative of the integrand is discontinuous. The only direct way of improving accuracy is to refine the grid. The decisive reason for choosing the trapezoidal rule formula is that, because of its relative simplicity, for a given computational effort it allows one to compute the integrand at a larger number of grid points.

Assume that we are given a sequence of deviator strain increments $de_k^{(m)}$ $(m = 1,2,3,\ldots)$ representing a strain history. The following equations govern the elemental stress vectors at points $(\theta_i \emptyset_j)$ of the finite grid:

$$
\begin{aligned}
&f_{ijk}^{(0)} = 0, \quad f_{ijk}^{(m)} = g_k \left\{ \begin{array}{ll} 1 & \text{if } g_t \le Y \\ Y/g_t & \text{if } g_t > Y \end{array} \right\}, \quad m = 1,2,3,\ldots \\
&g_k = f_{ijk}^{(m-1)} + \varkappa de_k^{(m)} n_k + \eta n_k (de_1^{(m)} n_1^2 + de_2^{(m)} n_2^2 + de_3^{(m)} n_3^2) \\
&g_t = [g_1^2 + g_2^2 + g_3^2 - (g_1 n_1 + g_2 n_2 + g_3 n_3)^2]^{\frac{1}{2}} \\
&n_1 = \cos\theta_i, \quad n_2 = \sin\theta_i \cos\emptyset_j, \quad n_3 = \sin\theta_i \sin\emptyset_j
\end{aligned}
\tag{6.9}
$$

where $i,j = 0,1,2,\ldots,N$ and $k = 1,2,3$ (no summation). The deviator strains and stresses are computed from the equations

$$e_k^{(0)} = 0, \quad e_k^{(m)} = de_k^{(m)} + e_k^{(m-1)}, \quad s_k = t_k - (t_1 + t_2 + t_3)/3$$

$$t_k = \sum_{i=0}^{N} \alpha_i' \left(\frac{f_{i0k} + f_{iNk}}{2} + \sum_{j=1}^{N-1} f_{ijk} \right), \quad (k = 1,2,3) \tag{6.10}$$

where $\alpha_i' = N^{-1}(\cos\theta_{i-1} - \cos\theta_{i+1})$, $i = 1,2,\ldots,N-1$

$$\alpha_0' = N^{-1}(1 - \cos\theta_1), \quad \alpha_N' = N^{-1}\cos\theta_{N-1} \quad .$$

Equation $(6.10)_2$ can represent either the ordinary trapezoidal rule or the modified trapezoidal rule, depending on whether the coordinates θ_i, ϕ_j in equations (6.9) are defined by equations (6.5) or $(6.8)_{3,4,5}$. Equations (6.9) and (6.10) have been incorporated into two computer programs, Programs A-2 and A-3 of Appendix A, representing the ordinary trapezoidal rule and the modified trapezoidal rule, respectively. These programs have been used to predict a variety of stress-strain behavior within the class of loadings defined by fixed principal axes.

Figure 9 shows stress-strain curves for shear-type loadings. The curves were computed for the case of <u>pure shear</u>, defined by $e_{11} = -e_{22} = e(t)$ and $e_{ij} = 0$ if $ij \neq 11$ or 22, which is included in the class of loadings discussed here. The results apply equally to the case of <u>simple shear</u>, defined by $e_{12} = e_{21} = e(t)$, $e_{ij} = 0$ if $ij \neq 12$ or 21. Simple shear is equivalent to pure shear plus a rotation, but it cannot be computed directly from Programs A-2 or A-3, which

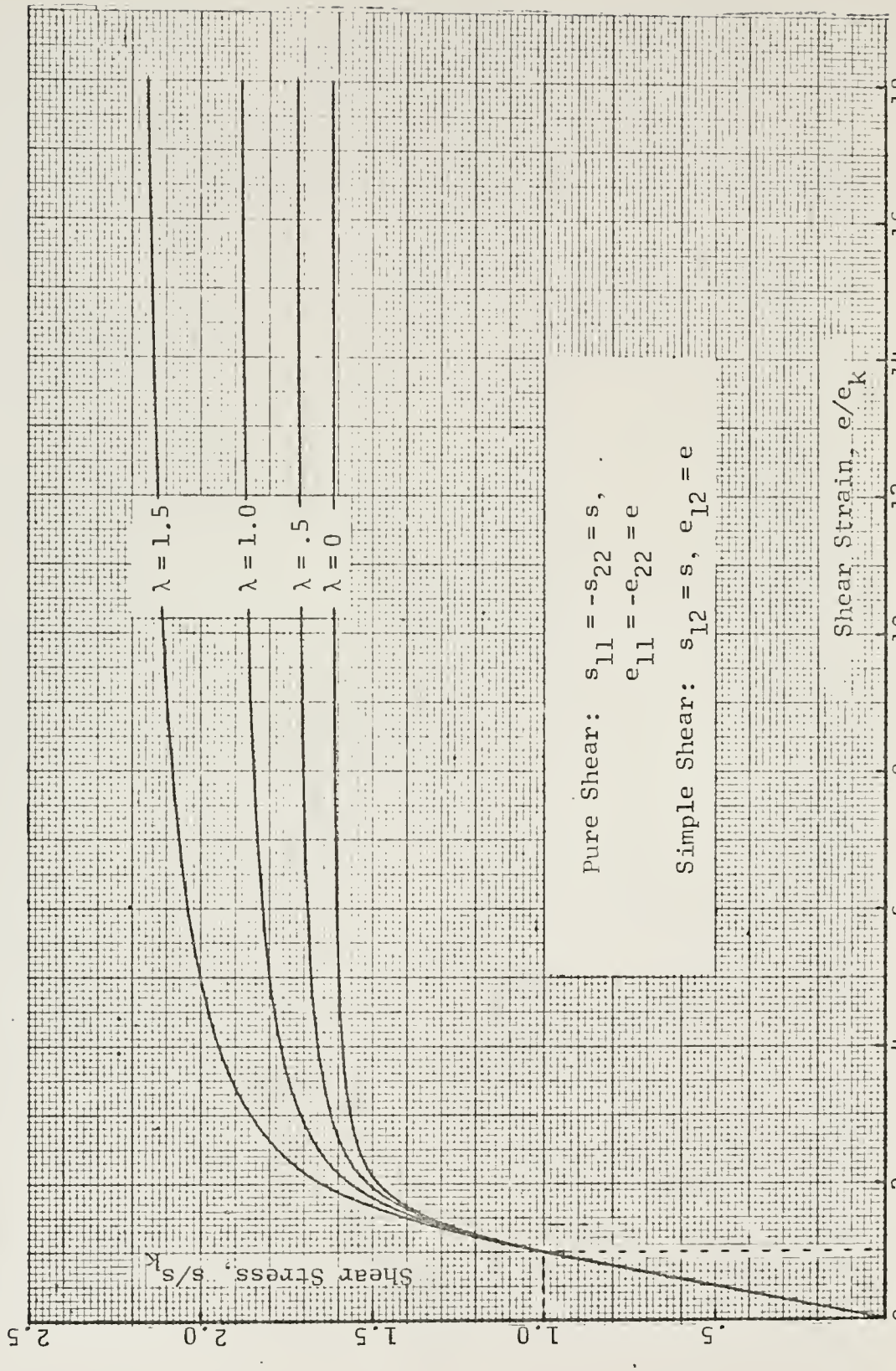

FIGURE 9. STRESS-STRAIN BEHAVIOR FOR SHEAR LOADINGS

input only the principal strains. Note that the stress-strain curves in shear depend on the work-hardening parameter λ in a manner similar to the case of axial loading, but that the degree of work-hardening is not as great. That is, the stress compared to yield and the slope of the stress-strain curve for a given moderate value of strain are less for shear loadings than for axial loadings.

The question of numerical errors now arises. How accurate are the numerical results, such as presented in Figure 9, that are computed using Programs A-2 or A-3? To answer this question we generated a large quantity of numerical results for the case of axial loading, using Programs A-2 and A-3. These numerical results, some of which are contained in Tables B-3 and B-4 of Appendix B, then were compared with highly accurate results computed from the closed-form solutions of Chapter V.

Figures 10-13 illustrate graphically the numerical errors for axial loading. The graphs show relative errors in the computed stress plotted against strain, for two values of λ and for the two integration formulae discussed earlier. We observe that the numerical error is constant in the elastic range $0 \leq e_1/e_k \leq 4/3$. However, after plasticity occurs the variation of numerical error with strain is very complicated, with many peaks and dips appearing. The peak numerical errors tend to increase proportionally with the strain; note that the numerical errors generally are less than 10^{-2}

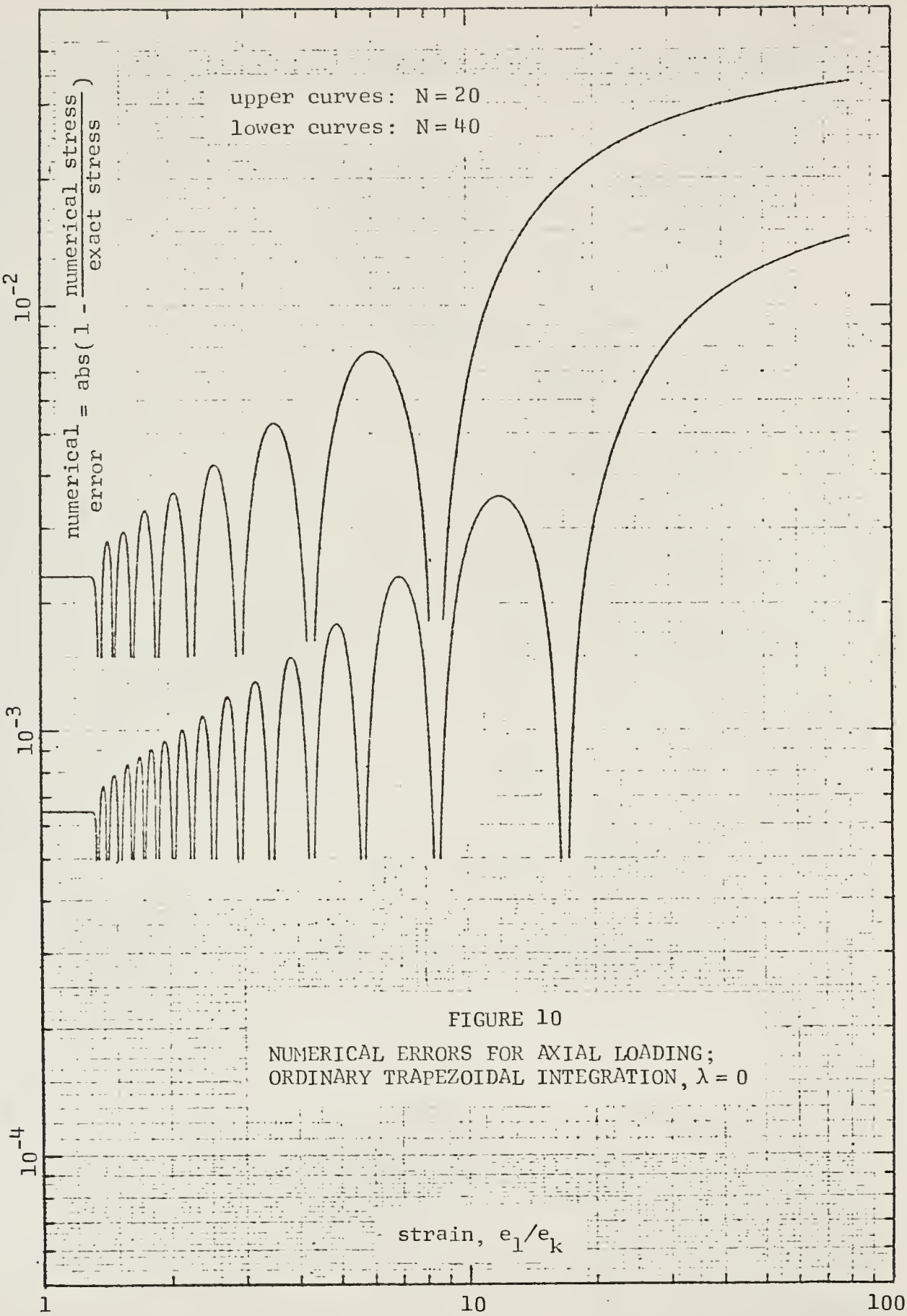

FIGURE 10

NUMERICAL ERRORS FOR AXIAL LOADING;
ORDINARY TRAPEZOIDAL INTEGRATION, $\lambda = 0$

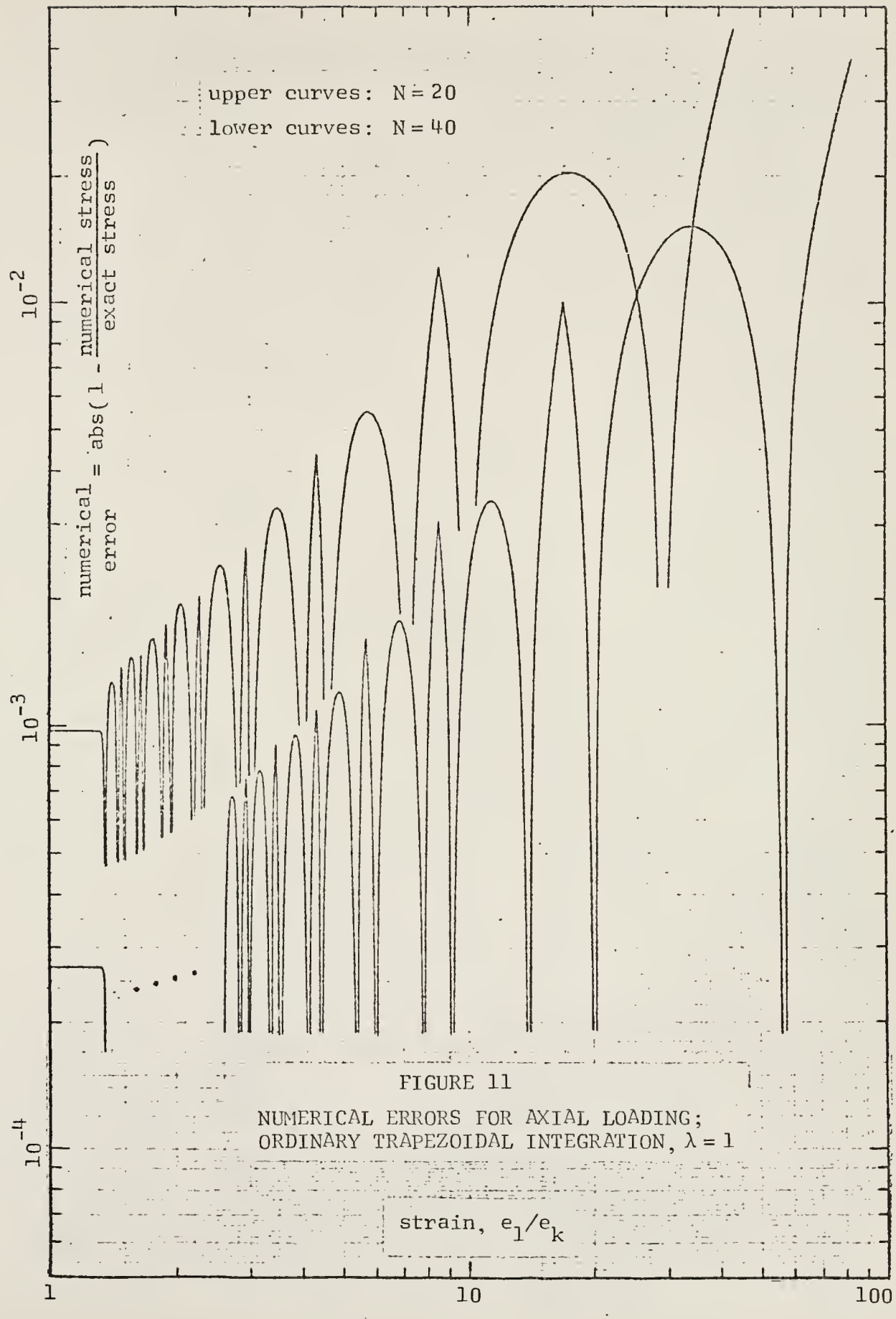

FIGURE 11

NUMERICAL ERRORS FOR AXIAL LOADING;
ORDINARY TRAPEZOIDAL INTEGRATION, $\lambda = 1$

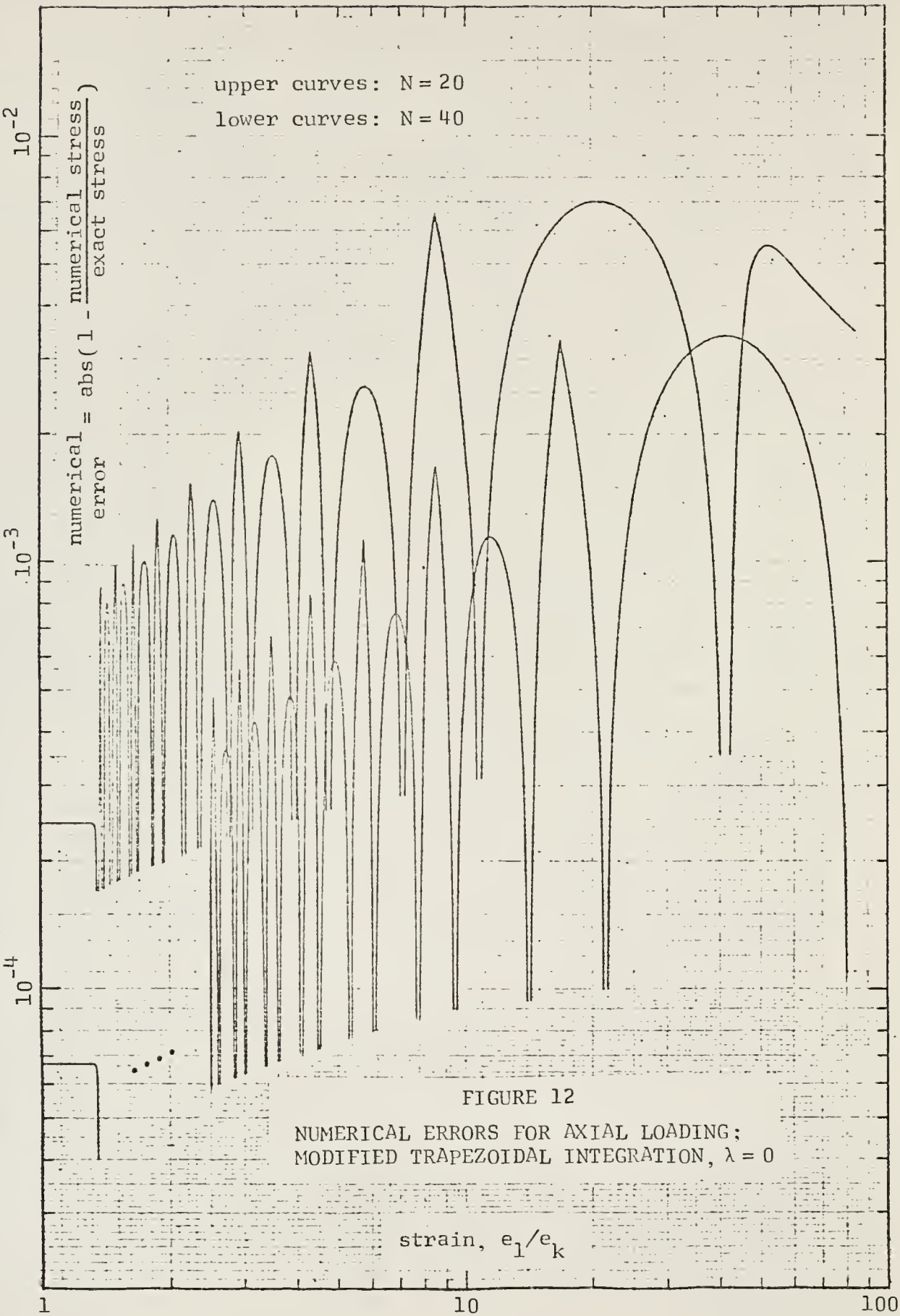

FIGURE 12

NUMERICAL ERRORS FOR AXIAL LOADING:
MODIFIED TRAPEZOIDAL INTEGRATION, $\lambda = 0$

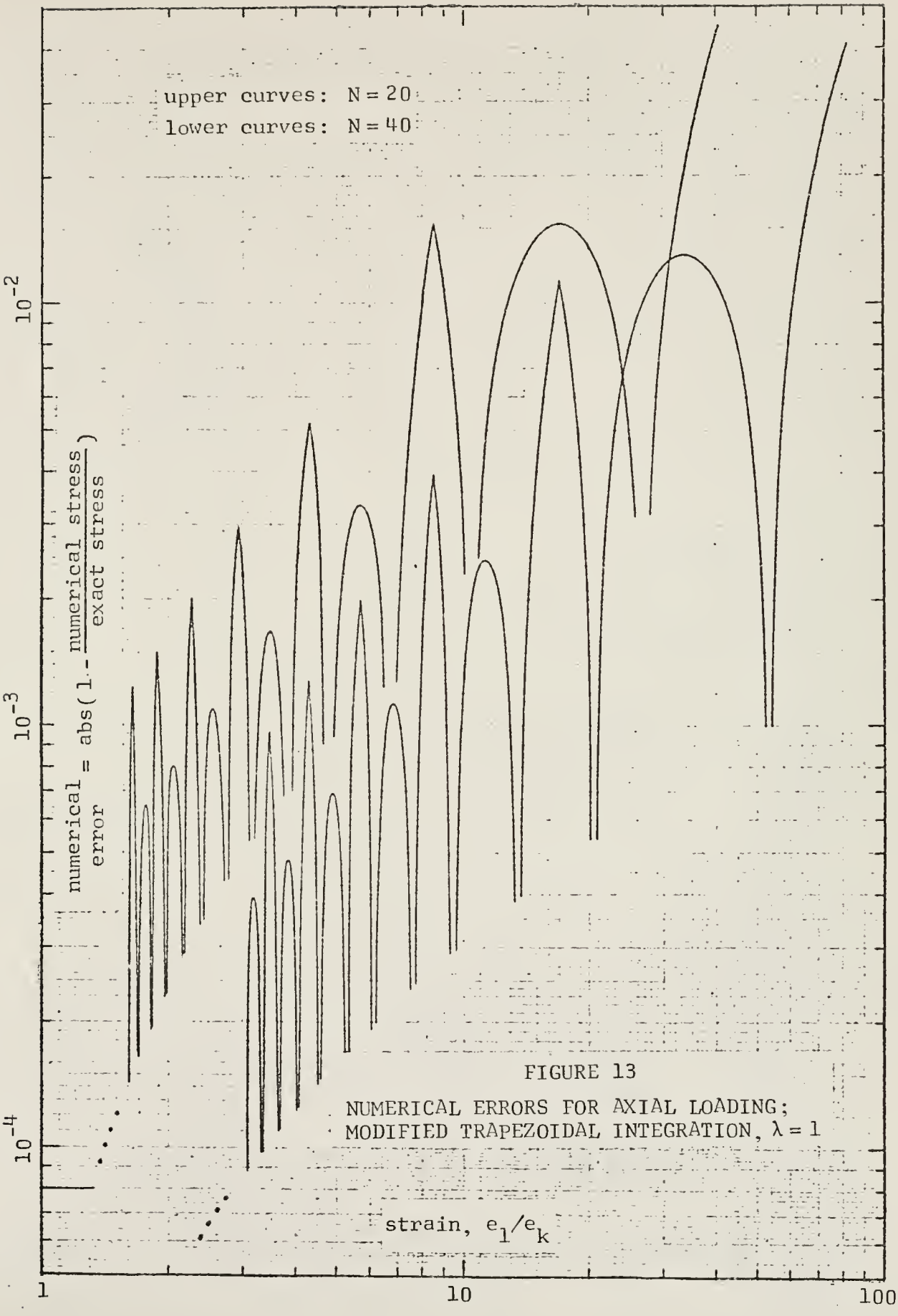

FIGURE 13

NUMERICAL ERRORS FOR AXIAL LOADING;
MODIFIED TRAPEZOIDAL INTEGRATION, $\lambda = 1$

(plotting accuracy) when the strain e_1/e_i is less than 10 and when the grid-spacing integer is 20 or larger. The dips are explained by the fact that for axial loading the elastic-plastic boundary coincides periodically with the finite grid. When this occurs the numerical integration involves only functions with continuous derivatives and hence the accuracy is greatly improved. For loadings other than axial loadings the dips in the numerical errors versus strain curves would not be as pronounced.

The effect of the grid-spacing integer N can be found by comparing the two sets of curves on each graph: the upper curve was computed with $N = 20$; the lower curve represents $N = 40$. When the integer N is doubled, we see that the numerical error is reduced by a factor of about 3.6, which implies that the error is approximately of order $N^{-1.85}$. This rule applies independent of λ and independent of the integration method. For $\lambda = 0$, the effect of the modified trapezoidal rule as compared with the ordinary trapezoidal rule is to reduce the numerical errors by factors of 9 and 3 in the elastic and plastic ranges, respectively. For $\lambda = 1$, the modified trapezoidal rule reduces the numerical error by a factor of 12 in the elastic range, and the numerical errors are approximately unchanged in the plastic range. From the latter observation we conclude that, in general, there is no clear advantage in using the modified trapezoidal rule,

or other higher-order integration formulae, instead of the ordinary trapezoidal rule.

The reader is referred to Table B-5 of Appendix B, where values of stress and strain are tabulated for the pure shear type of loading. Here again we see that the numerically computed stress depends on the parameter λ and on the grid-spacing integer N. In this case, however, we cannot establish the numerical accuracy by comparisons with exact solutions, since there are no exact solutions for pure shear loadings. We recall that classical estimates of the truncation errors are invalid due to discontinuous derivatives in the functions $f_k(\theta,\phi)$. Furthermore, classical methods such as Richardson's extrapolation technique [71, p. 186] are invalid due to the complicated variations in the numerical errors with N.

Henceforth, in lieu of any rational methods, we assume that the peak numerical errors versus strain are the same as shown in Figures 10-13 for any loading that is approximately radial. The strain measure for an arbitrary loading can be taken as the accumulated plastic strain, defined by

$$e_A = \int_o^t dt \left[\sum_{i=1}^{3} \sum_{j=1}^{3} (\dot{e}_{ij} - \dot{s}_{ij}/\mu)(\dot{e}_{ij} - \dot{s}_{ij}/\mu) \right]^{\frac{1}{2}} \qquad (6.11)$$

In consequence of this assumption we require at least N = 20 for any computed data which are to be plotted on a graph and at least N = 40 for any computed data which are to be included in a table. The cost penalty of using large values of N will be discussed later.

We shall have need of the deviatoric plane (or π-plane) representations of stress and strain, defined as follows: Consider a three-dimensional vector space with the principal stresses $\sigma_1, \sigma_2, \sigma_3$ assigned to a set of Cartesian axes. Any state of stress can be represented by a point $\underline{\sigma} = (\sigma_1, \sigma_2, \sigma_3)$ in this principal stress space together with a specification of the principal stress axes.[1] Consider a plane in principal stress space, called the deviatoric stress plane, defined as the locus of points that satisfy the equation $\sigma_1 + \sigma_2 + \sigma_3 = 0$. The vector $\underline{s} = (s_1, s_2, s_3)$ composed of the principal deviator stresses always is contained in the deviatoric stress plane. Any yield condition that is independent of mean stress can be represented at most by one closed curve in the deviatoric stress plane for each orientation of the principal stress axes.

Principal strain space and the deviatoric strain plane are defined simply by substituting "strain, ε, e" for "stress, σ, s" throughout the preceding paragraph. The following quantities are associated with the deviatoric planes:

$$s = \sqrt{3/8}\ (s_1^2 + s_2^2 + s_3^2)^{\frac{1}{2}} \quad \text{deviatoric stress intensity}$$

$$e = \sqrt{3/8}\ (e_1^2 + e_2^2 + e_3^2)^{\frac{1}{2}} \quad \text{deviatoric strain intensity}$$

$$e_o = \sqrt{3/8}\ \left[\sum_{i=1}^{3} (e_i - s_i/\mu)^2\right]^{\frac{1}{2}} \quad \text{residual strain intensity} \quad .$$

---

[1] This statement is true provided the stress tensor is symmetric. If stress is nonsymmetric, as occurs for certain loadings discussed in Chapter VII, then the stress couple must be specified also. The principal stress axes can be specified by a rotation tensor or by Euler angles.

The quantities s, e, e_o are proportional to the magnitudes of the vectors $\underline{s} = (s_1, s_2, s_3)$, $\underline{e} = (e_1, e_2, e_3)$, $\underline{e}_o = \underline{e} - \underline{s}/\mu$, respectively. The factor $\sqrt{3/8}$ is included so as to eventually simplify plotting of the data. With these definitions $\underline{s} = (4/3, -2/3, -2/3) \Rightarrow s = 1$ and $\underline{s} = (1, -1, 0) \Rightarrow s = \sqrt{3/4}$, etc. The residual strain e_o, as defined here, is a useful concept only when the principal axes of stress and strain coincide.

One objection which might be raised against the theory presented in this dissertation is that the predicted initial yield condition is a Tresca condition, whereas the observed initial yield condition for most real materials appears to be better described by a Mises yield condition. See Naghdi, et al. [41], Mair and Pugh [49], and Phillips, et al. [52,53]. In the deviatoric plane representation the Tresca condition is an equilateral hexagon and the Mises condition is a circle; both are symmetric about the origin. We can remove the above-mentioned objection by considering radial loadings in various directions and by defining yield — as experimentalists must do — in terms of an offset strain or proof strain. Let us temporarily define yield as the stress intensity s corresponding to some fixed residual strain intensity e_o along any radial loading path. Figures 14, 15, 16 show curves of constant offset strain in the deviatoric plane for several values of e_o.

Figure 14 shows curves of constant offset strain for an initially isotropic material, defined by $\underline{f}(\underline{n}) = 0$ at

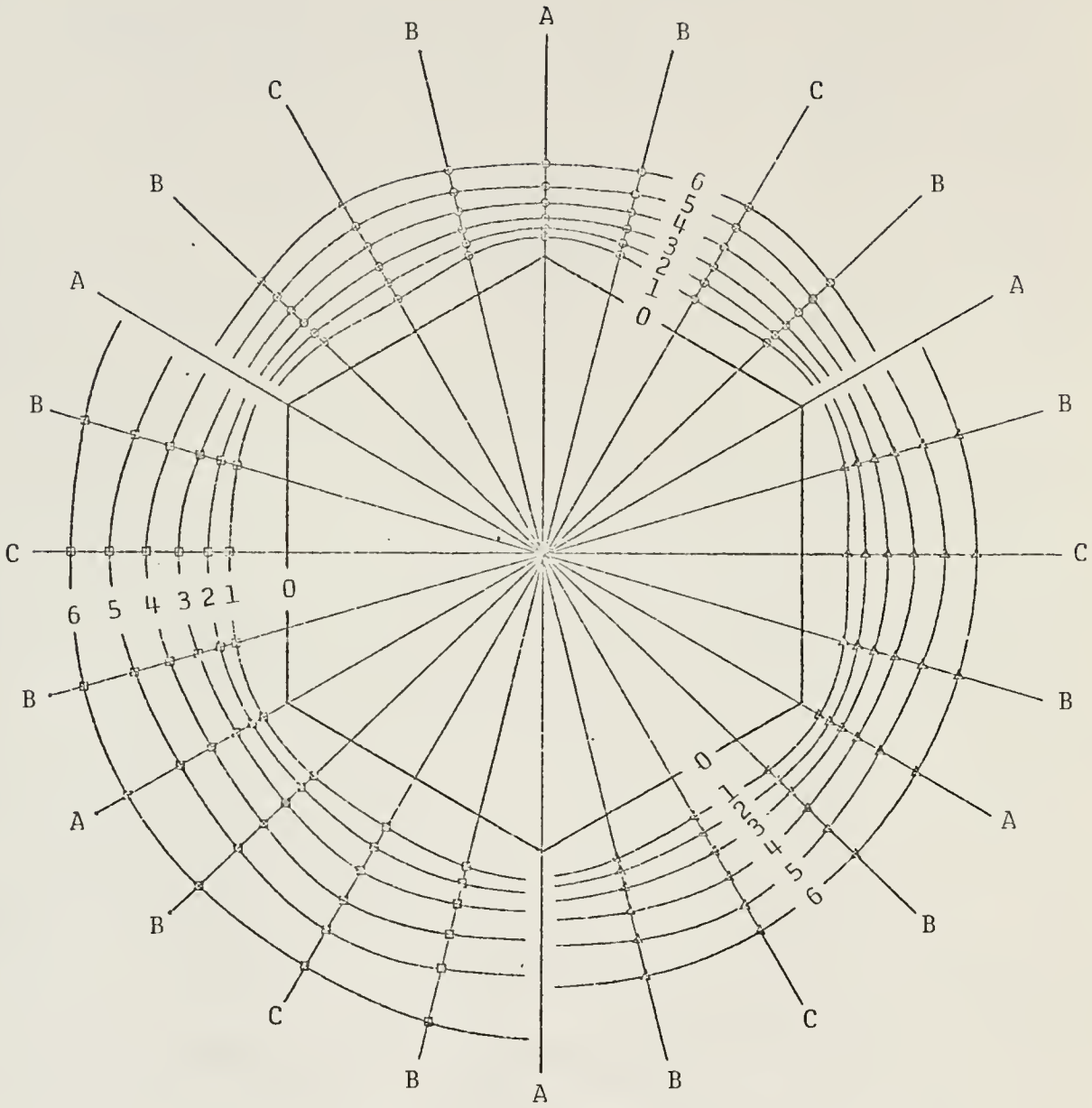

graph number: 0 1 2 3 4 5 6

offset strain, e_o/e_y: 0 .02 .05 .10 .20 .40 1.0

direction of loading: A(2,-1,-1), B(7,-2,-5), C(1,-1, 0)

work-hardening parameter: ○ $\lambda = 0$, △ $\lambda = 1.0$, □ $\lambda = 1.5$

FIGURE 14. SURFACES OF CONSTANT OFFSET STRAIN FOR AN INITIALLY ISOTROPIC MATERIAL

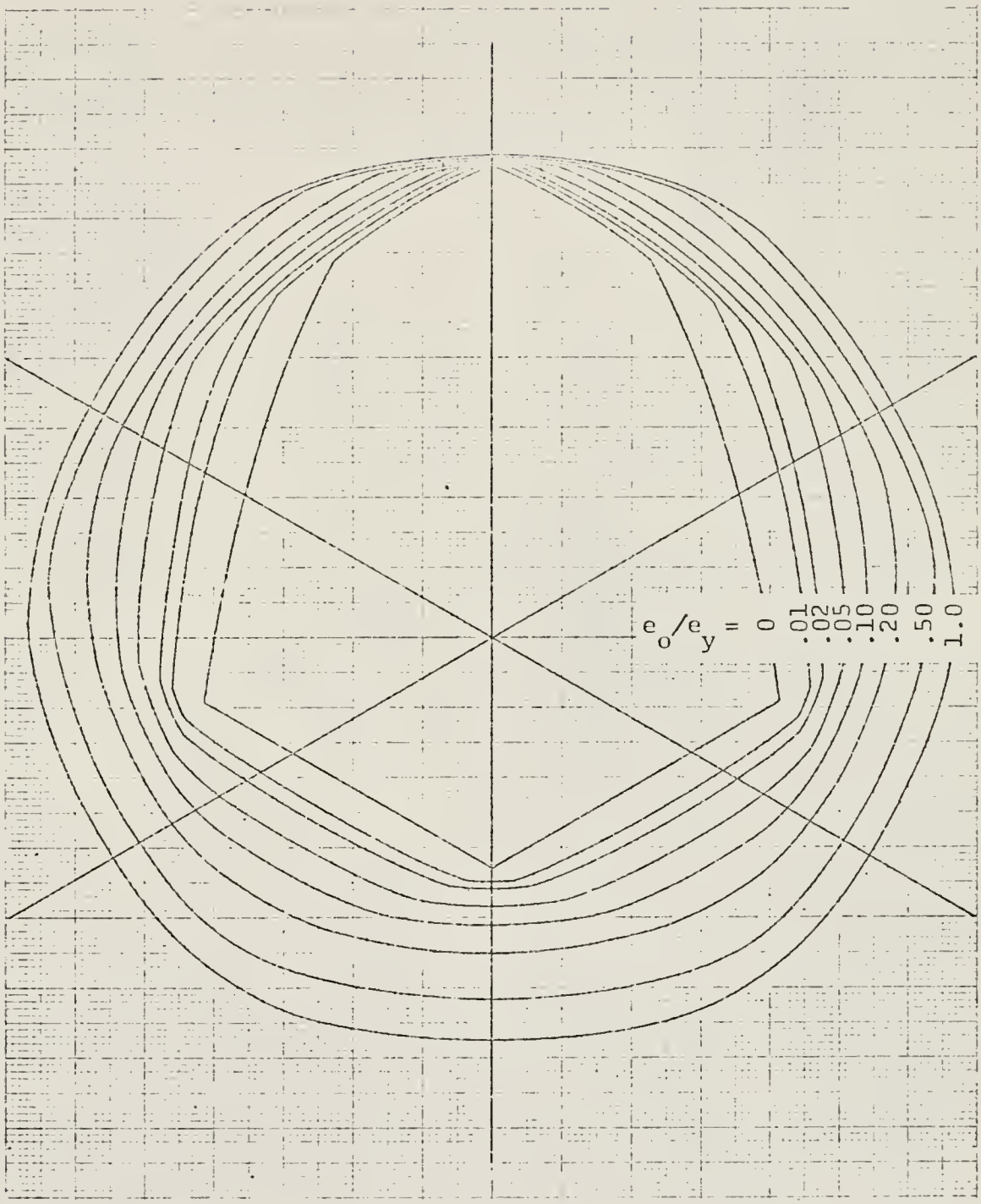

FIGURE 15. SURFACES OF CONSTANT OFFSET STRAIN AFTER AN AXIAL LOADING

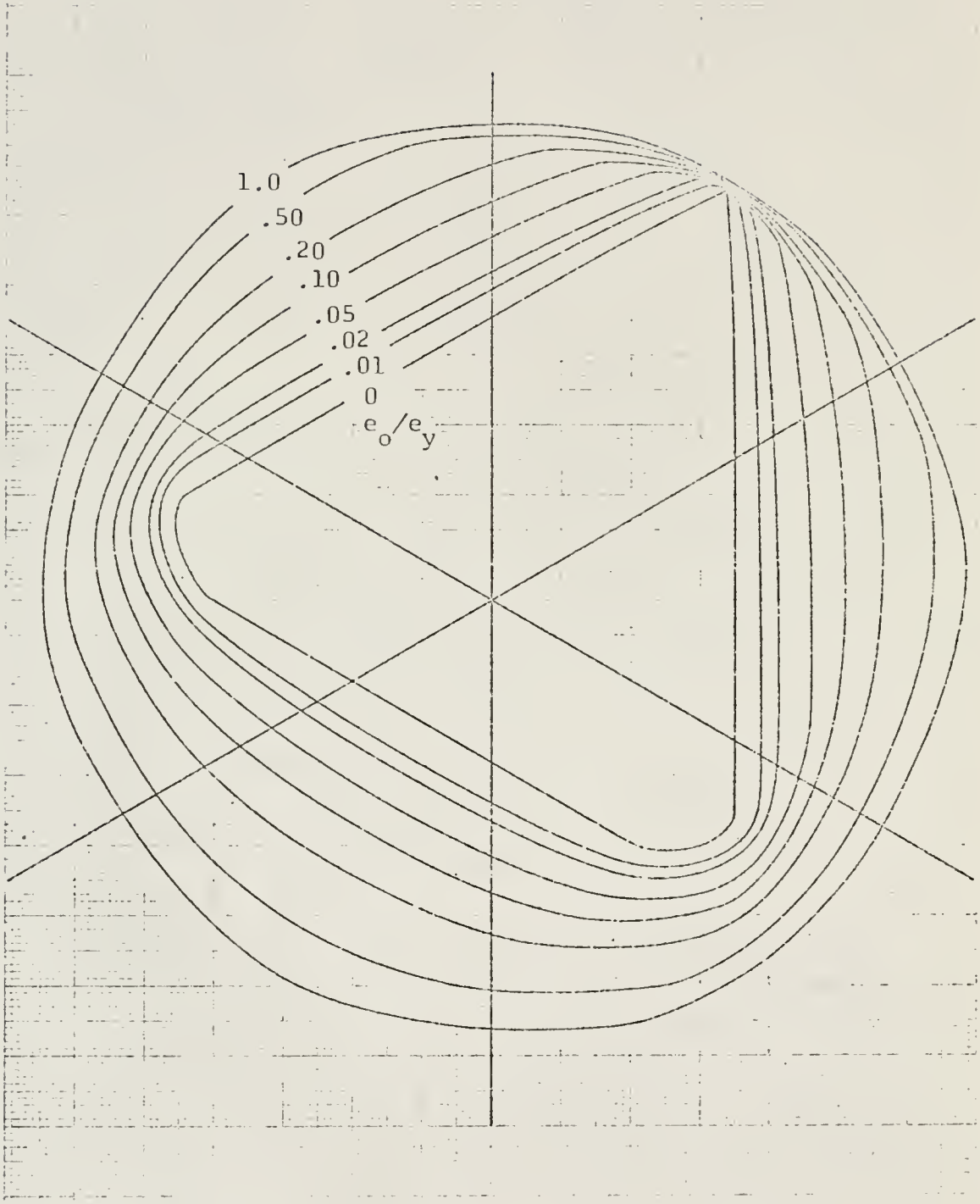

FIGURE 16. SURFACES OF CONSTANT OFFSET STRAIN AFTER A PURE SHEAR LOADING

time $t = 0$. The curves are shown as 120-degree segments rather than as complete closed curves in order to include data for three values of the work-hardening parameter λ on one graph. If completed, the curves would be symmetric about the origin in the same sense as the Tresca hexagon. We see that the "initial yield surface" can assume a variety of shapes depending on the offset strain used to define yield. It is apparent that any definition based on an offset strain in the range $.02 < e_o/e_y < 1.0$ will predict an initial yield surface that is closer to a Mises circle than to a Tresca hexagon. This is approximately the range of offset strain encountered in most experimental determinations of yield.

Figures 15 and 16 show curves of constant offset strain after the material has experienced plasticity during an initial axial loading and an initial pure shear loading, respectively. Here the data are computed for $\lambda = 0$ only. We see that the "subsequent yield surfaces" are not symmetric about the origin in the deviatoric stress plane, which implies the yield conditions are anisotropic. We observe in each case that the yield surfaces have expanded in the directions of loading and contracted or flattened in the directions opposite the loading. This phenomenon may be called the generalized Bauschinger effect. We also observe that the theoretical yield surface, defined by zero offset strain, exhibits a sharp corner at the point of loading, but that each yield surface defined by a finite offset strain, typical

of an experimental determination, exhibits a "blunt corner" at the point of loading. The latter observation agrees with conclusions by the majority of experimentalists who have investigated the question of whether there are corners in the yield surface. See Ivey [32], Bertsch and Findley [45], Mair [51], and Phillips, et al. [52,53].

An interesting and informative presentation of elastic-plastic stress-strain behavior involves the plotting of yield surfaces in the deviatoric planes for a sequence of stress or strain increments. Such a presentation can suggest rules-of-thumb that might be applicable in a general loading situation. Program A-4 of Appendix A is a modification of Program A-2 that computes a sequence of yield surfaces from a given sequence of strain increments with fixed principal stress and strain axes. The program first computes a given state of stress and strain, and then probes in various directions to find the yield surface — defined as the exact boundary of the elastic domain. Then the procedure is repeated for the next increment of stress or strain. Program A-4 was used to generate yield surfaces for several loading paths as described below.

Appendices C and D present yield surfaces computed for $\lambda = 0$ and for thirteen different loading paths. Three of the loading paths are purely radial and ten involve abrupt changes of direction. The yield surfaces are plotted in the deviatoric plane in both principal stress and principal strain space,

which enables one to construct the complete stress-strain histories. The plots were machine-made directly from the output of the computer program, which at least eliminates human errors and the tedium of hand-plotting. In some ways the yield surfaces in principal strain space, contained in Appendix D, are the most interesting. Here the yield surfaces gradually develop and pull away from the former yield surfaces when a new loading direction is taken.

By studying Appendices C and D, we see that most of the yield surfaces are composed of both straight and curved line segments. A sharp corner with curved sides tends to form around the point of loading, whereas the back sides of the yield surfaces generally retain the character of the initial yield surface (the Tresca hexagon). The generalized Bauschinger effect mentioned above is evident throughout Appendices C and D. For axial loadings the yield surfaces tend to shrink laterally, but for pure shear loadings the lateral shrinkage, or cross effect, is small. For all radial loadings the elastic range in the direction of loading is constant.

Phillips and co-workers investigated experimentally the effects of temperature and plastic deformation on the shape of the yield surface for annealed, commercially pure aluminum. The changes in the yield surfaces observed experimentally by Phillips, et al. [52,53] and Ivey [32] during plastic loadings are similar in some respects to the theoretical results contained in Appendices C and D. Among the

experimental observations are: (1) increased curvature at the point of loading and flattening on the backside of the yield surface, (2) translation of the yield surface away from the origin in the direction of loading in principal stress space, (3) no cross effect for either shear or axial loadings, (4) reduction of the elastic range in the direction of loading for both shear and axial loadings.

While these experimental observations do not entirely agree with the theoretical results, the differences are not serious. The author believes that further computations could be made that would bring the present theory into much better agreement with the experimental results of Phillips, et al. Item (1) above is essentially in agreement with the present theoretical results. Item (2) could be predicted theoretically by choosing a value of λ in the range $1 \leq \lambda \leq 2$. The differences between item (3) and the theoretical results could perhaps be traced to the fact that the experimental results are plotted in the shear-stress versus axial-stress plane whereas the theoretical results are plotted in the deviatoric planes. Item (4), dealing with reduction of the elastic range, is more serious. Prediction of this effect would require a major modification of the theory, which is not justified at this time since the simpler present version of the theory has not yet been fully explored.

CHAPTER VII

STRESS-STRAIN BEHAVIOR FOR BIAXIAL LOADINGS AND FOR A GENERAL LOADING HISTORY

Suppose we are given an arbitrary sequence of deviator strain increments comprising a deviator strain history at a material point.

$$\begin{aligned} &\underline{E}^{(o)} = 0, \quad \underline{E}^{(m)} = \underline{E}^{(m-1)} + d\underline{E}^{(m)}, \quad m = 1,2,3,\ldots \\ &d\underline{E}^{(m)} = [de_{ij}^{(m)}], \quad (i,j = 1,2,3) \end{aligned} \tag{7.1}$$

The following equations govern the elemental stress vectors and the resultant stresses. The notation is the same as in previous chapters.

$$\left.\begin{aligned} &\underline{f}^{(o)}(\underline{n}) = 0, \quad \underline{f}^{(m)} = \bar{g}\begin{cases} 1 & \text{if } g_t \le Y \\ Y/g_t & \text{if } g_t > Y \end{cases}, \quad m = 1,2,3,\ldots \\ &\bar{g} = \underline{f}^{(m-1)} + \chi d\underline{E}^{(m)}\cdot\underline{n} + \eta\underline{n}(\underline{n}\cdot d\underline{E}^{(m)}\cdot\underline{n}), \quad g_t = [\bar{g}\cdot\bar{g} - (\bar{g}\cdot\bar{n})^2]^{\frac{1}{2}} \end{aligned}\right\} \tag{7.2}$$

$$\left.\begin{aligned} &\underline{t}_1 = \frac{1}{\pi}\int_o^{2\pi} d\phi \int_o^{\pi/2} d\theta\, \underline{f}\sin\theta, \quad \underline{t}_2 = \frac{1}{\pi}\int_{-\pi/2}^{\pi/2} d\phi \int_o^{\pi/2} d\theta\, \underline{f}\sin\theta \\ &\underline{t}_3 = \frac{1}{\pi}\int_o^{\pi} d\phi \int_o^{\pi} d\theta\, \underline{f}\sin\theta \end{aligned}\right\} \tag{7.3}$$

We assume all vectors and tensors are referred to two coordinate systems: a given fixed Cartesian coordinate system[1] and an

---

[1] By a fixed coordinate system we actually mean a set of coordinate axes fixed relative to the material in the undeformed state. For use in the deformed state we require the coordinate axes to be rotated by the same rotation that carries the principal strain axes from the undeformed state to the deformed state. This distinction was not necessary in Chapters V and VI as all vectors were referred to the principal strain coordinates and these axes were fixed in the material.

arbitrary Cartesian coordinate system specified by the base vectors $\underline{N}_\alpha$ $(\alpha = 1,2,3)$. The spherical coordinates θ, ϕ in equations (7.3) are defined relative to the arbitrary coordinate system only. By symmetry considerations we can rewrite equations (7.3) as follows:

$$\left.\begin{aligned} \underline{t}_1 &= I_1 + I_2 + I_3 + I_4 \\ \underline{t}_2 &= I_1 - I_2 - I_3 + I_4 \\ \underline{t}_3 &= I_1 + I_2 - I_3 - I_4 \end{aligned}\right\} \tag{7.4}$$

where $$I_i = \frac{1}{\pi}\int_0^{\pi/2} d\phi \int_{S_i} d\theta\, \underline{f} \sin\theta, \quad (i = 1,2,3,4)$$

$$S_1 = (0,\pi/2), \quad S_3 = (\pi, 3\pi/2)$$

$$S_2 = (\pi/2,\pi), \quad S_4 = (3\pi/2, 2\pi) \quad .$$

The reason for considering the decomposition (7.4) is that it allows us to reduce the integration domain from seven octants to four octants on the unit sphere. Computer storage as required for the numerical integrations is reduced accordingly. For computational purposes we introduce a finite grid of points over one hemisphere of the unit sphere, and we introduce a set of unit vectors defined by these grid points. If $P = \pi/2N$, then

$$\begin{aligned} &\theta_i = i\,P, \quad \phi_j = j\,P, \quad (i = 0,\ldots,N;\ j = 0,\ldots,4N) \\ &\underline{n}_{ij} = (\cos\theta_i, \sin\theta_i\cos\phi_j, \sin\theta_i\sin\phi_j) \quad . \end{aligned} \tag{7.5}$$

We are now in a position to describe a numerical procedure for computing the stress history corresponding to a

given general strain history. The procedure, based on the ideas presented in Chapter II, follows:

1. Initialize the strain $\underline{E}^{(o)} = 0$, and initialize the elemental stress vectors $\underline{f}_{ij}^{(o)} = 0$ at each point $\underline{n}_{ij}$ of the finite grid. Let the arbitrary coordinate system coincide initially with the given fixed coordinate system. Thus $\underline{R} = [N_{i\alpha}] = I$, where I is the unit or identity matrix. Let $m = 1$.
2. Compute the elemental stress vectors $\underline{f}_{ij}^{(m)}$ at each point $\underline{n}_{ij}$ of the finite grid using equations (7.2) and the given strain increments $d\underline{E}^{(n)}$, $n = 1,\ldots,m$. The components of $d\underline{E}^{(n)}$ and $\underline{f}_{ij}^{(m)}$ are referred to the $\underline{N}_{\alpha}$-axes.
3. Compute the resultant stress vectors $\underline{t}_k = (t_{1k}, t_{2k}, t_{3k})$ using equations (7.4) and one of the numerical integration formulae (6.6) or (6.8). The components of $\underline{t}_k$ are referred to the $\underline{N}_{\alpha}$-axes.
4. To find the principal stress axes, compute a new set of unit vectors $\underline{N}_{\alpha}$ by operating on the resultant stress matrix $T = [t_{ik}]$ using the Jacobi method of matrix diagonalization [71, pp. 120-125]. The vectors $\underline{N}_{\alpha}$, which represent the arbitrary coordinate system, are the eigenvectors of the diagonalization process.
5. Compute the norm $M = (t_{12} + t_{21})^2 + (t_{23} + t_{32})^2 + (t_{31} + t_{13})^2$ and test it against a small convergence constant δ.

If $M > \delta$, then the vectors $\underline{N}_\alpha$ do not coincide sufficiently well with the principal stress axes; repeat steps 2, 3, 4. If $M \leq \delta$, then the vectors $\underline{N}_\alpha$ are sufficiently coincident with the principal stress axes so that we may continue.

6. Compute the deviator strain and stress tensors as follows:

$$\underline{E}^{(m)} = \underline{E}^{(m-1)} + d\underline{E}^{(m)}, \qquad \underline{S}^{(m)} = \underline{R} \cdot \underline{S}' \cdot \underline{R}^T$$

$$\underline{S}' = T - I \ \text{trace}(T)/3, \qquad \underline{R} = [N_{i\alpha}]$$

Here $\underline{S}'$ represents the deviator stress tensor referred to the $\underline{N}_\alpha$-axes; $\underline{S}^{(m)}$ and $\underline{E}^{(m)}$ are the deviator stress and strain tensors referred to the given fixed coordinate system.

7. Repeat steps 2 through 6 for $m = 2,3,4,\ldots$.

The above procedure has been incorporated into two computer programs, which are listed in Appendix A. Program A-6 uses the general procedure exactly as described above, but Program A-5 is restricted to biaxial loadings. Biaxial loadings are loadings for which one of the principal stress axes and one of the principal strain axes are fixed and coincident. For Program A-5 the strain is restricted by the relations $e_{23} = e_{32} = e_{31} = e_{13} = 0$, and the N_3-axis of the arbitrary coordinate system is required to coincide with the 3-axis of the given fixed coordinate system. Thus

$$\underline{R} = [N_{i\alpha}] = \begin{bmatrix} \cos\psi & -\sin\psi & 0 \\ \sin\psi & \cos\psi & 0 \\ 0 & 0 & 1 \end{bmatrix} .$$

The Jacobi method of diagonalizing the matrix T is replaced in Program A-5 by a method that simply involves finding the angle ψ.

$$\psi = \tfrac{1}{2}\tan^{-1}\left(\frac{t_{12}+t_{21}}{t_{11}-t_{22}}\right)$$

Except for the simplifications of the biaxial program just mentioned, Programs A-5 and A-6 are the same.

Program A-5 has been used to generate theoretical data for a variety of biaxial loadings. We distinguish between four classes of biaxial loadings as follows:

1. Biaxial strain e_{11} constant: $e_{11}=-2e_{22}=-2e_{33}=K$, $e_{12}=e_{21}=e(t)$;
2. Biaxial strain e_{12} constant: $e_{11}=-2e_{22}=-2e_{33}=e(t)$, $e_{12}=e_{21}=K$;
3. Biaxial stress s_{11} constant: $s_{11}=-2s_{22}=-2s_{33}=K$, $\frac{1}{2}(s_{12}+s_{21})=s(t)$;
4. Biaxial stress s_{12} constant: $s_{11}=-2s_{22}=-2s_{33}=s(t)$, $\frac{1}{2}(s_{12}+s_{21})=K$.

Here e(t), s(t) are functions of time, initially zero, and K is an appropriate constant. For each of these loadings we have $e_{23}=e_{32}=e_{31}=e_{13}=0$ and consequently $s_{23}=s_{32}=s_{31}=s_{13}=0$. These biaxial loadings are typical of the experimental situation whereby a plate is loaded by "middle surface" tensions and shears, and the situation in which a tube is loaded by axial force, axial torque, and/or internal pressure.

The input of Program A-5, as in fact the input of all computer programs in Appendix A, consists of a sequence of

deviator strain increments. Hence, the biaxial strain loadings, being defined explicitly in terms of strain components, are simple to compute. We merely input the given deviator strain increments and obtain the corresponding deviator stresses as output. Computations involving the biaxial stress loadings are more complicated. Here we must iteratively "mould" the input strain increments so as to predict constant stresses. If the stresses that are supposed to be constant during a loading instead tend to increase (decrease), then we must decrease (increase) the corresponding strain increments and run the computer program again. This process is continued until the appropriate stresses are essentially constant.

The reader should consult Tables B-6 and B-7 in Appendix B, where values of deviator stress and strain are tabulated for four biaxial strain loadings. The tables were generated for two values of axial strain ($e_{11}/e_k = 2,4$) and two values of the work-hardening parameter ($\lambda = 0,1$). The results were computed using $N = 30$ and the increments in e_{12} were as shown in the tables. Partial runs were made with $N = 40$ and with smaller increments in e_{12} as a check on convergence, which was found to be excellent. With axial strain held constant, we see that as shear strain increases the shear stress increases and the normal stresses decrease. The quantities θ_s and θ_e are the angles of rotation (in degrees) of the

principal stress and strain axes, respectively, about the 3-axis. We note that both θ_s and θ_e increase gradually throughout each loading and that, in general, the two sets of principal axes do not coincide.

The most unusual feature of Tables B-6 and B-7 is the occurrence of a nonsymmetric stress tensor. The quantities $\frac{1}{2}(s_{12} + s_{21})$ and $\frac{1}{2}(s_{12} - s_{21})$ are, respectively, the symmetric and antisymmetric parts of the shear stress. The latter quantity may be viewed as a stress couple tending to rotate the principal stress axes in a sense opposite from θ_s. We see that the magnitude of $\frac{1}{2}(s_{12} - s_{21})$ rises to a maximum and then falls during each loading. The maximum value of $\frac{1}{2}(s_{12} - s_{21})$ varies from 2 to 8 percent of the average shear stress $\frac{1}{2}(s_{12} + s_{21})$, depending on the parameters e_{11} and λ. We conclude that the theory predicts a nonsymmetric stress for loadings such as discussed here, where the principal stress and strain axes rotate relative to the material. We shall not explore the nonsymmetric stress effect further in this dissertation, other than to point out that if this effect actually exists it may become a significant factor in technological problems involving plasticity of metals. In the following discussions of biaxial loading we shall refer to the symmetric part $\bar{s}_{12} = \frac{1}{2}(s_{12} + s_{21})$ as the shear stress and we shall ignore the antisymmetric part $\frac{1}{2}(s_{12} - s_{21})$.

Figures 17 through 22 show theoretical results computed for each of the four classes of biaxial loadings mentioned

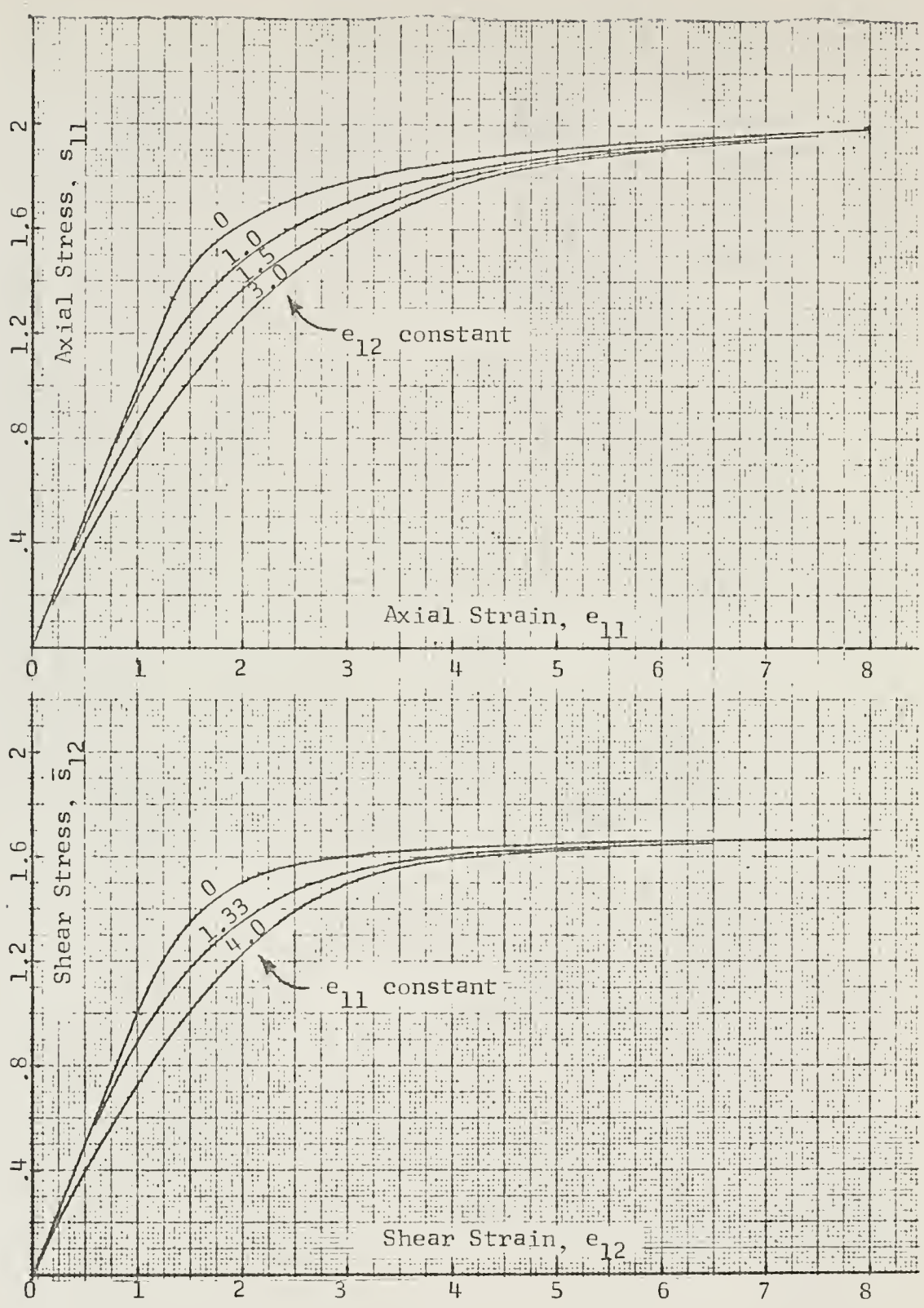

FIGURE 17. STRESS-STRAIN CURVES FOR BIAXIAL STRAIN LOADINGS

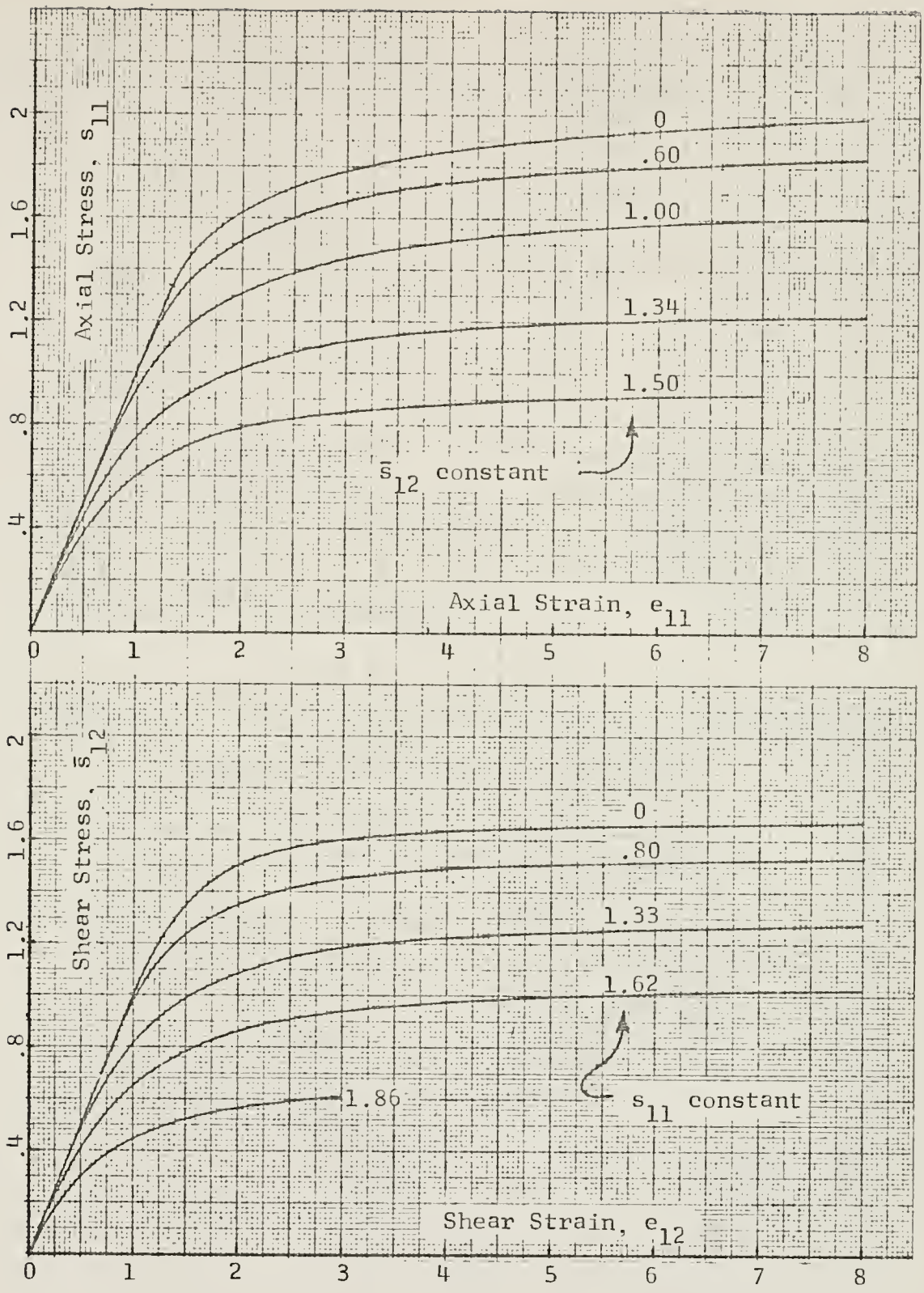

FIGURE 18. STRESS-STRAIN CURVES FOR BIAXIAL STRESS LOADINGS

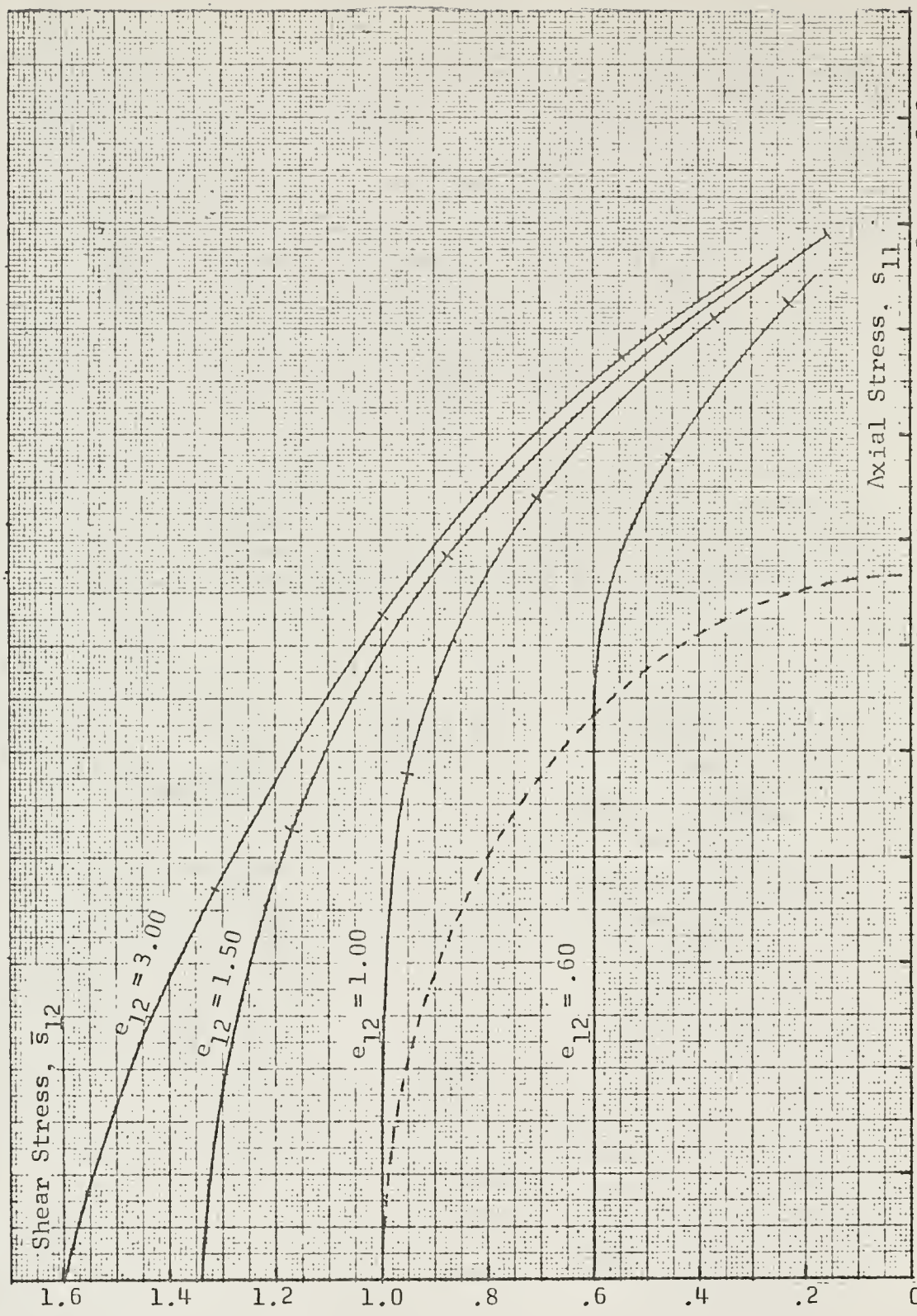

FIGURE 19. LOADING PATHS FOR BIAXIAL STRAIN WITH e_{12} CONSTANT

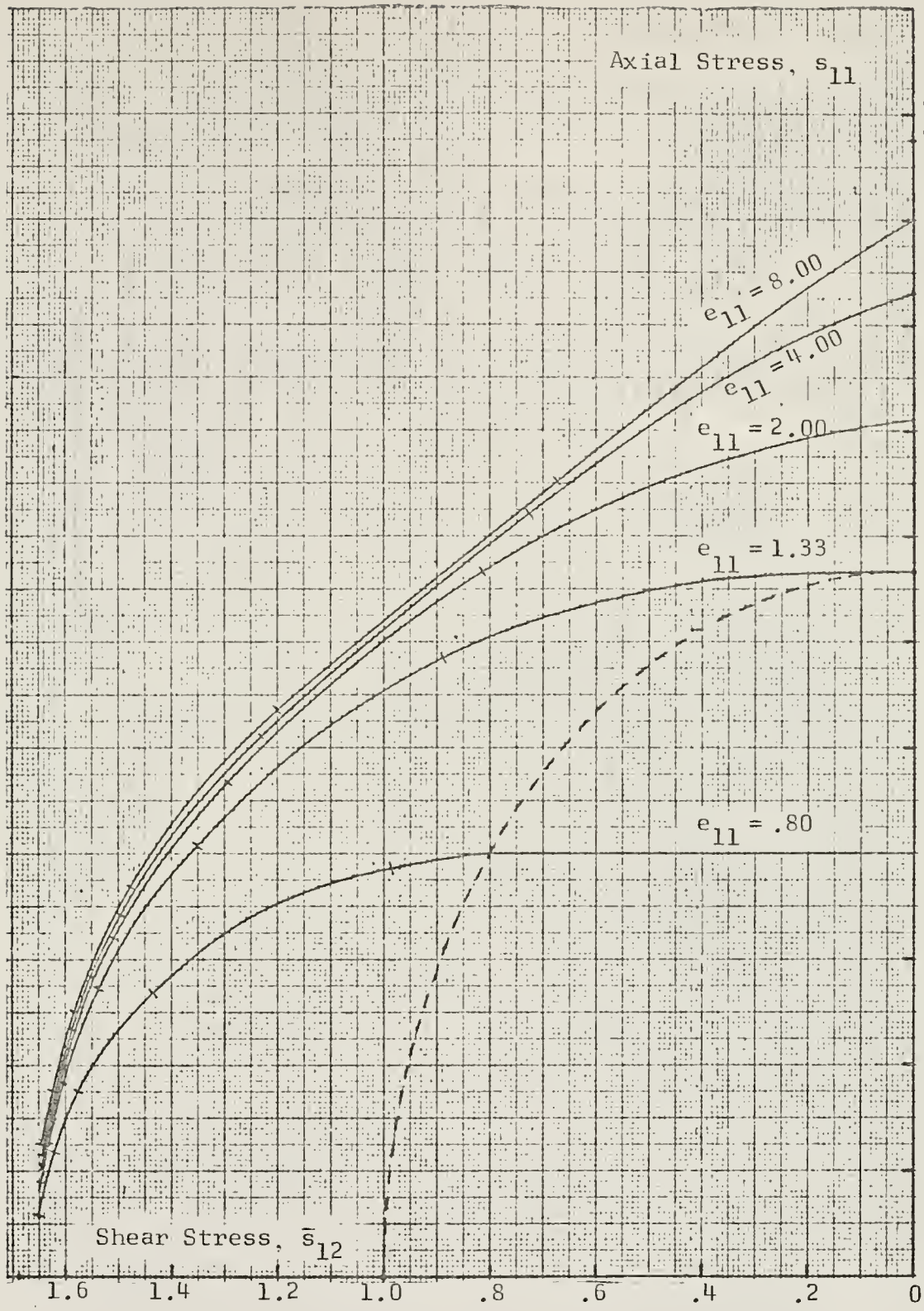

FIGURE 20. LOADING PATHS FOR BIAXIAL STRAIN WITH e_{11} CONSTANT

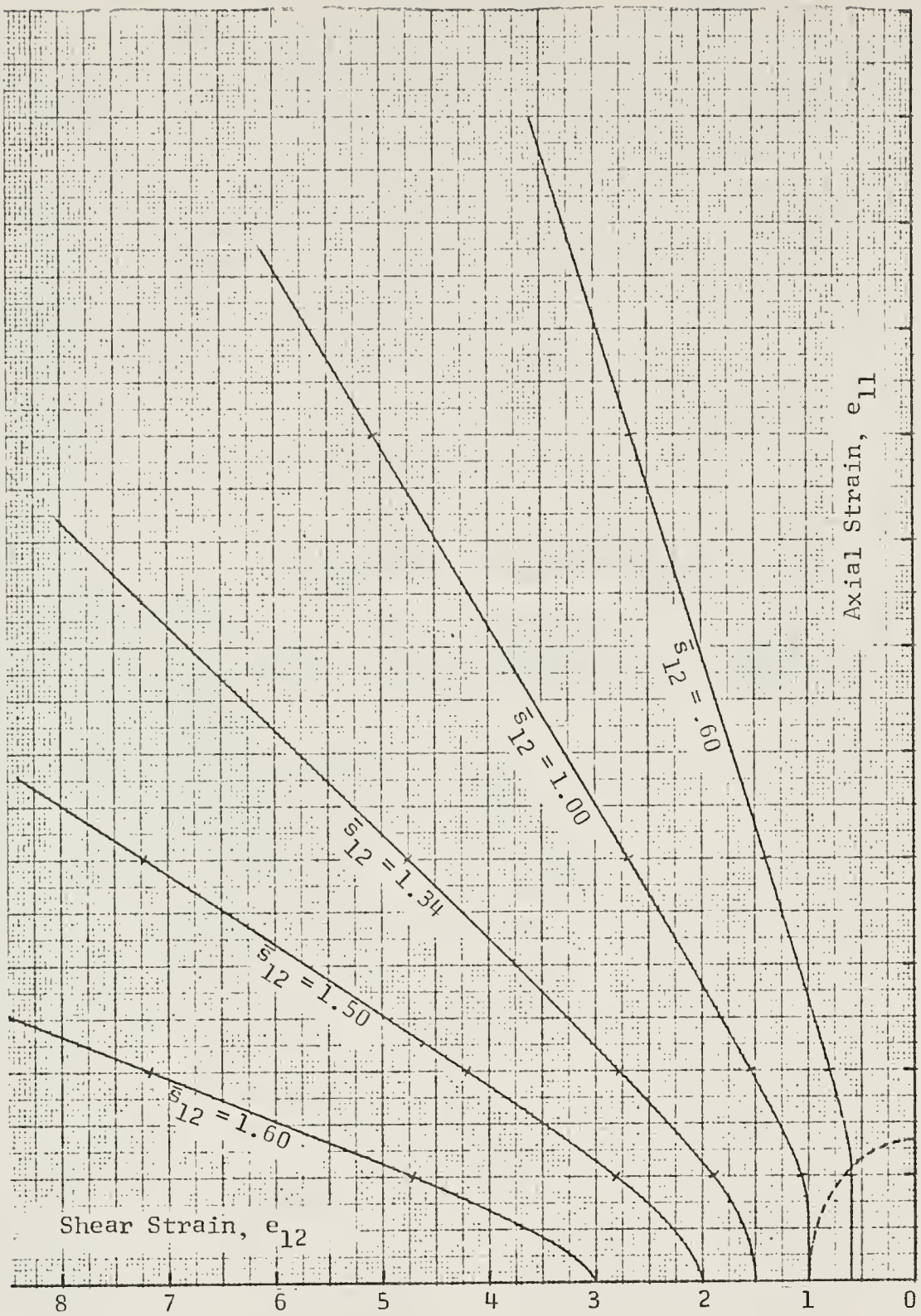

FIGURE 21. LOADING PATHS FOR BIAXIAL STRESS WITH s_{12} CONSTANT

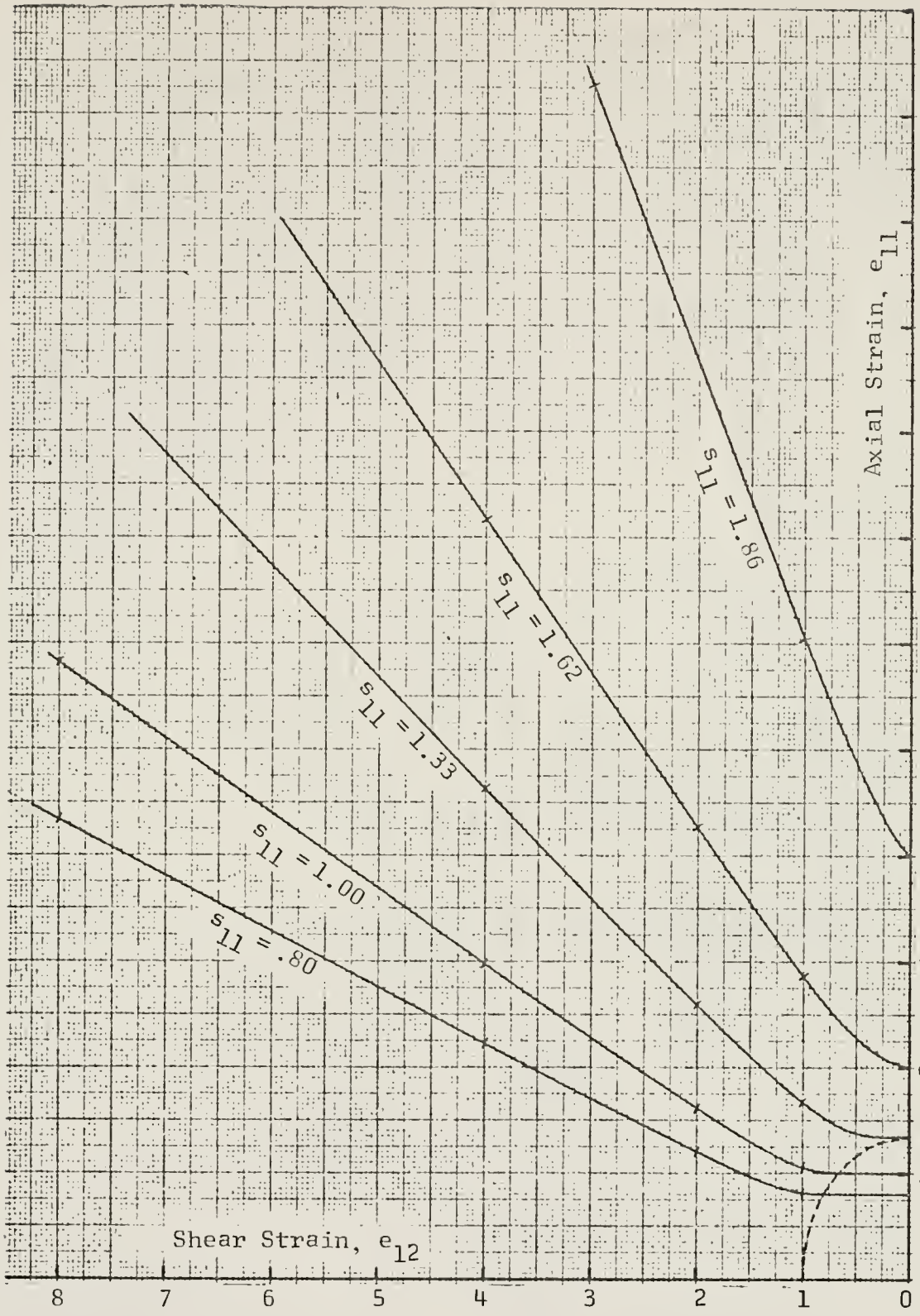

FIGURE 22. LOADING PATHS FOR BIAXIAL STRESS WITH s_{11} CONSTANT

above. The work-hardening parameter $\lambda = 1/3$ for these results was chosen to match the experimental data of Chapter VIII. The various graphs in Figures 17-22 illustrate the relationships between the four primary variables $e_{11}, e_{12}, s_{11}, \bar{s}_{12}$. Figures 17, 18 show graphs of deviator stress versus deviator strain; Figures 19, 20 show graphs of shear stress versus axial stress; and Figures 21, 22 show graphs of shear strain versus axial strain. For each figure appropriate deviator stresses or strains are held constant.

Figures 17 and 18 show curves of axial stress versus axial strain with either shear strain or shear stress constant, and curves of shear stress versus shear strain with either axial strain or axial stress constant. The curves in which strains are held constant (Figure 17) differ only slightly and they tend toward the same ultimate stress. The curves in which stresses are held constant (Figure 18) have a similar shape, but the stress for a given strain varies inversely with the constant stress parameter. Figures 19 and 20 show loading paths in stress space for e_{12} = constant and e_{11} = constant, respectively. These curves of shear stress versus axial stress are roughly parallel to the initial yield surface (shown as a dashed curve), and they tend toward a single point in stress space: $s_{11}/s_k \approx 2.15$ in Figure 19 and $\bar{s}_{12}/s_k \approx 1.69$ in Figure 20. Figures 21 and 22 show loading paths in strain space for $\bar{s}_{12}$ = constant and s_{11} = constant,

respectively. These graphs of shear strain versus axial strain initially are curved lines, but they become straight lines shortly after yield, projecting outward from the origin in directions that are roughly radial.

Figures 17 through 22 show a sufficient quantity of data that rough interpolations are possible not only upon the individual figures and graphs but also between the separate figures and graphs. For example, we know that data for a radial loading in the stress plane must fall between data in which $\bar{s}_{12}$ = constant and data in which s_{11} = constant, if all three loadings asymptotically approach the same point in stress space. Other examples are evident. One further observation is worthy of mention. If we compute, from the data of Figures 17-22, the ratio $\bar{s}_{12}/s_{11}$ and the slope de_{12}/de_{11} for any moderately large strain ($e_{11}^2 + e_{12}^2 > 100\, e_k^2$, say), we find these two quantities are numerically equal. That is,

$$\bar{s}_{12}/s_{11} = de_{12}/de_{11}, \text{ for large strains.}$$

Thus, the hypothesis proposed by Saint Venant in 1870, that the principal stress axes coincide with the principal axes of the strain increment, is valid for the present theory in the limit of large strains.

We now discuss cost penalties associated with the computer programs listed in Appendix A. The results presented here will allow the reader to estimate costs of running the various programs for his specific needs. We define the

cost penalty as the CPU (central processing unit) time in seconds necessary to compute the stress (and the yield surface in the case of Program A-4) for a single increment of strain. Table 1 gives the average cost penalties experienced while preparing this dissertation.

TABLE 1

COST PENALTY
CPU TIME IN SECONDS PER STRAIN INCREMENT

Program	N = 20	N = 40
A-1	.0003-.0004	(not dependent on N)
A-2,3	.03-.04	.06-.08
A-4	3 - 4	6 - 8
A-5,6	1.0-1.5	2.0-3.0

Program A-1 is the most efficient as it involves explicit calculations in terms of the simple transcendental functions. Programs A-2 and A-3 and Programs A-5 and A-6 are listed together as each pair employs essentially the same computational procedure and hence incurs essentially the same costs. Program A-4 is the least efficient, because for each strain increment we compute 24 points around the perimeter of the yield surface in the deviatoric stress plane in addition to the stress at the point of loading. If we desire a larger number of points on the yield surface for increased resolution, then the cost penalty of Program A-4 increases proportionally.

Program A-5 has been used to compute stress-controlled loading paths as well as strain-controlled loading paths. Stress-controlled loading paths cost approximately 10 times as much as shown in Table 1, due to additional iterations required for convergence.

The cost penalties in Table 1 are dependent on the characteristics of the IBM-370 computer located on the University of Florida campus. The actual costs in dollars can be obtained by multiplying the cost penalties in Table 1 by a factor of .20-.50 dollars per second, depending on the compiling cost, number of pages printed and cards punched, etc. Generally, the unit cost is reduced toward the factor .20 dollars per second as the amount of computations in a single run is increased. For uniformity I assumed all programs to be written in FORTRAN IV and compiled using the G-level compiler. If the WATFIV compiler is used or if the program is written in BASIC and submitted from a remote terminal, then the costs will be approximately two times or eight times higher, respectively, than those mentioned above.

CHAPTER VIII

COMPARISONS BETWEEN THE THEORY AND EXPERIMENTAL RESULTS FOR COMMERCIALLY PURE ALUMINUM

In Chapters II, III, IV, we introduced a new theory of plasticity and in Chapters V, VI, VII, we demonstrated this theory by computing stress-strain behavior for a variety of loading paths. Now we will attempt to relate this new theory to the actual stress-strain behavior of a real material. The material to be compared with the theory is commercially pure polycrystalline aluminum, designated as type 1100 by The Aluminum Association. This material contains at least 99.0 percent aluminum, with the main impurities being iron, silicon, and copper [72, Section 6]. The material was received in the form of ½-inch diameter extruded rods. Except for machining into test specimens, the material was tested exactly as fabricated without any heat treatment or annealing. The main advantage of the commercially pure aluminum is that it exhibits a smooth, reproducible stress-strain curve which is similar in shape to the curves of Figures 4 and 5. The main disadvantage of this material for comparison with the present theory is that it has a pronounced strain-rate effect; that is, the

stress in the plastic range depends on the rate of strain as well as on the strain itself.[1] This means that in order to obtain comparable data from different tests, all tests must be run at approximately the same constant strain rate.

A theory cannot be proven to represent a given material on the basis of agreement with experimental data in a single type of test, due to the extreme complexity of stress-strain behavior in general. This complexity of behavior becomes evident when we consider that plasticity involves a nonlinear — in fact, discontinuous — relationship between two second-order tensors, in which as many as eighteen variables — the tensor components — can be involved simultaneously. If we are to establish a definite correspondence between a theory and an actual material, then we must show agreement between theoretical and experimental results for at least two distinctly different loading paths, where the material (at the start of each test) and the theoretical parameters are maintained constant throughout [60, p. 10]. In a strict sense, we can never establish the exact degree of conformity between a theory and a real material by means of a finite number of tests and comparisons. However, agreement in a variety of loading situations does lend confidence that such conformity exists.

---

[1] Experiments show the strain rate effect is given approximately by $\sigma/\sigma_o = \log(k\dot{e})$, where $k \approx 10^{34}$ seconds, in the "static" range $e = 10^{-5}$ to 10^{-1} second^{-1}. Thus, each decade increase in strain rate increases the stress by approximately 3.3 percent.

In considering which experimental tests to perform I decided that at least one series of tests should involve reversed loadings. One of the main points to be resolved here is whether the Bauschinger effect, as predicted by the present theory and shown in Figures 7 and 8, reflects actual material behavior better than the existing incremental theories. The simplest tests that involve reversed loadings are pure tension followed by pure compression and conversely, which can be performed on a conventional testing machine. Therefore, I decided that the first series of tests should be tension-compression loadings of a solid cylindrical rod.

For the second series of tests I decided upon combined tension-torsion loadings of a thin-wall tube. This type of test is simple to perform, and the loading paths can be significantly different from purely axial loadings. Here the purpose was not to prove the superiority of the present theory over existing theories, since it has been shown [32] that the isotropic-hardening, Mises-yield, plastic potential theory provides fairly accurate predictions for biaxial loadings where the strain paths are essentially radial. Rather, the purpose of the tension-torsion tests was to find out whether the radial element theory <u>also</u> gave fairly accurate predictions for biaxial loadings. Results of tension-torsion tests can be compared with theoretical biaxial data such as shown in Figures 17-22. The main difficulty encountered

during the tension-torsion tests was the building of a special machine to apply the loadings.

Figure 23 shows the experimental setup for the tension-compression tests. The testing machine is a Tinius-Olsen Model U-Celotronic, mechanically driven, with a maximum capacity of 12000 pounds in tension or compression. This machine permits selection of discrete crosshead speeds in the range .002 to 20 inches per minute. The load applied to the specimen is recorded on a 12-inch-wide constant speed chart. The mechanical extensometer (shown in Figure 23b) is specially made and employs a Starrett No. 25-631 dial indicator with a resolution of .0005 inch and a range of 1 inch. The dial indicator is constrained to move directly with the specimen in a 2-inch gage length, thus giving a strain resolution of .00025 per division and a strain range of 50 percent. Figure 24 shows the specimen details and auxiliary apparatus. The specimen dimensions were chosen to accommodate the 2-inch gage length and yet to minimize buckling. The rectangular device in Figure 24a is a fixture for making punch marks on the specimen at cross sections exactly 2 inches apart. The extensometer is supported on the specimen by inserting pins into these punch marks.

The test procedure for the tension-compression tests consisted of the following steps: (1) mount the specimen on the testing machine while maintaining zero load; (2) mount the extensometer on the specimen and zero the extensometer

(a). Testing machine

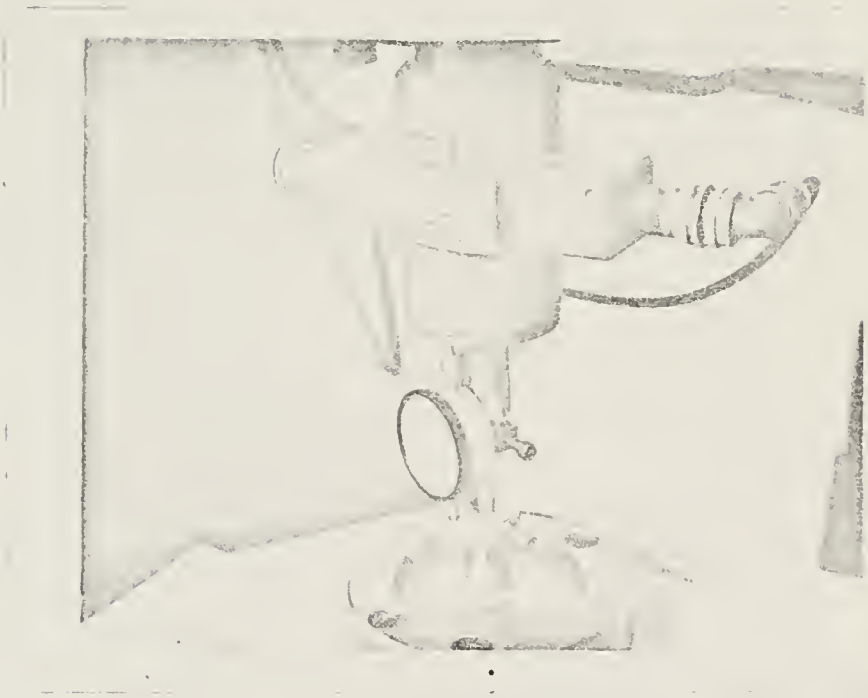

(b). Load cell and extensometer

FIGURE 23. APPARATUS FOR TENSION-COMPRESSION EXPERIMENTS

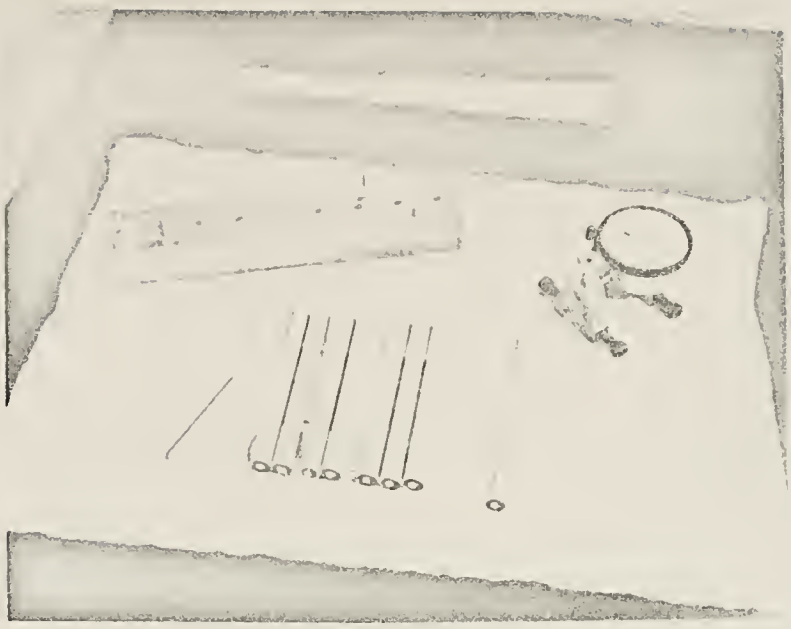

(a). Specimen and auxiliary apparatus

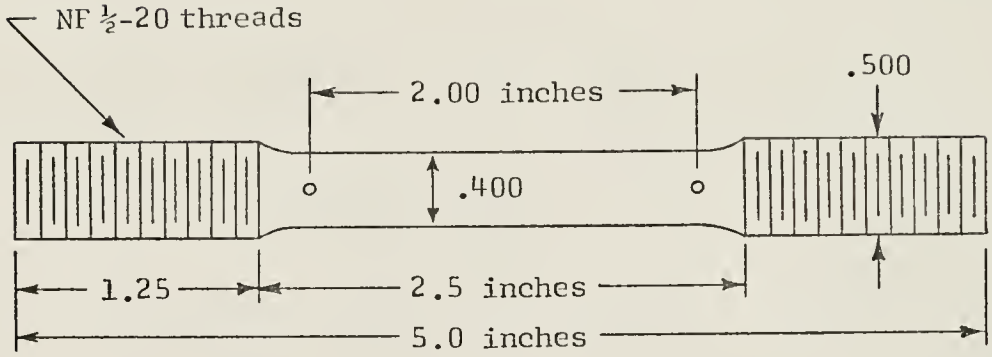

(b). Dimensions of cylindrical specimen

Note: Punch marks are made at two diametrally opposite locations and at two cross sections to support the extensometer.

FIGURE 24. SPECIMEN FOR TENSION-COMPRESSION EXPERIMENTS

dial; (3) zero the recorder pen at the center of the load chart and start the chart moving at an appropriate constant speed; (4) start the crosshead moving at a constant speed of .02 inch per minute for either tension or compression loading; (5) mark the load chart when appropriate strain readings appear on the extensometer using the event marker provided with the testing machine; (6) after an appropriate strain has accumulated, reverse the direction of loading while keeping the crosshead speed constant; and (7) repeat steps 5 and 6 twice. A small frictional drag in the extensometer was compensated during each reversed loading by resetting the dial indicator to zero at the moment the load on the specimen passed through zero, and then later allowing for this change while reducing and plotting the data. The crosshead speed of .02 inch per minute produced strain rates in the range .002 to .010 minute^{-1}, depending on the slope of the stress-strain curve. The stress was calculated as "true stress," or current load divided by current cross-sectional area. The strain measure was "engineering strain," or elongation divided by the initial gage length.

Figures 25-28 show experimental data for fifteen tension-compression tests. Eight tests were tension followed by compression followed by tension; seven tests were compression followed by tension followed by compression. The data of Figures 25-28 are seen to be consistent and reproducible. The stress-strain behavior is seen to be very nearly the same

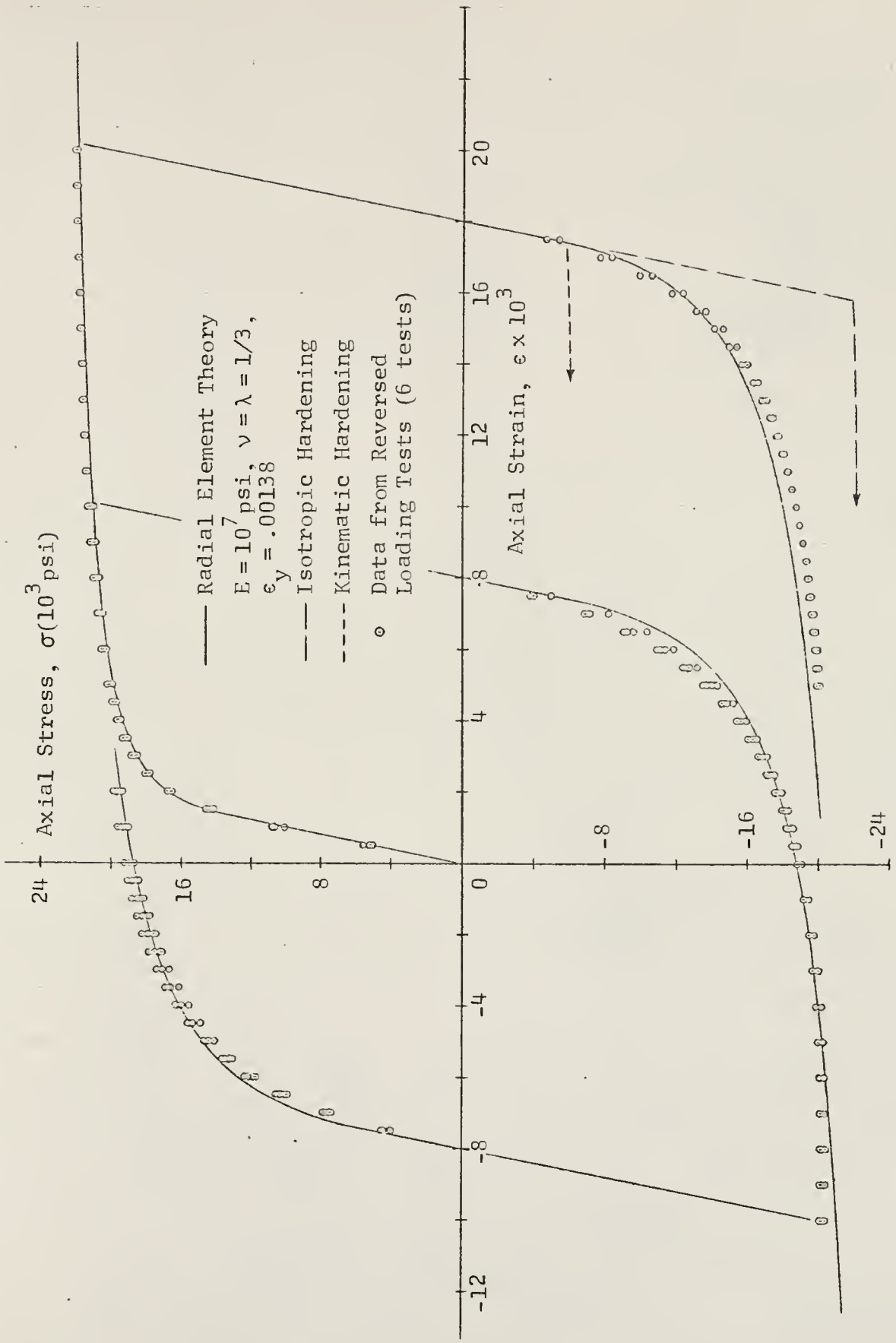

FIGURE 25. COMPARISON OF EXPERIMENT AND THEORY FOR TENSION-COMPRESSION-TENSION TESTS

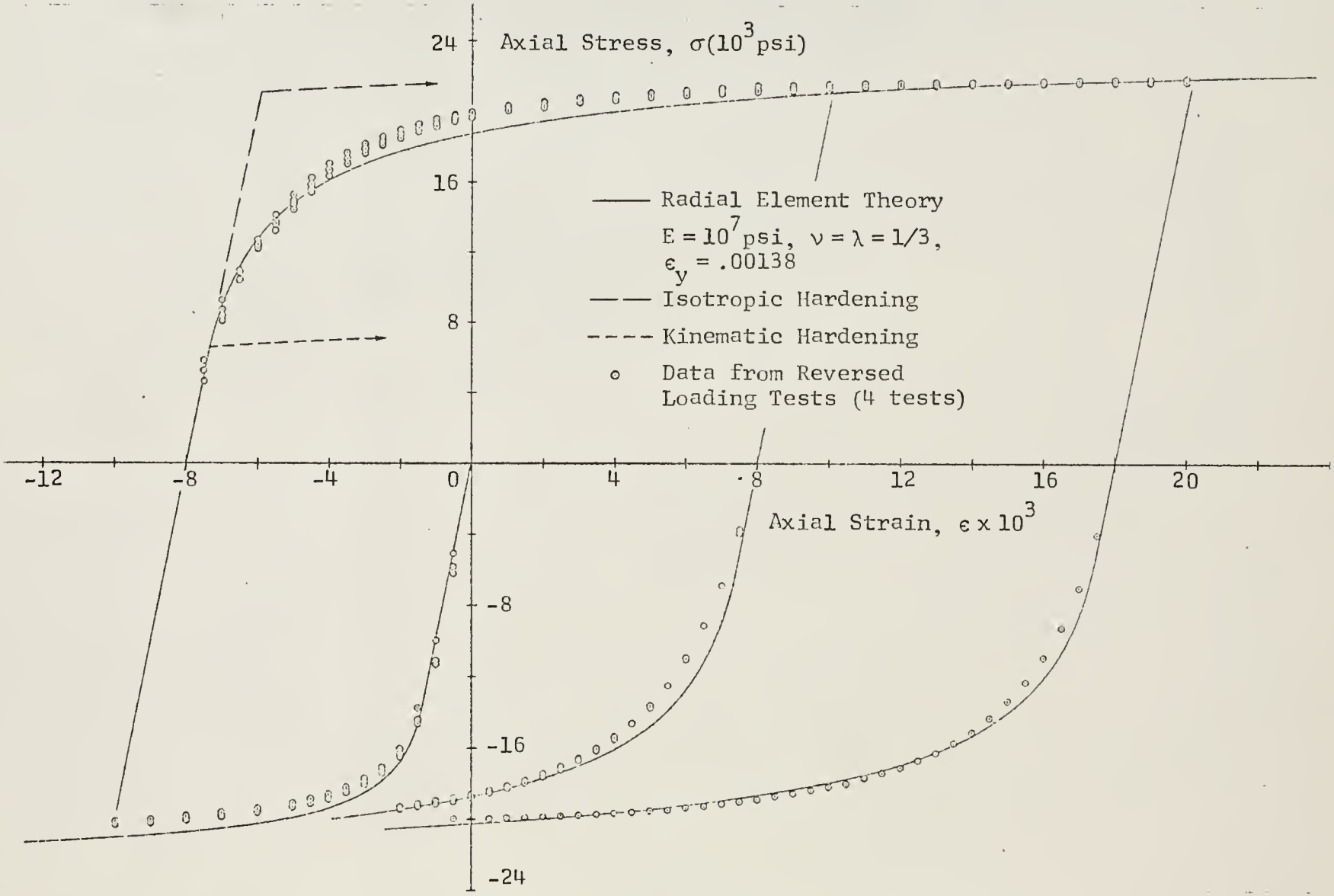

FIGURE 26. COMPARISON OF EXPERIMENT AND THEORY FOR COMPRESSION-TENSION-COMPRESSION TESTS

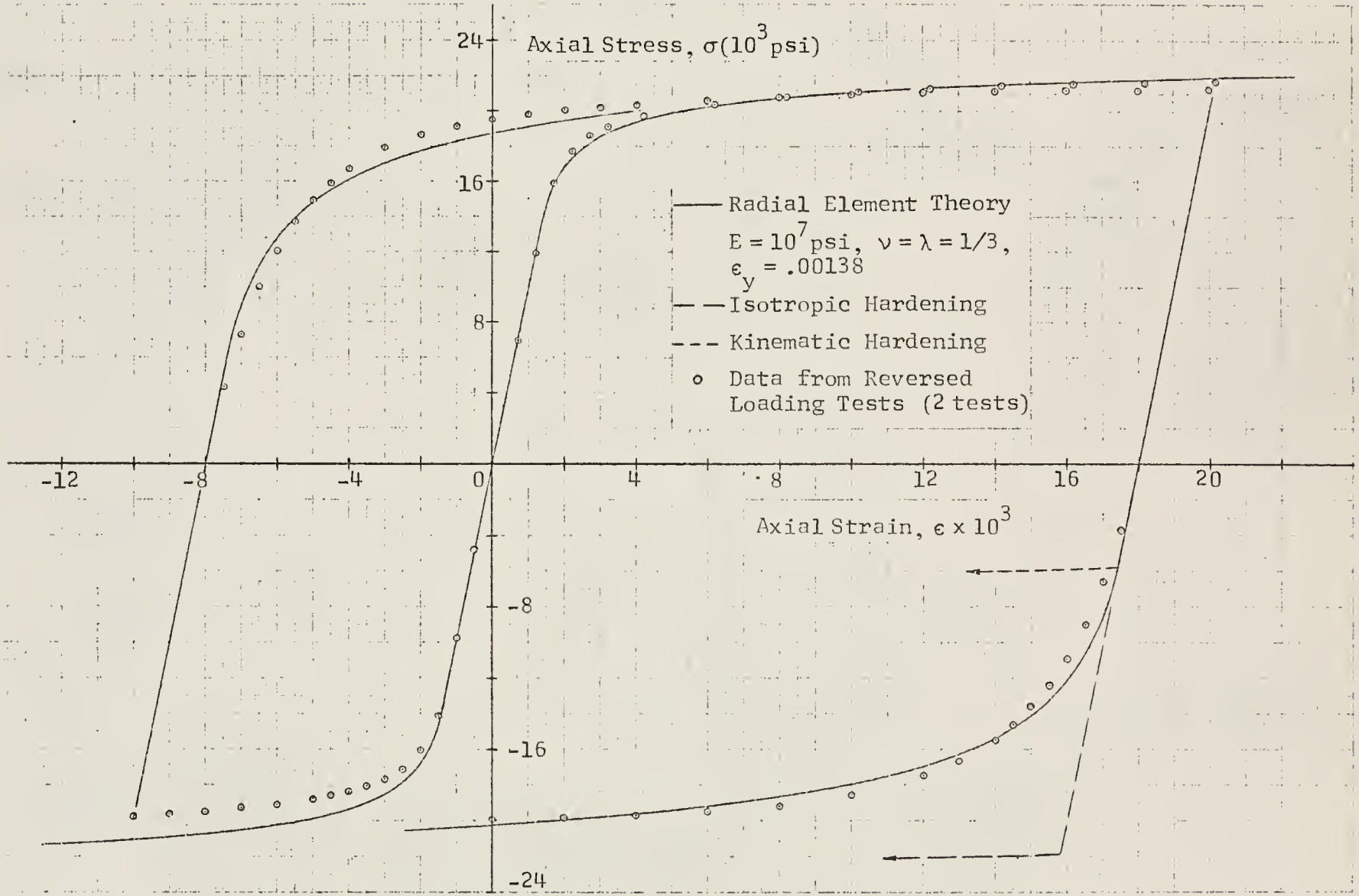

FIGURE 27. COMPARISON OF EXPERIMENT AND THEORY FOR AXIAL LOADING AND REVERSED AXIAL LOADING

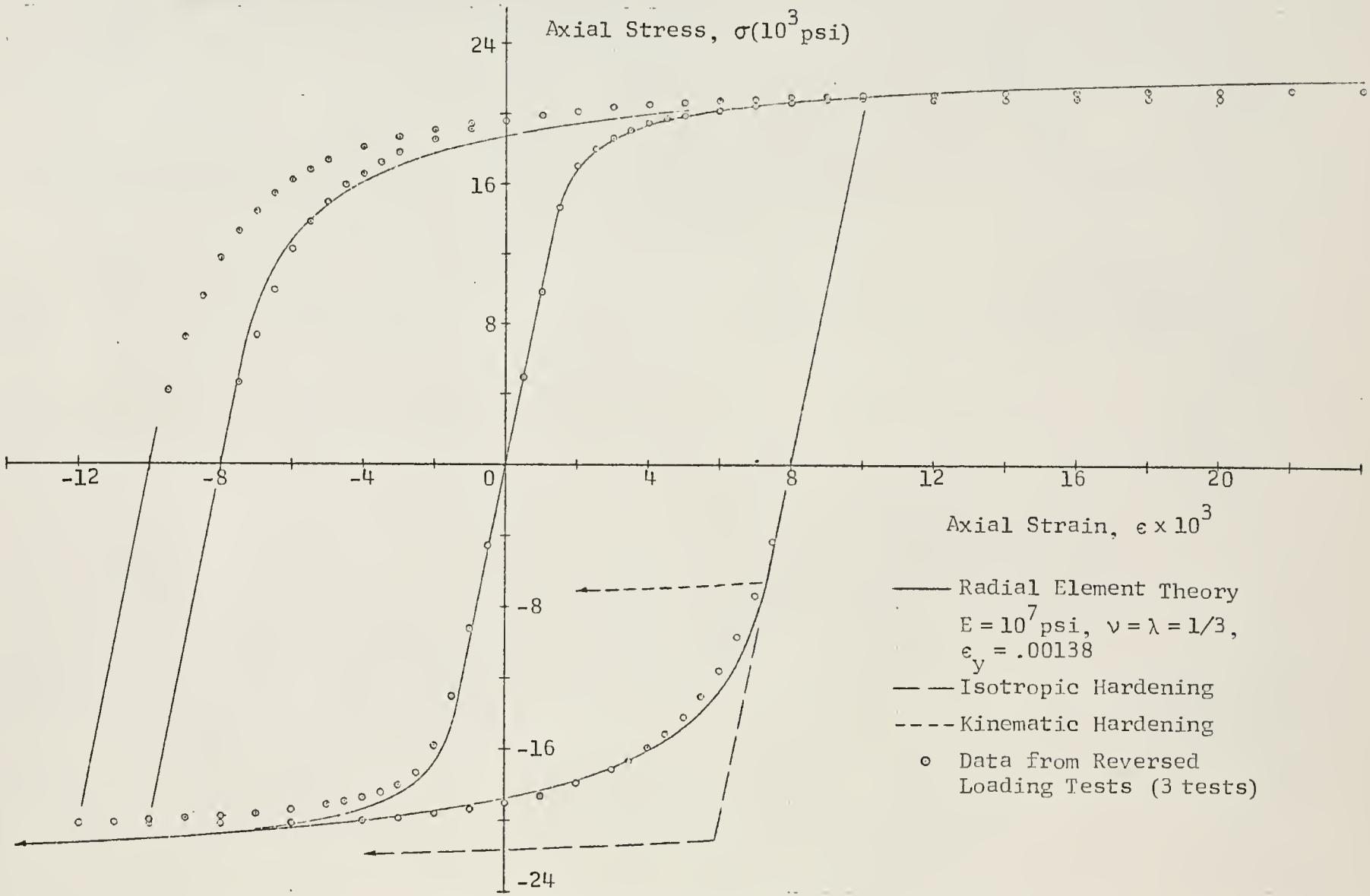

FIGURE 28. COMPARISON OF EXPERIMENT AND THEORY FOR AXIAL LOADING AND REVERSED AXIAL LOADING

for compression as for tension, which proves the material is initially isotropic at least in the axial direction. The exception here is that the slope $d\sigma/d\varepsilon$ becomes flat sooner for compression than for tension, which probably is due to plastic buckling and associated inhomogeneities of stress and strain. The Bauschinger effect is evident and occurs smoothly in a manner reminiscent of the Masing hypothesis. (Recall equations 5.20 of Chapter V.) This result is not surprising in view of similar results reported in the literature of cyclic loading; for example, see [35] and [36]. The following result is worth mentioning although not shown in Figures 25-28. During some of the tests we reloaded after unloading to zero stress, and in each case the stress followed the elastic line almost exactly to the maximum stress previously reached before plastic deformation resumed. This effect, which is also reported in [38], confirms the discontinuous nature of plastic material behavior.

Also included in Figures 25-28 are theoretical results for the radial element theory (solid lines) computed with the fixed parameters $E = 10^7$ psi, $\nu = \lambda = 1/3$, $\varepsilon_y = .00138$. The results were computed using a modified version of Program A-1 that includes both axial and reversed axial loadings. Actual stresses and strains were obtained from equations (5.11). The elasticity constants E, ν for aluminum can be found in any materials handbook, for example [72]. The plasticity constants λ, ε_y were found by the following fitting procedure:

stress-strain curves were computed for several combinations of λ, ϵ_y; then the correct values of λ, ϵ_y were determined by selecting the curve which best fitted the experimental data. We see that overall the agreement between theory and experiment is very good; most of the experimental data fall within 5 percent of the theoretical results. Especially remarkable is the agreement for reversed loadings, where the Masing-type Bauschinger effect is seen to occur for both theory and experiment.

The dashed lines in Figures 25-28 are reversed-loading curves for two types of incremental theory: the isotropic hardening theory and Prager's kinematic hardening theory. Particular yield surfaces are immaterial here, since for pure axial loading and reversed axial loading the shape of the yield surface cannot influence the reversed loading curves. As can be seen from the graphs, neither of these two incremental theories fits the data nearly as well as the present theory.

A second series of tests involved tension-torsion loadings of thin-wall tubes. The tubular specimens were fabricated from the same ½-inch-diameter extruded-rod stock of commercially pure aluminum as the specimens of the first test series. Tubes were drilled, reamed, and machined externally to the dimensions 3/8-inch inside diameter and .040-inch wall thickness. The specimens were loaded by a specially built testing machine shown in Figure 29. The mechanical strainometer and specimen details are shown in Figure 30.

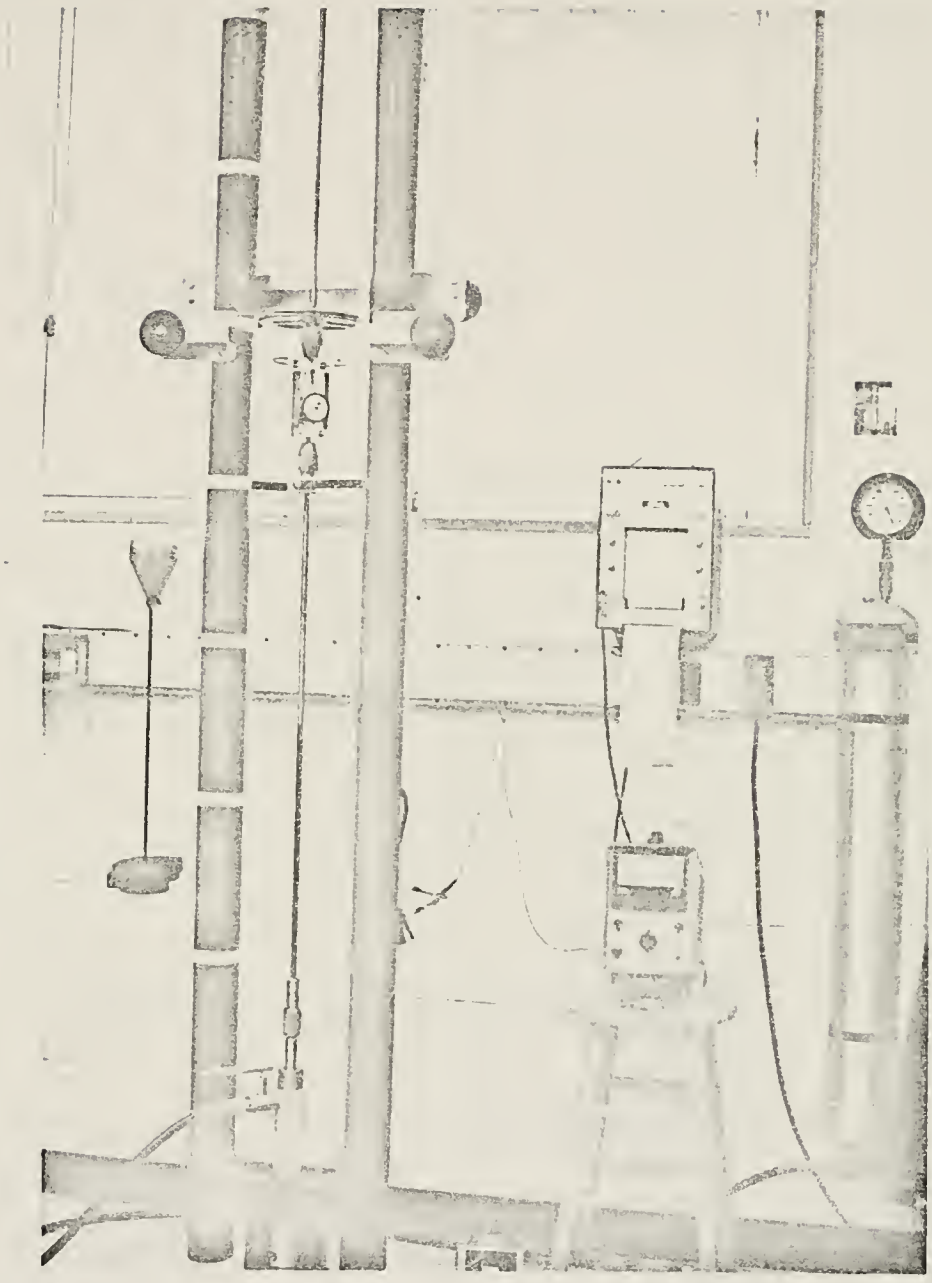

FIGURE 29. TESTING MACHINE FOR BIAXIAL STRESS EXPERIMENTS

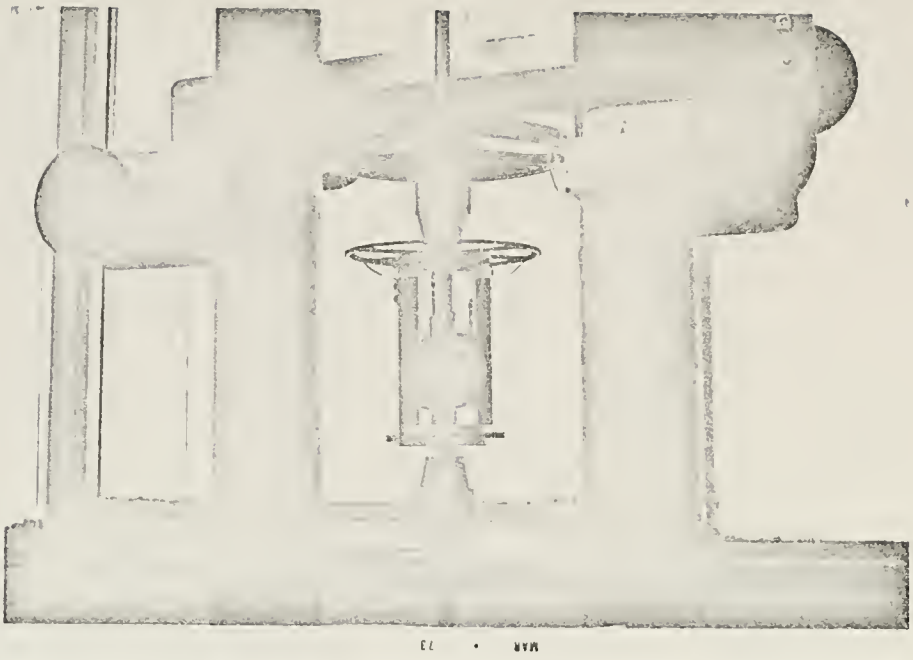

(a). Mechanical strainometer mounted on the tubular specimen

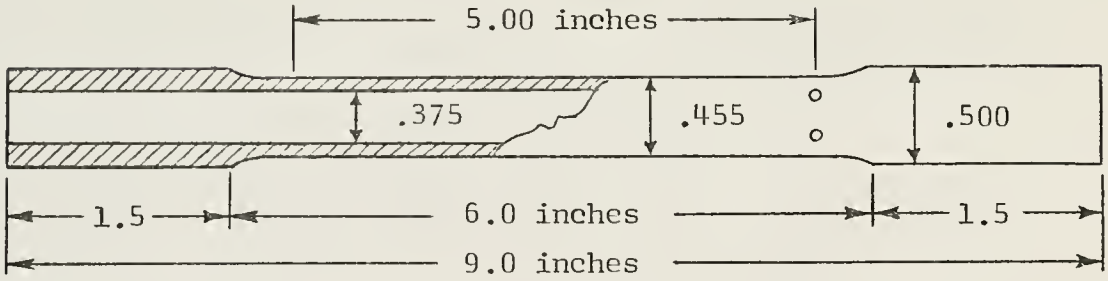

(b). Dimensions of the tubular specimen

Note: Punch marks are made at four equally spaced locations around the circumference and at two cross sections to support the strainometer.

FIGURE 30. STRAINOMETER AND SPECIMEN FOR BIAXIAL STRESS EXPERIMENTS

A description of the testing machine and instrumentation follows: The specimen is held between a pair of steel grips that can be tightened manually and that self-tighten as tension is applied. Each grip has a steel finger with longitudinal flutes that contacts the inside surface of the tubular specimen and prevents relative rotation. The grips are connected to the upper and lower parts of the machine by two long steel rods, which maintain accurate axial alignment of the specimen and the grips. The upper grip assembly is constrained to rotate but not translate by a thrust bearing located at the top of the machine (not shown). The lower grip assembly is constrained to translate but not rotate by a pair of horizontal levers located directly below the lower grip.

Axial load is applied by means of a hydraulic system consisting of a pump (not shown), an accumulator (shown at right in Figure 29), and a needle valve and hydraulic tension cylinder (shown at lower left in Figure 29). Axial load can be varied either in increments or continuously in the range zero to 3000 pounds (tension only). Torque is applied to the specimen by putting weights onto a load pan; the load pan is connected to the upper grip assembly through a system of strings and pulleys as shown in Figures 29 and 30a. The torque range is zero to approximately 370 inch-pounds, where the upper limit is achieved with 100 pounds on the load pan. The machine is capable of torsion in either direction if an additional load pan (not shown) is connected.

The axial load was measured and recorded by an electrical system consisting of a BLH type U3G1 load cell mounted at the top of the machine, a 6-volt dry cell, a Hewlett-Packard Model 425A microvoltmeter used as a preamplifier, and a Brush Model 220 chart recorder. The load-recording system was calibrated via dead weights before each test, and axial load was recorded on the constant-speed chart during each test. The usual chart speed was 5 mm/minute. Resolution of the load chart is about ± 5 pounds in a full scale range of 1000 pounds. During each test the torsional load was computed as the product of the radius of the main pulley and the total weight on the load pan, without any independent measurements. This procedure rests on the assumption that friction in the thrust bearing and the auxiliary pulleys is negligibly small. A special test involving an aluminum alloy tube instrumented with strain gages confirmed that friction in the torque apparatus was indeed small (± 2 percent) compared with the applied torque over the entire range of axial loads.

Extension and twist of the tubular specimen were measured using a specially built mechanical strainometer shown in Figure 30a. The strainometer has two main parts. The upper part consists of a polished aluminum disk and an attached fine-tooth gear. The lower part consists of an aluminum disk, two parallel spacers, two identical dial gages, and two pointers. The two parts are drilled so as to freely

straddle the specimen. Each part is supported on the tubular specimen by four pins, which are inserted into four matching punch marks on the specimen and held in place by rubber bands. The dial gages are spring-loaded against the disk of the upper part; readings of the dial gages provide two measures of the axial extension. The pointers touch the lower surface of the fine-tooth gear; relative positions of the pointers and the gear teeth give two measures of the axial twist. Effects of specimen bending and strainometer misalignment are minimized by averaging the two values of the extension and the twist.

Let δ_1, δ_2 be the dial gage readings in inches, and let n_1, n_2 be the twist angles measured in number of gear teeth having passed pointers 1 and 2 during the deformation. Then the axial strain and shear strain are given by

$$\epsilon_{11} = (\delta_1 + \delta_2)/2L \qquad \text{axial strain}$$

$$\epsilon_{12} = (n_1 + n_2)\,\pi d/4NL \qquad \text{shear strain}$$

where $L = 5$ inches is the gage length, $d = (OD + ID)/2$ is the average diameter of the specimen, and $N = 288$ is the total number of teeth on the gear. The minimum reading of each dial gage was about .0005 inch, which implies .0001 axial-strain resolution. Resolution of the twist measurements was about $\frac{1}{2}$-tooth, which implies approximately .0002 shear-strain resolution.

A torsion-tension test is defined as a constant torsional loading accompanied by a tension loading that increases

monotonically from zero. The procedure for performing a combined torsion-tension test follows: (1) retract the hydraulic tension cylinder; (2) calibrate the load cell; (3) insert and tighten the specimen in the lower grip; (4) mount the strainometer on the specimen; (5) insert and tighten the specimen in the upper grip, taking care not to plastically deform the specimen (This involves extending the tension cylinder while simultaneously aligning and tightening the upper grip.); (6) zero the strainometer dials and pointers; (7) apply a given constant torque on the specimen by placing an appropriate weight on the load pan; (8) close the needle valve on the tension cylinder and pressurize the accumulator to 2500 psi; (9) start the constant-speed load chart on the Brush recorder; (10) while watching the strainometer, apply an increment of axial strain by opening and closing the needle valve; (11) after an appropriate time (1-3 minutes) which allows the creep behavior to stabilize, read and record the axial load, the extension, and the twist; (12) repeat steps 10 and 11 until specimen failure.

Figures 31-34 show results of 14 torsion-tension tests including three pure tension tests. (Pure tension is a torsion-tension test with zero torque.) The experimental data are shown as open circles, triangles, and squares. Dashed curves are faired through the experimental points to illustrate the trend of the data. The number adjacent to each curve indicates the constant shear stress corresponding

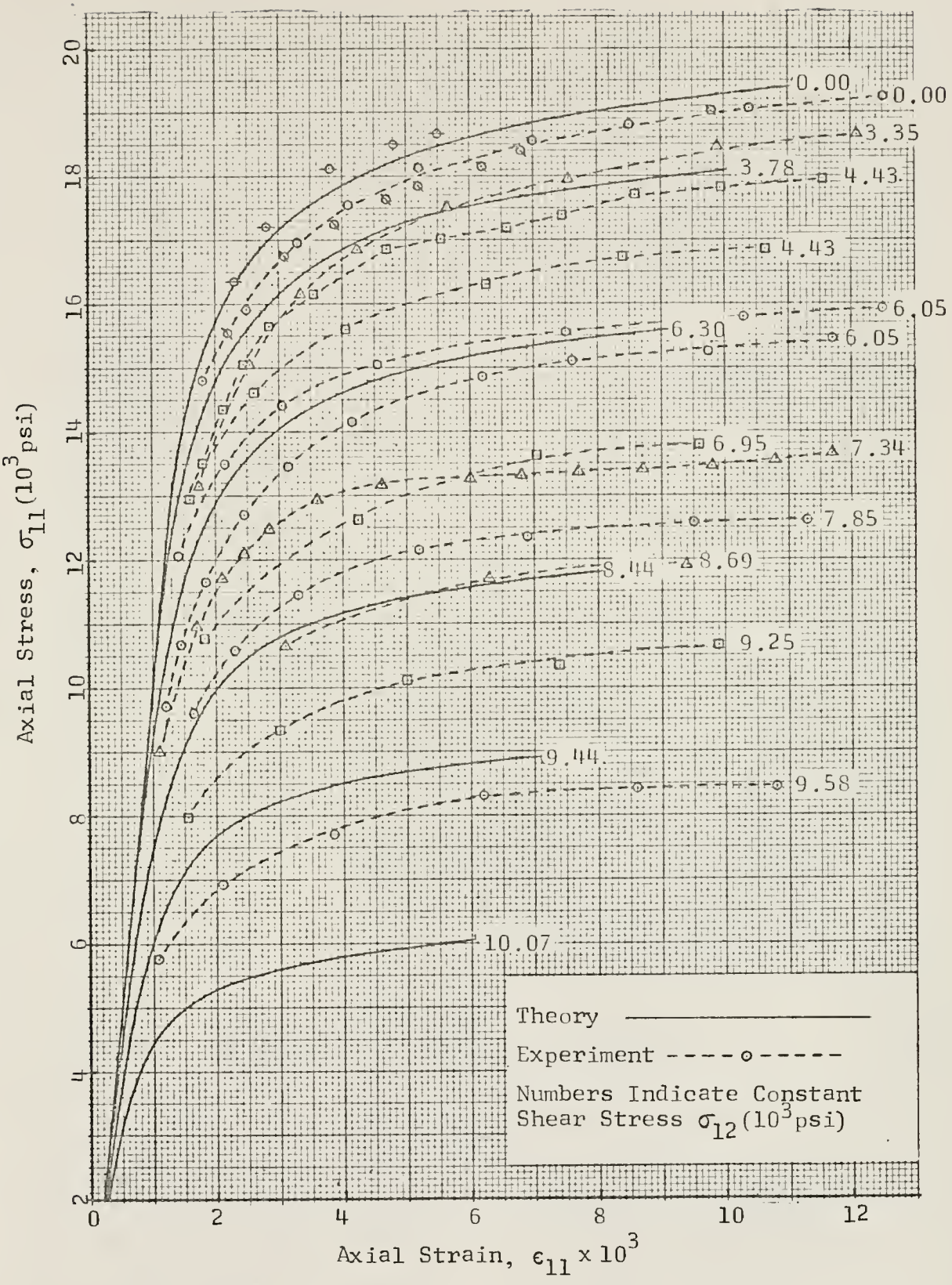

FIGURE 31. COMPARISON OF EXPERIMENT AND THEORY FOR BIAXIAL TESTS, AXIAL STRESS VERSUS AXIAL STRAIN

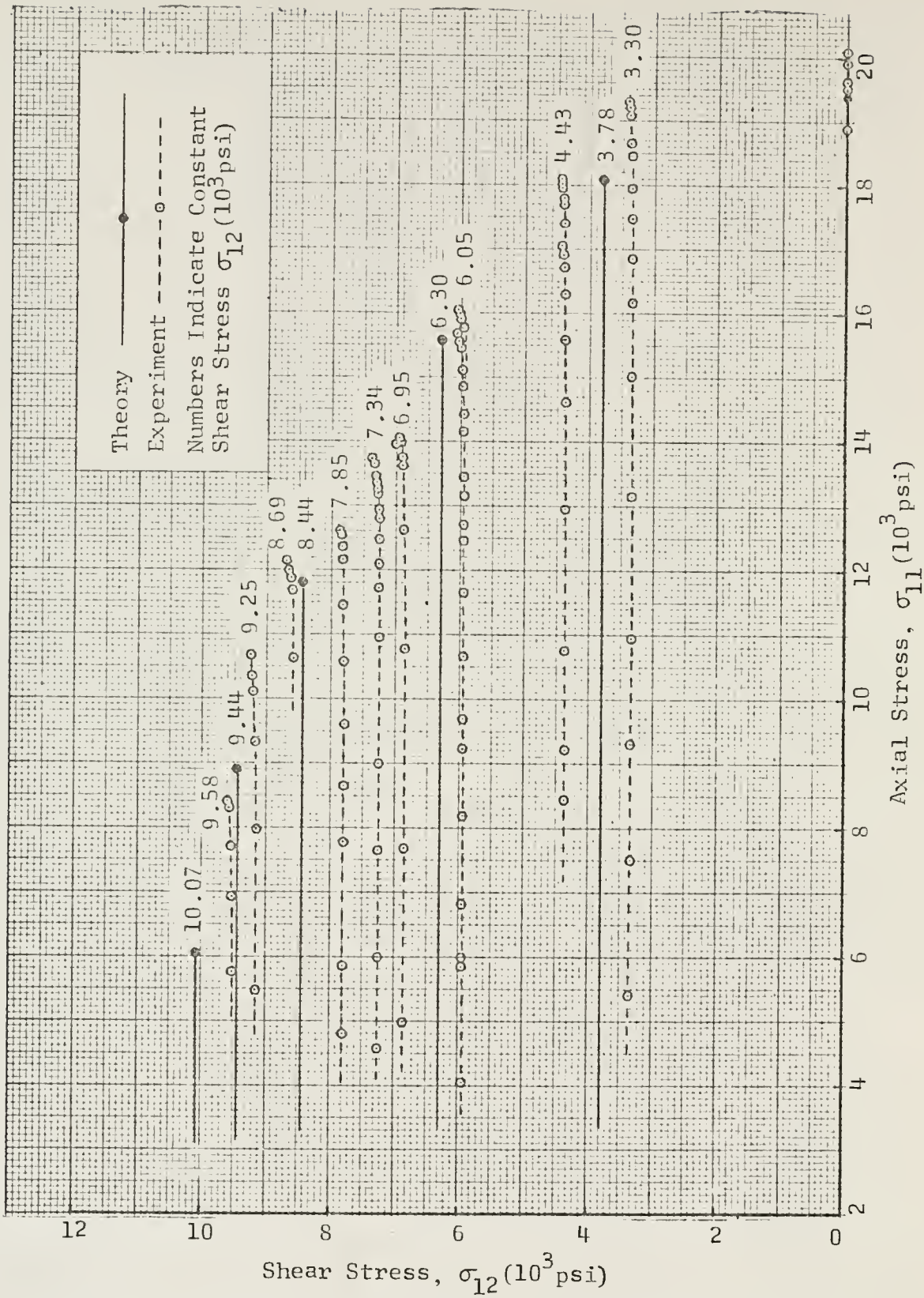

FIGURE 32. COMPARISON OF EXPERIMENT AND THEORY FOR BIAXIAL TESTS, SHEAR STRESS VERSUS AXIAL STRESS

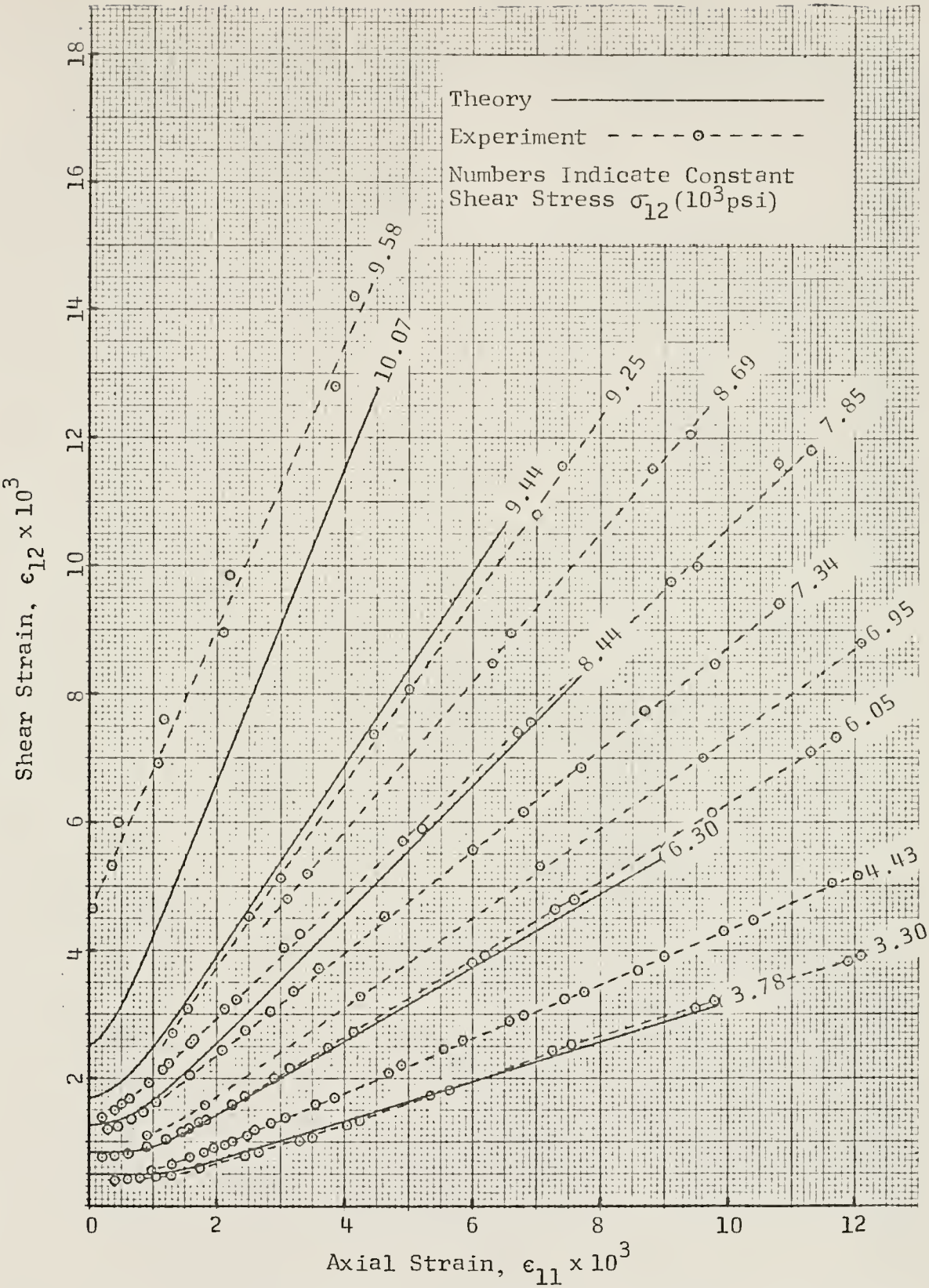

FIGURE 33. COMPARISON OF EXPERIMENT AND THEORY FOR BIAXIAL TESTS, SHEAR STRAIN VERSUS AXIAL STRAIN

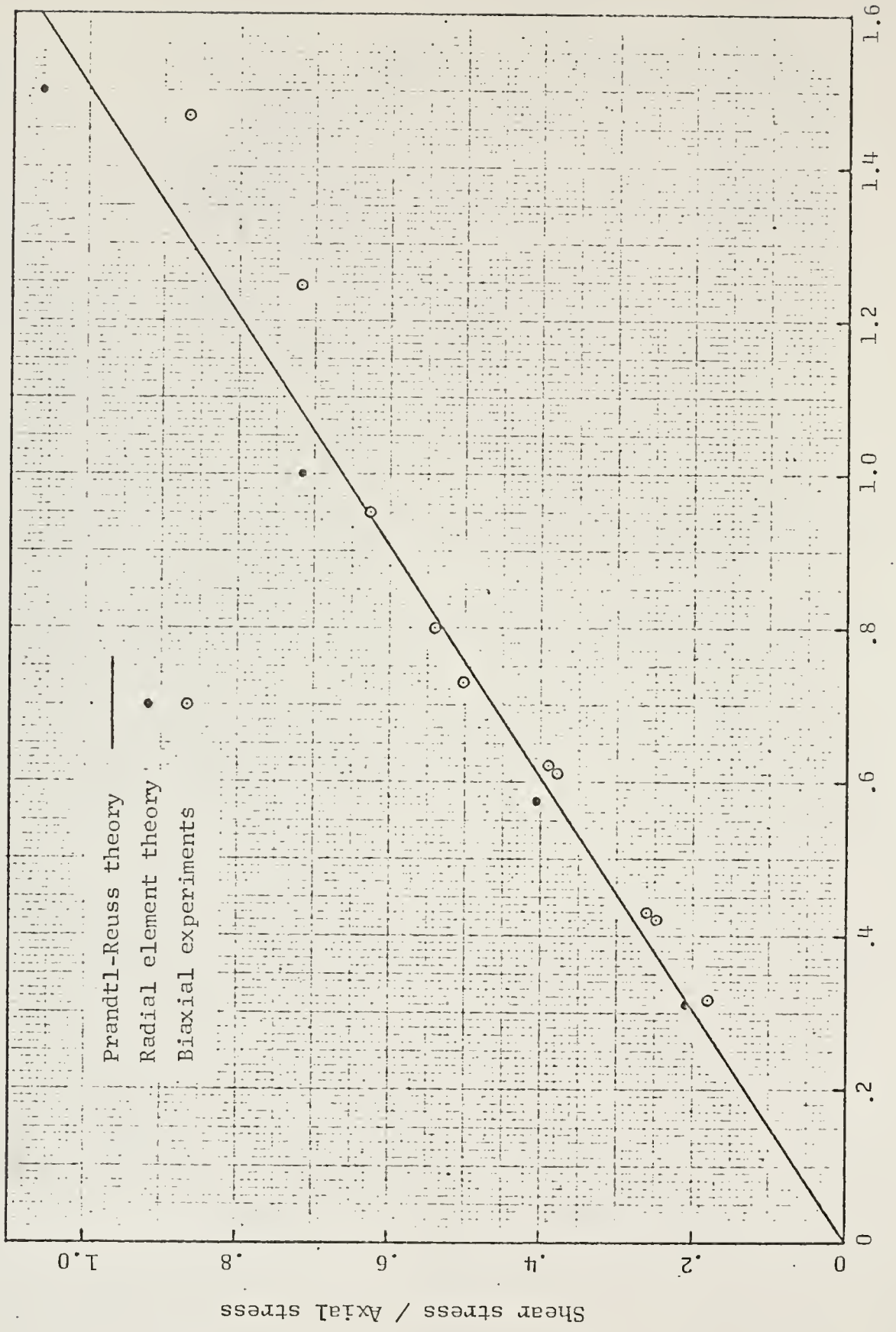

FIGURE 34. RATIO OF STRESSES COMPARED WITH SLOPE OF STRAIN PATH FOR LARGE STRAINS

to that test. The considerable scatter apparent in the experimental data is due partially to the following factors: (1) relatively inaccurate strain measurements; (2) small but finite friction in the torque mechanisms; and (3) imperfections in the specimen due to imprecise fabrication. Although no measurements were made, I estimate that the variations of wall thickness over the test sections were as large as 5 percent.

Figure 31 shows axial stress versus axial strain for several values of constant shear stress. The stress-strain curves are roughly similar in shape but we see that axial stress decreases with increasing shear stress. Figure 32 shows loading paths in the shear stress-axial stress plane. The data of Figure 32 suggest the existence of an ultimate stress envelope that might be similar in shape to the Tresca or the Mises yield curves. I feel that there is too much uncertainty in the present data to make a direct comparison with these two ellipses. Figure 33 shows loading paths in the shear strain-axial strain plane. After an initial transition period each strain path becomes essentially a straight line emanating in an approximately radial direction. Figure 34 correlates the ratio of the stresses with the slope of the strain path in the limit of large strains. The straight line in Figure 34 represents the equation

$$\frac{\sigma_{12}}{\sigma_{11}} = \frac{2\,\Delta e_{12}}{3\,\Delta e_{11}}$$

which is predicted by the Prandtl-Reuss theory and other incremental theories for large strains.

The solid points and lines shown in Figures 31-34 are results of the radial element theory computed using the following material parameters: $E = 10^7$ psi, $\nu = \lambda = 1/3$, $\varepsilon_y = .00126$. As before the elasticity constants E, ν were given handbook values for aluminum and the plasticity constants λ, ε_y were chosen so as to best fit the experimental data. Here the yield strain ($\varepsilon_y = .00126$) differs from that used previously ($\varepsilon_y = .00138$), when the theory was compared with tension-compression test data. A possible explanation of this discrepancy is that the material properties changed slightly during fabrication of the tubular specimens from the solid bar stock. This argument is made plausible by the observation that large amounts of heat were generated during the drilling operations in spite of continual flooding of the specimen with kerosene lubricant-coolant. Another factor contributing to the different yield stress concerns the strain-rate effect of aluminum. In the biaxial experiments we waited 1-3 minutes between load increments in order to minimize the effect of creep on the strain measurements. This amounted to an average strain rate of 10^{-4} to 10^{-3} minute^{-1} for the biaxial tests compared with .002 to .010 minute^{-1} for the tension-compression tests. Since the average strain rates were much smaller for the biaxial tests, we expect the stresses to be smaller also.

The theoretical data in Figures 31-34 are the same as the data in Figures 18a and 21, except that here the actual stress and strain components are plotted instead of the deviator components. The conversion is made through the following equations:

$$\sigma_{11} = 3s_{11}/2, \quad \sigma_{12} = \sigma_{21} = \bar{s}_{12}, \quad \epsilon_{12} = \epsilon_{21} = e_{12}$$

$$\epsilon_{11} = e_{11} + s_{11}/2\beta, \quad \epsilon_{22} = \epsilon_{33} = -e_{11}/2 + s_{11}/2\beta$$

where all other components of σ_{ij} and ϵ_{ij} are zero. Note that $\mu = 7.5 \times 10^6$ psi, $\beta = 30 \times 10^6$ psi by equations (3.1) and $e_k = .00084$, $s_k = 6300$ psi by equations (4.6).

The overall correlation between the radial element theory and the experimental data as shown in Figures 31-34 is good, and it is especially good considering the scatter in the experimental data. Two anomalies are worth mentioning. In Figure 33, the experimental strain path corresponding to $\sigma_{12} = 9580$ psi, starts at a shear strain that is obviously too high in relation to the theoretical curves, although its slope appears to be correct. This anomaly is due to a high initial creep; a high creep rate always occurs in aluminum when the applied stress is near the ultimate stress. The same phenomenon was observed for tests (not reported here) in which a high initial stress in tension was combined with an increasing shear stress. The second anomaly concerns the apparent difference between the radial element theory

and the Prandtl-Reuss theory in the limit of large strains, as shown in Figure 34. This difference exists partly because the computed results of the radial element theory are limited to relatively small strains. The two theories would agree more closely if the computed results were extended to larger strains, since the ratio of shear stress to axial stress is still decreasing and the slope of the strain path is essentially constant at the last point of each set of computed data.

CHAPTER IX

CONCLUSIONS AND RECOMMENDATIONS FOR FUTURE WORK

The following conclusions can be drawn from the work contained in this dissertation.

1. A new theory of plasticity, the radial element theory, is presented. Through the concept of radial element the theory directly exploits the anisotropic or directional aspects of material behavior. The theory is constructed in such a way that stress and strain transform as tensors for orthogonal coordinate transformations and for rotations of the material relative to fixed coordinates. The general form of this theory is not restricted to small deformations, nor is it restricted to any one type of material behavior.
2. The particular form of plasticity theory investigated here requires only four constants, two elasticity constants and two plasticity constants, for its complete specification. This contrasts with most other plasticity theories which require, in addition to the elasticity constants, specification of at least one work-hardening function.

3. Closed-form solutions were obtained for elastic-plastic stress-strain behavior in the cases of axial loading and reversed axial loading. A family of stress-strain curves is presented which depends on a work-hardening constant λ. The stress-strain curves are seen to be smooth and similar in shape to actual stress-strain curves of many metals. The reversed loading behavior is proved to satisfy the Masing hypothesis, a special simple form of Bauschinger effect.

4. Numerical solutions were obtained for the class of loadings involving fixed principal axes and for general loading histories. These numerical solutions, while not extremely complicated in principle, consume a considerable amount of computer time. Accordingly, these solutions could serve as a check on other simpler theories, but probably should not be used directly in the solution of complicated boundary value problems.

5. From the numerical solutions yield surfaces were computed and plotted in the deviator stress and strain planes for a variety of loading paths. Here yield surface is defined as the exact boundary of the elastic domain. These theoretical yield surfaces exhibit the following features: (a) the initial yield condition is an isotropic yield condition of the Tresca type; (b) after plastic deformation the

yield surface is anisotropic; usually it becomes expanded in directions surrounding the loading direction and compressed in directions opposite the loading; (c) the yield surface always is convex and generally is composed of both straight and curved line segments; (d) a sharp corner always develops at the point of loading during plastic deformation; (e) the elastic range in the direction of loading is constant for any radial loading; and (f) the yield surface shrinks in lateral directions during plastic deformation; this cross effect is greater for axial loadings than for pure shear loadings.

6. The numerical solutions also were used to generate surfaces of constant offset strain, for an initially undeformed material and also following plastic loadings in the axial and the pure shear directions. Here we observed: (a) for certain values of offset strain the initial "yield surface" is very close to a Mises condition; and (b) the corner in the yield surface at the loading point is "blunt" in the sense that for any finite offset strain it becomes a smooth curve of large radius. Both of these theoretical results have been observed experimentally by others.
7. The numerical solutions also were used to compute biaxial stress-strain data for the cases of constant shear strain - increasing axial strain, and vice versa,

and constant shear stress - increasing axial stress, and vice versa. The most unusual feature of the biaxial data is the appearance of a nonsymmetric stress tensor. This feature of the theory is genuine and seems to occur for any plastic loading that involves rotations of the principal strain axes relative to the material.

8. Experiments involving two widely different loading paths were performed to explore the quasi-static stress-strain behavior of commercially pure polycrystalline aluminum at room temperature. The two tests were tension-compression loadings of a solid rod and torsion-tension loadings of a tube. Comparisons between theoretical and experimental results showed good agreement throughout. Hence, it appears that the radial element theory predicts reasonably well the stress-strain behavior of at least this one material: commercially pure aluminum.
9. Especially good agreement was obtained in predicting the Bauschinger effect as observed during the tension-compression tests. In a reversed-loading type of test the common incremental theories (with either isotropic or kinematic hardening) fail to predict realistic results, and it is for these types of loading that the present theory has a clear advantage.

The following are recommendations for future work which could extend and improve the work contained in this dissertation.

1. The yield surfaces contained herein are too limited in kind to allow detailed comparisons with the literature on experimentally determined yield surfaces. Here yield surface computations were restricted to one value of the work-hardening constant ($\lambda = 0$) and to the class of loadings in which the principal axes of stress and strain are fixed and coincident. This loading situation is equivalent to applying any history of normal stresses to a rectangular block of material. It would be of interest to compute yield surfaces for other types of loading and for other values of the work-hardening constant λ. In particular, yield surfaces should be investigated in the shear stress-axial stress plane, which is the loading domain most often reported in the experimental literature. Several values of λ should be tried in order to gain a better understanding of the overall theoretical stress-strain behavior. Zigzag loading paths should be tried in order to study the dependence of the plastic strain increment on the stress and the stress increment. There are numerous experimental studies of zigzag loading paths in the literature. Surfaces of constant offset strain should be computed along with yield surfaces defined by the elastic limit. Offset strain surfaces surrounding a given yield surface supplement the

information provided by the yield surface alone and they provide a realistic tie with experimental data.

2. The general concept of yield surface should be investigated more fully. For example, the anisotropic yield surface corresponding to a given initial plastic loading could be computed relative to a variety of rotated coordinate systems. These results would demonstrate that a given anisotropic yield surface requires at least five independent variables for its complete description: in this case, two deviator-plane variables and three Euler angles.

3. The nonsymmetric stress that was computed for combined axial stress - shear stress loadings should be studied in more detail. In the absense of an externally applied body couple, a nonsymmetric stress tensor implies the existence of a couple stress tensor. The nonsymmetric stress and the couple stress should be investigated together as a function of the loading path. The possibility of detecting this effect experimentally also should be investigated. For most practical purposes it should be possible simply to define and use the symmetric part of the stress tensor as the stress itself, and to simply ignore the antisymmetric part. As justification for ignoring the antisymmetric part of the stress and the couple stress we note that the antisymmetric stress components are

small compared with the symmetric stress components in all computations reported here. In addition, we note that the common yield and strength criteria and the majority of boundary value problems are formulated exclusively in terms of the symmetric stress.

4. Comparisons between experimental and theoretical data reported herein are too limited in quantity and quality to definitely establish the relationship of the present theory to other theories. In Chapter VIII we showed that the radial element theory predicts reasonably well the behavior of aluminum for tension-compression loadings and for torsion-tension loadings. The radial element theory was shown to be superior to two simple incremental theories for the reversed axial loadings. A question arises as to whether the present theory is superior for other types of reversed loadings as well. To answer this question some highly accurate biaxial tests should be performed for complex loading paths that include reversed loadings in the shear stress - axial stress domain. These results then should be compared with the present theory and with various incremental theories of plasticity.

5. There is a need to generalize the radial element theory, to make it more flexible in the sense of fitting a wider class of material behavior. In Chapter VIII we fitted the present theory to experimental data for

aluminum by choosing appropriate values of the four constants $E, \nu, \lambda, \epsilon_y$. However, there exist other materials for which such a fitting is not possible. One example is mild steel, which exhibits an irregular behavior at the initial yield point. Other examples are the pure metals (aluminum, copper, zinc, etc.) when dead annealed, which exhibit work-hardening far in excess of the range predicted by the radial element theory. In addition, most metals exhibit changes in the shapes of the stress-strain curves under cyclic loading. The hysteresis curve of a metal generally either shrinks or grows depending on the prior history of the specimen, whereas the radial element theory predicts a stationary hysteresis curve if the stress or strain limits are fixed. One way to achieve greater flexibility in the theory is to generalize the elastic-perfectly-plastic relationship governing the elemental stress vectors. Thus, we might allow isotropic and kinematic hardening at each point on the unit sphere, and we might somehow include temperature and time effects into this basic relationship between the elemental stress vector and the deformation of the radial element. Obviously, such changes could greatly complicate the present theory. A simpler, although perhaps less satisfactory, modification of the theory is obtained by letting the yield constant Y (and maybe

also the work-hardening constant λ) depend on the temperature T, the time t, and the accumulated plastic strain e_A. The proposed relationship might assume the form

$$F(Y, \dot{Y}, \ddot{Y}, \ldots, T, e_A) = 0$$

where F is a function of the variables shown, where $\dot{Y} = dY/dt$, $\ddot{Y} = d^2Y/dt^2$, ... , and where e_A is defined by equation (6.11).

6. Another generalization of the theory is obtained by including a set of intrinsic material directions in the set of independent variables. By this means we could obtain anisotropic elasticity, and anisotropic initial yield conditions, in addition to the anisotropic effects already predicted following an initial plastic loading. An important application of this proposed theory, which has not yet been investigated concerns derivation of stress-strain relations for fibrous materials. Here we refer to materials such as steel- and glass-fiber reinforced plastics and tire rubber, that have numerous cords and fibers penetrating the material in various directions.

7. The radial element theory also might be useful for nonlinear elasticity, visco-elasticity, and other theories of material behavior where finite strains are likely to occur. As observed in Chapter III,

the radial element theory is not intrinsically limited to small strains although we chose to limit ourselves in this manner for mathematical simplicity. The advantage of the present theory for these large strain applications is that a person needs merely to postulate a simple relationship between an elemental stress vector and the deformation of a radial element. Then he can compute the complicated tensor relationship between stress and strain by a straightforward mathematical procedure.

BIBLIOGRAPHY

1. R. Hill, The Mathematical Theory of Plasticity, Clarendon Press, Oxford, 1950.

2. W. Prager and P. G. Hodge, Theory of Perfectly Plastic Solids, John Wiley, New York, 1951.

3. (a) D. C. Drucker, "Plasticity," Proc. First Symp. on Naval Structural Mech., edited by J. N. Goodier and N. J. Hoff, Pergamon Press, 1960, pp. 407-448; (b) G. A. Zizicas, Discussion of Ref. 3a, pp. 448-451.

4. P. M. Naghdi, "Stress-strain relations in plasticity and thermo-plasticity," Proc. Second Symp. on Naval Structural Mech., edited by E. H. Lee and P. S. Symonds, Pergamon Press, 1960, pp. 121-169.

5. A. E. Green and P. M. Naghdi, "A general theory of an elastic-plastic continuum," Arch. Rational Mech. Anal., vol. 18, 1965, pp. 251-281.

6. B. Crossland, "The effect of fluid pressure on the shear properties of metals," Proc. Inst. of Mechanical Engineers, vol. 168, 1954, pp. 935-944.

7. H. Tresca, "Mémoire sur l'écoulement des corps solides," Mém. Sav. Acad. Sci. Paris, vol. 18, 1868, pp. 733-799.

8. B. de Saint Venant, "Mémoire sur l'établissement des équations différentielles des mouvements intériors opérés dans les corps solides ductiles au delà des limites où l'élasticité pourrait les ramener à leur premier état," Comptes Rendus Acad. Sci. Paris, vol. 70, 1870, pp. 473-480.

9. M. Levy, "Mémoire sur les équations générales des mouvements intériers des corps solides ductiles au delà des limites où l'élasticité pourrait les ramener à leur premier état," Comptes Rendus Acad. Sci. Paris, vol. 70, 1870, 1323-1325.

10. R. von Mises, "Mechanik der festen Körper im plastisch deformablen Zustand," Göttinger Nachrichten, math.-phys. Klasse, 1913, pp. 582-592.

11. L. Prandtl, "Spannungsverteilung in plastischen Körpern," Proc. First International Congress of Applied Mech., 1924, pp. 43-54.

12. H. Hencky,"Zur Theorie plastischer Deformationen und der hierdurch hervorgerufenen Nebenspannungen," Proc. First International Congress of Applied Mech., 1924, pp. 312-317.

13. L. Prandtl, "Ein Gedankmodell zur kinetischen Theorie fester Körper," Zeitschrift fur angewandte Math. und Mech., vol. 8, 1928, pp. 85-106.

14. R. von Mises, "Mechanik der plastischen Formänderungen von Kristallen," Zeitschrift fur angewandte Math. und Mech., vol. 8, 1928, pp. 161-165.

15. E. Reuss, "Berücksichtigung der elastischen Formänderungen in der Plastizitätstheorie," Zeitschrift fur angewandte Math. und Mech., vol. 10, 1930, pp. 266-274.

16. M. Ros and A. Eichinger,"Metalle Diskussionsbericht No. 34 der eidgenossen Materialprüfungsanstalt,"Proc. Third International Congress of Applied Mech., 1930, p. 254.

17. E. Melan, "Zur Plastizitat des Raumlichen Kontinuums," Ingenieur-Arch., vol. 9, 1938, pp. 116-126.

18. W. Prager, "Strain hardening under combined stress," J. Applied Phys., vol. 16, 1945, pp. 837-840.

19. R. Hill, "A theory of yielding and plastic flow of anisotropic metals," Proc. Royal Society (London), vol. A193, 1948, pp. 281-297.

20. D. C. Drucker, "A more fundamental approach to plastic stress-strain relations," Proc. First U. S. National Congress of Applied Mech., ASME, 1952, pp. 487-491.

21. W. Koiter, "Stress-strain relations, uniqueness and variational theorems for elastic-plastic materials with a singular yield surface," Quarterly of Applied Math., vol. 11, 1953, pp. 350-354.

22. J. L. Sanders, "Plastic stress-strain relations based on infinitely many plane loading surfaces," Proc. Second U. S. National Congress of Applied Mech., ASME, 1954, pp. 455-460.

23. I. U. Ishlinskii, "General theory of plasticity with linear strain hardening" (in Russian), Ukr. Mat. Zh., vol. 6, 1954, pp. 314-324.

24. W. Prager, "The theory of plasticity: A survey of recent achievements," Proc. Inst. of Mechanical Engineers, vol. 169, 1955, pp. 41-47.

25. W. Prager, "A new method of analyzing stresses and strains in work-hardening plastic solids," J. Applied Mech., Trans. ASME, vol. 78, 1956, pp. 493-496.

26. P. G. Hodge, "Piecewise linear plasticity," Proc. Ninth International Congress of Applied Mech., 1956, pp. 65-72.

27. H. Ziegler, "A modification of Prager's hardening rule," Quarterly of Applied Math., vol. 17, 1959, pp. 55-65.

28. Z. Mroz, "On the description of anisotropic work-hardening," J. Mech. and Phys. of Solids, vol. 15, 1967, pp. 163-175.

29. W. R. Osgood, "Combined stress tests on 24ST aluminum tubes," J. Applied Mech., Trans. ASME, vol. 69, 1947, pp. 147-153.

30. J. L. Morrison and W. M. Shepherd, "An experimental investigation of plastic stress-strain relations," Proc. Inst. of Mechanical Engineers, vol. 163, 1950, pp. 1-9.

31. I. Kadashevich and V. V. Novizhilov, "The theory of plasticity which takes into account residual microstresses," TPMM, vol. 22, 1959, pp. 104-118.

32. H. J. Ivey, "Plastic stress-strain relations and yield surfaces for aluminum alloys," J. Mechanical Engr. Sci., vol. 3, 1961, pp. 15-31.

33. W. D. Iwan, "On a class of models for the yielding behavior of continuous and composite systems," J. Applied Mech., Trans. ASME, vol. 89, 1967, pp. 612-617.

34. S. B. Batdorf and B. Budiansky, "Polyaxial stress-strain relations of a strain-hardening metal," J. Applied Mech., Trans. ASME, vol. 76, 1954, pp. 323-326.

35. E. Krempl, "Cyclic plasticity: Some properties of the hysteresis curve of structural metals at room temperature," J. Basic Engr., Trans. ASME, vol. 93, 1971, pp. 317-323.

36. C. E. Feltner and R. W. Landgraf, "Selecting materials to resist low cycle fatigue," J. Basic Engr., Trans. ASME, vol. 93, 1971, pp. 444-452.

37. G. Masing, "Eigenspannung und Verfestigung beim Messing," Proc. Second International Congress of Applied Mech., 1926, pp. 332-335.

38. D. C. Drucker and F. D. Stockton, "Instrumentation and fundamental experiments in plasticity," Proc. Society for Experimental Stress Analysis, vol. 10, 1951, pp. 127-142.

39. P. M. Naghdi, J. C. Rowley, and C. W. Beadle, "Experiments concerning the yield surface and the assumption of linearity in the plastic stress-strain relations," J. Appl. Mech., Trans. ASME, vol. 77, 1955, pp. 416-420.

40. L. W. Hu and J. F. Bratt, "Effect of tensile plastic deformation on yield conditions," J. Appl. Mech., Trans. ASME, vol. 80, 1958, p. 411.

41. P. M. Naghdi, F. Essenberg, and W. Koff, "An experimental study of initial and subsequent yield surfaces in plasticity," J. Applied Mech., Trans. ASME, vol. 80. 1958, pp. 201-209.

42. S. S. Gill and J. Parker, "Plastic stress-strain relationships — some experiments on the effect of loading path and loading history," J. Appl. Mech., Trans. ASME, vol. 81, 1959, pp. 77-87.

43. H. G. McComb, "Some experiments concerning subsequent yield surfaces in plasticity," NASA Technical Note: D-396, 1960.

44. A. Phillips and G. A. Gray, "Experimental investigation of corners in the yield surface," J. Basic Engr., Trans. ASME, vol. 83, 1961, pp. 275-289.

45. P. K. Bertsch and W. N. Findley, "An experimental study of subsequent yield surfaces — corners, normality, Bauschinger and allied effects," Proc. Fourth U. S. National Congress of Applied Mech., ASME, 1962, pp. 893-907.

46. B. Paul, W. Chen, and L. Lee, "Experimental study of plastic flow under step-wise increments of tension and torsion," Proc. Fourth U. S. National Congress of Applied Mech., ASME, 1962, pp. 1031-1038.

47. W. Szezepinski, "On the effect of plastic deformation on the yield condition," Arch. Mech. Stosowanej, vol. 15, 1963, pp. 275-294.

48. J. Parker and M. B. Bassett, "Plastic stress-strain relationships — some experiments to derive a subsequent yield surface," J. Appl. Mech., Trans. ASME, vol. 86, 1964, pp. 671-682.

49. W. M. Mair and H. Ll. D. Pugh, "Effect of pre-strain on yield surfaces in copper," J. Mechanical Engr. Sci., vol. 6, 1964, pp. 150-163.

50. J. Miastkowski and W. S. Szczepinski, "An experimental study of yield surfaces of prestrained brass," International J. of Solids and Structures, vol. 1, 1965, pp. 189-194.

51. W. M. Mair, "The yield surface in metals," NEL Report No. 215, Glasgow, 1966.

52. A. Phillips, C. S. Liu, and J. W. Justusson, "An experimental investigation of yield surfaces at elevated temperatures," Acta Mech., vol. 14, 1972, pp. 119-146.

53. A. Phillips and J. L. Tang, "The effect of loading path on the yield surface at elevated temperatures," International J. of Solids and Structures, vol. 8, 1972, pp. 463-474.

54. J. F. Besseling, "A theory of elastic, plastic, and creep deformations of an initially isotropic material showing anisotropic strain-hardening, creep recovery, and secondary creep," J. Applied Mech., Trans. ASME, vol. 80, 1958, pp. 529-536.

55. (a) J. W. Hutchinson, "Plastic stress-strain relations of f.c.c. polycrystalline metals hardening according to Taylor's rule," J. Mech. Phys. Solids, vol. 12, 1964, pp. 11-24; and (b) J. W. Hutchinson, "Plastic stress-strain relations of b.c.c. polycrystals," J. Mech. Phys. Solids, vol. 12, pp. 25-33.

56. T. H. Lin and M. Ito, "Theoretical plastic distortion of a polycrystalline aggregate under combined and reversed stresses," J. Mech. and Phys. of Solids, vol. 13, 1965, pp. 103-115.

57. T. H. Lin and M. Ito, "Theoretical plastic stress-strain relationship of a polycrystal and comparisons with the von Mises and the Tresca plasticity theories," Int. J. of Engr. Science, vol. 4, 1966, pp. 543-561.

58. C. H. Wells and P. R. Paslay, "A small-strain plasticity theory for planar slip materials," J. Applied Mech., Trans. ASME, vol. 91, 1969, pp. 15-21.

59. A. H. Cottrell, Dislocations and Plastic Flow in Crystals, Clarendon Press, Oxford, 1953.

60. C. Truesdell and W. Noll, "The non-linear field theories of mechanics," Handbuch der Physik, vol. III/3, edited by S. Flugge, Springer-Verlag, 1965.

61. E. Kröner, "Allgemeine Kontinuumstheorie der Verzetzungen und Eigenspannungen," Arch. Rational Mech. Anal., vol. 4, 1960, pp. 273-334.

62. (a) J. L. Ericksen, "Anisotropic fluids," Arch. Rational Mech. Anal., vol. 4, 1960, pp. 231-237; and (b) J. L. Ericksen, "Poiseuille flow of certain anisotropic fluids," Arch. Rational Mech. Anal., vol. 8, 1961, pp. 1-8.

63. A. A. Ilyushin, Plastichnost, Izdatel'stvo Akademii Nauk, Moscow, 1963.

64. F. Riesz and B. Sz.-Nagy, Functional Analysis, Frederick Ungar, New York, 1955.

65. V. S. Lensky, "Analysis of plastic behavior of metals under complex loading," Proc. Second Symp. on Naval Structural Mech., edited by E. H. Lee and P. S. Symonds, Pergamon Press, 1960, pp. 259-278.

66. C. Truesdell and R. A. Toupin, "The classical field theories," Handbuch der Physik, vol. III/1, edited by S. Flugge, Springer-Verlag, 1960. (Pages 241-324 constitute a treatise on deformation of a continuum.)

67. L. E. Malvern, Introduction to the Mechanics of a Continuous Medium, Prentice-Hall, Englewood Cliffs, New Jersey, 1969.

68. C. F. Elam, Distortion of Metal Crystals, Clarendon Press, Oxford, 1935.

69. D. C. Drucker, "A definition of stable inelastic material," J. Applied Mech., Trans. ASME, vol. 81, 1959, pp. 101-106.

70. C. R. Wylie, Advanced Engineering Mathematics, McGraw-Hill, New York, 1960.

71. C-E. Fröberg, Introduction to Numerical Analysis, Addison-Wesley, Reading, Massachusetts, 1969.

72. F. A. Lewis, "Aluminum-base materials," Engineering Materials Handbook, edited by C. L. Mantell, McGraw-Hill, New York, 1958.

APPENDIX A

COMPUTER PROGRAMS

PROGRAM A-1. AXIAL LOADING. EXACT SOLUTION.

```
0000    READ L
0001    PRINT "PARAMETER L =",L
0002    PRINT
0003    PRINT "E1/EY","S1/SY","E1/EK","S1/SK"
0004    P=3.141593
0005    Q=2/P
0006    M=3-L
0007 1  READ F
0008    E=.75*F
0009    IF E>1 THEN 2
0010    PRINT E,E,F,F
0011    GOTO 1
0012 2  T=SQR(E*E-1)
0013    Z=ATN(T)
0014    X=COS(P/4-Z/2)
0015    Y=COS(P/4+Z/2)
0016    A=(Z-T)/1.5
0017    B=(1-Q*Z/3)*E
0018    C=Q*T*(1-L)/(E*M)
0019    D=Q*L/(1.5*M)
0020    S=A+B+C+D*(LOG(X)-LOG(Y))
0021    T=S/.75
0022    PRINT E,S,F,T
0023    GOTO 1
0024    DATA 1,1,2,3,4,5,6,7,8,9,10
END OF WORK FILE
/b
```

```
PARAMETER L =   1

E1/EY           S1/SY           E1/EK           S1/SK
 .75             .75             1               1
 1.5             1.251866        2               1.669155
 2.25            1.42417         3               1.898893
 3               1.525433        4               2.03391
 3.75            1.596273        5               2.128364
 4.5             1.650401        6               2.200534
 5.25            1.694045        7               2.258726
 6               1.730536        8               2.307381
 6.75            1.761846        9               2.349128
 7.5             1.789242        10              2.385656

    .03 SECONDS CPU TIME 00000 4
PROCEED
_
```

PROGRAM A-2. LOADING WITH FIXED PRINCIPAL AXES.
NUMERICAL SOLUTION USING ORDINARY TRAPEZOIDAL INTEGRATION.

```
0000    DIM A(30),X(30,32)
0001    DIM Y(30,32),Z(30,32)
0002    READ L,N
0003    PRINT L,N
0004    G=(4-2*L)/(3-L)
0005    H=(4*L-4)/(3-L)
0006    P=1.570796
0007    B=P/N
0008    A(0)=1-COS(B/2)
0009    FOR I=1 TO N-1
0010    C=B*(I-.5)
0011    D=B*(I+.5)
0012    A(I)=(COS(C)-COS(D))/(1+I/2)
0013    NEXT I
0014    A(N)=COS(D)/(1+N/2)
0015    FOR I=0 TO N
0016    FOR J=0 TO I+2
0017    X(I,J)=Y(I,J)=Z(I,J)=0
0018    NEXT J
0019    NEXT I
0020    E1=E2=E3=0
0021 1  READ D1,D2,D3
0022    FOR I=0 TO N
0023    C1=COS(B*I)
0024    S1=SIN(B*I)
0025    S=P/(I+2)
0026    FOR J=0 TO I+2
0027    C2=S1*COS(S*J)
0028    C3=S1*SIN(S*J)
0029    F=D1*C1*C1+D2*C2*C2+D3*C3*C3
0030    C=X(I,J)+C1*(F*H+G*D1)
0031    D=Y(I,J)+C2*(F*H+G*D2)
0032    E=Z(I,J)+C3*(F*H+G*D3)
0033    F=C*C1+D*C2+E*C3
0034    F=C*C+D*D+E*E-F*F
0035    IF F<G*G THEN 2
0036    F=SQR(F)/G
0037    C=C/F
0038    D=D/F
0039    E=E/F
0040 2  X(I,J)=C
0041    Y(I,J)=D
0042    Z(I,J)=E
0043    NEXT J
0044    NEXT I
0045    U=V=W=0
0046    FOR I=0 TO N
0047    C=(X(I)+X(I,I+2))/2
0048    D=(Y(I)+Y(I,I+2))/2
0049    E=(Z(I)+Z(I,I+2))/2
0050    FOR J=1 TO I+1
0051    C=C+X(I,J)
0052    D=D+Y(I,J)
0053    E=E+Z(I,J)
0054    NEXT J
0055    U=U+C*A(I)
0056    V=V+D*A(I)
0057    W=W+E*A(I)
0058    NEXT I
0059    S=(U+V+W)/3
0060    S1=U-S
0061    S2=V-S
0062    S3=W-S
0063    E1=E1+D1
0064    E2=E2+D2
0065    E3=E3+D3
0066    PRINT E1,E2,E3,S1,S2,S3
0067    GOTO 1
0068    DATA 1,30
0069    DATA 1,-.5,-.5,1,-.5,-.5
0070    DATA 1,-.5,-.5,1,-.5,-.5
0071    DATA 1,-.5,-.5,1,-.5,-.5
0072    DATA 1,-.5,-.5,1,-.5,-.5
0073    DATA 1,-.5,-.5,1,-.5,-.5
PROCEED
```

```
PROCEED
—
 1            30
 1.000000    -0.500000   -0.500000   0.999541   -0.499771   -0.499770
 2.000000    -1.000000   -1.000000   1.669422   -0.834711   -0.834711
 3.000000    -1.500000   -1.500000   1.896647   -0.948324   -0.948323
 4.000000    -2.000000   -2.000000   2.032299   -1.016150   -1.016149
 5.000000    -2.500000   -2.500000   2.123879   -1.061940   -1.061939
```

PROGRAM A-3. LOADING WITH FIXED PRINCIPAL AXES.
NUMERICAL SOLUTION USING MODIFIED TRAPEZOIDAL INTEGRATION.

```
0000    DIM A(30),X(30,32)
0001    DIM Y(30,32),Z(30,32)
0002    READ L,N
0003    PRINT L,N
0004    G=(4-2*L)/(3-L)
0005    H=(4*L-4)/(3-L)
0006    P=1.570796
0007    B=P/N
0008    A(0)=1-COS(B/2)
0009    FOR I=1 TO N-1
0010    C=B*(I-.5)
0011    D=B*(I+.5)
0012    A(I)=(COS(C)-COS(D))/(1+I/2)
0013    NEXT I
0014    A(N)=COS(D)/(1+N/2)
0015    FOR I=0 TO N
0016    FOR J=0 TO I+2
0017    X(I,J)=Y(I,J)=Z(I,J)=0
0018    NEXT J
0019    NEXT I
0020    E1=E2=E3=0
0021 1  READ D1,D2,D3
0022    FOR I=0 TO N
0023    C=B*I
0024    IF I>0 THEN 2
0025    C=B/6
0026 2  IF I<N THEN 3
0027    C=P-B/6
0028 3  C1=COS(C)
0029    S1=SIN(C)
0030    S=P/(I+2)
0031    FOR J=0 TO I+2
0032    C=S*J
0033    IF J>0 THEN 4
0034    C=S/6
0035 4  IF J<I+2 THEN 5
0036    C=P-S/6
0037 5  C2=S1*COS(C)
0038    C3=S1*SIN(C)
0039    F=D1*C1*C1+D2*C2*C2+D3*C3*C3
PROCEED
_
```

```
0040    C=X(I,J)+C1*(F*H+G*D1)
0041    D=Y(I,J)+C2*(F*H+G*D2)
0042    E=Z(I,J)+C3*(F*H+G*D3)
0043    F=C*C1+D*C2+E*C3
0044    F=C*C+D*D+E*E-F*F
0045    IF F<G*G THEN 6
0046    F=SQR(F)/G
0047    C=C/F
0048    D=D/F
0049    E=E/F
0050 6  X(I,J)=C
0051    Y(I,J)=D
0052    Z(I,J)=E
0053    NEXT J
0054    NEXT I
0055    U=V=W=0
0056    FOR I=0 TO N
0057    C=(X(I)+X(I,I+2))/2
0058    D=(Y(I)+Y(I,I+2))/2
0059    E=(Z(I)+Z(I,I+2))/2
0060    FOR J=1 TO I+1
0061    C=C+X(I,J)
0062    D=D+Y(I,J)
0063    E=E+Z(I,J)
0064    NEXT J
0065    U=U+C*A(I)
0066    V=V+D*A(I)
0067    W=W+E*A(I)
0068    NEXT I
0069    S=(U+V+W)/3
0070    S1=U-S
0071    S2=V-S
0072    S3=W-S
0073    E1=E1+D1
0074    E2=E2+D2
0075    E3=E3+D3
0076    PRINT E1,E2,E3,S1,S2,S3
0077    GOTO 1
0078    DATA 1,30
0079    DATA 1,-.5,-.5,1,-.5,-.5
PROCEED
_
```

```
 1            30
 1.000000    -0.500000   -0.500000   1.000034    -0.500018   -0.500017
 2.000000    -1.000000   -1.000000   1.670351    -0.835176   -0.835175
 3.000000    -1.500000   -1.500000   1.897929    -0.948965   -0.948965
 4.000000    -2.000000   -2.000000   2.033916    -1.016958   -1.016958
 5.000000    -2.500000   -2.500000   2.125821    -1.062911   -1.062910
```

PROGRAM A-4. PAGE 1 OF 2.
YIELD SURFACES RELATIVE TO FIXED PRINCIPAL AXES.

```
0000    DIM A(20),X(20,22),Y(20,22)
0001    DIM Q(23),R(23),Z(20,22)
0002    DATA 8,-4,7,-5,6,-6,5,-7
0003    DATA 4,-8,2,-7,0,-6,-2,-5
0004    DATA -4,-4,-5,-2,-6,0,-7,-2
0005    DATA -8,-4,-7,-5,-6,6,-5,7
0006    DATA -4,8,-2,7,0,6,2,5
0007    DATA 4,4,5,2,6,0,7,-2
0008    FOR I=0 TO 23
0009    READ Q(I),R(I)
0010    NEXT I
0011    READ L,N
0012    PRINT L,N
0013    G=(4-2*L)/(3-L)
0014    H=(4*L-4)/(3-L)
0015    P=1.570796
0016    B=P/N
0017    A(0)=1-COS(B/2)
0018    FOR I=1 TO N-1
0019    C=B*(I-.5)
0020    D=B*(I+.5)
0021    A(I)=(COS(C)-COS(D))/(1+I/2)
0022    NEXT I
0023    A(N)=COS(D)/(1+N/2)
0024    FOR I=0 TO N
0025    FOR J=0 TO I+2
0026    X(I,J)=Y(I,J)=Z(I,J)=0
0027    NEXT J
0028    NEXT I
0029    E1=E2=E3=0
0030  1 READ D1,D2,D3
0031    FOR I=0 TO N
0032    C1=COS(B*I)
0033    S1=SIN(B*I)
0034    S=P/(I+2)
0035    FOR J=0 TO I+2
0036    C2=S1*COS(S*J)
0037    C3=S1*SIN(S*J)
0038    F=D1*C1*C1+D2*C2*C2+D3*C3*C3
0039    C=X(I,J)+C1*(F*H+G*D1)
0040    D=Y(I,J)+C2*(F*H+G*D2)
0041    E=Z(I,J)+C3*(F*H+G*D3)
0042    F=C*C1+D*C2+E*C3
0043    F=C*C+D*D+E*E-F*F
0044    IF F<G*G THEN 2
0045    F=SQR(F)/G
PROCEED
```

```
0046    C=C/F
0047    D=D/F
0048    E=E/F
0049  2 X(I,J)=C
0050    Y(I,J)=D
0051    Z(I,J)=E
0052    NEXT J
0053    NEXT I
0054    U=V=W=0
0055    FOR I=0 TO N
0056    C=(X(I)+X(I,I+2))/2
0057    D=(Y(I)+Y(I,I+2))/2
0058    E=(Z(I)+Z(I,I+2))/2
0059    FOR J=1 TO I+1
0060    C=C+X(I,J)
0061    D=D+Y(I,J)
0062    E=E+Z(I,J)
0063    NEXT J
0064    U=U+C*A(I)
0065    V=V+D*A(I)
0066    W=W+E*A(I)
0067    NEXT I
0068    E1=E1+D1
0069    E2=E2+D2
0070    E3=E3+D3
0071    S=(U+V+W)/3
0072    S1=U-S
0073    S2=V-S
0074    S3=W-S
0075    PRINT
0076    PRINT E1,E2,E3
0077    PRINT S1,S2,S3
0078    PRINT
0079    FOR K=0 TO 23
0080    F1=Q(K)/6
0081    F2=R(K)/6
0082  3 T=0
0083    D1=F1-S1
0084    D2=F2-S2
0085    D3=-D1-D2
0086    FOR I=0 TO N
0087    C1=COS(B*I)
0088    U=SIN(B*I)
0089    S=P/(I+2)
0090    FOR J=0 TO I+2
0091    C2=U*COS(S*J)
PROCEED
```

PROGRAM A-4. PAGE 2 OF 2.
YIELD SURFACES RELATIVE TO FIXED PRINCIPAL AXES.

```
0092    C3=U*SIN(S*J)
0093    F=D1*C1*C1+D2*C2*C2+D3*C3*C3
0094    C=X(I,J)+C1*(F*H+G*D1)
0095    D=Y(I,J)+C2*(F*H+G*D2)
0096    E=Z(I,J)+C3*(F*H+G*D3)
0097    F=C*C1+D*C2+E*C3
0098    F=C*C+D*D+E*E-F*F
0099    IF F<T THEN 4
0100    T=F
0101 4  NEXT J
0102    NEXT I
0103    F=SQR(T)/G
0104    F1=F1/F
0105    F2=F2/F
0106    E=ABS(F-1)
0107    IF E>.01 THEN 3
0108    PRINT F1,F2,-F1-F2
0109    NEXT K
0110    GOTO 1
0111    DATA 0,10
0112    DATA 4,-2,-2
PROCEED
/b


 0              10

 4              -2              -2
 1.788328       -.8941646       -.8941634

 1.786601       -.8933018       -.8932992
 1.563043       -1.116459       -.4465837
 1.202357       -1.202357       0
 .7985362       -1.117949       .3194132
 .5196369       -1.039272       .5196353
 .2746201       -.9611699       .6865498
 0              -.8685517       .8685517

   2.21 SECONDS CPU TIME 00000 4
PROCEED
-
```

PROGRAM A-5. PAGE 1 OF 2.
STRESS HISTORY FOR A GIVEN BIAXIAL STRAIN HISTORY.

```
0000    DIM A(15),M(7),U(3),V(3),W(3)
0001    DIM X(1152),Y(1152),Z(1152)
0002    M(0)=M(3)=M(4)=M(5)=1
0003    M(1)=M(2)=M(6)=M(7)=-1
0004    L=1
0005    N=15
0006    PRINT L,N
0007    N1=N+1
0008    N2=N1*(N+3)
0009    G=(4-2*L)/(3-L)
0010    H=(4*L-4)/(3-L)
0011    P1=1.570796
0012    B=P1/N
0013    P=1
0014    A(0)=(1-COS(B/2))/4
0015    FOR I=1 TO N-1
0016    C=B*(I-.5)
0017    D=B*(I+.5)
0018    A(I)=(COS(C)-COS(D))/(4+2*I)
0019    NEXT I
0020    A(N)=COS(D)/(4+2*N)
0021    E1=E2=E3=E4=Z1=Q=0
0022 1  FOR I=0 TO 4*N2
0023    X(I)=Y(I)=Z(I)=0
0024    NEXT I
0025    FOR O=1 TO P
0026    READ D1,D2,D3,D4
0027    C=COS(Q)
0028    S=SIN(Q)
0029    D=C*C
0030    E=S*S
0031    F=C*S
0032    T1=D*D1+E*D2+2*F*D4
0033    T2=D*D2+E*D1-2*F*D4
0034    T4=(D-E)*D4+F*(D2-D1)
0035    FOR I=0 TO N
0036    C=B*I
0037    IF I>0 THEN 2
0038    C=B/6
0039 2  IF I<N THEN 3
0040    C=P1-B/6
0041 3  C1=COS(C)
0042    S1=SIN(C)
0043    S=P1/(I+2)
0044    FOR J=0 TO I+2
0045    C=S*J
0046    IF J>0 THEN 4
0047    C=S/6
0048 4  IF J<I+2 THEN 5
0049    C=P1-S/6
0050 5  C2=S1*COS(C)
0051    C3=S1*SIN(C)
0052    FOR K=0 TO 3
0053    C4=C2*M(K)
0054    C5=C3*M(K+4)
0055    L=I+N1*J+N2*K
0056    C=C1*T1+C4*T4
0057    D=C1*T4+C4*T2
0058    E=C5*D3
0059    F=H*(C1*C+C4*D+C5*E)
0060    C=X(L)+C1*F+C*G
0061    D=Y(L)+C4*F+D*G
0062    E=Z(L)+C5*F+E*G
0063    F=C1*C+C4*D+C5*E
0064    F=C*C+D*D+E*E-F*F
0065    IF F<G*G THEN 6
0066    F=SQR(F)/G
0067    C=C/F
0068    D=D/F
0069    E=E/F
0070 6  X(L)=C
0071    Y(L)=D
0072    Z(L)=E
0073    NEXT K
0074    NEXT J
0075    NEXT I
0076    NEXT O
0077    RESTORE
0078    FOR K=0 TO 3
0079    U(K)=V(K)=W(K)=0
0080    FOR I=0 TO N
0081    J=I+N2*K
0082    L=J+N1*(I+2)
0083    C=(X(J)+X(L))/2
0084    D=(Y(J)+Y(L))/2
0085    E=(Z(J)+Z(L))/2
0086    FOR J=1 TO I+1
0087    L=I+N1*J+N2*K
0088    C=C+X(L)
0089    D=D+Y(L)
0090    E=E+Z(L)
0091    NEXT J
0092    U(K)=U(K)+C*A(I)
0093    V(K)=V(K)+D*A(I)
0094    W(K)=W(K)+E*A(I)
0095    NEXT I
0096    NEXT K
0097    T1=U(0)+U(1)+U(2)+U(3)
0098    T2=U(0)-U(1)-U(2)+U(3)
0099    T4=V(0)+V(1)+V(2)+V(3)
```

PROGRAM A-5. PAGE 2 OF 2.
STRESS HISTORY FOR A GIVEN BIAXIAL STRAIN HISTORY.

```
0100    T5=V(0)-V(1)-V(2)+V(3)
0101    T9=W(0)+W(1)-W(2)-W(3)
0102    F=(T1+T5+T9)/3
0103    T1=T1-F
0104    T5=T5-F
0105    T9=T9-F
0106    E=T2+T4
0107    F=T1-T5
0108    Q=Q+.5*ATN(E/F)
0109    IF E*E>.000001 THEN 1
0110    C=COS(Q)
0111    S=SIN(Q)
0112    D=C*C
0113    R=S*S
0114    S1=D*T1+R*T5-C*S*E
0115    S2=D*T2-R*T4+C*S*F
0116    S4=D*T4-R*T2+C*S*F
0117    S5=D*T5+R*T1+C*S*E
0118    E1=E1+D1
0119    E2=E2+D2
0120    E3=E3+D3
0121    E4=E4+D4
0122    PRINT
0123    PRINT E1,E4,Z1,S1,S2,Z1
0124    PRINT E4,E2,Z1,S4,S5,Z1
0125    PRINT Z1,Z1,E3,Z1,Z1,T9
0126    P=P+1
0127    GOTO 1
0128    DATA 2,-1,-1,0
0129    DATA 0,0,0,.1
0130    DATA 0,0,0,.1
0131    DATA 0,0,0,.1
```

PROGRAM A-6. PAGE 1 OF 2.
STRESS HISTORY FOR A GIVEN GENERAL STRAIN HISTORY.

```
0000    DIM A(15),M(7),R(2,2)
0001    DIM T(2,2),U(2,2),V(3),W(3)
0002    DIM X(1152),Y(1152),Z(1152)
0003    M(0)=M(3)=M(4)=M(5)=1
0004    M(1)=M(2)=M(6)=M(7)=-1
0005    L=1
0006    N=15
0007    PRINT L,N
0008    N1=N+1
0009    N2=N1*(N+3)
0010    G=(4-2*L)/(3-L)
0011    H=(4*L-4)/(3-L)
0012    P1=1.570796
0013    B=P1/N
0014    A(0)=(1-COS(B/2))/4
0015    FOR I=1 TO N-1
0016    C=B*(I-.5)
0017    D=B*(I+.5)
0018    A(I)=(COS(C)-COS(D))/(4+2*I)
0019    NEXT I
0020    A(N)=COS(D)/(4+2*N)
0021    E1=E2=E3=E4=E5=E6=0
0022    FOR I=1 TO 7
0023    R(I)=0
0024    NEXT I
0025    R(0)=R(4)=R(8)=P=1
0026 1  FOR I=0 TO 4*N2
0027    X(I)=Y(I)=Z(I)=0
0028    NEXT I
0029    FOR Q=1 TO P
0030    READ D1,D2,D3,D4,D5,D6
0031    U(0)=D1
0032    U(4)=D2
0033    U(8)=D3
0034    U(1)=U(3)=D4
0035    U(2)=U(6)=D5
0036    U(5)=U(7)=D6
0037    FOR I=0 TO 2
0038    FOR J=0 TO 2
0039    T(I,J)=0
0040    FOR K=0 TO 2
0041    FOR L=0 TO 2
0042    D=R(I,K)*R(J,L)
0043    T(I,J)=T(I,J)+D*U(K,L)
0044    NEXT L
0045    NEXT K
0046    NEXT J
0047    NEXT I
0048    FOR I=0 TO N
0049    C=B*I
PROCEED
-
```

```
0050    IF I>0 THEN 2
0051    C=B/6
0052 2  IF I<N THEN 3
0053    C=P1-B/6
0054 3  C1=COS(C)
0055    S1=SIN(C)
0056    S=P1/(I+2)
0057    FOR J=0 TO I+2
0058    C=S*J
0059    IF J>0 THEN 4
0060    C=S/6
0061 4  IF J<I+2 THEN 5
0062    C=P1-S/6
0063 5  C2=S1*COS(C)
0064    C3=S1*SIN(C)
0065    FOR K=0 TO 3
0066    C4=C2*M(K)
0067    C5=C3*M(K+4)
0068    L=I+N1*J+N2*K
0069    C=C1*T(0)+C4*T(1)+C5*T(2)
0070    D=C1*T(3)+C4*T(4)+C5*T(5)
0071    E=C1*T(6)+C4*T(7)+C5*T(8)
0072    F=H*(C1*C+C4*D+C5*E)
0073    C=X(L)+C1*F+C*G
0074    D=Y(L)+C4*F+D*G
0075    E=Z(L)+C5*F+E*G
0076    F=C1*C+C4*D+C5*E
0077    F=C*C+D*D+E*E-F*F
0078    IF F<G*G THEN 6
0079    F=SQR(F)/G
0080    C=C/F
0081    D=D/F
0082    E=E/F
0083 6  X(L)=C
0084    Y(L)=D
0085    Z(L)=E
0086    NEXT K
0087    NEXT J
0088    NEXT I
0089    NEXT Q
0090    RESTORE
0091    FOR K=0 TO 3
0092    U(K)=V(K)=W(K)=0
0093    FOR I=0 TO N
0094    J=I+N2*K
0095    L=J+N1*(I+2)
0096    C=(X(J)+X(L))/2
0097    D=(Y(J)+Y(L))/2
0098    E=(Z(J)+Z(L))/2
0099    FOR J=1 TO I+1
PROCEED
-
```

PROGRAM A-6. PAGE 2 OF 2.
STRESS HISTORY FOR A GIVEN STRAIN HISTORY.

```
0100    L=I+N1*J+N2*K
0101    C=C+X(L)
0102    D=D+Y(L)
0103    E=E+Z(L)
0104    NEXT J
0105    U(K)=U(K)+C*A(I)
0106    V(K)=V(K)+D*A(I)
0107    W(K)=W(K)+E*A(I)
0108    NEXT I
0109    NEXT K
0110    T(0)=U(0)+U(1)+U(2)+U(3)
0111    T(1)=U(0)-U(1)-U(2)+U(3)
0112    T(2)=U(0)+U(1)-U(2)-U(3)
0113    T(3)=V(0)+V(1)+V(2)+V(3)
0114    T(4)=V(0)-V(1)-V(2)+V(3)
0115    T(5)=V(0)+V(1)-V(2)-V(3)
0116    T(6)=W(0)+W(1)+W(2)+W(3)
0117    T(7)=W(0)-W(1)-W(2)+W(3)
0118    T(8)=W(0)+W(1)-W(2)-W(3)
0119    F=(T(0)+T(4)+T(8))/3
0120    T(0)=T(0)-F
0121    T(4)=T(4)-F
0122    T(8)=T(8)-F
0123    C=T(1)+T(3)
0124    D=T(2)+T(6)
0125    E=T(5)+T(7)
0126    F=C*C+D*D+E*E
0127    IF F<.000001 THEN 9
0128    FOR I=0 TO 2
0129    J=I+1
0130    K=I+2
0131    IF J<3 THEN 7
0132    J=J-3
0133  7 IF K<3 THEN 8
0134    K=K-3
0135  8 E=T(J,K)+T(K,J)
0136    F=T(J,J)-T(K,K)
0137    D=.5*ATN(E/F)
0138    C=COS(D)
0139    S=SIN(D)
0140    C2=C*C
0141    S2=S*S
0142    E=E*C*S
0143    F=F*C*S
0144    FOR L=0 TO 2
0145    D=R(J,L)
0146    R(J,L)=S*R(K,L)+C*D
0147    R(K,L)=C*R(K,L)-S*D
0148    NEXT L
0149    D=T(I,J)
PROCEED
-
0150    T(I,J)=S*T(I,K)+C*D
0151    T(I,K)=C*T(I,K)-S*D
0152    D=T(J,I)
0153    T(J,I)=S*T(K,I)+C*D
0154    T(K,I)=C*T(K,I)-S*D
0155    D=T(J,K)
0156    T(J,K)=C2*D-S2*T(K,J)-F
0157    T(K,J)=C2*T(K,J)-S2*D-F
0158    D=T(J,J)
0159    T(J,J)=C2*D+S2*T(K,K)+E
0160    T(K,K)=C2*T(K,K)+S2*D-E
0161    NEXT I
0162    GOTO 1
0163  9 FOR I=0 TO 2
0164    FOR J=0 TO 2
0165    U(I,J)=0
0166    FOR K=0 TO 2
0167    FOR L=0 TO 2
0168    D=R(K,I)*R(L,J)
0169    U(I,J)=U(I,J)+D*T(K,L)
0170    NEXT L
0171    NEXT K
0172    NEXT J
0173    NEXT I
0174    E1=E1+D1
0175    E2=E2+D2
0176    E3=E3+D3
0177    E4=E4+D4
0178    E5=E5+D5
0179    E6=E6+D6
0180    PRINT
0181    PRINT E1,E4,E5,U(0),U(1),U(2)
0182    PRINT E4,E2,E6,U(3),U(4),U(5)
0183    PRINT E5,E6,E3,U(6),U(7),U(8)
0184    P=P+1
0185    GOTO 1
0186    DATA 2,-1,-1,0,0,0
0187    DATA 0,0,0,.1,0,0
0188    DATA 0,0,0,.1,0,0
0189    DATA 0,0,0,.1,0,0
PROCEED
-
```

APPENDIX B

TABULATED RESULTS

TABLE B-1

AXIAL LOADING BEHAVIOR (E2 = E3 = -E1/2; S2 = S3 = -S1/2)
EXACT SOLUTIONS

E1/EY	λ = 0 S1/SY	λ = 0.5 S1/SY	λ = 1.0 S1/SY	λ = 1.5 S1/SY	λ = 2.0 S1/SY
1.0	1.00000	1.00000	1.00000	1.00000	1.00000
1.1	1.06906	1.07135	1.07479	1.08051	1.09196
1.2	1.11640	1.12230	1.13116	1.14593	1.17547
1.3	1.15270	1.16267	1.17763	1.20256	1.25241
1.4	1.18181	1.19600	1.21728	1.25275	1.32370
1.5	1.20580	1.22423	1.25187	1.29793	1.39005
1.6	1.22599	1.24860	1.28251	1.33903	1.45207
1.7	1.24324	1.26994	1.30999	1.37673	1.51023
1.8	1.25817	1.28885	1.33487	1.41157	1.56496
1.9	1.27123	1.30577	1.35758	1.44393	1.61662
2.0	1.28276	1.32104	1.37845	1.47414	1.66552
2.2	1.30220	1.34759	1.41567	1.52913	1.75606
2.4	1.31798	1.37001	1.44806	1.57815	1.83832
2.6	1.33104	1.38930	1.47669	1.62234	1.91364
2.8	1.34204	1.40614	1.50230	1.66255	1.98306
3.0	1.35144	1.42104	1.52543	1.69943	2.04742
3.2	1.35956	1.43434	1.54651	1.73347	2.10738
3.4	1.36664	1.44633	1.56586	1.76508	2.16351
3.6	1.37288	1.45722	1.58372	1.79456	2.21624
3.8	1.37842	1.46718	1.60031	1.82219	2.26596
4.0	1.38337	1.47633	1.61578	1.84818	2.31299
4.2	1.38782	1.48480	1.63027	1.87271	2.35761
4.4	1.39184	1.49266	1.64389	1.89593	2.40003
4.6	1.39549	1.49999	1.65674	1.91798	2.44047
4.8	1.39882	1.50685	1.66889	1.93896	2.47910
5.0	1.40187	1.51329	1.68042	1.95897	2.51607
5.5	1.40849	1.52785	1.70689	2.00529	2.60209
6.0	1.41395	1.54059	1.73054	2.04712	2.68029
6.5	1.41855	1.55189	1.75190	2.08525	2.75194
7.0	1.42246	1.56202	1.77137	2.12027	2.81807
7.5	1.42584	1.57120	1.78924	2.15265	2.87945
8.0	1.42878	1.57958	1.80577	2.18275	2.93672
8.5	1.43137	1.58727	1.82112	2.21088	2.99039
9.0	1.43366	1.59438	1.83547	2.23727	3.04087
9.5	1.43571	1.60099	1.84891	2.26212	3.08854
10.	1.43754	1.60716	1.86158	2.28561	3.13368
11.	1.44070	1.61837	1.88487	2.32904	3.21737
12.	1.44333	1.62835	1.90589	2.36845	3.29357
13.	1.44554	1.63734	1.92503	2.40453	3.36351
14.	1.44743	1.64550	1.94261	2.43779	3.42814
15.	1.44907	1.65298	1.95885	2.46863	3.48819
16.	1.45050	1.65988	1.97394	2.49739	3.54428
17.	1.45176	1.66628	1.98805	2.52433	3.59691
18.	1.45287	1.67223	2.00127	2.54968	3.64648
19.	1.45387	1.67781	2.01373	2.57358	3.69330
20.	1.45478	1.68307	2.02550	2.59622	3.73767

TABLE B-2

AXIAL LOADING BEHAVIOR (E2 = E3 = -E1/2 ; S2 = S3 = -S1/2)
EXACT SOLUTIONS

E1/EK	λ = 0 S1/SK	λ = 0.5 S1/SK	λ = 1.0 S1/SK	λ = 1.5 S1/SK	λ = 2.0 S1/SK
1.0	1.00000	1.00000	1.00000	1.00000	1.00000
1.1	1.10000	1.10000	1.10000	1.10000	1.10000
1.2	1.20000	1.20000	1.20000	1.20000	1.20000
1.3	1.30000	1.30000	1.30000	1.30000	1.30000
1.4	1.38505	1.38618	1.38789	1.39072	1.39639
1.5	1.44303	1.44719	1.45344	1.46386	1.48468
1.6	1.48853	1.49640	1.50822	1.52791	1.56729
1.7	1.52588	1.53779	1.55565	1.58543	1.64498
1.8	1.55733	1.57343	1.59757	1.63781	1.71828
1.9	1.58430	1.60463	1.63513	1.68597	1.78763
2.0	1.60774	1.63231	1.66916	1.73057	1.85341
2.2	1.64659	1.67947	1.72881	1.81103	1.97547
2.4	1.67756	1.71847	1.77983	1.88209	2.08662
2.6	1.70290	1.75146	1.82431	1.94572	2.18854
2.8	1.72402	1.77988	1.86366	2.00329	2.28256
3.0	1.74193	1.80471	1.89889	2.05586	2.36979
3.2	1.75730	1.82668	1.93075	2.10420	2.45109
3.4	1.77065	1.84631	1.95979	2.14893	2.52720
3.6	1.78236	1.86399	1.98644	2.19053	2.59871
3.8	1.79270	1.88004	2.01106	2.22941	2.66612
4.0	1.80192	1.89471	2.03391	2.26590	2.72989
4.2	1.81018	1.90820	2.05523	2.30027	2.79036
4.4	1.81762	1.92065	2.07518	2.33275	2.84787
4.6	1.82437	1.93220	2.09394	2.36351	2.90266
4.8	1.83051	1.94296	2.11163	2.39275	2.95499
5.0	1.83613	1.95302	2.12836	2.42060	3.00506
5.5	1.84827	1.97560	2.16658	2.48490	3.12152
6.0	1.85828	1.99518	2.20053	2.54279	3.22731
6.5	1.86666	2.01241	2.23105	2.59543	3.32420
7.0	1.87379	2.02776	2.25873	2.64366	3.41353
7.5	1.87993	2.04158	2.28405	2.68818	3.49643
8.0	1.88527	2.05411	2.30738	2.72949	3.57372
8.5	1.88996	2.06557	2.32900	2.76804	3.64611
9.0	1.89411	2.07612	2.34913	2.80415	3.71419
9.5	1.89780	2.08587	2.36797	2.83813	3.77845
10.	1.90112	2.09493	2.38566	2.87019	3.83927
11.	1.90682	2.11134	2.41811	2.92939	3.95196
12.	1.91155	2.12584	2.44729	2.89302	4.05450
13.	1.91553	2.13883	2.47379	3.03204	4.14855
14.	1.91893	2.15058	2.49805	3.07718	4.23542
15.	1.92187	2.16129	2.52043	3.11899	4.31611
16.	1.92443	2.17113	2.54118	3.15793	4.39143
17.	1.92669	2.18023	2.56054	3.19439	4.46209
18.	1.92870	2.18869	2.57867	3.22864	4.52858
19.	1.93048	2.19657	2.59571	3.26094	4.59139
20.	1.93209	2.20397	2.61180	3.29150	4.65092

TABLE B-3

AXIAL LOADING BEHAVIOR (E2 = E3 = -E1/2; S2 = S3 = -S1/2)
ORDINARY TRAPEZOIDAL INTEGRATION

	NUMERICAL SOLUTIONS $\lambda = 0$			NUMERICAL SOLUTIONS $\lambda = 1$		
	N = 20	N = 30	N = 40	N = 20	N = 30	N = 40
E1/EK	S1/SK	S1/SK	S1/SK	S1/SK	S1/SK	S1/SK
1.0	0.99768	0.99890	0.99936	0.99903	0.99954	0.99973
1.1	1.09745	1.09879	1.09929	1.09893	1.09950	1.09970
1.2	1.19721	1.19868	1.19923	1.19883	1.19945	1.19968
1.3	1.29698	1.29857	1.29916	1.29874	1.29940	1.29965
1.4	1.38262	1.38385	1.38432	1.38720	1.38752	1.38765
1.5	1.44081	1.44109	1.44232	1.45306	1.45249	1.45326
1.6	1.48459	1.48645	1.48730	1.50645	1.50719	1.50760
1.7	1.52172	1.52367	1.52456	1.55372	1.55452	1.55497
1.8	1.55269	1.55633	1.55599	1.59532	1.59764	1.59688
1.9	1.58211	1.58179	1.58348	1.63538	1.63379	1.63499
2.0	1.60234	1.60677	1.60638	1.66624	1.66942	1.66850
2.2	1.64281	1.64438	1.64512	1.72797	1.72793	1.72809
2.4	1.67217	1.67457	1.67574	1.77723	1.77811	1.77875
2.6	1.69574	1.70092	1.70172	1.81999	1.82397	1.82405
2.8	1.71932	1.72112	1.72217	1.86276	1.86221	1.86266
3.0	1.73903	1.73827	1.74068	1.90043	1.89665	1.89872
3.2	1.75036	1.75541	1.75500	1.92703	1.93109	1.92925
3.4	1.76169	1.76820	1.76932	1.95363	1.95935	1.95977
3.6	1.77302	1.77820	1.78076	1.98024	1.98367	1.98605
3.8	1.78436	1.78820	1.79010	2.00684	2.00799	2.00923
4.0	1.79569	1.79820	1.79944	2.03344	2.03230	2.03242
4.2	1.80702	1.80820	1.80878	2.06005	2.05662	2.05561
4.4	1.81506	1.81600	1.81646	2.08105	2.07720	2.07600
4.6	1.81866	1.82084	1.82193	2.09452	2.09276	2.09262
4.8	1.82225	1.82568	1.82740	2.10800	2.10832	2.10924
5.0	1.82585	1.83051	1.83287	2.12147	2.12388	2.12585
5.5	1.83485	1.84261	1.84654	2.15515	2.16278	2.16740
6.0	1.84384	1.85471	1.85617	2.18884	2.20168	2.20062
6.5	1.85284	1.86538	1.86282	2.22252	2.23738	2.22772
7.0	1.86183	1.86927	1.86948	2.25620	2.25792	2.25483
7.5	1.87083	1.87316	1.87613	2.28988	2.27846	2.28194
8.0	1.87982	1.87705	1.88279	2.32357	2.29899	2.30904
8.5	1.88882	1.88094	1.88944	2.35725	2.31953	2.33615
9.0	1.88923	1.88483	1.89181	2.36724	2.34007	2.35140
9.5	1.88923	1.88871	1.89396	2.37608	2.36061	2.36608
10.	1.88923	1.89260	1.89612	2.38492	2.38114	2.38076
11.	1.88923	1.90038	1.90043	2.40261	2.42222	2.41012
12.	1.88923	1.90815	1.90474	2.42029	2.46330	2.43948
13.	1.88923	1.91403	1.90905	2.43798	2.49715	2.46884
14.	1.88923	1.91403	1.91336	2.45566	2.50872	2.49820
15.	1.88923	1.91403	1.91767	2.47334	2.52028	2.52756
16.	1.88923	1.91403	1.92198	2.49103	2.53185	2.55692
17.	1.88923	1.91403	1.92627	2.50871	2.54341	2.58614
18.	1.88923	1.91403	1.92627	2.52639	2.55498	2.59473
19.	1.88923	1.91403	1.92627	2.54408	2.56654	2.60331
20.	1.88923	1.91403	1.92627	2.56176	2.57811	2.61190

TABLE B-4

AXIAL LOADING BEHAVIOR (E2 = E3 = -E1/2; S2 = S3 = -S1/2)
MODIFIED TRAPEZOIDAL INTEGRATION

	NUMERICAL SOLUTIONS λ = 0			NUMERICAL SOLUTIONS λ = 1		
	N = 20	N = 30	N = 40	N = 20	N = 30	N = 40
E1/EK	S1/SK	S1/SK	S1/SK	S1/SK	S1/SK	S1/SK
1.0	0.99976	0.99989	0.99993	1.00008	1.00003	1.00002
1.1	1.09973	1.09987	1.09993	1.10009	1.10004	1.10002
1.2	1.19971	1.19986	1.19992	1.20010	1.20004	1.20002
1.3	1.29968	1.29985	1.29991	1.30011	1.30005	1.30002
1.4	1.38552	1.38522	1.38513	1.38867	1.38821	1.38805
1.5	1.44389	1.44255	1.44317	1.45462	1.45323	1.45368
1.6	1.48786	1.48800	1.48820	1.50811	1.50796	1.50805
1.7	1.52515	1.52529	1.52551	1.55547	1.55534	1.55544
1.8	1.55629	1.55803	1.55698	1.59715	1.59850	1.59737
1.9	1.58587	1.58357	1.58452	1.63729	1.63429	1.63550
2.0	1.60627	1.60862	1.60746	1.66824	1.67035	1.66904
2.2	1.64706	1.64637	1.64628	1.73013	1.72893	1.72867
2.4	1.67672	1.67671	1.67699	1.77954	1.77919	1.77937
2.6	1.70060	1.70319	1.70305	1.82246	1.82512	1.82471
2.8	1.72447	1.72354	1.72357	1.86538	1.86343	1.86336
3.0	1.74448	1.74081	1.74216	1.90320	1.89793	1.89946
3.2	1.75611	1.75809	1.75656	1.92995	1.93244	1.93003
3.4	1.76773	1.77101	1.77096	1.95671	1.96077	1.96059
3.6	1.77936	1.78114	1.78247	1.98346	1.98515	1.98690
3.8	1.79098	1.79127	1.79188	2.01021	2.00954	2.01013
4.0	1.80261	1.80140	1.80130	2.03696	2.03392	2.03335
4.2	1.81423	1.81153	1.81071	2.06371	2.05830	2.05658
4.4	1.82255	1.81946	1.81847	2.08486	2.07895	2.07700
4.6	1.82644	1.82443	1.82401	2.09848	2.09457	2.09366
4.8	1.83032	1.82939	1.82955	2.11209	2.11020	2.11031
5.0	1.83420	1.83436	1.83509	2.12571	2.12582	2.12697
5.5	1.84390	1.84678	1.84894	2.15975	2.16488	2.16861
6.0	1.85361	1.85919	1.85874	2.19379	2.20394	2.20191
6.5	1.86331	1.87018	1.86558	2.22783	2.23980	2.22911
7.0	1.87301	1.87438	1.87241	2.26187	2.26050	2.25630
7.5	1.88272	1.87858	1.87924	2.29591	2.28119	2.28350
8.0	1.89242	1.88278	1.88607	2.32995	2.30189	2.31070
8.5	1.90212	1.88698	1.89291	2.36399	2.32258	2.33789
9.0	1.90324	1.89118	1.89545	2.37433	2.34328	2.35323
9.5	1.90394	1.89538	1.89778	2.38352	2.36397	2.36800
10.	1.90464	1.89958	1.90011	2.39271	2.38467	2.38277
11.	1.90603	1.90798	1.90476	2.41109	2.42606	2.41230
12.	1.90743	1.91638	1.90942	2.42947	2.46744	2.44184
13.	1.90883	1.92288	1.91408	2.44785	2.50161	2.47138
14.	1.91023	1.92349	1.91874	2.46622	2.51349	2.50091
15.	1.91163	1.92411	1.92340	2.48460	2.52536	2.53045
16.	1.91303	1.92473	1.92806	2.50298	2.53723	2.55998
17.	1.91442	1.92535	1.93269	2.52136	2.54910	2.58937
18.	1.91583	1.92596	1.93304	2.53974	2.56098	2.59813
19.	1.91723	1.92658	1.93339	2.55812	2.57285	2.60689
20.	1.91863	1.92720	1.93373	2.57649	2.58472	2.61565

TABLE B-5

PURE SHEAR LOADING (E2 = -E1; S2 = -S1; E3 = S3 = 0)
ORDINARY TRAPEZOIDAL INTEGRATION

	NUMERICAL SOLUTIONS $\lambda = 0$			NUMERICAL SOLUTIONS $\lambda = 1$		
	N = 20	N = 30	N = 40	N = 20	N = 30	N = 40
E1/EK	S1/SK	S1/SK	S1/SK	S1/SK	S1/SK	S1/SK
1.0	0.99768	0.99890	0.99936	0.99903	0.99954	0.99973
1.1	1.08866	1.09015	1.09060	1.09223	1.09291	1.09308
1.2	1.16501	1.16643	1.16704	1.17395	1.17452	1.17480
1.3	1.22950	1.23111	1.23180	1.24592	1.24660	1.24693
1.4	1.28472	1.28611	1.28671	1.30995	1.31039	1.31061
1.5	1.33103	1.33310	1.33365	1.36603	1.36703	1.36719
1.6	1.37123	1.37298	1.37377	1.41637	1.41704	1.41741
1.7	1.40543	1.40734	1.40809	1.46108	1.46173	1.46203
1.8	1.43426	1.43631	1.43711	1.50014	1.50099	1.50130
1.9	1.45830	1.46080	1.46161	1.53436	1.53547	1.53581
2.0	1.47833	1.48079	1.48152	1.56381	1.56501	1.56520
2.2	1.50664	1.50876	1.50973	1.60884	1.60924	1.60971
2.4	1.52517	1.52833	1.52905	1.64123	1.64285	1.64288
2.6	1.53948	1.54243	1.54350	1.66777	1.66899	1.66946
2.8	1.55014	1.55318	1.55435	1.68888	1.69034	1.69089
3.0	1.55904	1.56177	1.56289	1.70763	1.70830	1.70877
3.2	1.56580	1.56878	1.56982	1.72315	1.72397	1.72411
3.4	1.57117	1.57413	1.57531	1.73586	1.73662	1.73702
3.6	1.57540	1.57858	1.57987	1.74662	1.74778	1.74837
3.8	1.57887	1.58251	1.58371	1.75650	1.75792	1.75819
4.0	1.58204	1.58559	1.58693	1.76512	1.76635	1.76705
4.2	1.58484	1.58830	1.58978	1.77278	1.77419	1.77517
4.4	1.58718	1.59085	1.59213	1.77980	1.78172	1.78204
4.6	1.58904	1.59293	1.59402	1.78606	1.78828	1.78814
4.8	1.59057	1.59470	1.59584	1.79180	1.79396	1.79395
5.0	1.59204	1.59614	1.59744	1.79703	1.79900	1.79924
5.5	1.59563	1.59910	1.60049	1.80960	1.80993	1.81016
6.0	1.59835	1.60144	1.60304	1.81967	1.81898	1.81996
6.5	1.59991	1.60325	1.60483	1.82793	1.82652	1.82749
7.0	1.60080	1.60455	1.60619	1.83392	1.83293	1.83371
7.5	1.60154	1.60564	1.60727	1.83822	1.83849	1.83920
8.0	1.60224	1.60673	1.60823	1.84212	1.84404	1.84394
8.5	1.60295	1.60770	1.60899	1.84603	1.84870	1.84807
9.0	1.60366	1.60835	1.60960	1.84993	1.85269	1.85176
9.5	1.60417	1.60883	1.61008	1.85369	1.85643	1.85492
10.	1.60439	1.60914	1.61053	1.85637	1.85925	1.85797
11.	1.60474	1.60962	1.61142	1.86082	1.86353	1.86372
12.	1.60509	1.61004	1.61203	1.86527	1.86691	1.86831
13.	1.60537	1.61047	1.61239	1.86939	1.87028	1.87217
14.	1.60537	1.61083	1.61262	1.87229	1.87361	1.87488
15.	1.60537	1.61097	1.61280	1.87398	1.87614	1.87684
16.	1.60537	1.61107	1.61298	1.87560	1.87811	1.87871
17.	1.60537	1.61118	1.61316	1.87722	1.88008	1.88058
18.	1.60537	1.61128	1.61334	1.87885	1.88205	1.88245
19.	1.60537	1.61138	1.61344	1.88047	1.88402	1.88426
20.	1.60537	1.61140	1.61349	1.88209	1.88541	1.88555

TABLE B-6

BIAXIAL STRAIN BEHAVIOR FOR $\lambda = 0$ (E22 = E33 = -E11/2)

E11	E12=E21	S11	S22	S33	$\frac{S12+S21}{2}$	$\frac{S12-S21}{2}$	θ_s	θ_e
2	0	1.6063	-.8031	-.8031	0	0	0	0
2	.2	1.5715	-.7825	-.7890	.1853	-.0052	4.47	3.80
2	.4	1.5224	-.7553	-.7672	.3604	-.0116	8.78	7.47
2	.6	1.4607	-.7226	-.7380	.5221	-.0185	12.78	10.90
2	.8	1.3887	-.6863	-.7024	.6689	-.0252	16.41	14.04
2	1.0	1.3100	-.6484	-.6616	.8007	-.0309	19.64	16.85
2	1.2	1.2284	-.6113	-.6171	.9178	-.0361	22.47	19.33
2	1.4	1.1445	-.5744	-.5701	1.0203	-.0394	24.95	21.51
2	1.6	1.0633	-.5410	-.5223	1.1086	-.0438	27.06	23.42
2	1.8	.9841	-.5089	-.4752	1.1856	-.0457	28.90	25.10
2	2.0	.9097	-.4800	-.4297	1.2531	-.0465	30.50	26.57
2	2.2	.8383	-.4526	-.3858	1.3117	-.0451	31.90	27.86
2	2.4	.7710	-.4269	-.3442	1.3609	-.0442	33.12	29.00
2	2.6	.7086	-.4033	-.3053	1.4025	-.0426	34.19	30.01
2	2.8	.6513	-.3824	-.2690	1.4372	-.0403	35.11	30.91
2	3.0	.5990	-.3622	-.2367	1.4653	-.0375	35.92	31.72
2	3.5	.4905	-.3121	-.1784	1.5117	-.0317	37.57	33.40
2	4.0	.4036	-.2659	-.1377	1.5405	-.0284	38.87	34.72
2	4.5	.3341	-.2266	-.1075	1.5591	-.0251	39.91	35.78
2	5.0	.2775	-.1931	-.0845	1.5716	-.0216	40.74	36.65
2	5.5	.2316	-.1647	-.0669	1.5799	-.0184	41.43	37.37
2	6.0	.1944	-.1416	-.0533	1.5862	-.0156	41.98	37.98
4	0	1.8026	-.9013	-.9013	0	0	0	0
4	.2	1.7372	-.8631	-.8740	.1677	-.0134	3.67	1.91
4	.4	1.6577	-.8189	-.8387	.3255	-.0268	7.36	3.80
4	.6	1.5623	-.7684	-.7939	.4688	-.0409	10.95	5.66
4	.8	1.4632	-.7197	-.7435	.5993	-.0550	14.38	7.47
4	1.0	1.3686	-.6761	-.6925	.7222	-.0667	17.61	9.22
4	1.2	1.2772	-.6361	-.6411	.8354	-.0759	20.56	10.90
4	1.4	1.1903	-.6000	-.5903	.9386	-.0827	23.18	12.51
4	1.6	1.1067	-.5660	-.5407	1.0336	-.0864	25.51	14.04
4	1.8	1.0263	-.5341	-.4922	1.1189	-.0864	27.56	15.48
4	2.0	.9494	-.5040	-.4454	1.1963	-.0840	29.36	16.85
4	2.2	.8765	-.4757	-.4007	1.2645	-.0780	30.93	18.13
4	2.4	.8074	-.4500	-.3574	1.3226	-.0719	32.29	19.33
4	2.6	.7430	-.4261	-.3169	1.3706	-.0656	33.45	20.46
4	2.8	.6842	-.4049	-.2792	1.4092	-.0602	34.44	21.51
4	3.0	.6304	-.3850	-.2454	1.4410	-.0546	35.30	22.50
4	3.5	.5199	-.3355	-.1845	1.4931	-.0446	37.01	24.70
4	4.0	.4312	-.2895	-.1417	1.5256	-.0380	38.36	26.57
4	4.5	.3596	-.2490	-.1107	1.5466	-.0333	39.43	28.16
4	5.0	.3017	-.2145	-.0873	1.5615	-.0285	40.31	29.52
4	5.5	.2539	-.1846	-.0693	1.5720	-.0239	41.03	30.62
4	6.0	.2147	-.1592	-.0556	1.5798	-.0200	41.63	31.72

TABLE B-7

BIAXIAL STRAIN BEHAVIOR FOR $\lambda = 1$ (E22 = E33 = -E11/2)

E11	E12=E21	S11	S22	S33	$\frac{S12+S21}{2}$	$\frac{S12-S21}{2}$	θ_s	θ_e
2	0	1.6694	-.8347	-.8347	0	0	0	0
2	.2	1.6371	-.8162	-.8209	.1905	-.0034	4.42	3.80
2	.4	1.5935	-.7924	-.8011	.3741	-.0078	8.71	7.47
2	.6	1.5380	-.7629	-.7751	.5480	-.0123	12.74	10.90
2	.8	1.4715	-.7283	-.7432	.7097	-.0168	16.42	14.04
2	1.0	1.3973	-.6904	-.7070	.8580	-.0207	19.71	16.85
2	1.2	1.3202	-.6520	-.6682	.9914	-.0231	22.58	19.33
2	1.4	1.2412	-.6137	-.6275	1.1121	-.0247	25.09	21.51
2	1.6	1.1613	-.5750	-.5863	1.2198	-.0263	27.28	23.42
2	1.8	1.0833	-.5380	-.5453	1.3155	-.0265	29.18	25.10
2	2.0	1.0089	-.5034	-.5055	1.3999	-.0254	30.81	26.57
2	2.2	.9375	-.4708	-.4667	1.4733	-.0240	32.23	27.86
2	2.4	.8708	-.4408	-.4300	1.5374	-.0216	33.45	29.00
2	2.6	.8069	-.4121	-.3947	1.5924	-.0182	34.53	30.01
2	2.8	.7485	-.3868	-.3617	1.6395	-.0138	35.45	30.91
2	3.0	.6937	-.3624	-.3313	1.6785	-.0090	36.26	31.72
2	3.5	.5744	-.3034	-.2710	1.7413	-.0041	37.91	33.40
2	4.0	.4750	-.2510	-.2240	1.7793	-.0025	39.21	34.72
2	4.5	.3938	-.2071	-.1867	1.8035	-.0020	40.24	35.78
2	5.0	.3288	-.1722	-.1566	1.8199	-.0016	41.05	36.65
2	5.5	.2766	-.1442	-.1324	1.8316	-.0010	41.68	37.37
2	6.0	.2346	-.1219	-.1127	1.8402	-.0003	42.19	37.98
4	0	2.0323	-1.016	-1.016	0	0	0	0
4	.2	1.9696	-.9793	-.9903	.1699	-.0041	3.29	1.91
4	.4	1.8984	-.9408	-.9577	.3300	-.0069	6.54	3.80
4	.6	1.8157	-.8980	-.9177	.4811	-.0087	9.76	5.66
4	.8	1.7274	-.8552	-.8722	.6264	-.0094	12.94	7.47
4	1.0	1.6355	-.8111	-.8244	.7689	-.0124	16.08	9.22
4	1.2	1.5450	-.7681	-.7769	.9041	-.0168	19.01	10.90
4	1.4	1.4563	-.7265	-.7298	1.0311	-.0206	21.69	12.51
4	1.6	1.3692	-.6853	-.6839	1.1484	-.0326	24.09	14.04
4	1.8	1.2841	-.6452	-.6389	1.2553	-.0243	26.23	15.48
4	2.0	1.2024	-.6074	-.5951	1.3515	-.0224	28.10	16.85
4	2.2	1.1240	-.5711	-.5530	1.4380	-.0180	29.74	18.13
4	2.4	1.0461	-.5338	-.5123	1.5124	-.0126	31.21	19.33
4	2.6	.9708	-.4958	-.4750	1.5759	-.0086	32.52	20.46
4	2.8	.8988	-.4590	-.4398	1.6286	-.0045	33.69	21.51
4	3.0	.8309	-.4237	-.4072	1.6713	-.0012	34.71	22.50
4	3.5	.6885	-.3458	-.3427	1.7404	.0025	36.73	24.70
4	4.0	.5693	-.2783	-.2911	1.7803	.0022	38.31	26.57
4	4.5	.4731	-.2246	-.2486	1.8051	.0021	39.53	28.16
4	5.0	.3964	-.1827	-.2138	1.8217	.0016	40.49	29.52
4	5.5	.3350	-.1496	-.1854	1.8334	.0015	41.24	30.70
4	6.0	.2855	-.1238	-.1617	1.8420	.0014	41.83	31.72

APPENDIX C

YIELD SURFACES IN PRINCIPAL STRESS SPACE

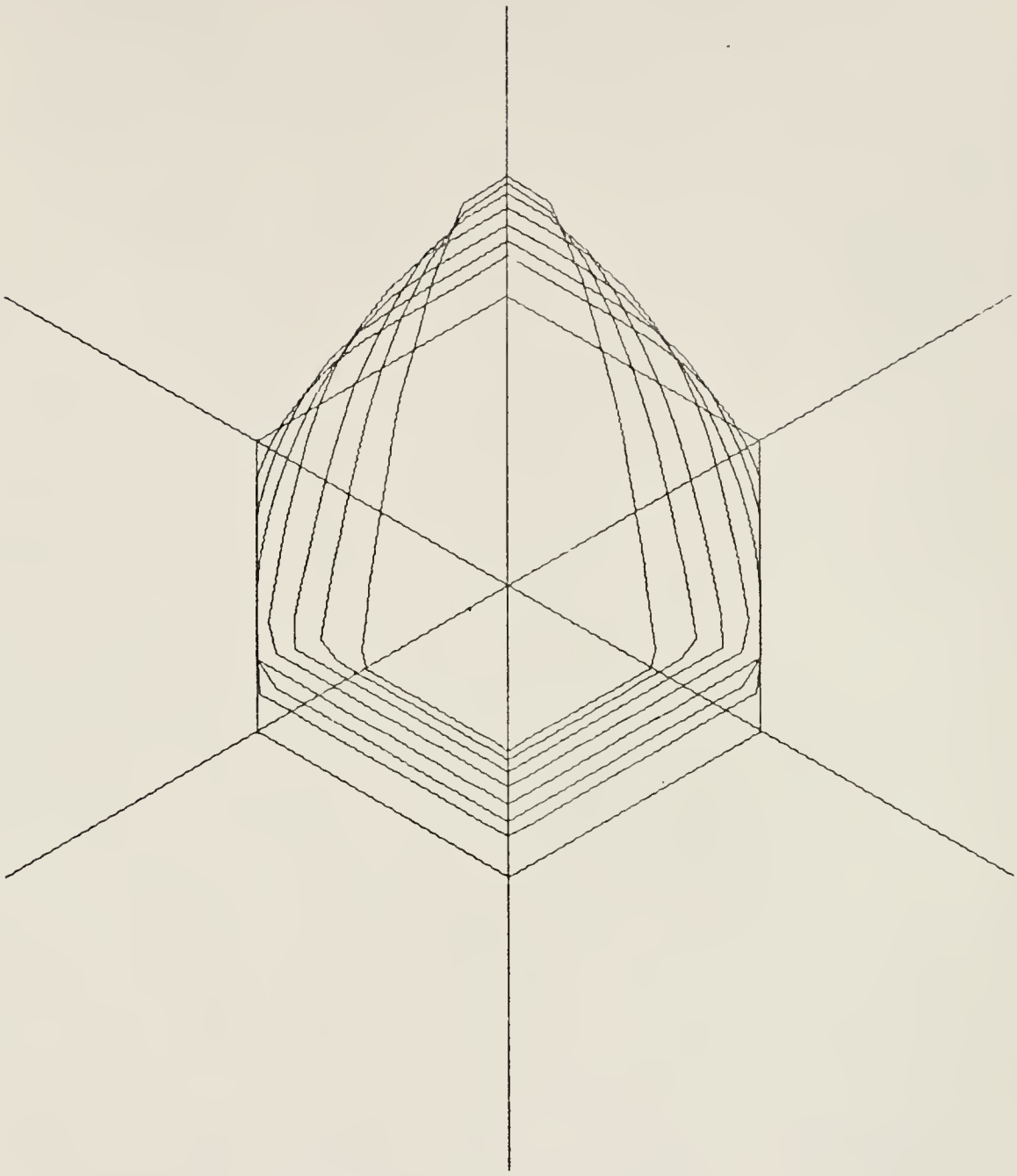

FIGURE C-1. (2,-1,-1) AXIAL LOADING
YIELD SURFACES IN PRINCIPAL STRESS SPACE ($\lambda = 0$)

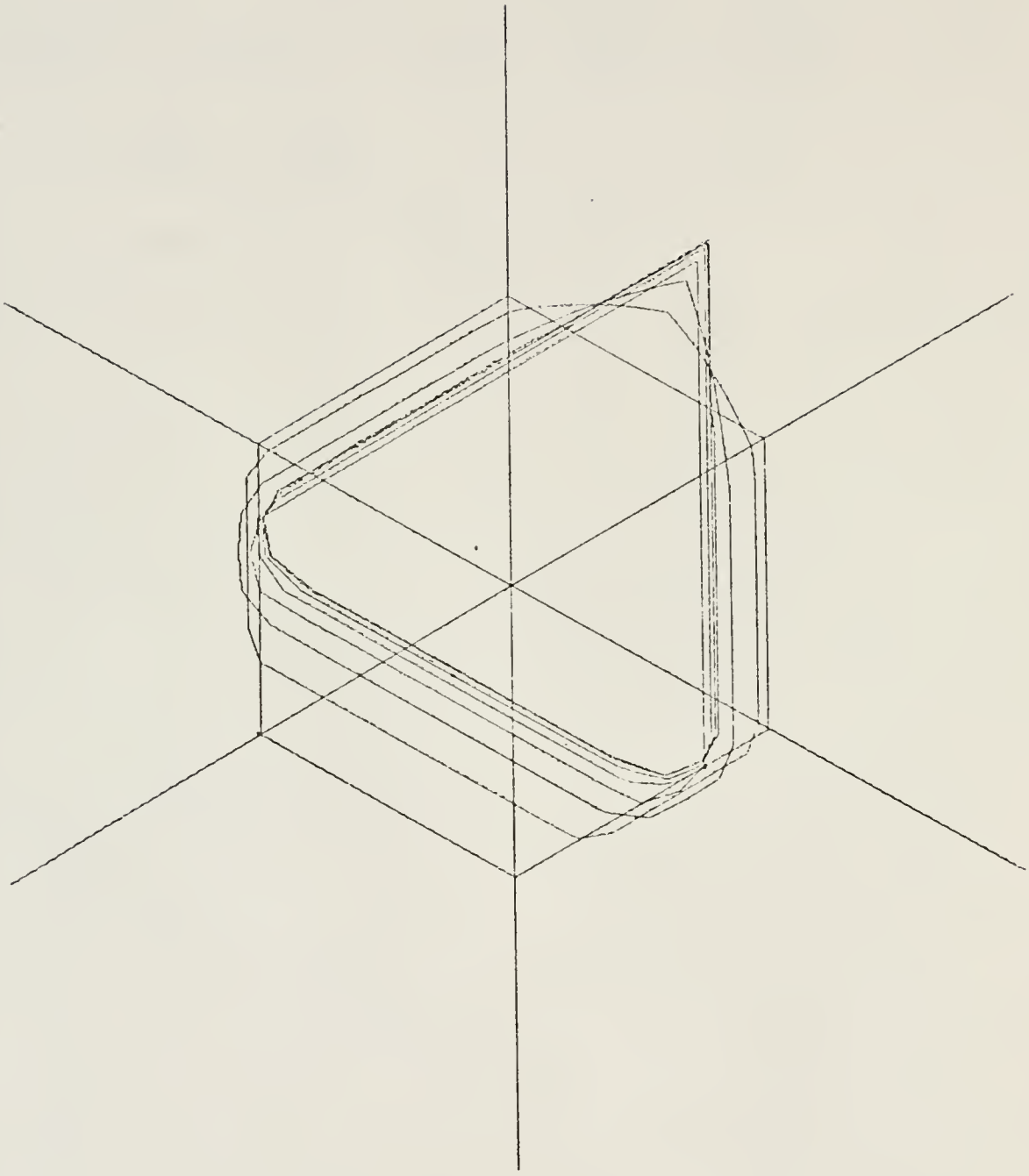

FIGURE C-2. (1,-1,0) SHEAR LOADING
YIELD SURFACES IN PRINCIPAL STRESS SPACE ($\lambda = 0$)

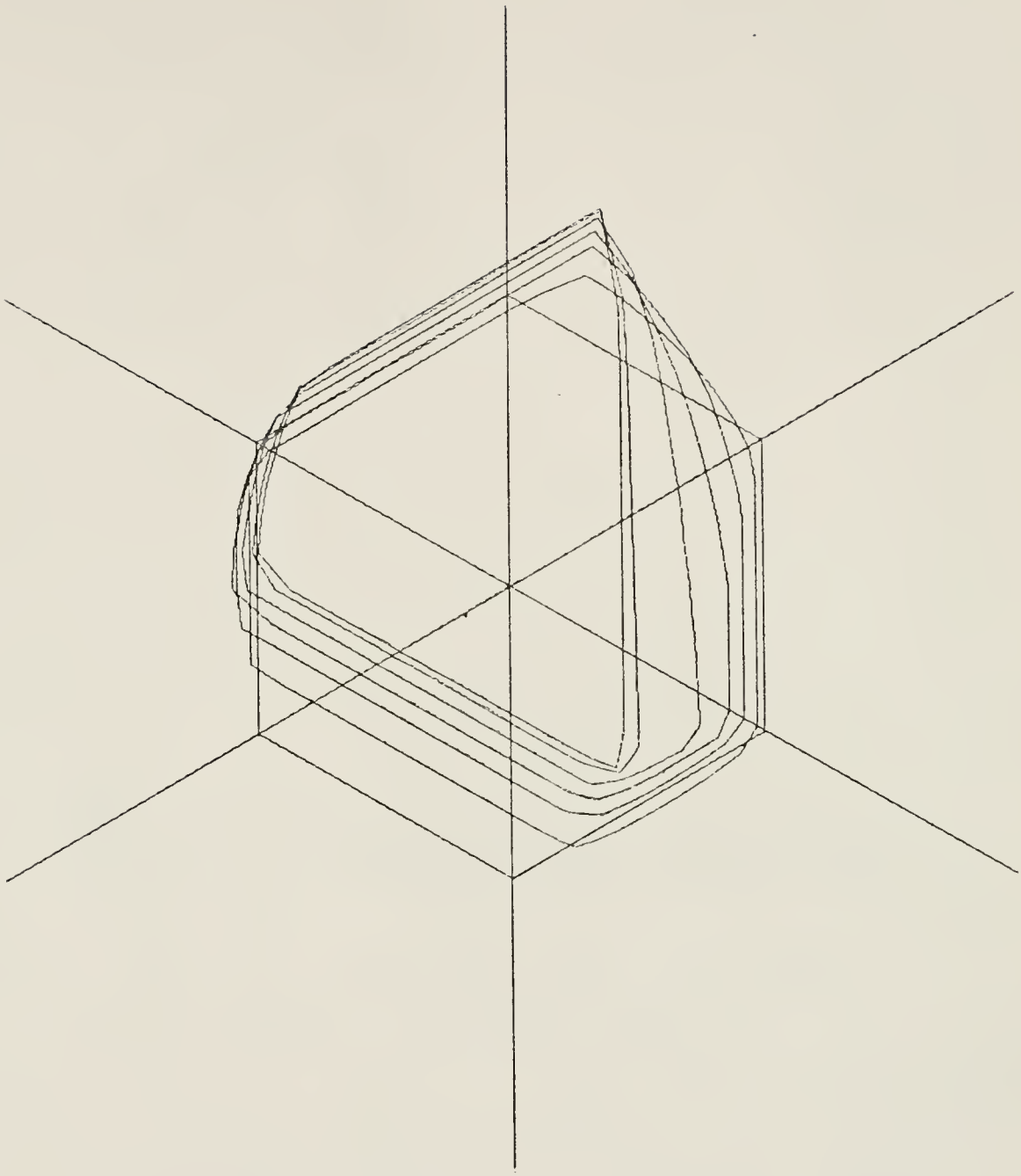

FIGURE C-3. (7,-5,-2) RADIAL LOADING
YIELD SURFACES IN PRINCIPAL STRESS SPACE ($\lambda = 0$)

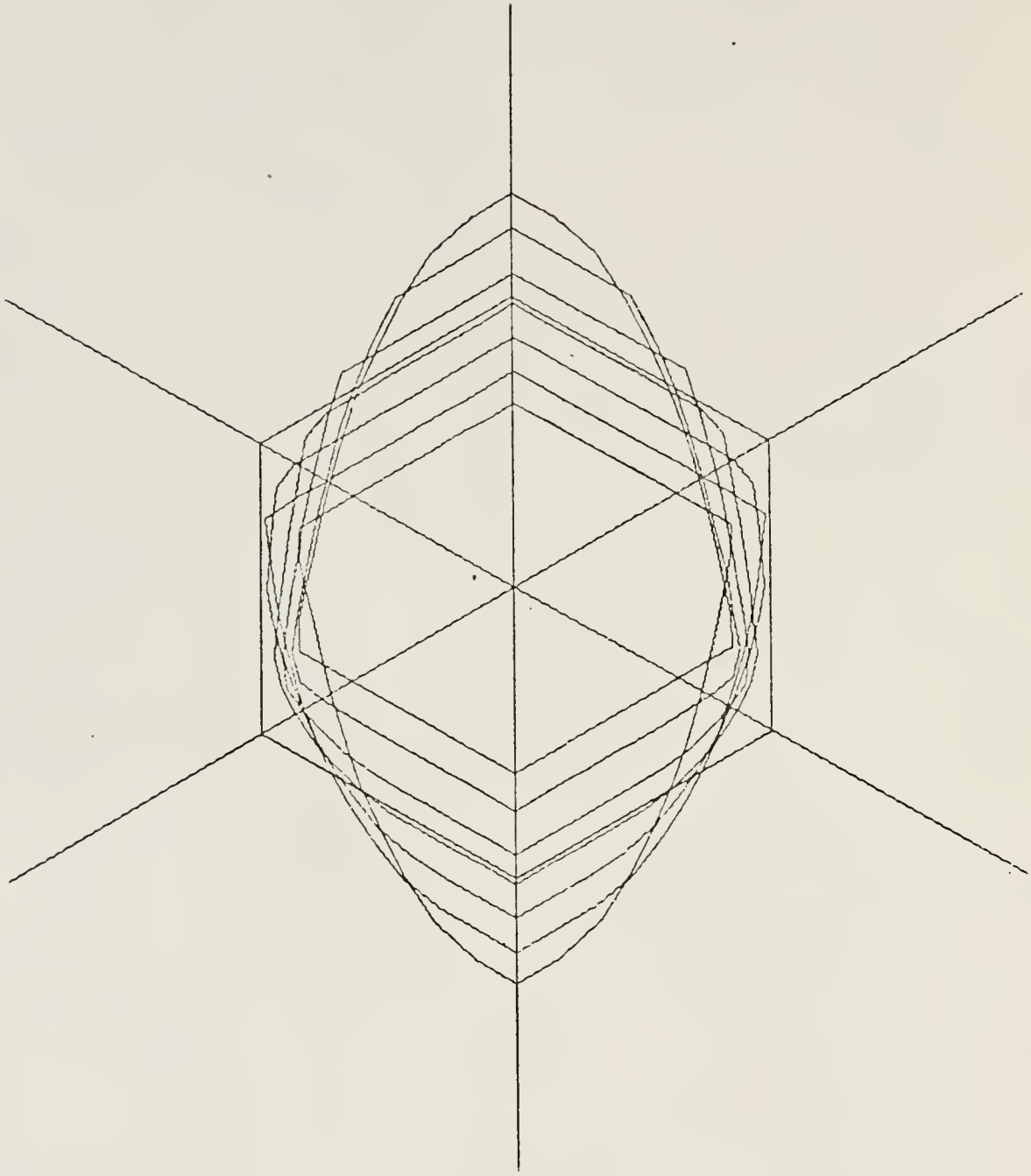

FIGURE C-4. (2,-1,-1) LOADING + REVERSED LOADING
YIELD SURFACES IN PRINCIPAL STRESS SPACE ($\lambda = 0$)

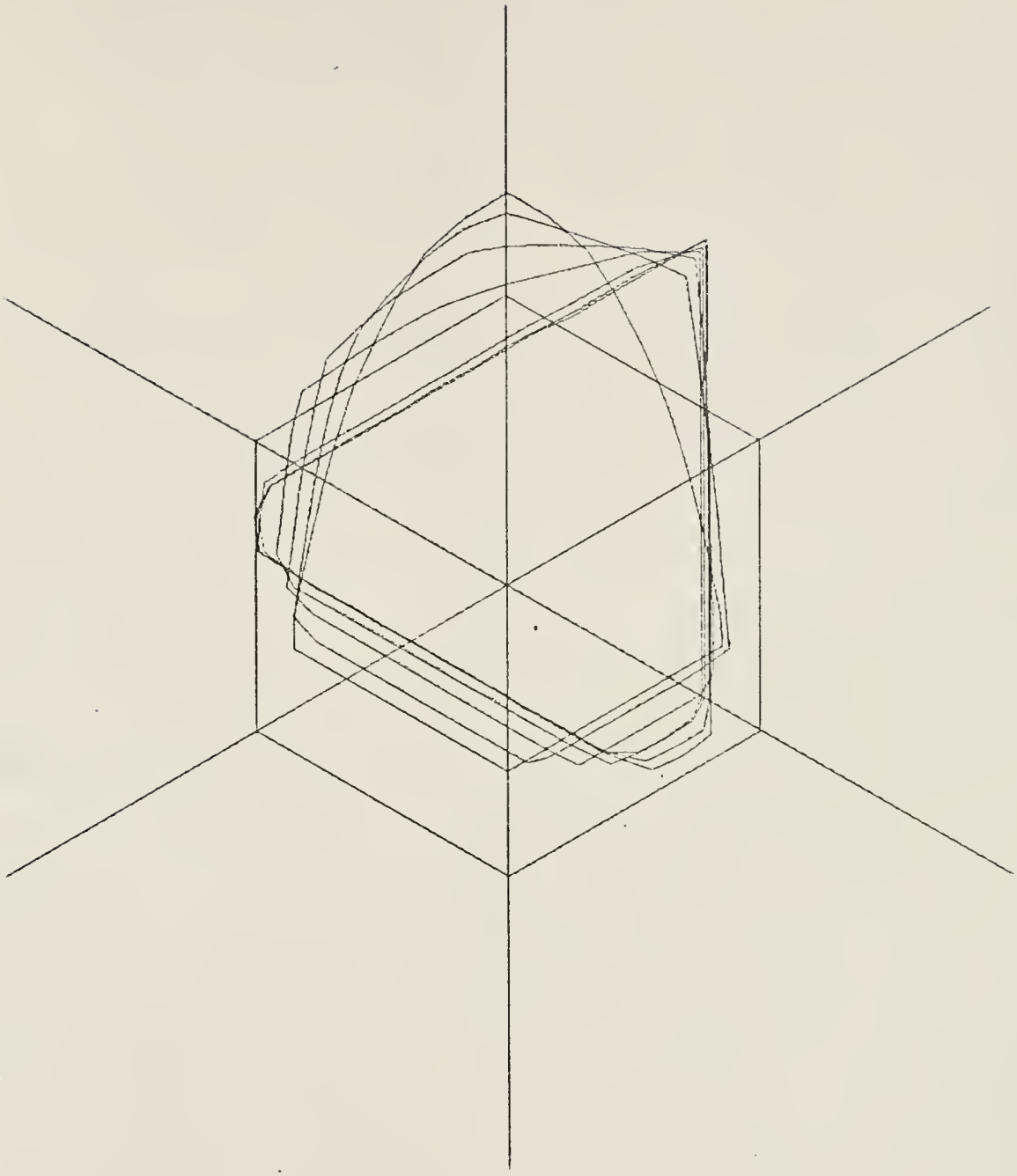

FIGURE C-5. (2,-1,-1) LOADING + (1,-1,0) STRESS LOADING
YIELD SURFACES IN PRINCIPAL STRESS SPACE ($\lambda = 0$)

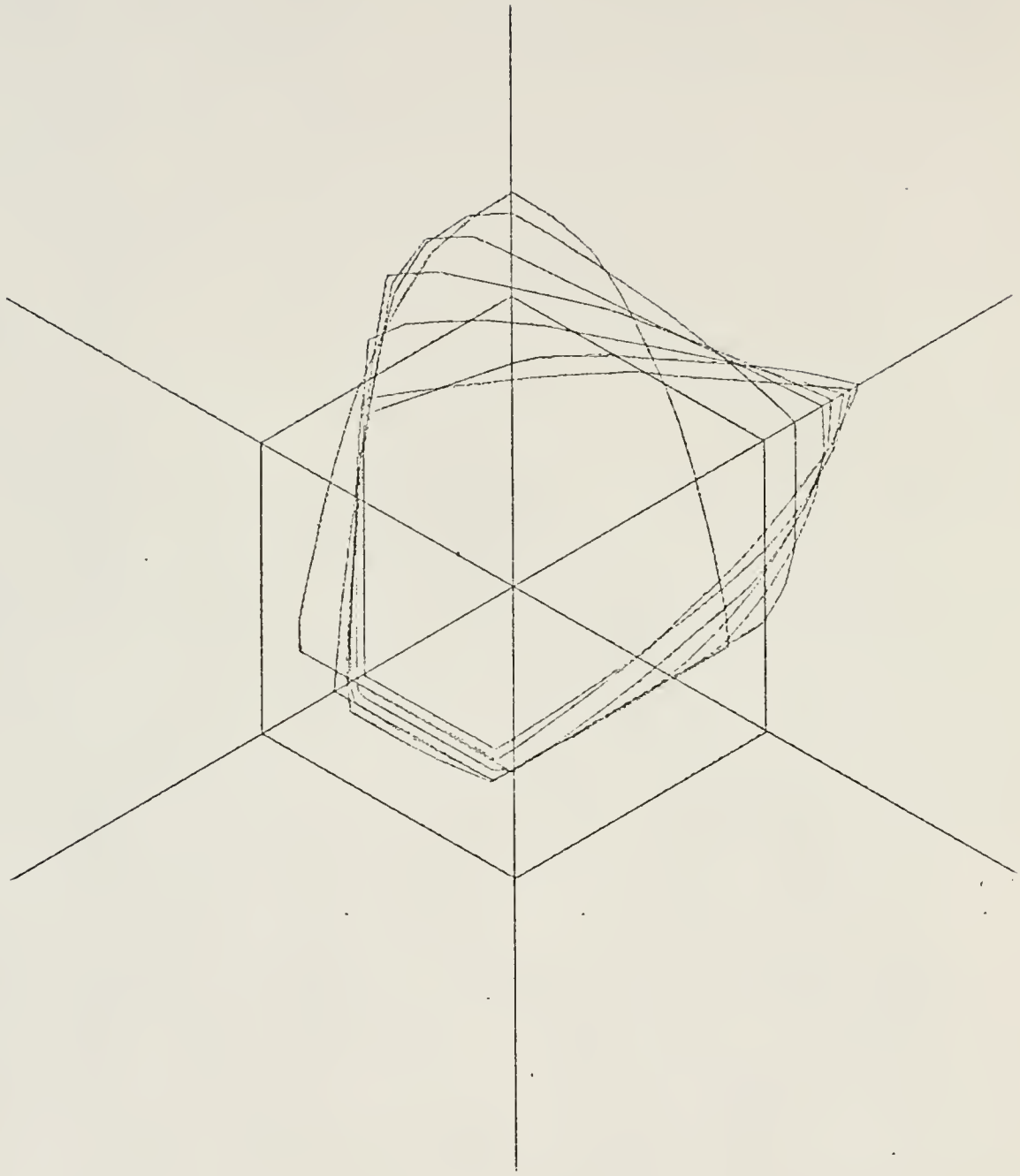

FIGURE C-6. (2,-1,-1) LOADING + (1,-2,1) STRESS LOADING
YIELD SURFACES IN PRINCIPAL STRESS SPACE ($\lambda = 0$)

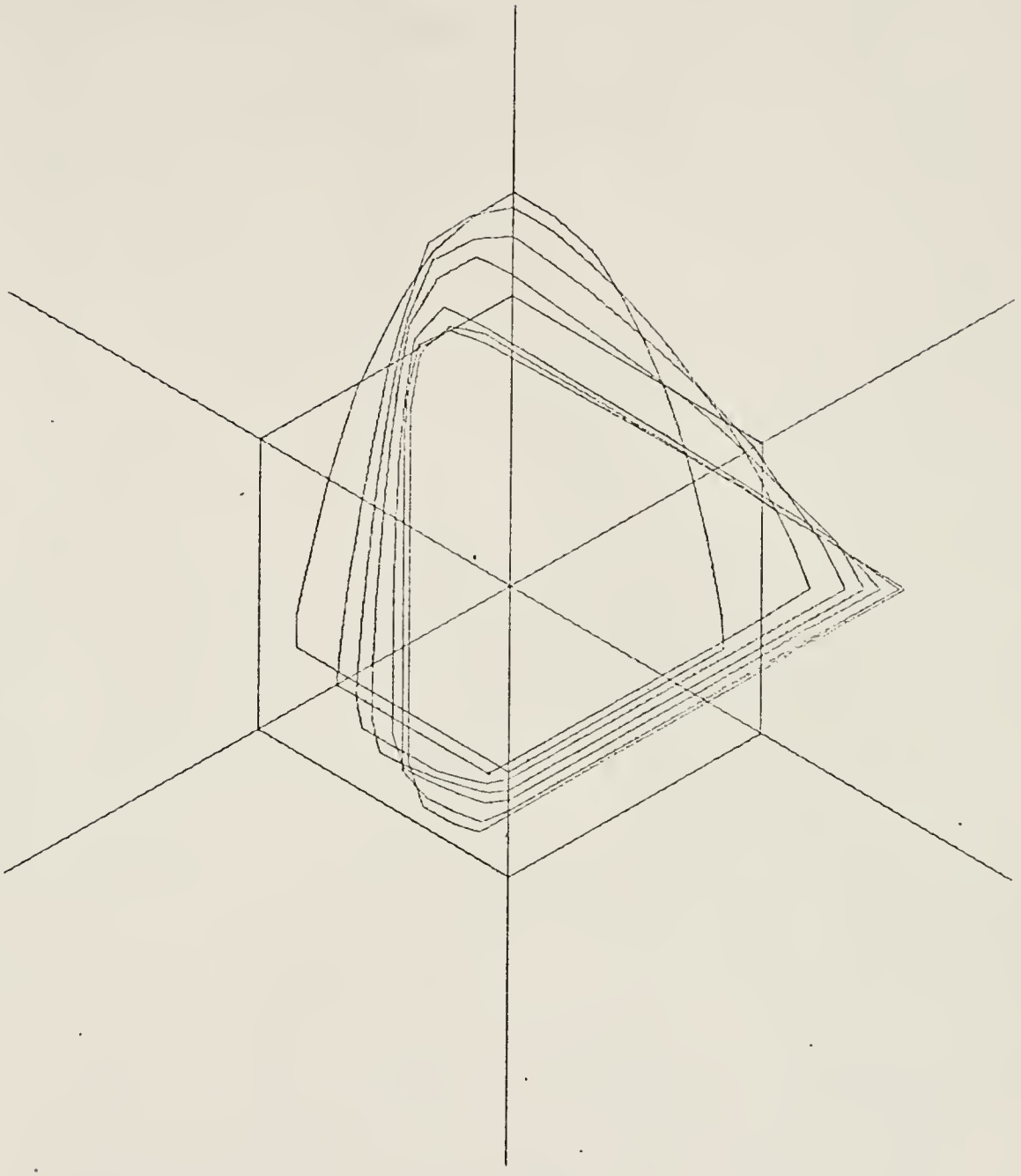

FIGURE C-7. (2,-1,-1) LOADING + (0,-1,1) STRESS LOADING
YIELD SURFACES IN PRINCIPAL STRESS SPACE ($\lambda = 0$)

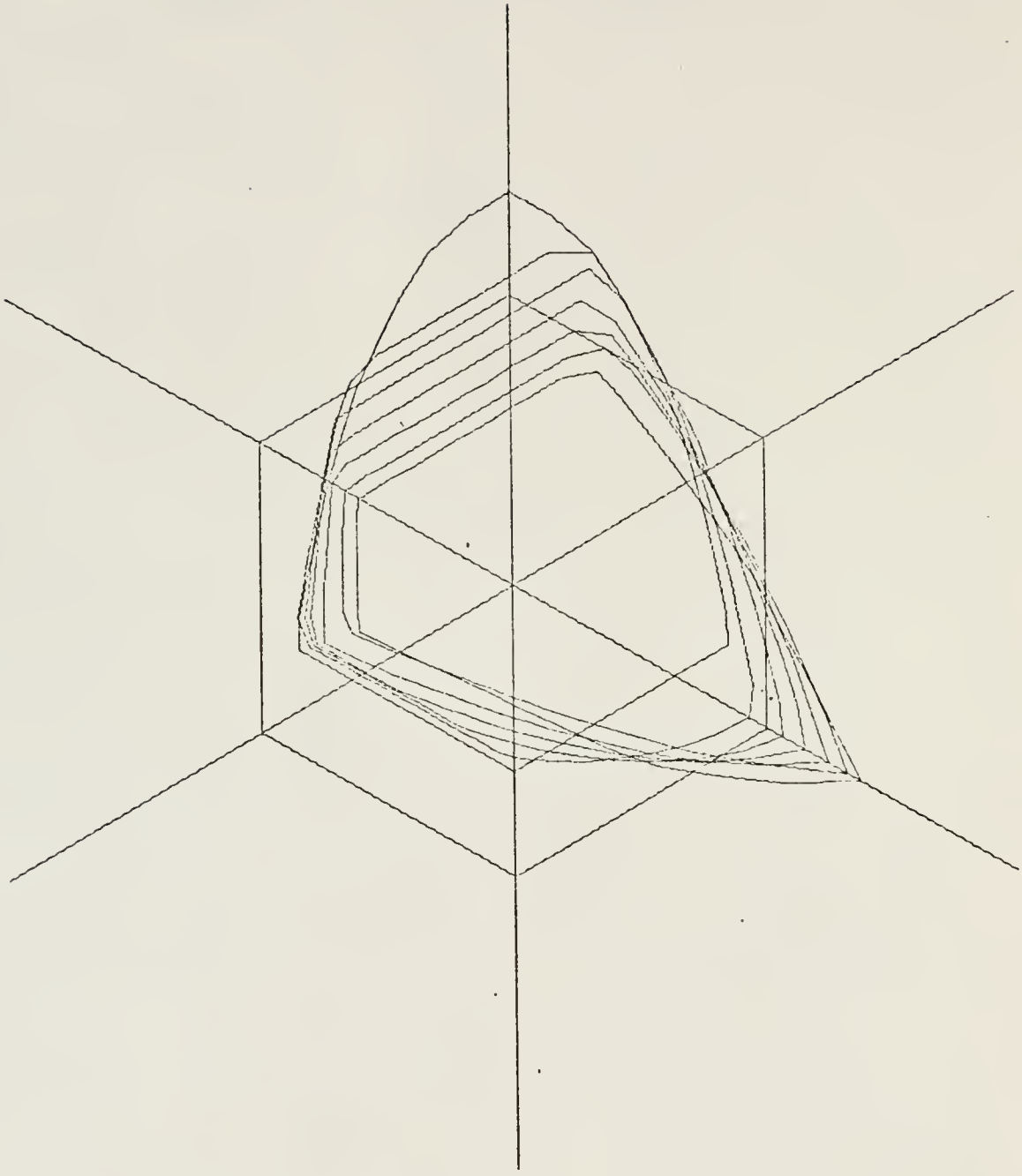

FIGURE C-8. (2,-1,-1) LOADING + (-1,-1,2) STRESS LOADING YIELD SURFACES IN PRINCIPAL STRESS SPACE ($\lambda = 0$)

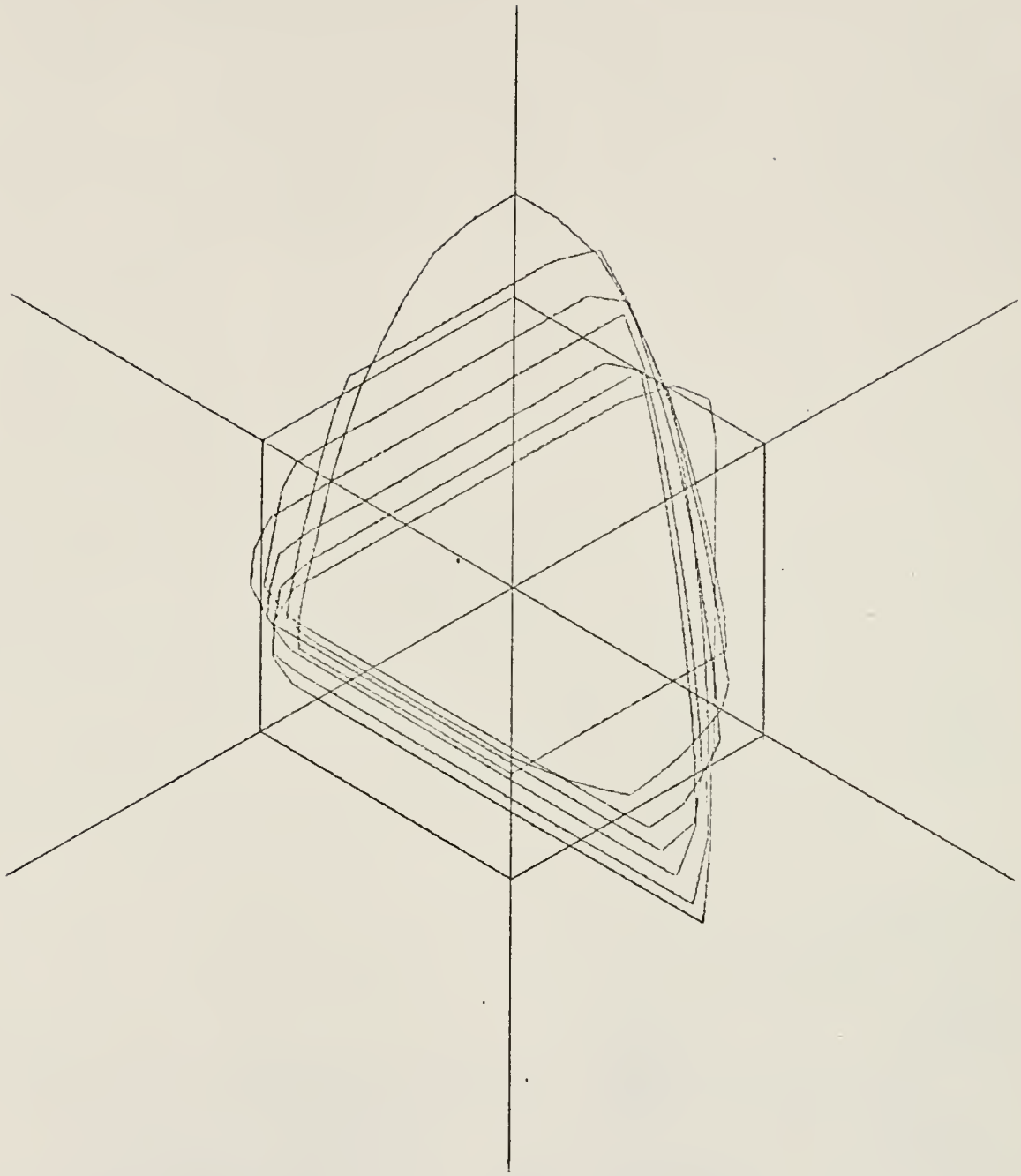

FIGURE C-9. (2,-1,-1) LOADING + (-1,0,1) STRESS LOADING YIELD SURFACES IN PRINCIPAL STRESS SPACE ($\lambda = 0$)

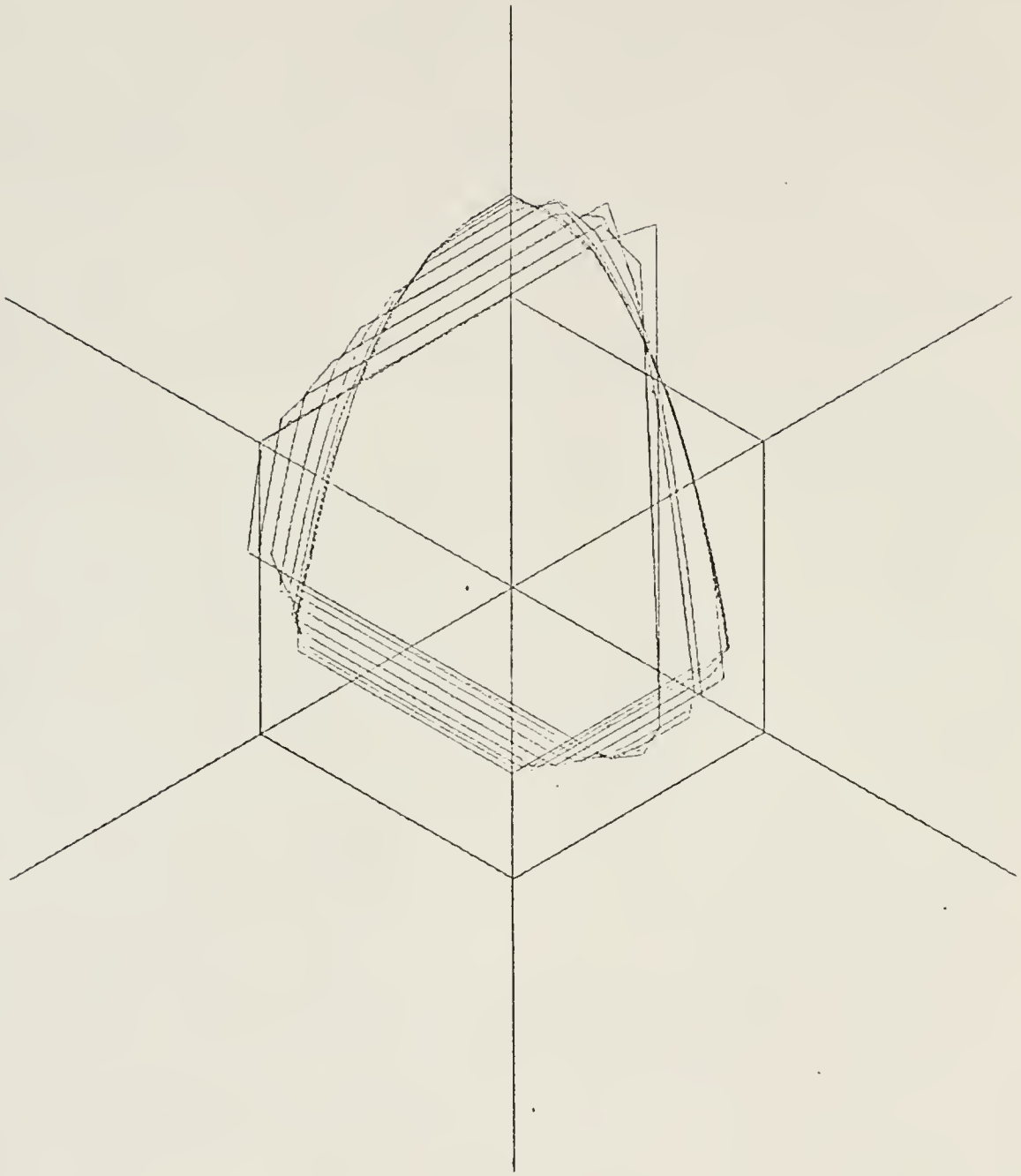

FIGURE C-10. (2,-1,-1) LOADING + (1,-1,0) STRAIN LOADING YIELD SURFACES IN PRINCIPAL STRESS SPACE ($\lambda = 0$)

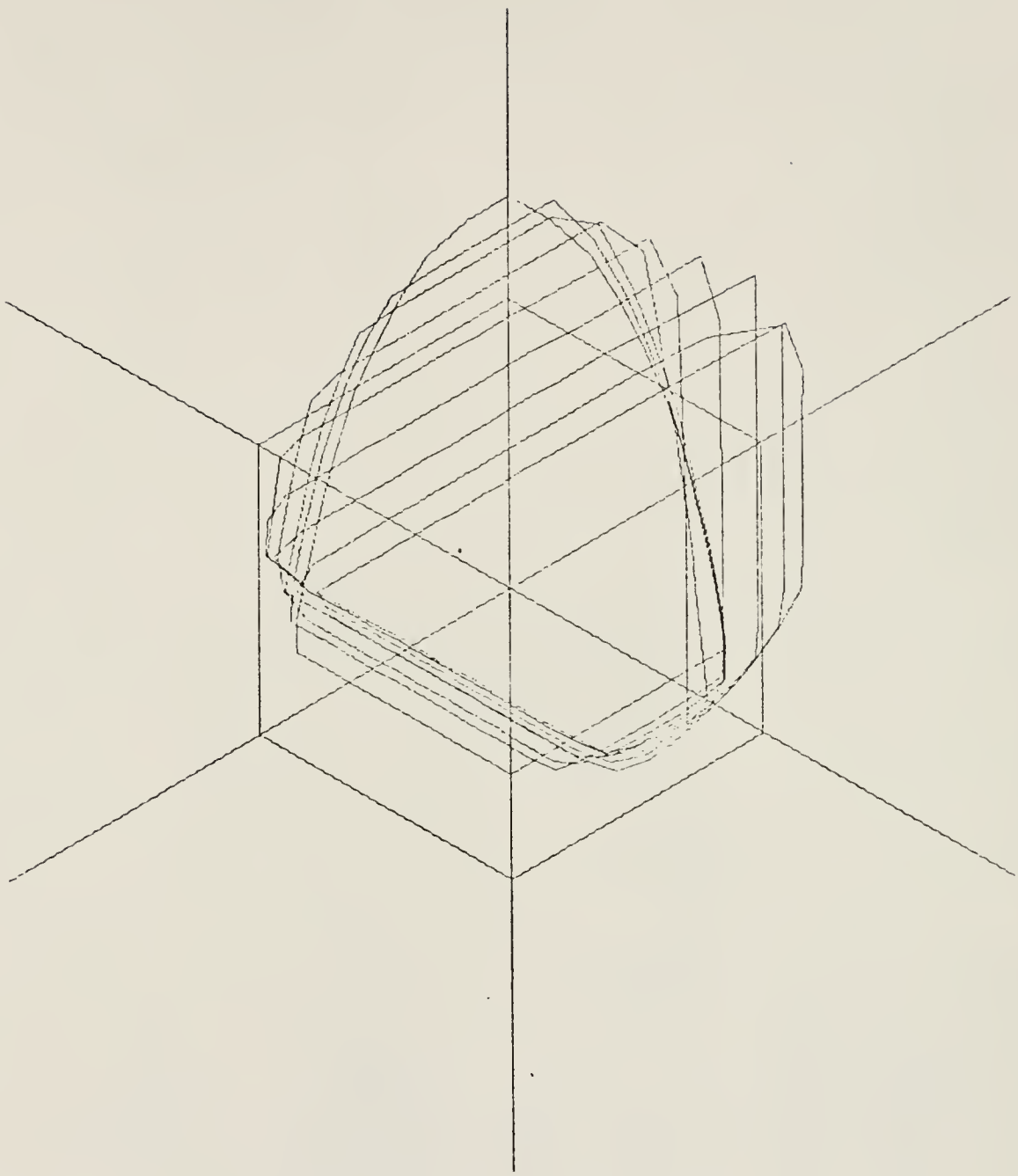

FIGURE C-11. (2,-1,-1) LOADING + (1,-2,1) STRAIN LOADING YIELD SURFACES IN PRINCIPAL STRESS SPACE ($\lambda = 0$)

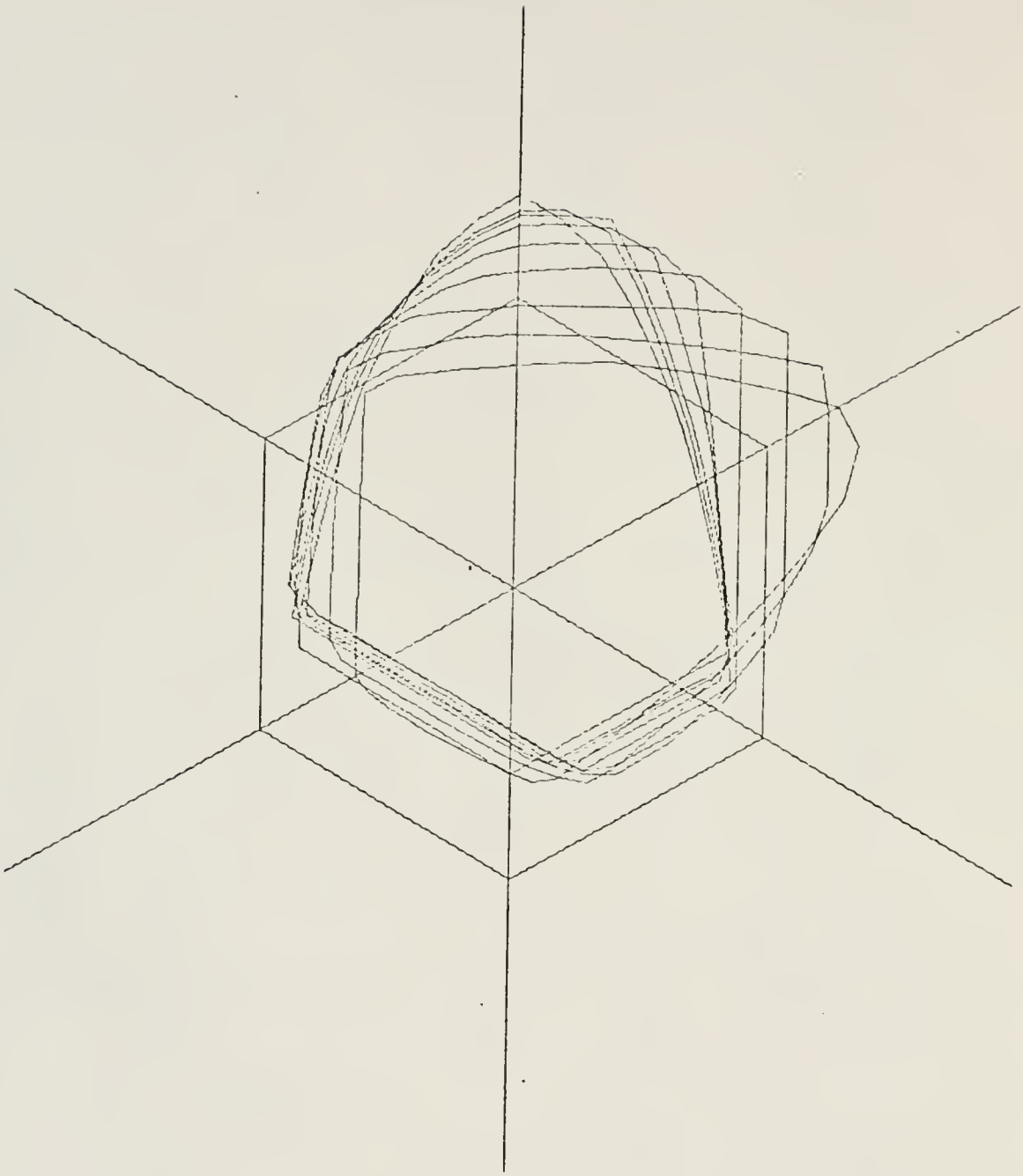

FIGURE C-12. (2,-1,-1) LOADING + (0,-1,1) STRAIN LOADING YIELD SURFACES IN PRINCIPAL STRESS SPACE ($\lambda = 0$)

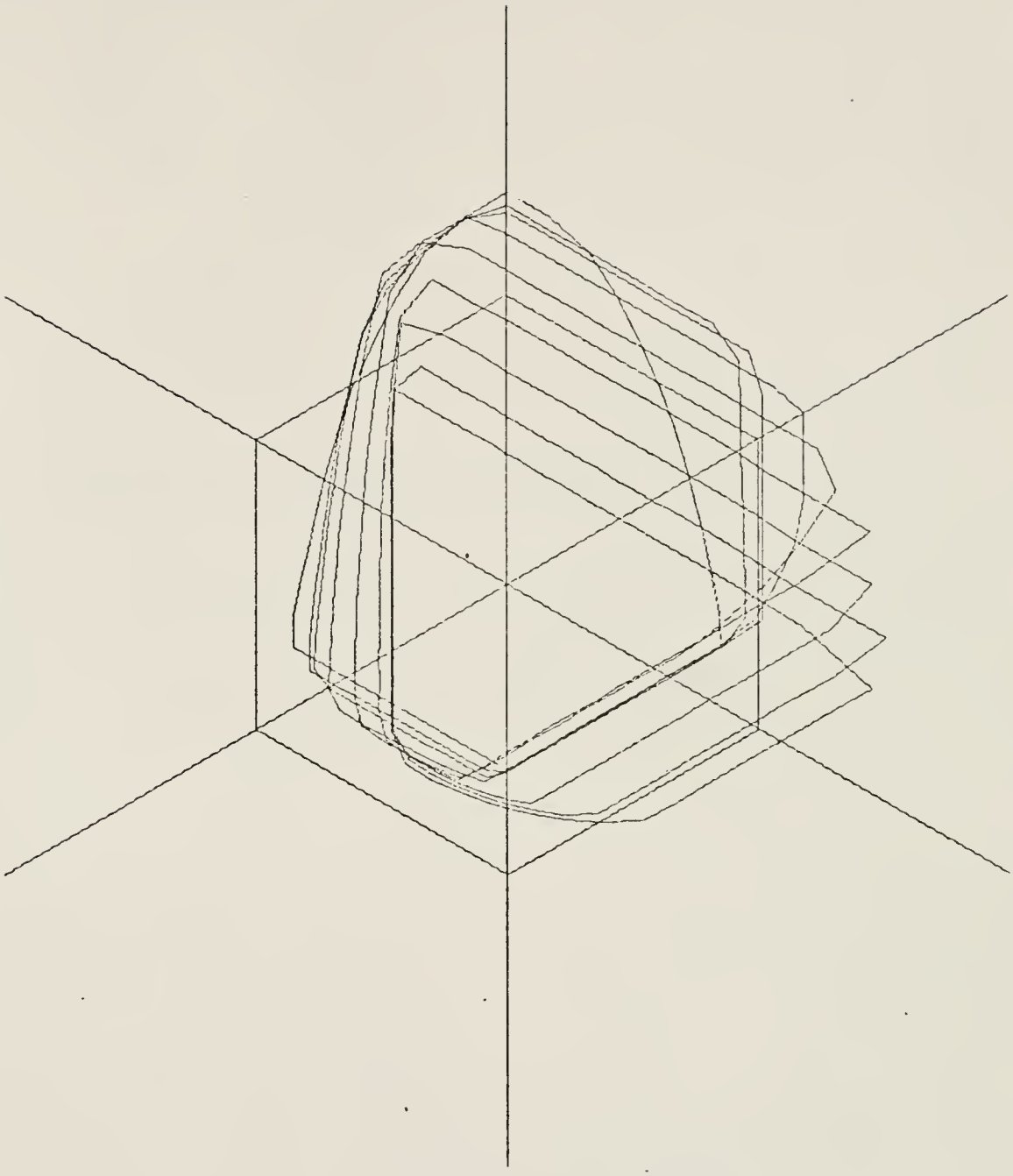

FIGURE C-13. (2,-1,-1) LOADING + (-1,-1,2) STRAIN LOADING YIELD SURFACES IN PRINCIPAL STRESS SPACE ($\lambda = 0$)

APPENDIX D

YIELD SURFACES IN PRINCIPAL STRAIN SPACE

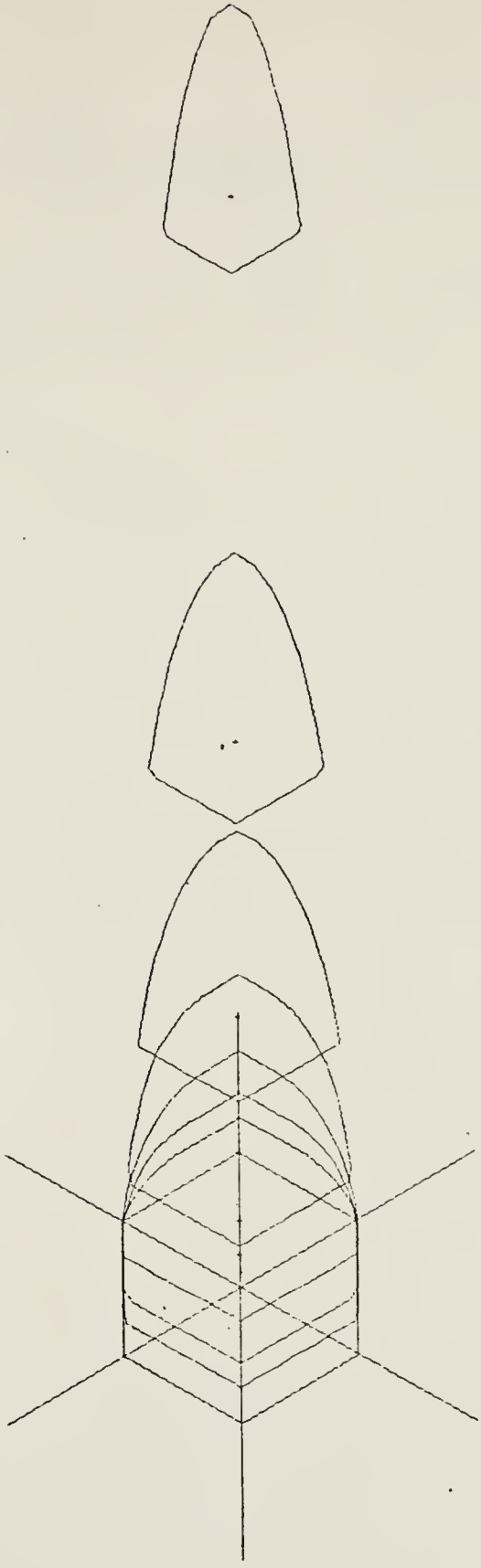

FIGURE D-1. (2,-1,-1) AXIAL LOADING
YIELD SURFACES IN PRINCIPAL STRAIN SPACE ($\lambda = 0$)

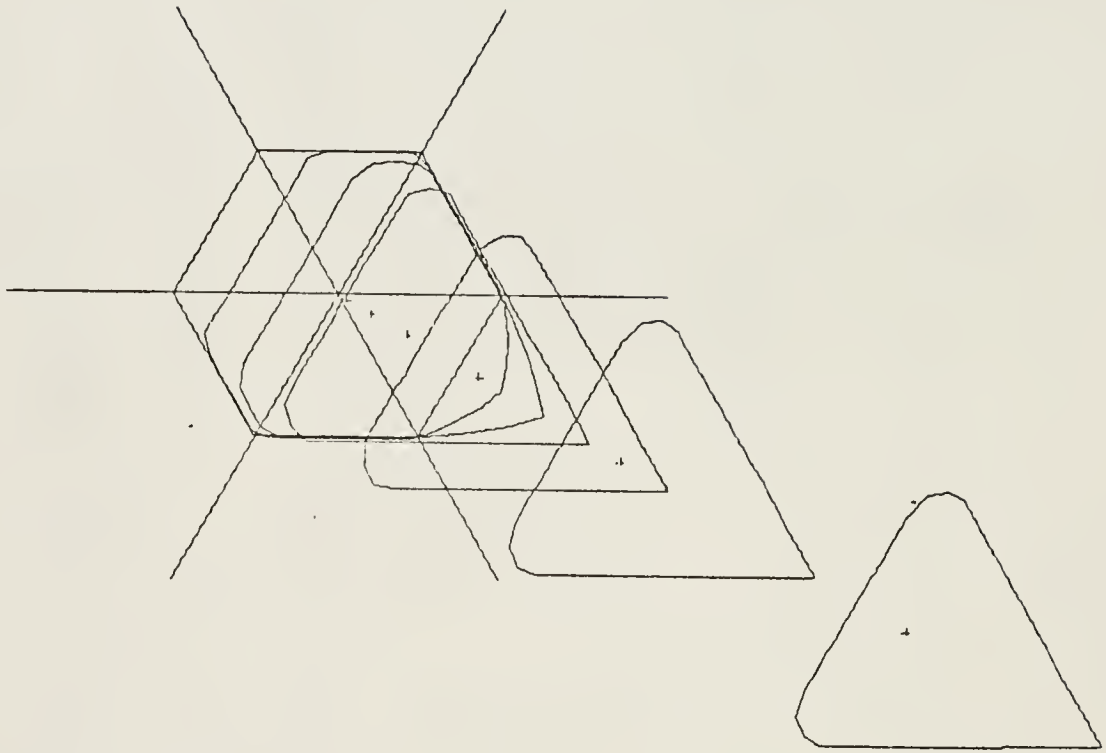

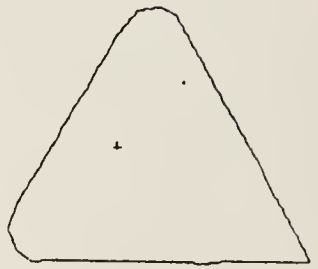

FIGURE D-2. (1,-1,0) SHEAR LOADING
YIELD SURFACES IN PRINCIPAL STRAIN SPACE ($\lambda = 0$)

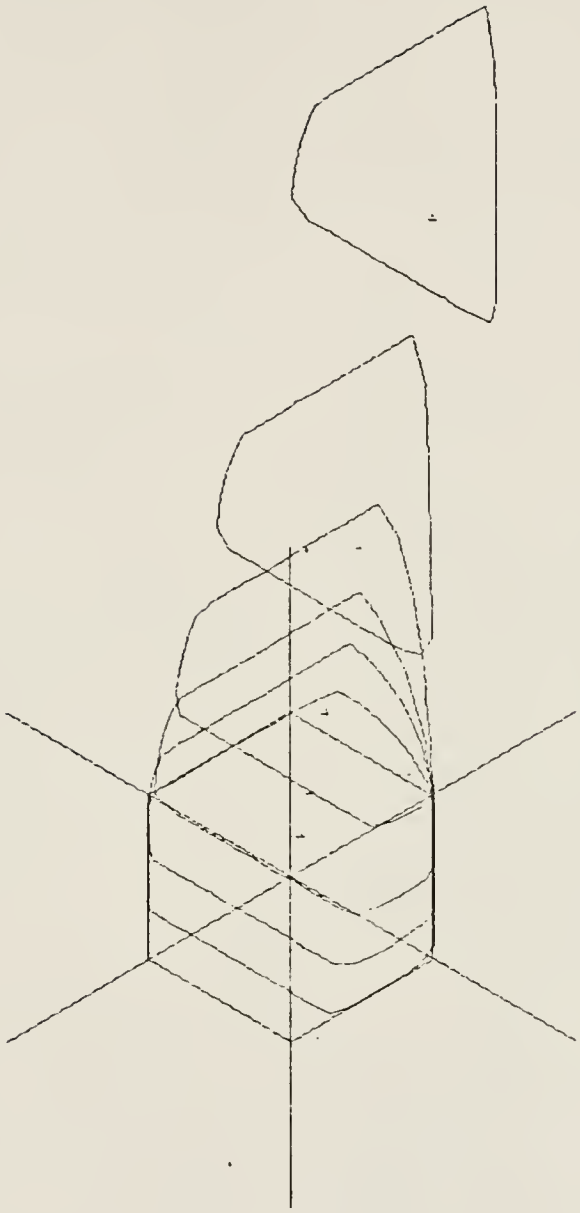

FIGURE D-3. (7,-5,-2) RADIAL LOADING
YIELD SURFACES IN PRINCIPAL STRAIN SPACE ($\lambda = 0$)

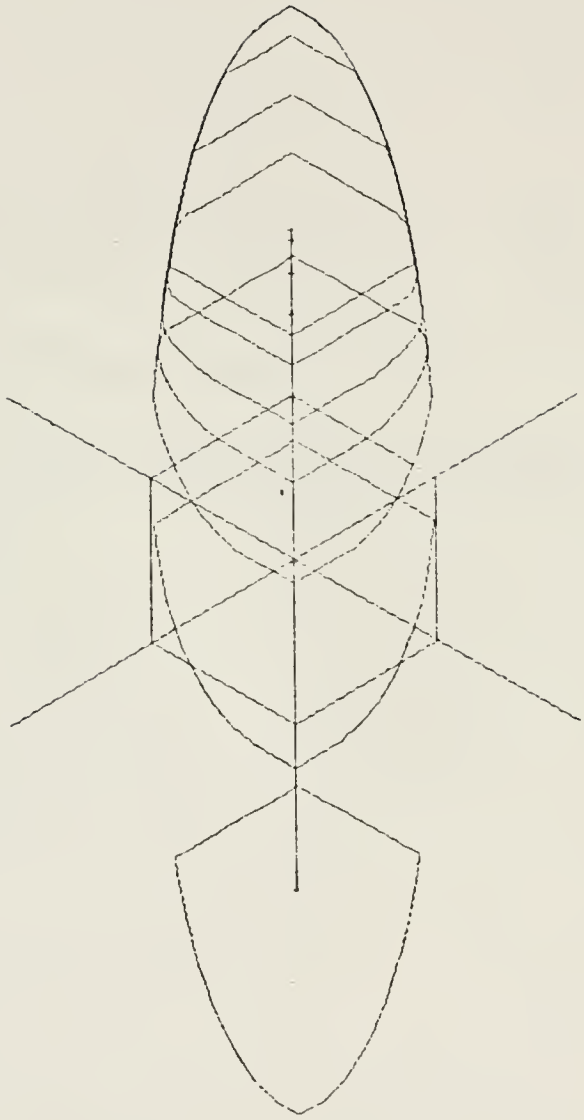

FIGURE D-4. (2,-1,-1) LOADING + REVERSED LOADING YIELD SURFACES IN PRINCIPAL STRAIN SPACE ($\lambda = 0$)

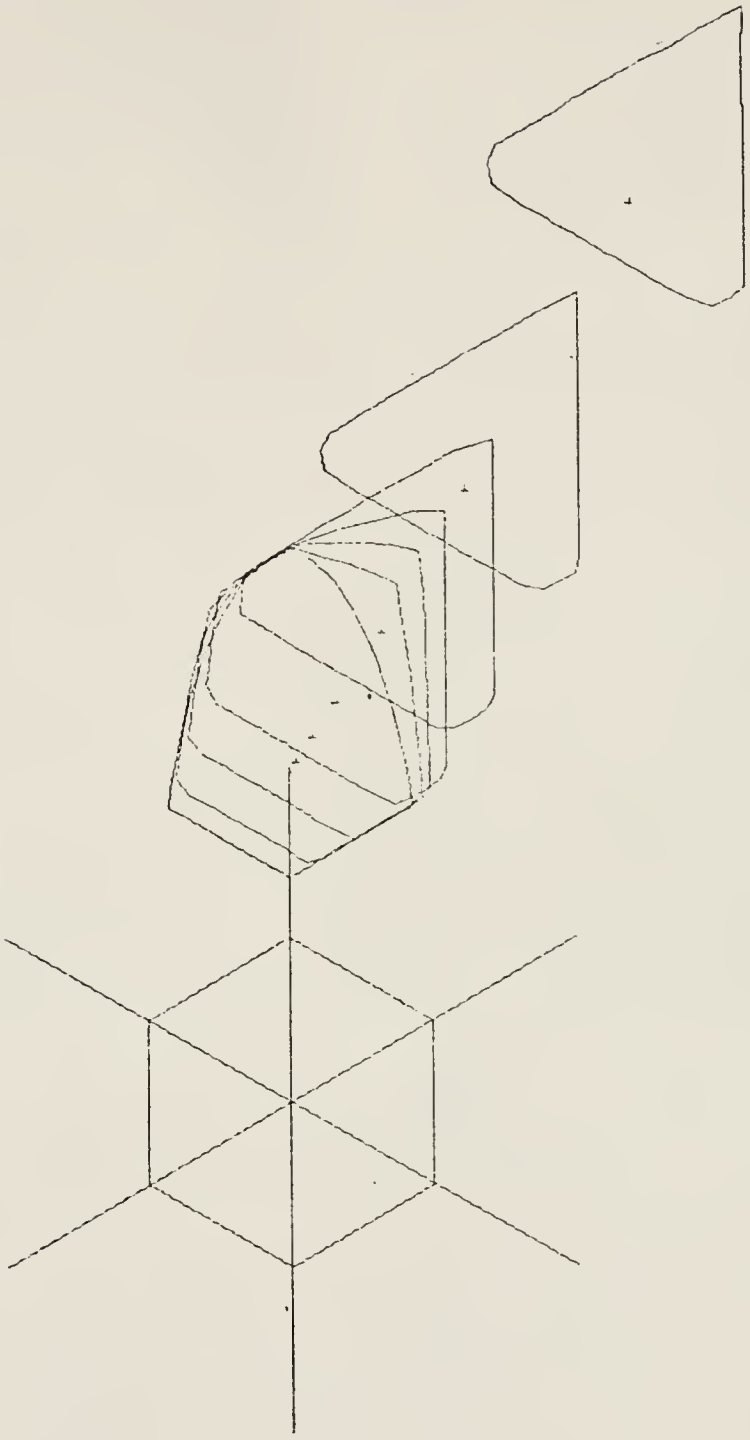

FIGURE D-5. (2,-1,-1) LOADING + (1,-1,0) STRESS LOADING YIELD SURFACES IN PRINCIPAL STRAIN SPACE ($\lambda = 0$)

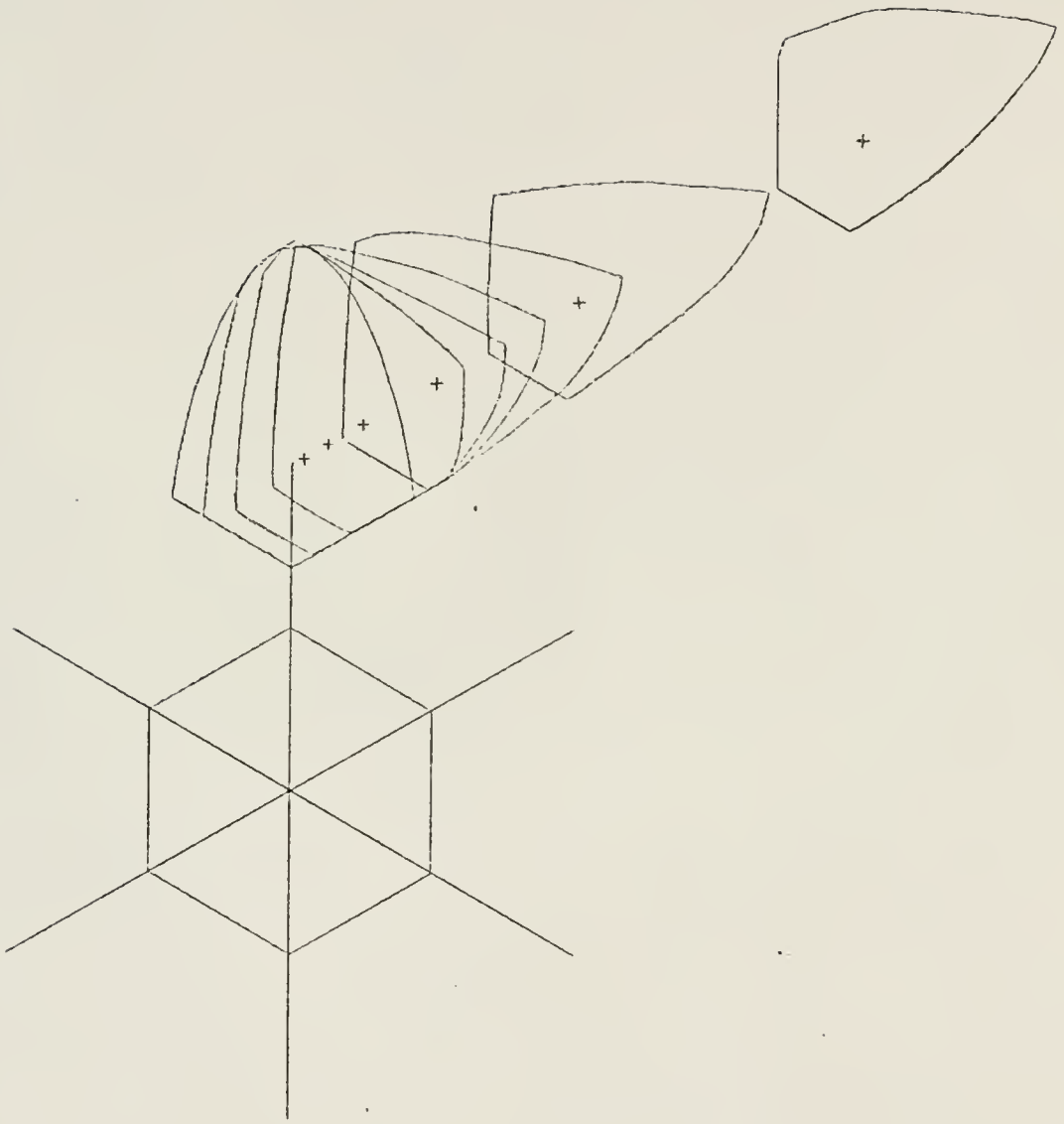

FIGURE D-6. (2,-1,-1) LOADING + (1,-2,1) STRESS LOADING
YIELD SURFACES IN PRINCIPAL STRAIN SPACE ($\lambda = 0$)

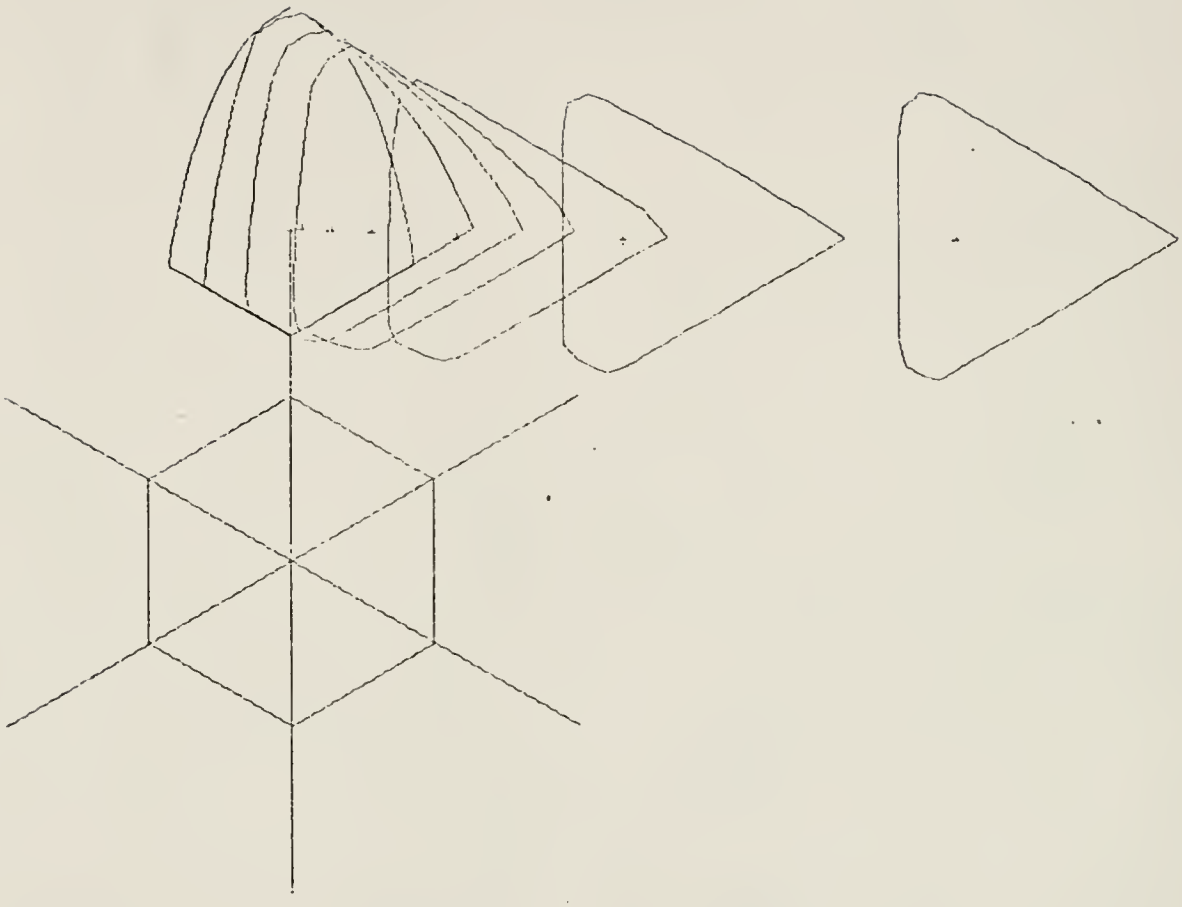

FIGURE D-7. (2,-1,-1) LOADING + (0,-1,1) STRESS LOADING
YIELD SURFACES IN PRINCIPAL STRAIN SPACE ($\lambda = 0$)

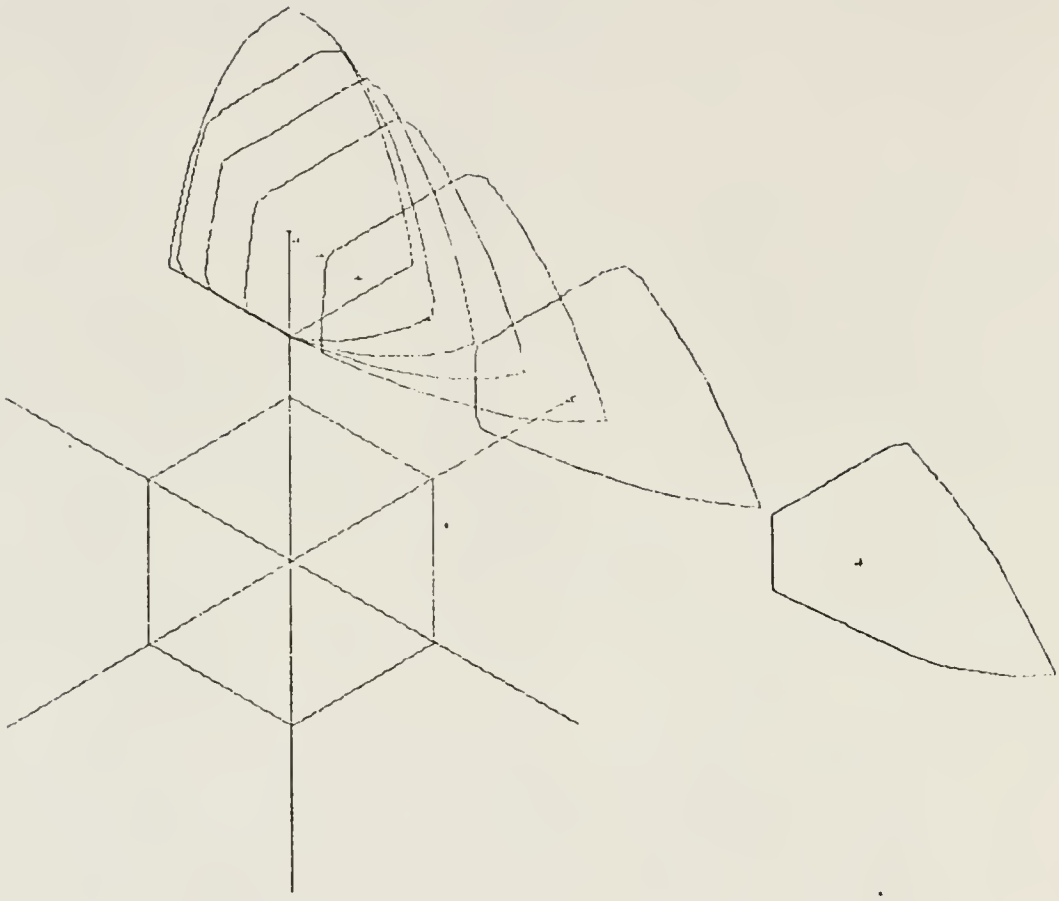

FIGURE D-8. (2,-1,-1) LOADING + (-1,-1,2) STRESS LOADING YIELD SURFACES IN PRINCIPAL STRAIN SPACE ($\lambda = 0$)

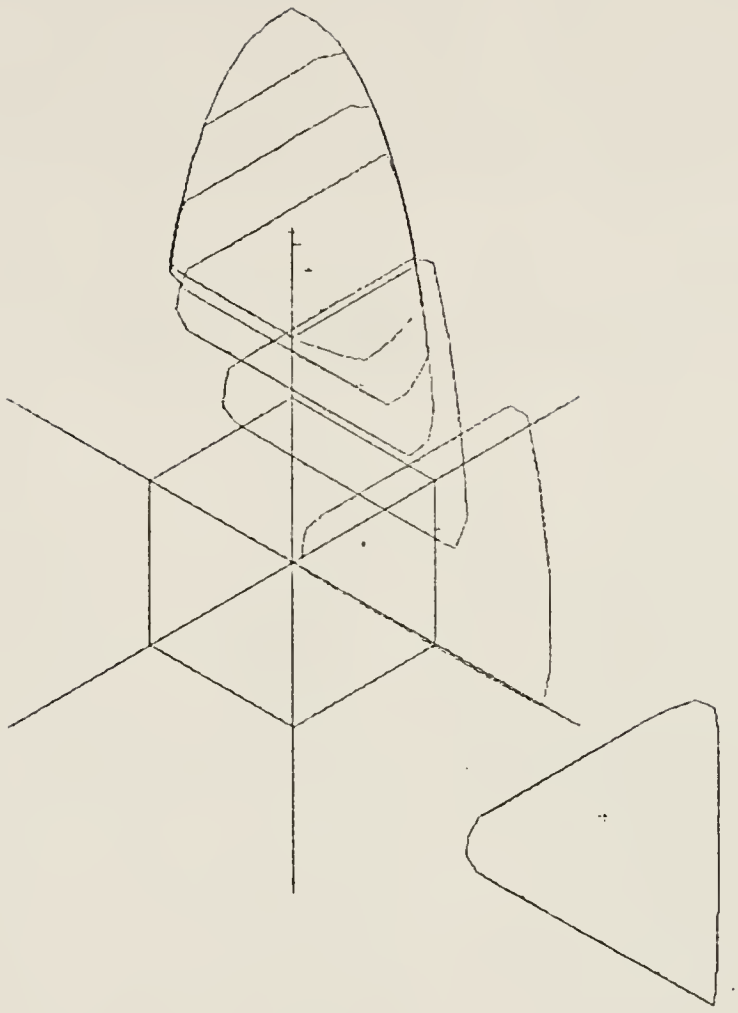

FIGURE D-9. (2,-1,-1) LOADING + (-1,0,1) STRESS LOADING YIELD SURFACES IN PRINCIPAL STRAIN SPACE ($\lambda = 0$)

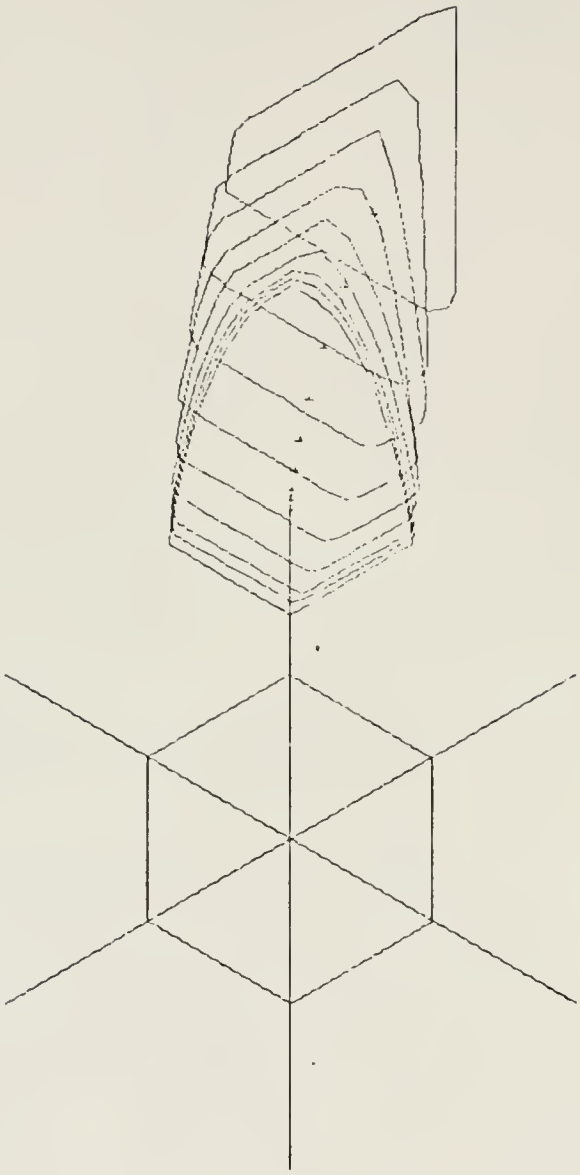

FIGURE D-10. (2,-1,-1) LOADING + (1,-1,0) STRAIN LOADING YIELD SURFACES IN PRINCIPAL STRAIN SPACE ($\lambda = 0$)

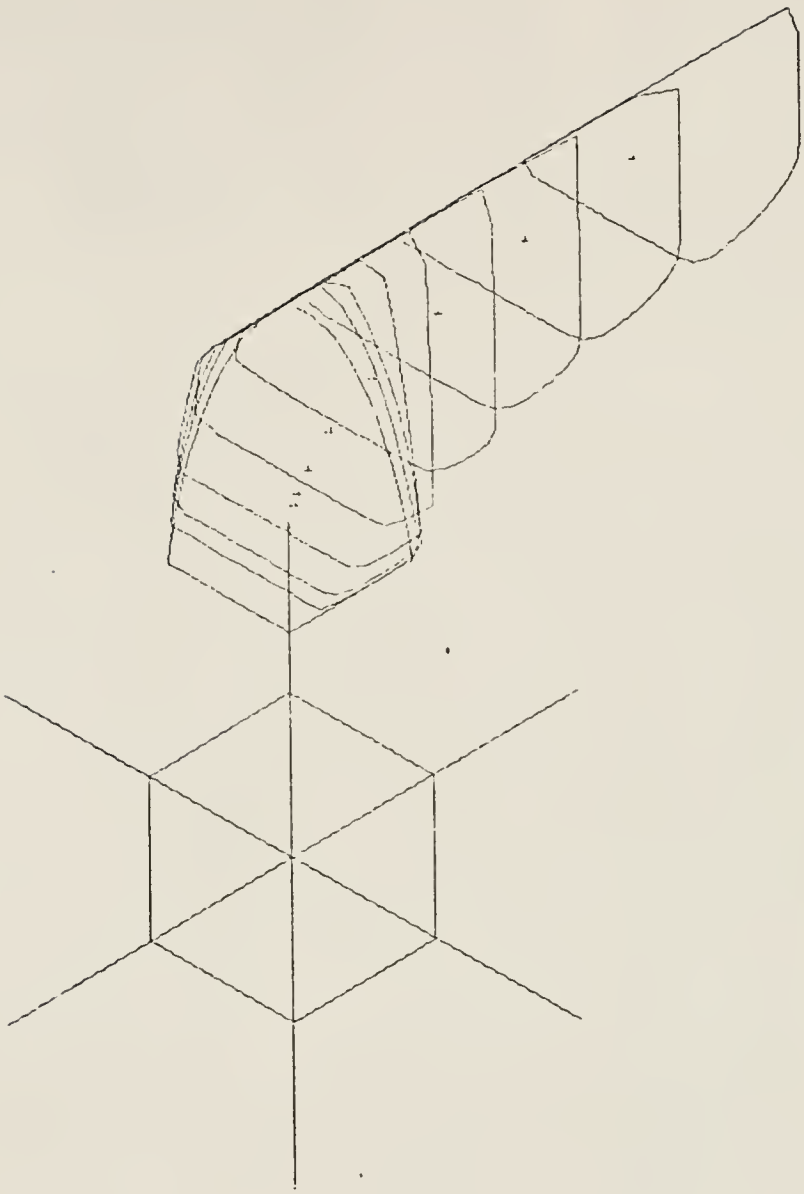

FIGURE D-11. (2,-1,-1) LOADING + (1,-2,1) STRAIN LOADING YIELD SURFACES IN PRINCIPAL STRESS SPACE ($\lambda = 0$)

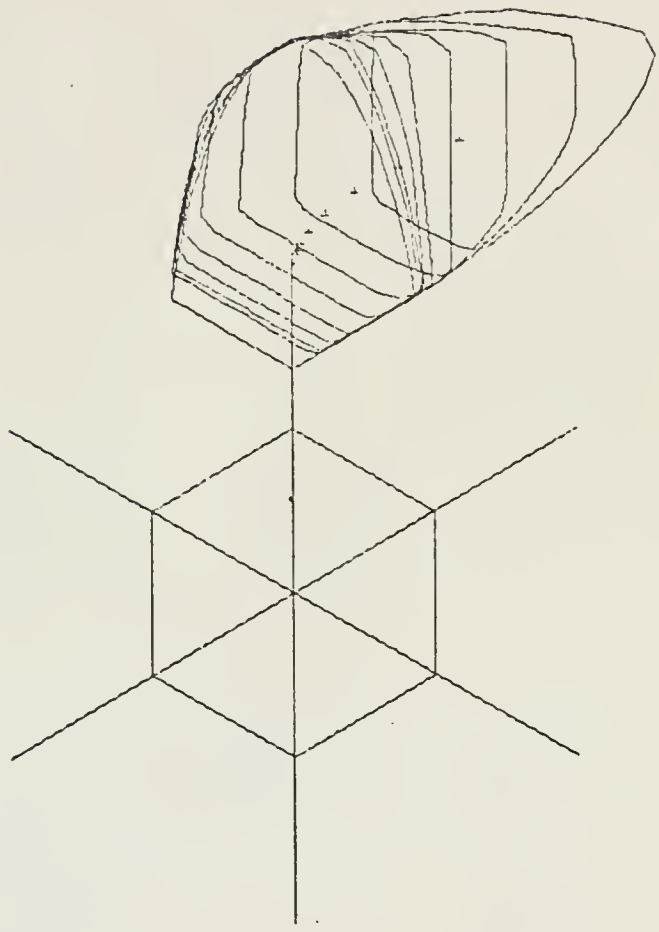

FIGURE D-12. (2,-1,-1) LOADING + (0,-1,1) STRAIN LOADING YIELD SURFACES IN PRINCIPAL STRAIN SPACE ($\lambda = 0$)

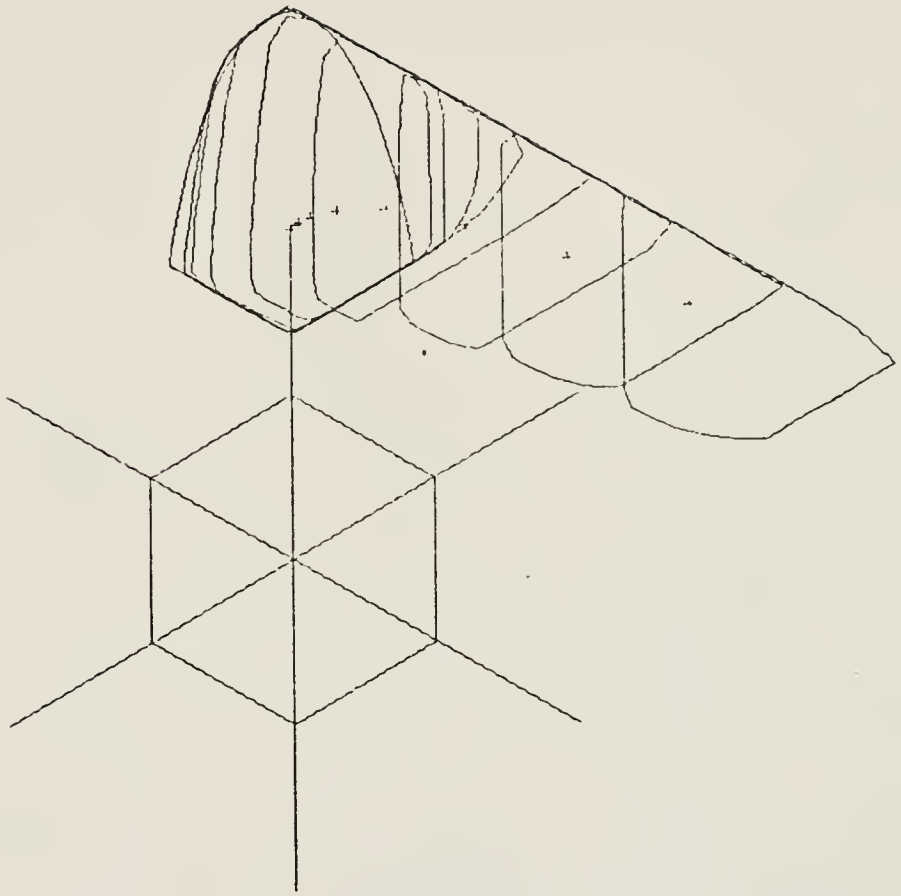

FIGURE D-13. (2,-1,-1) LOADING + (-1,-1,2) STRAIN LOADING YIELD SURFACES IN PRINCIPAL STRAIN SPACE ($\lambda = 0$)

BIOGRAPHICAL SKETCH

Carl Gottlieb Langner is a native Texan. He was born 30 November 1938, in Brownsville and he grew up in Seguin, where he graduated from high school. He attended the following colleges and universities: Texas Lutheran College (1956-1958), The University of Texas (1958-1960), Rice University (1960-1962), Johns Hopkins University (1965-1966), and the University of Florida (1970-1973). He received a Bachelor of Science degree in June 1960, from The University of Texas and a Master of Science degree in June 1963, from Rice University; both degrees were conferred in Mechanical Engineering. His M.S. thesis concerned dynamic stresses in a finite elastic body of revolution due to longitudinal impact.

Mr. Langner has worked for the following industrial organizations: Mission Manufacturing Company in Houston; Allegany Ballistics Laboratory in Cumberland, Maryland; Southwest Research Institute in San Antonio; and Shell Pipe Line Corporation in Houston. His work experience includes: analysis of a pneumatic drill, analysis of thermal stresses in a rocket nozzle, optimum design of anti-slosh baffles for rocket fuel tanks, vibration analysis of a hydrofoil boat, experiments on inelastic deformations of conical

shells, experiments on plasticity of cubes of pure aluminum, and various analyses involving the mechanics of a suspended pipe.

While at Shell Pipe Line Corporation, Mr. Langner was the engineer on two offshore pipeline projects: one repair project and one construction project. The former project involved a pipeline damaged during hurricane Camille. The latter project represented the deepest pipeline ever laid (at that time) in the Gulf of Mexico with a water depth of 375 feet. At the University of Florida Mr. Langner designed and built various pieces of equipment for the Dynamic Plasticity Laboratory, including the biaxial testing machine described herein.

Mr. Langner's publications include his M.S. thesis, studies of a spray-deposited explosive, description of the articulated stinger — a tool for laying offshore pipelines, and an article on citrus harvest mechanization. Mr. Langner is co-author of two patents concerned with construction of offshore pipelines, and he has two other patents pending.

I certify that I have read this study and that in my opinion it conforms to acceptable standards of scholarly presentation and is fully adequate, in scope and quality, as a dissertation for the degree of Doctor of Philosophy.

Lawrence E. Malvern

Lawrence E. Malvern, Chairman
Professor of Engineering Mechanics

I certify that I have read this study and that in my opinion it conforms to acceptable standards of scholarly presentation and is fully adequate, in scope and quality, as a dissertation for the degree of Doctor of Philosophy.

Ibrahim K. Ebcioglu

Ibrahim K. Ebcioglu
Professor of Engineering Mechanics

I certify that I have read this study and that in my opinion it conforms to acceptable standards of scholarly presentation and is fully adequate, in scope and quality, as a dissertation for the degree of Doctor of Philosophy.

Edward K. Walsh

Edward K. Walsh
Associate Professor
of Engineering Mechanics

I certify that I have read this study and that in my opinion it conforms to acceptable standards of scholarly presentation and is fully adequate, in scope and quality, as a dissertation for the degree of Doctor of Philosophy.

Robert E. Reed-Hill

Robert E. Reed-Hill
Professor of Materials Science

This dissertation was submitted to the Dean of the College of Engineering and to the Graduate Council, and was accepted as partial fulfillment of the requirements for the degree of Doctor of Philosophy.

August, 1973

Dean, College of Engineering

Dean, Graduate School

UNIVERSITY OF FLORIDA
3 1262 08553 7966